Vital Sign Monitoring and Analysis in Acute Coronary Syndrome Patients



Christina B. Vilakazi
St John's College

Supervised by: Professor Lionel Tarassenko and Dr Gari Clifford
Trinity Term, 2012

This DPhil Thesis is submitted to the
Department of Engineering Science, University of Oxford

Vital Sign Monitoring and Analysis in Acute Coronary Syndrome Patients

Christina B. Vilakazi
St John's College

DPhil in Engineering Science
Trinity Term, 2012

Abstract

Distinguishing patients with acute coronary syndromes (ACS) within the very large proportion with suspected cardiac pain is a diagnostic challenge, especially in individuals without clear symptoms or electrocardiographic features. This thesis presents the development of a patient data fusion system that would ultimately be able to assist with early identification of patients with non-ST-elevation Acute Coronary Syndrome (NSTEACS) in the pre-hospital setting.

In order to identify high-risk ACS patients, patients with ST changes need to be identified. A rule-based ST segment analysis technique was developed and validated on two publicly available databases. Even in subjects who are known to have myocardial ischaemia (MI), ST changes are not considered as a basis for a definitive diagnosis of individual episodes of ischaemia. A technique to differentiate between ST changes caused by MI and those caused by non-ischaemic ST changes such as body position changes or conduction changes was also developed.

At the outset of this research there was no available database with continuous vital-sign data for recorded during the ambulance transport. A clinical study was set up to collect vital-sign data and ECG during ambulance transport. Additional parameters from the ECG such as heart rate variability that can be used for detecting ACS, particularly NSTEACS, were investigated. High-risk patients may be identified early by appropriate combination of vital-sign data, demographic information and ECG analysis.

This thesis contributes to the literature on early identification of NSTEACS patient during the ambulance transportation. Firstly, it differentiate between ischaemic and non-ischaemic ST episodes using non-linear classifiers. pre-hospital data to ensure . Secondly, it investigates the diagnostic and prognostic value of heart rate variability in identifying high-risk NSTEACS patients in a pre-hospital setting. Thirdly, the thesis attempts to show how data fusion of vital-sign data and additional parameters from the ECG can be used to differentiate between non-cardiac and NSTEACS patients in a pre-hospital setting. Lastly, the thesis also provides some insight into the data collection process in a pre-hospital setting.

Acknowledgements

First and foremost, I would like to thank my supervisor, Prof. Lionel Tarassenko for his support, guidance and continued encourangement throughout the course of this research. I have benefited enormously from Lionel's wisdom during my time in Oxford. I am also grateful to my co-supervisor, Dr. Gari Clifford for the support, direction, constant encourangement and inspiration. I could not have imagined having better supervisors for my DPhil.

Thanks are also due to clinical collaborators in the John Radcliffe, Department of Cardiovascular Science and particularly Prof. Keith Channon, Dr. Robin Choudhury and Dr. Rajesh Kharbanda who have supported this project from the start and assisted with the collection of the data for the Pre-hospital Monitoring of Acute Coronary Syndrome Study. Special thanks go to Lisa Gaughran, who without her hardwork the Pre-hospital Monitoring of Acute Coronary Syndrome Study would not have been possible.

I am grateful for the support and assistance of all my colleagues in the Biomedical Signal Processing group. Particular thanks to David Wong for the endless ideas about 'ACS data fusion project' data analysis; Christina for the encouragement and proof-reading; and Gao Li for help with the Signal Quality Index work. I would also like to extend special thanks to Val Mitchell, who has been a great help regarding administration and paperwork, and for the much need hugs.

Finally, I would like to thank my parents, Susan and Abram Vilakazi for their support and love; my sister, Sonti for always believing in me; and my nephew Tshepo for inspiration. To my partner in life, Lufuno for the love, patience, encouragement and willingness to listen to me go on about my research.

Dedication

To my mother, my friend and my biggest cheer leader...
Susan Vilakazi
(21 April 1958 - 29 January 2009)

Contents

1 Introduction **1**
- 1.1 Classification of acute coronary syndrome . . . 3
- 1.2 Motivation for early diagnosis of myocardial ischaemia . . . 7
- 1.3 Early monitoring of acute coronary syndrome . . . 8
  - 1.3.1 Pre-hospital monitoring of acute coronary syndrome . . . 9
  - 1.3.2 Continuous ECG monitoring . . . 11
- 1.4 Risk stratification and diagnosis of acute coronary syndrome . . . 13
  - 1.4.1 Risk scores . . . 14
  - 1.4.2 Braunwald risk stratification . . . 15
- 1.5 Treatment and therapy . . . 17
- 1.6 Overview of the thesis . . . 18

2 Signal processing techniques for ECG analysis **20**
- 2.1 Basic anatomy of the heart . . . 20
- 2.2 Electrophysiology . . . 22
- 2.3 The Electrocardiogram . . . 24
  - 2.3.1 ECG recording . . . 24
  - 2.3.2 The ECG waveform . . . 27
  - 2.3.3 ECG analysis . . . 28
  - 2.3.4 Sources of noise in ECG waveforms . . . 29
  - 2.3.5 Selection of leads for diagnosing ST segment changes . . . 30
- 2.4 Causes of ST segment deviation in myocardial ischaemia . . . 32
  - 2.4.1 Stages in the development of myocardial ischaemia . . . 33
- 2.5 Signal processing tools for ECG analysis . . . 35
  - 2.5.1 Pre-processing of the ECG . . . 36
  - 2.5.2 QRS detection . . . 38
  - 2.5.3 Beat filtering . . . 39
  - 2.5.4 Baseline wander removal . . . 40
  - 2.5.5 Locating the PQ junction . . . 42
- 2.6 Dealing with noisy records . . . 42
  - 2.6.1 Signal Quality Index . . . 45
- 2.7 Heart rate variability . . . 47
  - 2.7.1 The physiological background of heart rate variability . . . 50
  - 2.7.2 Measures of heart rate variability . . . 51
  - 2.7.3 Methodology for computing heart rate variability . . . 54
- 2.8 Conclusion . . . 58

3 Automated ST segment analysis **59**
3.1 Available reference databases . . . 60
3.1.1 European ST-T Database . . . 60
3.1.2 Long Term ST Database . . . 61
3.2 Overview of ST segment analysis approaches . . . 63
3.2.1 Performance measures . . . 64
3.2.2 Digital-filter based systems . . . 64
3.2.3 Rule-based systems . . . 65
3.2.4 Machine learning techniques . . . 68
3.2.5 Comparison of different systems . . . 69
3.3 Implementation of an ischaemic detection algorithm . . . 70
3.4 Determining the J point and ST level . . . 72
3.4.1 Building a time series of the ST level function . . . 74
3.4.2 Computation of ST segment deviation . . . 74
3.5 Results of applying the algorithm to LTST DB . . . 75
3.6 Results of applying the algorithm to the ESC ST-T database . . . 78
3.7 Discussion . . . 79

4 Discriminating between ischaemic and non-ischaemic ST changes **80**
4.1 Existing techniques for discrimination between ischaemic and non-ischaemic ST changes . . . 81
4.2 Non-linear methodology outline . . . 83
4.3 Feature generation . . . 83
4.3.1 Heart rate . . . 84
4.3.2 Heart rate variability as a feature . . . 87
4.3.3 Depolarization Indices . . . 88
4.3.4 QRS complex features . . . 91
4.3.5 Feature extraction using Principal Component Analysis . . . 91
4.4 Feature selection . . . 95
4.4.1 Stepwisefit method . . . 96
4.5 Performance measures . . . 96
4.6 Classification . . . 97
4.6.1 Linear regression . . . 97
4.6.2 Neural networks . . . 98
4.6.3 Support Vector Machine . . . 99
4.6.4 Relevance Vector Machine . . . 101
4.7 Experimental methods . . . 102
4.7.1 Cross-validation . . . 103
4.7.2 Bootstrapping . . . 103
4.7.3 Data processing . . . 104
4.8 Experimental results . . . 105
4.8.1 Feature selection results . . . 108
4.8.2 Classification results . . . 110
4.8.3 Comparison of different models . . . 115
4.8.4 Discrimination between ischaemic and non-ischaemic ST episodes . . . 116
4.9 Discussion . . . 117

5 Pre-hospital monitoring of acute coronary syndrome patients 119
5.1 Introduction . . . 119
5.2 The protocol . . . 121
5.3 Software and hardware . . . 123
5.3.1 Heart rate . . . 124
5.3.2 Blood pressure . . . 124
5.3.3 Peripheral oxygen saturation . . . 125
5.3.4 ECG and ST level . . . 125
5.4 Summary of the data . . . 126
5.4.1 Demographic and clinical data . . . 127
5.4.2 Classification of patients into groups based on diagnosis . . . 127
5.5 Vital-sign data . . . 130
5.5.1 Signal Quality Index of records in the pre-hospital monitoring study . . . 132
5.6 Summary . . . 134

6 Spectral analysis of ECG-derived information as a diagnostic tool for acute coronary syndrome 136
6.1 Introduction . . . 136
6.1.1 Changes of HRV related to myocardial infarct . . . 136
6.2 Computation of heart rate variability . . . 139
6.2.1 Respiratory sinus arrhythmia as an index of vagal tone control . . . 139
6.2.2 Extraction of respiratory rate from amplitude modulation of the ECG . . . 144
6.2.3 Tracking changes in parasympathetic activity . . . 146
6.3 Vagal tone control in acute coronary syndrome patients . . . 148
6.3.1 Analysis of results from the two patient groups . . . 151
6.4 Discussion . . . 156

7 Data fusion for pre-hospital patient monitoring 158
7.1 Overview of data fusion techniques . . . 159
7.2 Data statistics . . . 161
7.3 Comparison of data fusion techniques . . . 165
7.3.1 Data pre-preprocessing . . . 165
7.4 Experimental results . . . 165
7.4.1 Linear regression . . . 166
7.4.2 Logistic regression . . . 167
7.4.3 Multi-layer perceptron . . . 168
7.4.4 Support Vector Machine . . . 169
7.4.5 Relevance Vector Machine . . . 170
7.5 Using additional features to discriminate between non-cardiac and NSTEACS . . . 171
7.5.1 Variability indices . . . 171
7.5.2 Demographic information . . . 172
7.5.3 Feature selection and classification . . . 175
7.6 Discussion . . . 176

8 Conclusions **177**
8.1 Overview of the thesis 177
8.2 Future work 179
8.2.1 Heart rate variability measures 179
8.2.2 Data fusion models 180

A Support Vector Machine **181**

B Relevance Vector Machine **189**

C Signal quality index assessment **194**
C.1 Established signal quality assessment techniques 194
C.1.1 Comparison of multiple beat detection algorithms on a single lead: bSQI 195
C.1.2 Beat detection comparison using different ECG leads: iSQI 195
C.1.3 Kurtosis of the ECG: kSQI 196
C.1.4 Spectral distribution of ECG: sSQI 197
C.1.5 Combined ECG SQI 197
C.1.6 Database 198
C.1.7 Additive noise 198
C.2 Comparison of ECGSQI with a template-based method, TSQI 200

List of Figures

1.1 Evaluation of acute coronary syndrome. ACS - Acute Coronary Syndrome, ECG - Electrocardiogram, NSTEMI - non-ST-elevated Myocardial Infarction, STEACS - ST elevation Acute Coronary Syndrome. 4

2.1 Blood flow in the heart. 21
2.2 A typical action potential from a ventricular myocardial cell. Phases 0 through 4 are marked. An action potential is generated when the membrane potential is partially depolarized from the resting level(E_m) to the threshold potential(E_t). . 23
2.3 (a) The ECG lead vectors in the frontal and transverse plane of the human body. (b) The placement of the ten surface electrodes from which the standard 12-lead ECG is derived. 25
2.4 Examples of standard 12-lead ECG recordings. 26
2.5 Schematic representation of a single cycle of the electrocardiogram signal corresponding to one heart beat. The characteristic features are labelled P, Q, R, S, T and U waves. Of particular interest to this are the J point, ST segment and ST level. 27
2.6 Examples of different types of ECG noises. 31
2.7 Power line removal after applying a two stage filtering procedure using notch filters and low pass filtering. (a) Original ECG and (b) corresponding PSD. (c) ECG after 50 Hz notch filter (d) corresponding PSD. (e) ECG after 50 and 60 Hz (f) corresponding PSD (g) ECG after 50 and 60 Hz and low-pass Butterworth filter (h) corresponding PSD. 37
2.8 The common structure of a QRS detector. 39
2.9 Block diagram for Pan and Tompkins Algorithm. 40
2.10 Removing baseline wander from a 10-second ECG recording using cubic spline interpolation. Panel A shows the original ECG signal, Panel B shows the original signal with PQ points (red circles), panel C shows the fitting of the cubic spline at 5 Hz, and panel D shows the final ECG signal, constructed by subtracting the baseline from the original signal. 43
2.11 Flowchart of the algorithm for computing the Signal Quality Index. 46
2.12 Illustration of template creating using one-minute window from patient 0031. The red stars are the R-peak. 48
2.13 Illustration of template matching using high-quality beat and the low-quality beats. The high-quality beat has a correlation coefficient of 0.97 and the low-quality beat has a correlation coefficient of 0.25. 49
2.14 Flow diagram of the methodology used for computing HRV using spectral analysis. 56

2.15 Illustration of removal and replacement of ectopic beat. (a) Detection of R-peaks using the Hamilton and Tompkins algorithm; (b) Ectopic beat removal. (c) Replacement with a "phantom" beat using linear interpolation. 57

3.1 Flowchart of the proposed ST analysis algorithm. 72
3.2 Salient points on an ECG beat after QRS detection and determination of the J point and ST amplitude. 73
3.3 An example of a real ischaemic episode of (a) 105 seconds ECG (record s20131 of the LTST DB). The corresponding (b) ST level (c) ST reference (ST ref.), and (d) ST episodes found by our algorithm described in this chapter using the criteria according to protocol B. S and E indicate the start and end of an event as annotated in the database. The solid red lines are the start and end of episode as found by our algorithm. The horizontal dashed lines in (d) indicate the threshold from protocol B used to detect an episode. 76

4.1 Typical transient ischaemic ST segment deviation episode (record, lead, reference), time series of the ST segment deviation (blue) and heart rate, (green). (b) Typical heart-rate related non-ischaemic ST segment deviation (record, lead, reference), time series of the ST segment deviation (blue) and heart rate, (green). 85
4.2 Evolution of the ST amplitude (J60(80)) with respect to the heart rate for an ischaemic ST segment from record s30651 in the LTST DB (b). Evolution of the ST amplitude with respect to heart rate for heart-rate related non-ischaemic ST segment from record s30651 in the LTST DB. 86
4.3 Example showing the delineation using the number of samples to evaluate the QRS slopes. 90
4.4 An example of temporal evolution of the upslope, $\mathrm{I_{US}}$, and downslope, $\mathrm{I_{DS}}$, during an ST episode. 90
4.5 Diagram of a generalised neural network model. 98
4.6 Block diagram of the RVM. 102
4.7 Evolution of different metric on the training (blue) and testing (green) for when increasing model dimensionality (k). The selected dimensionality for the model (k=12) is indicated by a red star. 109
4.8 ROC plot showing the median curve and the 5th and 95th percentiles over the 1000 independent splits of the data for linear regression on annotation protocol B using 12 most relevant features obtained from the stepwise fit. 110
4.9 Empirical probability distribution of outputs of linear regression for each class. 111
4.10 ROC plot showing the median curve and the 5th and 95th percentiles over the 10000 independent splits of the data for the MLP on protocol B together with corresponding statistics. 112
4.11 ROC plot showing the median curve and the 5th and 95th percentiles over the 1000 independent split of the data for SVM. 113
4.12 ROC plot showing the median curve and the 5th and 95th percentiles over the 1000 independent split of the data achieved using RVM to discriminate between ischaemic and heart-rate related ST episodes. 114
4.13 Comparison of areas under the ROC curves for the four different classifiers used in this study. Each boxplot has a central mark at the median, while the edges of the box are the 5th and 95th centiles. 115

5.1 Flowchart for the clinical study. 122
5.2 The Medtronic Lifepak 12/15 used for recording the data in the study 123
5.3 Flowchart of the study. 126
5.4 Percentage of collected vital-sign data grouped per 100 patients. The blue is the heart rate, green represent SpO_2, yellow represent BP and red is the ST level. 131
5.5 Percentage of complete records grouped per 100 patients for all 500. 132
5.6 Signal Quality Index for patient 0031 for a 40-second window shown in green, with the ECG signal shown in blue. 133
5.7 Histogram of the SQIs for the 500 patients in the database. 134

6.1 Flow diagram of the methodology used for computing heart rate variability from RSA and extraction respiratory information from baseline wander. 140
6.2 Illustration of the steps involved in processing the ECG to extract the RSA signal. (a) R-peak detection. (b) After detrending the RR-interval (c) After band-pass filtering (d) After resampling at 7Hz. 141
6.3 Illustration for estimating the power spectral density of the HRV for a one-minute window using the Lomb-Scargle periodogram. (a) Extraction of RR interval (b) The RSA signal. (c) Power spectral estimated from the Lomb-Scargle periodogram. In this example the dominant peak is at 0.33Hz. 142
6.4 Evolution of the energy normalised power spectral density for the RSA signal for the duration of the recording. The dominant peak remained around the same region of about 0.38Hz for the first two-thirds of the recording. 143
6.5 Extracting the baseline wander signal using a bandpass filter. (a) The ECG waveform. (b) The extracted baseline wander signal using the band-pass FIR filter described in the text. (c) The baseline wander signal after detrending. (d) The baseline wander signal after downsampling from 125Hz to 25Hz. 146
6.6 Power spectral density of the baseline wander for a one-minute window of the same subject as in Figure 6.5. (a) Extraction of baseline wander signal from the ECG (b) The baseline wander signal. (c) Power spectral estimated from the Lomb-Scargle periodogram. For this example the dominant peak is at 0.33Hz. . 147
6.7 Evolution of the normalised power spectral density (PSD) computed using Lomb-Scargle periodogram for the duration of the recording. The dominant peak remains close to 0.38Hz for the first two-thirds of the recording. 148
6.8 Extracting the respiratory frequencies from baseline wander signal using the Lomb-Scargle periodogram. The red circles are respiratory frequencies after median filtering. The black solid lines are the respiratory frequencies $\pm$ 0.05Hz ($\pm$ 3 breaths per minute). 149
6.9 Illustration of the three methods used for defining the bands to compute the HF component of the HRV from the ECG recording in Figure 6.6 (baseline wander signal). (a) Standard band (0.15Hz and 0.4Hz). (b) Half the mean HR. (c) Limits set using the ECG-derived respiratory sinus arrhythmia (RSA). 150
6.10 The frequency trends of the power in LF and HF using dynamics bands set using respiratory frequency. The components were computed from the PSD estimated using the Lomb-Scargle periodogram. The red graphs are the median filtered plots. 151

6.11 Boxplots showing low- (LF) and high frequency (HF) components of RR-interval in normalized units and their LF/HF-ratio between non-cardiac and ACS groups (both STEMI and NSTEACS). The boxplot is placed around the median (50%), represents centile 25-75%. 153

7.1 Distribution of vital-sign data for the non-cardiac group (blue) and the NSTEACS group (green). 163
7.2 Vital sign record for patient 0297 from the NSTEACS group. The HR, $\mathrm{SpO_2}$. 164
7.3 ROC curve and empirical probability for linear regression. 167
7.4 ROC curves for logistic regression. (a) The median curve is in blue and the 5th and 95th centile as shown as dashed lines. (b) Empirical probability of the NSTEACS group and normal non-cardiac group. 168
7.5 ROC curves of multi-layer perceptron. The median curve is in blue and the 5th and 95th centiles as shown as dashed lines. 169
7.6 ROC curves for SVM. The median curve is in blue and the 5th and 95th centile as shown as dashed lines. 170
7.7 ROC curves for Relevance Vector Machine. The median curve is in blue and the 5th and 95th centile as shown as dashed lines. 171
7.8 ROC curves using means and standard deviations as features (7-dimensional feature vector) for (a) Logistic regression, (b)Multi-layer perceptron (MLP), (c) Support Vector Machine(SVM), (d) Relevance Vector Machine (RVM). . . 173
7.9 ROC curves using means and demographic information as features for (a) Logistic regression, (b)Multi-layer perceptron (MLP). 174
7.10 ROC curves using the subset of selected features (a) Logistic regression, (b)Multi-layer perceptron (MLP). 175

C.1 An example of 30 s of evaluation data. (a) EM noise at different SNRs, (a) BW noise at different SNRs (a) MA noise at different SNRS (SNR = 24, 18, 12, 6, 0 and -6 dB) 199
C.2 An example of a comparison of the two SQI algorithms on a ECG signal added with -6dB movement artefacts (MA) noise. The SQI were computed for 1-minute window with no overlaps. Gold standard human annotated SQI in blue. Template-based SQI (this work) in black. ECGSQI in green) 201

List of Tables

3.1 Comparison of existing methods for ischaemic ST episode detection and beat classification. Beat classification techniques classified individual beats as normal or ST elevated/depressed. Ref. stands for references. Se -Sensitivity, PPV - Positive Predictive Value. 71

3.2 Overall performance of the proposed algorithm on the ST episodes annotated according to the annotation protocol B of the LTST DB. The gross and average sensitivity, Se and gross and average specificity, Sp, in determining ST events are used to characterise performance. 75

3.3 Performance of the proposed technique for all ECG recording for the ST episode detection according to the annotation protocol B of the LTST database. The table shows the results of all ST episodes. The second column on the table is correctly detected events ⁄ total number of events. 77

3.4 The gross and average sensitivity, Se and gross and average specificity, Sp, of the algorithm proposed in this thesis in determining ST events on the ESC ST-T database. 78

4.1 Number of ischaemic, heart-rate related and sudden-step changes used in discrimination for each annotation protocol. The numbers in brackets represent the number of episodes with start and end points. 105

4.2 List of the selected features by groups, their means and standard deviations ($\mu \pm \sigma$) for ischaemic and heart-rate related ST episodes annotated according to the annotation protocol B of the LTST DB, *p-value* from the ANOVA. ‡ indicates significance of $p < 0.05$. 107

4.3 List of the selected features identified by stepwise fit with performance measures for ischaemic and heart-rate related ST episodes annotated according to the annotation protocol B of the LTST DB. The results were obtained using linear regression. 108

4.4 summary of the classification performance in terms of sensitivity, specificity and accuracy between ischaemic ST and heart-rate related ST episodes using linear regression for annotation protocols A, B and C from the LTST DB database. 111

4.5 Summary of the classification performance in terms of sensitivity, specificity and accuracy between ischaemic ST and heart-rate related ST episodes using an MLP for annotation protocols A, B and C from the LTST DB database. . . . 112

4.6 Summary of the classification performance in terms of sensitivity, specificity and accuracy between ischaemic ST and heart-rate related ST episodes using SVM for annotation protocols A, B and C from the LTST DB. 113

4.7 Summary of the classification performance in terms of sensitivity, specificity and accuracy between ischaemic ST and heart-rate related ST episode using RVM for annotation protocols A, B and C from the LTST DB database. 115
4.8 Summary of the classification performance in terms of sensitivity, specificity and accuracy between ischaemic and non-ischaemic ST episodes using RVM for annotation protocols B from the LTST DB database. 116

5.1 Demographic and risk factors of the overall population along with the ACS group and non-cardiac group. n represents the number of patients. 128
5.2 Patient demographics and cardiac risk factors for each age category. n represent stands for the number of patients. 129
5.3 Patient demographics, risk factors and pharmacological factors for subgroups of acute coronary syndrome (ACS). The subgroup are ST elevation Myocardial Infarction (STEMI), non-ST elevation Myocardial Infarction (NSTEMI) and unstable angina (UA). n stands for the number of patients in that subgroup. . . 130
5.4 Percentage of records with high-quality beats for records with all vital-sign parameters (heart rate, blood pressure, oxygen saturation and ST level.) 133

6.1 A list of patients included in non-cardiac and ACS subsets for analysis. 152
6.2 The ACS subset has 20 patients and the non-cardiac subset also has 20 patients. The values given are median and interquartile range (IQR). 154
6.3 Results of statistical significance test between the ACS and the non-cardiac group using frequency domain measures of heart rate variability. The ACS subset has 20 patients and the non-cardiac subset also has 20 patients. The values given are mean (μ) and standard deviation (σ). The *p-values* of F-test, K-S test unequal t-test and Mann-Whitney test are shown. The statistical significance level was set at < 0.05. 155
6.4 Results of the non-cardiac and the NSTEACS group using frequency domain measures of heart rate variability. The non-cardiac group had a subset of 7 patients and the NSTEACS subset had 7 patients. The values given are median and interquartile range (IQR). 155

7.1 Physiological upper and lower bounds for the vital-sign parameters. 161
7.2 Mean and standard deviation of vital-sign parameters for the ACS, cardiac and non-cardiac groups. 162
7.3 Mean and standard deviation of vital-sign data for non-cardiac and NSTEACS groups. 162
7.4 Median (5%-95%) of AUC, sensitivity and specificity of logistic regression, MLP, SVM and RVM using 7-dimensional vector with the means and standard deviations of the four vital signs. 172
7.5 Median (5%-95%) AUC, sensitivity and specificity of logistic regression and MLP using the means of the HR, $\mathrm{SpO_2}$, MAP and ST level and the demographic factors; age, previous MI and smoker or not. 174
7.6 Median (5%-95%) AUC, sensitivity and specificity of logistic regression and MLP using the subset of selected features, mean values of $\mathrm{SpO_2}$, standard deviation values of $\mathrm{SpO_2}$, previous MI and smoker or not. 176

B.1 Sparse Bayesian Learning Algorithm 193

C.1 Performance of ECGSQI and TSQI on the entire subset of data selected from the MIMIC II database in this study, with three different types of noise added; electrode motion (EM), muscle artifact (MA) and and baseline wander (BW) . . 202

Glossary of clinical terms

In the interest of clarity and since the nature of this thesis is cross-disciplinary, a glossary of clinical terms and explanations of contextual descriptors are provided.

- Angina: Chest pain due to an inadequate supply of oxygen to the heart muscle. The chest pain of angina is typically severe and crushing. There is a feeling just behind the breastbone (the sternum) of pressure and suffocation.

- Arrhythmia: Any variation from the normal (sinus) rhythm of the heart beat, including premature beats, heart block, atrial fibrillation and atrial flutter.

- Artefact: A product or effect that is not present in the natural state (of an organism, etc.) but occurs during or as a result of investigation or is brought about by some extraneous agency such as electrode movement.

- Atherosclerosis: A process of progressive thickening and hardening of the walls of medium-sized and large arteries as a result of fat deposits on their inner lining.

- Autonomic Nervous System (ANS): The system of nerves of the glands and of the involuntary muscle that regulates key functions including the activity of the cardiac muscle, smooth muscles (e.g., of the gut), and glands. In 1940 R. S. Woodworth defined the autonomic nerves to be those that run to the heart, blood vessels, lungs, stomach, intestines, and other viscera. These nerves are composed of extra-slender nerve fibres, which grow out from cells in the brain stem and cord. The ANS comprises the sympathetic nervous system (which accelerates the heart rate, constricts blood vessels, and raises blood pressure) plus the parasympathetic nervous system (which slows the heart rate, increases intestinal and gland activity, and relaxes sphincter muscles).

- Baroreflex: A reflex whereby the heart speeds up and beats more forcefully when BP falls.

- Blood Pressure (BP): The pressure that must be applied to an artery in order to stop the pulse in the vessel beyond the point of pressure. It is generally assumed to be equivalent to the systolic pressure to which the blood is subjected by the force of the heart and the

elasticity of the vessels, but also depends upon thickness and hardness of vessel wall, and of volume of blood thrown out of the heart at each beat. BP is greatest at each heart beat (systolic blood pressure - SBP) and lowest between beats (diastolic blood pressure DBP).

- Bradychardia: A slowness of the beating of the heart (to less than of 60 breaths per minute).
- Cardiac Output: HR over stroke volume.
- Cardiomyopathy: A weakness of the heart muscle, often leading to heart failure. Can be caused by a number of underlying disorders including coronary artery disease, valvular heart disease, viral infection, diabetes, alcohol abuse, or connective tissue disorders. Sometimes no specific cause can be identified, in which case the cardiomyopathy is referred to as idiopathic.
- Coronary Artery Disease (CAD): Is a chronic disease in which there is a atherosclerosis (hardening) of the arteries on the surface of the heart. It is also referred to as coronary heart disease (CHD).
- Diastole: The time, in between ventricular contractions (systole), at which ventricular filling occurs.
- Diastolic Blood Pressure: The pressure exerted on the walls of the arteries when the heart is in the relaxation phase (diastole). Considered abnormally elevated if consistently over 90 mmHg.
- Efferent Nerve: Carry impulses away from the muscle/gland/organ
- Ejection Fraction: a measure of the function of the left ventricle, also called left ventricular ejection fraction (LVEF). The ejection fraction is the percentage of blood ejected from the left ventricle with each heart beat. An LVEF of 50% indicates that the left ventricle ejects half its volume each time it contracts. A normal ejection fraction is 50% or higher. A reduced ejection fraction can indicate that cardiomyopathy is present.
- Fibrillation: A small, local, involuntary contraction of muscle, invisible under the skin, resulting from spontaneous activation of single muscle cells or muscle fibres.

- Heart Beat: A full cycle depolarisation and repolarisation of the cardiac muscle. Each heart beat is followed by a period of rest where ventricular filling occurs.
- Heart Rate (HR): The number of heart beats per minute (bpm)
- Hypertension: Persistently high arterial blood pressure. Hypertension may have no known cause (essential or idiopathic hypertension) or be associated with other primary diseases (secondary hypertension).
- Infarction: The formation of an infarct, an area of tissue death due to a local lack of oxygen.
- Inferior: In anatomy, below or toward the feet. As opposed to superior. The liver is inferior to the lungs.
- Ischaemia: Is a restriction in blood supply to tissues, causing a shortage of oxygen and glucose needed for cellular metabolism (to keep tissue alive).
- Norepinephrine: or noradrenaline; a precursor of adrenaline whose main function is to mediate the impulses in the sympathetic nervous system. Increased levels are associated with stress and it is often referred to as the fight or flight hormone.
- Noise: A collective term for: fluctuations or disturbances which are not part of a wanted signal or which interfere with its intelligibility or usefulness such as muscle activity (for ECG analysis) and ectopic beats (for HRV analysis).
- Myocardial Infarction (MI): A blockage in the normal electrical conduction paths of the heart that cause the muscle contraction, often leading to permanent damage to the heart muscle.
- Parasympathetic system: Part of the autonomic nervous system which is connected with the brain and spinal cord through certain nerve centres in the mid-brain, medulla, and lower end of the cord, including the vagus (see below). Its action is usually antagonistic to that of the sympathetic system in that it inhibits the action of the heart and stimulates the intestine.

- Sympathetic system: Part of the autonomic nervous system consisting of ganglia united by an irregular network of nerve fibres. The major part of the sympathetic system consists of two ganglionated cords that run through the neck, chest and abdomen, lying close in front of the spine. Its action is usually antagonistic to that of the parasympathetic system in that it stimulates the action of the heart and inhibits the intestine.

- Systole: The time at which ventricular contraction occurs; a contraction of the heart that alternates with the diastole occupying, respectively.

- Systolic Blood Pressure (SBP): The pressure exerted on the walls of the arteries during the contraction phase of the heart. Considered abnormally elevated if consistently over 150 mmHg. Systolic blood pressure varies with age, sex, size and relative condition.

- Tachycardia: The excessive rapidity in the action of the heart, the term is usually applied to a heart rate above 100 per minute and may be qualified as atrial, junctional (nodal) or ventricular and as paroxysmal.

Chapter 1

Introduction

Coronary artery diseases (CAD) are one of the leading causes of death globally and the most common type of heart disease [1, 2]. According to the World Health Organization (WHO), 3.8 million men and 3.4 million women die each year from CAD globally [3]. CAD was the most common cause of premature death in the United Kingdom (UK) in 2008 and approximately 18% of premature deaths in men and 9% premature deaths in women were due to CAD. The British Heart Foundation estimates that in the UK, 191,000 people die each year from cardiovascular disease of which almost half (46%) is caused by CAD [4].

CAD occurs when the arteries that supply blood to the heart muscle become hardened and narrowed due to the buildup of cholesterol and plaque on their inner walls. This buildup is called atherosclerosis [1]. Atherosclerosis streaks within the walls of the coronary arteries represent the early stages of heart disease in asymptomatic individuals, but do not initially obstruct the flow of blood. Over a period of time these streaks increase in thickness as the plaques expand into the walls of the arteries, eventually expanding into the lumen of the vessel and affecting the blood flow to the heart. Plaques can become unstable, rupture, and additionally promote a thrombus (blood clot) that occludes the artery.

Acute coronary syndrome (ACS) is the most prevalent manifestation of CAD and is associated with high mortality and morbidity [2]. The syndrome is caused by a sudden rupture of plaque in the coronary arteries with occlusive or sub-occlusive thrombus formation leading to

myocardial ischaemia and necrosis. If the ischaemia is left untreated for a sufficient period of time, it can cause damage to, or death (infarction) of, heart muscle tissue (myocardium). Acute coronary syndrome is broadly classified into two major categories: unstable angina (UA), in which the heart tissue is not permanently damaged; and myocardial infarction (MI), in which it is damaged.

Myocardial ischaemia stems from an insufficient supply of blood to the myocardium due to blockages in the coronary artery. Supply ischaemia results from a partial occlusion of coronary arteries, reducing the amount of oxygenated blood to the myocardium. This differs from demand ischaemia which refers to a condition in which an increased oxygen demand caused by exercise, tachycardia or emotion, leads to a transitory imbalance [1]. A distinction should also be made between myocardial ischaemia and myocardial infarction. Ischaemia means that the amount of oxygen supplied to the tissue is inadequate to supply the needs of the tissue. When the myocardium becomes ischaemic, it does not function efficiently. If the blood flow to the tissues is improved, myocardial ischaemia can be reversed. The term infarction describes necrosis or damage of myocardial cells, and means that the tissue has undergone irreversible damage due to lack of sufficient oxygen-rich blood.

The diagnosis of myocardial infarction is made after assessing the patient's complaints and physical status. Among the diagnostic tests available to detect heart muscle damage are an electrocardiogram (ECG), echocardiography, cardiac medical resonance imaging (MRI), coronary angiography and various blood tests. The ECG gives valuable clues to identify the location of myocardial damage while a coronary angiogram allows visualisation of narrowing or obstructions in the heart vessels.

The primary means by which the heart's functionality is assessed is through the analysis of the surface ECG, a non-invasive signal that captures the projection of the electrical activity of the heart on the body surface. As large areas of the heart's muscle become ischaemic, its relaxation and contraction patterns are affected, which causes variations in the features of the ECG due to the development of an injury current between the ischaemic and non-ischaemic regions of the heart [1].

The feature of the ECG that most clearly reflects the development of this injury current is known as the ST segment. The cellular modifications generated by acute ischaemia affect the ST segment such that changes in the ST segment are an early indication of ischaemia. If the blood supply to the heart muscle is restored, myocardial ischaemia can be reversed. Therefore an early diagnosis of myocardial ischaemia is important to ensure a good outcome for the patient.

Previous work in the area of ACS has focused mainly on the analysis of ECG for diagnosis and risk stratification. This thesis describes the development of a system to identify high-risk ACS patients in the pre-hospital setting, using non-invasive measurements of vital signs such as heart rate, oxygen saturation, blood pressure and additional parameters from the ECG. In this context, the vital-sign monitoring would be initiated by an ambulance crew, and analysed by a computer to identify high-risk ACS patients. This result could then be used by the clinician in conjunction with other information to make a diagnosis and/or determine a course of treatment. Although the intended application of the system is the pre-hospital environment, the problem of identifying high-risk ACS is also present in-hospital environments. Some techniques used in-hospital setting may therefore inform the development of a tool for use in pre-hospital care, provided that the limitations of the pre-hospital are considered.

1.1 Classification of acute coronary syndrome

Chest pains are the leading symptom that initiates the diagnosis and treatment of ACS but the classification of patients is based on the ECG [2]. Two categories of patients may be encountered; patients with ST-elevation ACS (STEACS) and patients with non-ST-elevated ACS (NSTEACS) and both are discussed below. The classification of ACS is also given in Figure 1.1.

Patients with acute chest pain and persistent ST segment elevation are generally diagnosed as having STEACS, which usually reflects an acute total coronary occlusion. Most of these patients ultimately develop an ST-elevation MI (STEMI). In combination with the clinical

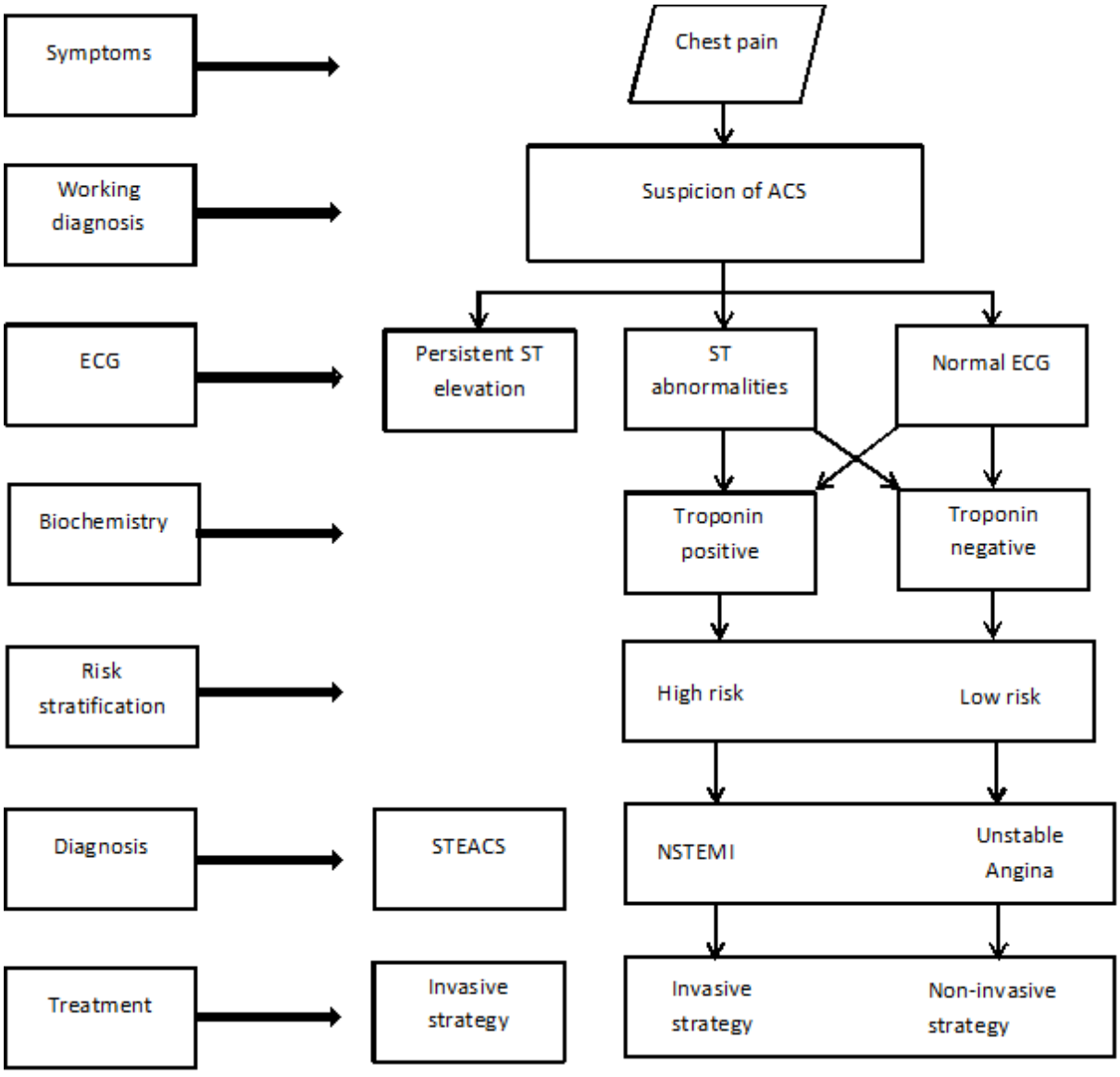


Figure 1.1: Evaluation of acute coronary syndrome. ACS - Acute Coronary Syndrome, ECG - Electrocardiogram, NSTEMI - non-ST-elevated Myocardial Infarction, STEACS - ST elevation Acute Coronary Syndrome [2].

presentation, STEACS is defined by the presence of 0.1mV ST elevation in at least two adjacent limb leads in the ECG, 0.2mV ST elevation in at least two contiguous precordial leads, or new onset bundle branch block [2] (See Section 2.3.5).

Patients with acute chest pain but without persistent ST segment elevation are diagnosed with NSTEACS. In NSTEACS, a clot narrows the lumen enough to limit blood flow and cause myocardial ischaemia. ECG changes may or may not be seen with ischaemia alone. Ischaemia without changes in the ECG that reflect damage to heart muscle is referred to as silent ischaemia. At presentation, the working diagnosis of NSTEACS is based on the measurement of cardiac biomarkers, these are substances that are released into the blood when the heart muscle is damaged. Further classification into non-ST-elevation MI (NSTEMI) or UA is based on whether the cardiac biomarkers are abnormal or normal respectively [2]. In the case of UA, diagnosis may await further diagnostic studies, such as coronary angiography or imaging studies, to confirm the diagnosis and to distinguish it from non-coronary causes of chest pain. Coronary angiography is a specialised X-ray test to find out detailed information about heart arteries. A flexible tube called a catheter is inserted into a blood vessel in a groin or arm. A special type of dye called contrast medium is injected into the catheter and X-ray images (angiograms) are taken. The contrast medium is visible on the angiograms, showing the blood vessels that the fluid travels through. This clearly highlights any of the blood vessels that are narrowed or blocked.

Cardiac marker determinations play a vital role in the diagnosis of acute myocardial infarction. Cardiac biomarkers are protein components of cell structures that are released into circulation when myocardial injury occurs [5]. They play an important role in the diagnosis, risk stratification and treatment of patients with chest pain and suspected ACS and those with acute heart failure. Cardiac biomarkers also make it possible to distinguish between NSTEMI and UA. There are various types of cardiac biomarkers with varying degree of sensitivity and specificity, the most popular being troponin and cardiac enzymes. Generally, troponins are the preferred test for a suspected MI because they are more specific for heart damage than other tests. Levels in the serum rise three to four hours after the occurrence of cardiac symptoms.

Elevated troponin levels then persist in the blood owing to the slow release and degradation of the muscle structural pool [6].

An elevated troponin level indicates patients that are at increased risk of death or the development of acute myocardial infarction; increased risk is related quantitatively to the serum troponin level. The troponin test can also be used to identify low risk patients who may be sent home with close follow-up.

In patients with non-diagnostic 12-lead ECGs and negative cardiac biomarkers but suspected ACS, stress imaging may be performed, provided the patient is free of chest pain. Imaging techniques have been used to assist in ruling out or confirming the presence of acute infarction or ischaemia in the Emergency Department; identifying non-ischaemic conditions causing chest pain; defining short- and long-term prognoses; and identifying mechanical complications of acute infarction. The underlying rationale is that regional myocardial hypoperfusion and ischaemia lead to a cascade of events including myocardial dysfunction and cell death. Important imaging parameters are therefore perfusion, myocyte viability, myocardial thickness, thickening, and motion, and the effects of fibrosis on the kinetics of radio labelled and paramagnetic contrast agents [7]. Commonly used imaging techniques in acute and chronic infarction are echocardiography, radionuclide ventriculography and magnetic resonance imaging (MRI). Positron emission tomography (PET) and X-ray computed tomography (CT) are less common [7].

Echocardiography is an excellent real-time imaging technique with moderate spatial and temporal resolution. Its strength is the assessment of myocardial thickness, thickening, and motion at rest [8]. Given its safety and ease of use, echocardiography represents a useful screening tool for patients with suspected ACS, despite its limitations in distinguishing old myocardial scars from acute severe ischaemia.

1.2 Motivation for early diagnosis of myocardial ischaemia

Research has shown that patients with ACS continue to have poor outcomes despite advances in modern therapies [9, 10]. The in-hospital mortality rate within six months of first presentation among patients admitted with ACS is 7% with STEMI, 6% with NSTEMI and 3% with UA. At three months 33% of patients will have died, been readmitted or had a subsequent acute cardiac event [11]. The risk of death after four years rises to 25% in both STEMI and NSTEMI presentations.

The immediate management of a patient with ACS is determined by the characteristics of the presenting ECG and, in particular, the presence or absence of ST segment elevation. The therapeutic objective is to achieve rapid, complete and sustained reperfusion by primary angioplasty or fibrinolytic therapy. Many treatments, especially for STEACS, are critically time dependent and the immediate diagnosis and risk stratification of all patients with a suspected ACS is essential [12].

STEMI occurs in 30% to 45% of MI patients [11, 13]. Over the past several decades, the mortality rate associated with STEMI has progressively declined, caused in part by an associated fall in the overall incidence of MI and an increased postMI survival rate. However, there has been a steady decrease in the proportion of ACS patients presenting with STEMI rather than NSTEMI.

The GUSTO-IIb trial found that patients who suffered a NSTEMI had mortality rates of 5.7% within 30 days and 11.1% within one year; for UA patients the mortality rates were 2.4% and 7.0% respectively [9]. In addition 9.8% of NSTEMI patients and 6.2% of UA patients suffered a myocardial (re)infarction within six months. There are two main reasons for this increased risk. First, the underlying cause of the cardiovascular disease may cause future heart attacks. Second, ACS often leads to scarred or damaged cardiac tissues, the presence of which can interfere with the normal electrical conduction patterns of the heart. This may lead to arrhythmias (abnormal heart rhythm) which increases the risk of a patient developing adverse events [14].

In the last few years the prevalence of NSTEACS relative to STEMI has been determined from multiple surveys and registries [11, 15–21]. Overall, research suggests that the annual incidence of NSTEACS is higher than that of STEMI. In contrast to STEMI, where most events occur before or shortly after presentation, NSTEACS events continue over days and weeks [15]. However, mortality rates for STEMI and NSTEACS after six months are comparable, 12% versus 13%, respectively [11]. In a cohort study comparing NSTEMI and STEMI, patients with NSTEMI had statistically similar mortality at one year after intervention as compared to patients with STEMI (3.4% versus 4.4%) [22]. However, NSTEMI patients had significantly more "major cardiac events" (death, myocardial infarction, disabling stroke, or requiring revascularization) at one year (24.0% versus 16.6%).

1.3 Early monitoring of acute coronary syndrome

Monitoring of various physiological parameters is carried out in all hospital settings with the aim of detecting changes in the physiological state of the patient. Ideally, such changes should be detected in time to allow interventions to be carried out to stabilise the patients condition and prevent any further deterioration. Various methods have been proposed for identifying those patients who are at high risk of deterioration or require urgent intervention.

Research has shown that treatment offers the greatest potential benefit for myocardial salvage in the first few hours after diagnosis of STEACS [2, 12]. Thus, it is imperative that healthcare providers evaluate, triage, and treat patients with ACS as quickly as possible. It has also been shown that delays to therapy occur during three intervals: from onset of symptoms to patient recognition, during out-of-hospital transport, and during in-hospital evaluation [12].

According to Van de Werf *et al.* [23], the aim of management of ACS can be divided into four phases.

- Emergency care when the main considerations are to make a rapid diagnosis and early risk stratification, to relieve pain and to prevent or treat cardiac arrest.
- Early care in which the main considerations are to initiate reperfusion therapy as soon as

possible to prevent or limit infarct expansion and to treat immediate complications such as pump failure, shock and life-threatening arrhythmias.

- Subsequent care in which the complications that usually ensue later are addressed.
- Risk assessment and measures to prevent progression of coronary artery disease.

These phases correspond to pre-hospital care, the emergency department or coronary care unit and the ordinary ward. The ultimate goal of any patient monitoring system is to be able to track the patient physiological state from ambulance to discharge. This type of a system would allow for early identification of ACS and early detection of patient health status. The focus of this thesis is on pre-hospital setting and this stage is discussed in more depth in sections below.

1.3.1 Pre-hospital monitoring of acute coronary syndrome

Prompt diagnosis and treatment offers the greatest potential benefit for myocardial salvage in the first hours of STEMI; and early, focused management of UA and NSTEMI reduces adverse events and improves outcome. Thus, it is imperative that healthcare providers recognize patients with potential ACS in order to initiate the evaluation, appropriate triage, and management as expeditiously as possible; in the case of STEMI, this recognition also allows for prompt notification of the receiving hospital and preparation for emergency reperfusion therapy.

The aim of the pre-hospital phase of patient monitoring is to ensure early risk stratification of high-risk patients. At acute presentation this stratification guides triage and directs initial therapeutic options. A consensus statement endorsing the use of pre-hospital electrocardiograms to rapidly diagnose and triage patients transported by emergency medical services with a suspected STEMI before hospital arrival was drafted by the American Society of Cardiologists and the European Society of Cardiologists [12, 13]. Multiple studies have demonstrated the benefits of pre-hospital ECG monitoring for decreasing door-to-treatment time in patients with STEMI [2, 24–29]. The direction and magnitude of the time savings are clinically relevant, resulting in an approximately 10-minute decrease in door-to-drug time and in a 15- to

20-minute decrease in door-to-balloon [1] time [26]. Other studies have shown further reductions in door-to-balloon time when pre-hospital ECGs are used to activate the catheterization laboratory while the patient is en route to the hospital [30–33].

According to the American Heart Association [34], for patients transported by emergency medical services (EMS) without a pre-hospital ECG, delay from symptom onset to reperfusion therapy, which reflects the overall period of ischaemic injury, can be divided into four time intervals: (1) symptom onset to EMS arrival, (2) EMS arrival to hospital arrival, (3) hospital arrival to ECG, and (4) ECG to reperfusion. Pre-hospital ECG programs, if effectively implemented and coordinated with hospital systems of care, would be expected to decrease the latter three time intervals. The second interval is composed of time from first medical contact by EMS to hospital door, and EMS personnel may behave with more urgency if a diagnosis of STEMI has been made. The third interval is essentially eliminated with a pre-hospital ECG. The fourth interval can be decreased by advanced notification of the hospital to receive and evaluate the patient, to activate the catheterization laboratory while the patient is en route, or to bypass the emergency department and transport the patient directly to the catheterization laboratory. Scholz *et al.* [35] reported the impact of pre-hospital ECG monitoring on these time intervals using 114 patients with STEMI treated within an integrated system of care. The system consisted of acquiring a pre-hospital ECG by emergency responders, transmitting the pre-hospital ECG to a fax machine at the percutaneous coronary intervention (PCI) hospital cardiac intensive care unit, activating the catheterization laboratory en route if STEMI was diagnosed, and bypassing the emergency department when the catheterization laboratory team was on-site. Pertinent time intervals were collected for one year. Comparing performance in the last quarter of implementing this system with the first quarter (reference group), the time spent at the scene decreased from 25 to 19 minutes, time spent in the emergency department decreased from 14 to 3 minutes, time from arterial access to balloon decreased from 21 to 11 minutes, door-to-balloon time decreased from 54 to 26 minutes, and first medical contact to

[1] Balloon refers to the procedure used during Percutaneous Coronary Intervention (PCI). A catheter is inserted into an artery at the wrist, arm or groin. The narrowed coronary artery is stretched by inflating a tiny balloon which is at the tip of the catheter.

balloon time decreased from 113 to 74 minutes [35].

Although the focus of ECG monitoring has been on patients with STEMI, other manifestations of ACS are commonly encountered. It might be argued that early detection of NSTEMI and UA patients is not as critical as early identification of patients with STEMI who benefit from immediate reperfusion therapy. However, the failure to diagnose ischaemia in patients with NSTEMI or UA in the emergency department may result in failure to initiate antithrombotic therapies in a timely fashion. More importantly, UA patients without ECG evidence for ischaemia or elevated biomarkers may be mistakenly sent home with a noncardiac diagnosis.

1.3.2 Continuous ECG monitoring

The standard ECG at rest does not adequately reflect the dynamic nature of coronary thrombosis and myocardial ischaemia. Almost two-thirds of all ischaemic episodes in the phase of instability are clinically silent, and hence are unlikely to be detected by a conventional ECG [12]. Accordingly, the 12-lead ECG remains the main tool for performing diagnosis to assist in determining the treatment strategy for STEACS and in further stratifying the patient's risk for NSTEACS. However, the basis of this distinction is based on the 'snapshot' ECG which does not adequately reflect the dynamic nature of myocardial ischaemia and in a large number of patients the ECG may itself not change.

On-line continuous computer-assisted 12-lead ST segment monitoring is a valuable diagnostic tool in risk profiling of patients. Studies have revealed that 15% to 30% of patients with NSTEACS have transient episodes of ST segment changes, predominantly ST segment depression and these patients have an increased risk of subsequent cardiac events [36, 37]. In 2004, the American College Cardiology (ACC) and American Heart Association (AHA) jointly published a recommendation that standard practice should include continuous ST segment monitoring of patients in the early phases of ACS [12]. A short review of the impact of continuous ST segment monitoring on the evaluation of treatment is described in the next section. Furthermore, the importance of continuous ECG monitoring of patients with no traditional changes on the ECG due to ischaemia (also referred to as silent ischaemia) is also

reviewed.

Importance of continuous ST segment monitoring for patient with silent ischaemia

Reported rates of NSTEACS among hospitalized patients vary from 21% to 77% depending on the type of patient, hours of monitoring and the method of continuous ST segment monitoring [38–40].

Kress *et al.* [41] used continuous 3-lead Holter monitors with blinded ST segment analysis by a cardiologist to detect ischaemia in intensive care unit (ICU) patients who had risk factors for coronary artery disease and were receiving mechanical ventilation. Ischaemia was defined as ST segment elevation or depression of more than 0.1mV from baseline and was detected among 24% of patients, who subsequently had a longer ICU stay than patients without ischaemia. The study involved patients receiving continuous ST segment monitoring to detect ischaemia while being awakened from sedation. Continuous ST segment monitoring was a more helpful end point for detecting myocardial ischaemia than troponin level because many patients had preexisting troponin leaks.

Importance of continuous ST segment monitoring for evaluation of treatment

Jernberg *et al.* [42] found that the use of multi-lead ST segment monitoring in patients with ACS allowed prospective identification of patients that respond better to longer treatment with low-molecular-weight heparin, resulting in lower rates of mortality, myocardial infarction and revascularization. Researchers in a sub-study of the Global Utilization of Streptokinase and TPA for Occluded Coronary Arteries (GUSTO-I) trial concluded that recurrent ST segment elevation as detected via continuous ST segment monitoring was an independent predictor of mortality, even after consideration of multiple clinical risk factors in the GUSTO mortality model [43].

In a multi-site study of 1777 patients Maas *et al.* [44] found that age, heart rate and late ST segment elevation were independent risk factors for adverse clinical outcomes. ST sub-groupings resulted in significant stratification for both low and high-risk patients for the

composite end points (in-hospital death and combined death, reinfarction, or congestive heart failure). The study concluded that continuous ST segment monitoring is helpful in assessing response to therapy, especially in high-risk patients older than seventy years old.

In a study conducted at various sites in Canada, 681 patients admitted with non-ST elevation ACS were randomly assigned to receive either enoxaparin or intravenous unfractionated heparin [45]. At thirty months, patients with ST segment shifts were more likely to die and to reach the composite end point for worse outcomes than were patients without such shifts. After adjustments for risk scores, the presence of ST segment shifts on continuous ECGs was a stronger independent predictor of mortality than the findings from 12-lead ECGs on admission [45]. Several other investigators reported that using continuous ST segment monitoring helped to predict severity of disease at various time points: during hospitalization [44, 46]; after discharge; and in long-term follow up [37].

In the first study involving a comprehensive evaluation of ST segment changes before, during, and after PCI, Terkelsen *et al.* [27] performed continuous ST segment monitoring in ninety-two patients with STEMI, from ambulance through the percutaneous procedure until ninety minutes after the procedure. The results indicated that a pre-specified ST-monitoring classification was useful for stratifying patients at the time of PCI into groups at low, intermediate, and high risk. Terkelsen *et al.* [27] recommended the use of continuous ST segment monitoring for an early indication of the degree of reperfusion after percutaneous intervention.

1.4 Risk stratification and diagnosis of acute coronary syndrome

Diagnosis and risk stratification of patients with ACS is extremely important to avoid unnecessary hospitalizations and improve prognosis. This stratification guides triage and directs initial therapeutic options. The goal of risk stratification is to identify patients whose outcomes can be improved through specific clinical interventions at different points of care, thus reducing risk of clinically significant outcomes such as death, cardiac arrest or admission to the intensive

care unit (ICU). The major challenges faced by clinicians in managing ACS is distinguishing those with ACS within the very large proportion with suspected cardiac pain, especially those without clear symptoms or distinguishing ECG features.

Diagnosis and risk stratification are closely linked in ACS. During the process of establishing the diagnosis of ACS and excluding differential diagnoses the risk is repeatedly assessed and serves as a guide for the therapeutic management. Patients with NSTEACS are at high risk for MI, recurrence of MI, or death.

Risk stratification means classifying patients according to the severity of their illness. Implicit in this definition is the ability to predict outcomes from a given intervention based on pre-existing illness or the severity of intervention. The usefulness of any risk stratification system is based on how the system links severity to a specific outcome. Several risk stratification scores have been developed and validated for ACS in large patient populations and these are reviewed in this section.

1.4.1 Risk scores

Scores represent a simple and convenient method of risk stratification, in which a number of independent risk factors on presentation are shown to have prognostic significance. The three major determinants of prognosis in ACS are the extent of myocardial injury, the extent of coronary artery disease and the instability of the disease and its refractoriness to management. Numerous scoring systems have been developed to risk stratify ACS patients during the first few hours of clinical presentation so as to assist clinicians in selecting appropriate pharmacological therapies and percutaneous interventions in the acute setting. These include Braunwald risk stratification, Thrombolysis in Myocardial Infarction (TIMI), Global Registry of Acute Coronary Events (GRACE) and Platelet glycoprotein IIb/IIIa in Unstable Angina Receptor Suppression Using Integrilin (PURSUIT) all of which are described below [15, 47–49].

1.4.2 Braunwald risk stratification

The ACC/AHA Guidelines recommend that all patients be risk stratified for the selection of an initial management strategy and site of care. A well-recognized approach is the one initially proposed and later refined by Braunwald and colleagues and published in ACC/AHA Guidelines on the Management of Patients With Unstable Angina and non-ST segment Elevation MI [47]. This approach is based on a combination of historical, clinical, laboratory, and ECG variables and answers two questions: what is the likelihood that signs and symptoms represent ACS secondary to obstructive CAD, and what is the likelihood of an adverse clinical outcome?

Patients are initially risk-stratified according to the likelihood that symptoms are due to unstable CAD. Patients at intermediate or high risk for CAD are further classified by their risk of major adverse cardiac events. This second classification is useful for prospectively identifying patients at intermediate or high risk who can benefit from an invasive strategy and more aggressive pharmacology.

TIMI risk score

The Thrombolysis in Myocardial Infarction risk score is a simple risk stratification technique that incorporates clinical variables easily acquired at the time of admission and is designed to be evaluated without the use of a computer [48]. It can therefore be used in triage and initial decision making with regard to treatment options. The TIMI risk score was developed to assess a patient's risk of death, recurrent MI or ischaemia, thereby allowing doctors to make better therapeutic decisions. The score is derived from seven independent factors all of which are associated with poor cardiac outcome. These factors are:

- Age: 65 years or older.
- At least three risk factors for coronary artery disease among the following
  - Hypertension

  - Hypercholeterplemia
  - Diabetes mellitus
  - Family history of coronary artery disease
  - Current or former smoker
- Prior coronary stenosis (narrowing of an artery) of 50%.
- ST segment deviation on ECG at presentation
- Severe anginal symptoms (at least two anginal events)
- Use of aspirin in prior seven days.
- Elevated cardiac markers.

One point is counted for each of the above variables that is observed and the TIMI risk score is the total number of points (between 0 and 7). The set of variables was obtained by selecting independent prognostic variables from a set of 12 prospective clinical variables after multivariate logistic regression [50]. The other five variables considered but not included in the TIMI score were prior MI, prior coronary artery bypass (CABG), prior angioplasty (PTCA), prior history of congestive heart failure and use of intravenous heparin within 24 hours of receiving to the medication.

GRACE risk score

The GRACE risk score is based upon a large unselected population of an international registry of the full spectrum of ACS patients [15]. The risk factors were derived with independent predictive power for in-hospital deaths and post-discharge deaths at 6 months. Easy-to-assess clinical, electrocardiographic and laboratory variables such as age, heart rate, systolic blood pressure, serum creatinine level, Killip class at admission, presence of ST-depression, and elevated cardiac biomarkers as well as cardiac arrest were included in the calculation. The Killip classification system is a measure of the severity of heart failure based on physical symptoms [51].

PURSUIT risk score

The PURSUIT risk score was developed from a trial that studied the effects of drugs versus placebo in 9461 patients with ACS without persistent ST segment elevation [49]. This population covers a variety of patients, hospital settings, and treatment policies and was therefore suitable for development of a clinical risk model. The model uses similar clinical variables as TIMI and GRACE.

1.5 Treatment and therapy

The goals of therapy in acute MI are the quick restoration of normal coronary blood flow (revascularization) and the maximum salvage of functional myocardium. These goals can be met by a number of medical interventions and therapies. When patients present to a hospital, there are a variety of interventions to achieve treatment goals. Immediate treatment for suspected acute myocardial infarction includes oxygen, aspirin, and sublingual nitroglycerin [52].

Most cases of STEMI are treated with reperfusion therapy, such as PCI or thrombolysis. Patients who have multiple blockages of their coronary arteries, particularly if they also have diabetes mellitus, are often treated using CABG [52, 53]. The European Society of Cardiology guidelines in 2011 proposed treating the blockage causing the myocardial infarction by PCI and performing CABG later when the patient is more stable [52].

PCI involves stretching open narrowed areas of coronary arteries to improve the blood flow [53]. Using a local anaesthetic, a catheter is inserted into an artery at a wrist, arm or groin. The narrowed coronary artery is stretched by inflating a tiny balloon which is at the tip of the catheter. In the majority of cases a metal stent is also placed in the artery. A stent is a cylinder of metal mesh which acts like a scaffold to keep the artery open and prevents the narrowing coming back. The artery heals around the stent making it a permanent part of the artery [52].

As explained earlier, individuals without ST segment elevation are presumed to be experiencing either UA or NSTEMI. NSTEMI is usually managed with medication, although PCI may be required if the patient's risk warrants it. NSTEMI patients receive many of the same

initial therapies and are often stabilized with antiplatelet drugs, beta-blockers and anticoagulated. Anti-platelet drugs are blood thinning drugs of which aspirin is the most common [53]. Aspirin thins the blood making it less likely to form clots, reducing the risk of further heart problems or stroke. Beta-blockers reduce the work the heart has to do by slowing down the heart rate and lowering the blood pressure.

If an NSTEMI patient remains hemodynamically stable, they can be offered either late coronary angiography with subsequent restoration of blood flow, or non-invasive stress testing to determine if there is significant ischaemia that would benefit from revascularization. If hemodynamic instability develops in individuals with NSTEMIs, they may undergo urgent coronary angiography and subsequent revascularization [52].

The basis for this distinction in treatment regimens is that ST segment elevations on an ECG are typically due to complete occlusion of a coronary artery. On the other hand, in NSTEMIs there is typically a sudden narrowing of a coronary artery with preserved but diminished flow to the myocardium.

1.6 Overview of the thesis

The remainder of this thesis describes the development of a patient monitoring system to assist with diagnosis and management of ACS patients using data fusion of vital signs and additional features from the ECG. The next chapter defines key physiological concepts and delineates ways in which MI can occur. This chapter also describes most of the signal processing techniques used in this thesis. The aim is to develop a patient data fusion system that is able to assist with early identification and risk stratification of patients with ACS during the pre-hospital phase. To be able to identify high-risk ACS patients ST segment elevation needs to be detected. Chapter 3 reviews the state-of-the-art in automated ST segment analysis, describes the development of the automated ECG analysis algorithm used in this thesis and compares the performance of the algorithm with existing methods.

Even in subjects who are known to have myocardial ischaemia, ST changes are not con-

sidered as a basis for a definitive diagnosis of individual episodes. A previous myocardial infarct may exist and cause permanent distortion in an ST segment with a persistently abnormal pattern in the heart's frame of reference. This fixed pattern appears to change with the subject's body position because of the movement of the ECG electrodes relative to the heart. Chapter 4 investigates techniques to differentiate between ST changes caused by myocardial ischaemia and non-ischaemic events such as heart-rate, body position changes or conduction changes.

At the start of the work described in this thesis no data sources containing pre-hospital data for ACS patients were available. A clinical study was set up to collect vital-sign data and ECG during ambulance transport. The summary of the data collected during the study is described in detail in Chapter 5.

The beating of the heart and respiration are two prominent physiological functions which are both modulated by fluctuations of the autonomic nervous system. Hence, they carry information which may be used to gain insight into the autonomic control of the heart. Additional parameters from the ECG such as heart rate variability that can be used for detecting ACS, particularly NSTEACS are investigated in Chapter 6.

High-risk patients may be identified early by appropriate combination of vital-sign data, demographics and ECG analysis. This hypothesis is tested in Chapter 7. Finally, Chapter 8 summarizes the contributions of this thesis and identifies avenues for further research.

Chapter 2

Signal processing techniques for ECG analysis

This chapter introduces the main characteristics of the electrocardiogram (ECG) and the bi-opotentials associated with the contractions of the heart muscle. A description of some of the common types of signals that can be derived from the ECG is also presented, together with the motivation behind the analysis of these signals.

2.1 Basic anatomy of the heart

In order to appreciate the different waveform features of the ECG it is necessary to understand the basics of cardiac anatomy and electrophysiology. The heart is a four-chambered pump which provides the driving force for the circulation of the blood around the body. A wall divides the heart cavity to form a double-pump configuration. Each side of the heart is then further divided into an upper chamber known as the atrium, and a lower chamber known as the ventricle. In general, blood moves through the heart in the following series of steps (see Figure 2.1). First, unoxygenated blood moves into the right atrium of the heart through the superior and inferior atrium. The atrium then contracts and pushes the blood through a one-way valve. The right ventricle then contracts pushing the blood out of the heart to the pulmonary arteries

and then lungs for the exchange of carbon dioxide and oxygen. The blood then returns to the heart's left atria via the pulmonary veins. The atrium again contracts and pushes the blood through another one-way valve. The left ventricle then contracts, pushing the blood out of the heart to the aorta, which then branches off to the rest of the arteries.

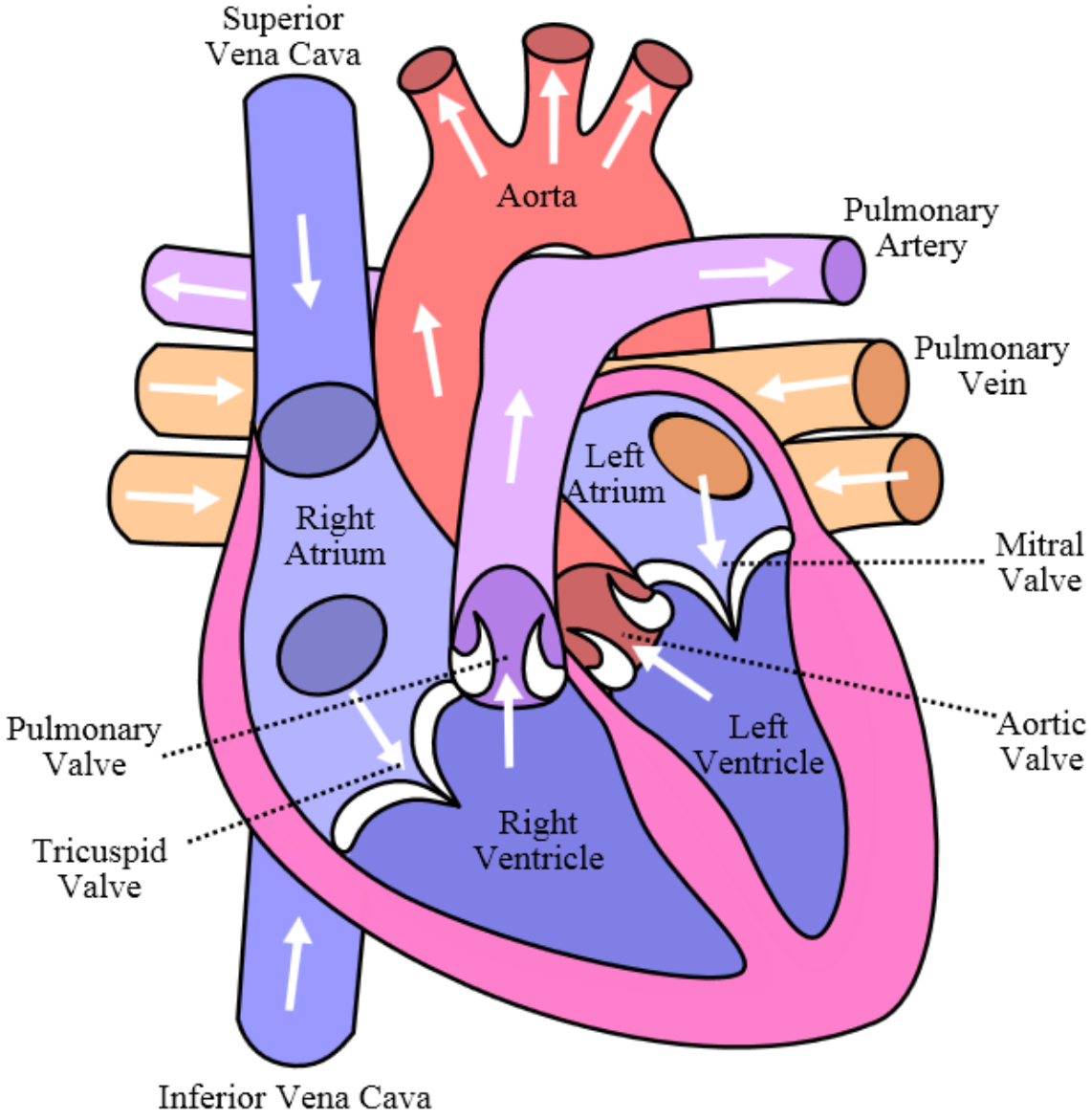


Figure 2.1: Blood flow in the heart [54].

2.2 Electrophysiology

The atria and the ventricles in the heart are composed of muscle cells (myocytes). The rhythmic contractions of the heart stem from the flow of ions through channels in the membranes of the heart's muscle cells. The cell membrane is the dividing medium between the extracellular and the intracellular fluids, each of which has a different ionic concentration. When a cell is stimulated electrically the permeabilities of the membrane to ionic transfer are modified. The resulting flow of ions through the cell membrane gives rise to an electrical signal known as an action potential. This in turn results in a mechanical contraction of the cell [55]. The propagation of action potentials through the atria and the ventricles during each heartbeat results in a set of distinct features in the characteristic ECG waveform. These features represent either depolarisation (electrical discharging) or repolarisation (electrical recharging) of the heart muscle cells in the atria and the ventricles.

Before the action potential is propagated, it must be initiated by pacemakers, cardiac cells that possess the property of automaticity. That is, they have the ability to spontaneously depolarize, and therefore function as pacemaker cells for the rest of the heart. Such cells are found in the sino-atrial node (SA node), in the atrio-ventricular node (AV node) and in certain specialized conduction systems within the atria and ventricles. Under normal operating conditions, the SA node determines the heart rate, the lower pacemakers being reset during each cardiac cycle. However, in some pathological circumstances, the rate of lower pacemakers can exceed that of the SA node, and then the lower pacemakers determine the overall heart rate [55].

The time course of the action potential as the cells depolarize and repolarise is illustrated for a ventricular cell in Figure 2.2, with the five conventional phases (0 through 4) marked. When cardiac cells are depolarized to a threshold voltage of about -70mV, there is a rapid depolarization that is caused by a transient increase in fast sodium channel conductance in the cell membrane. This results in the rapid upstroke of Phase 0 of the action potential.

Phase 1 represents an initial repolarisation that is caused by the opening of a potassium channel. During Phase 2 there is an approximate balance between an inward calcium current

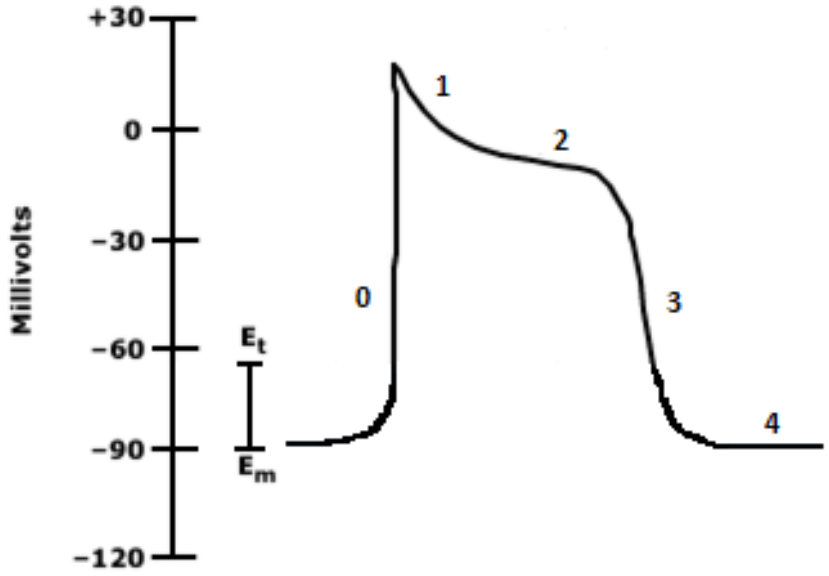


Figure 2.2: A typical action potential from a ventricular myocardial cell. Phases 0 through 4 are marked. An action potential is generated when the membrane potential is partially depolarized from the resting level(E_m) to the threshold potential(E_t) [54].

and an outward potassium current, causing a plateau in the action potential and a delay in repolarisation. The inward calcium movement occurs through long-lasting calcium channels that open up when the membrane potential depolarizes to about -40 mV [55].

Phase 3 is a complex process and several mechanisms are thought to be important. The potassium conductance increases, tending to repolarise the cell via a potassium-mediated outward current. In addition, there is a time-dependent decrease in calcium conductivity which also contributes to cellular repolarisation. Phase 4, the resting condition, is characterized by open potassium channels and a negative transmembrane potential [55].

After Phase 0, there is also a parallel set of cellular and molecular processes known as excitation-contraction coupling: the cell depolarization leads to high intracellular calcium concentrations, which in turn unlocks the energy-dependent contraction apparatus of the cell [55].

2.3 The Electrocardiogram

The technique of electrocardiography originated in the early part of the 20th century through the pioneering work of Augustus Waller and, independently, Willem Einthoven [56]. Einthoven, a Dutch doctor and physiologist, used a galvonometer to register the electrical activity of the heart from the surface of the body. The resulting electrical signal was termed the electrocardiogram, and earned Einthoven the 1924 Nobel prize for medicine.

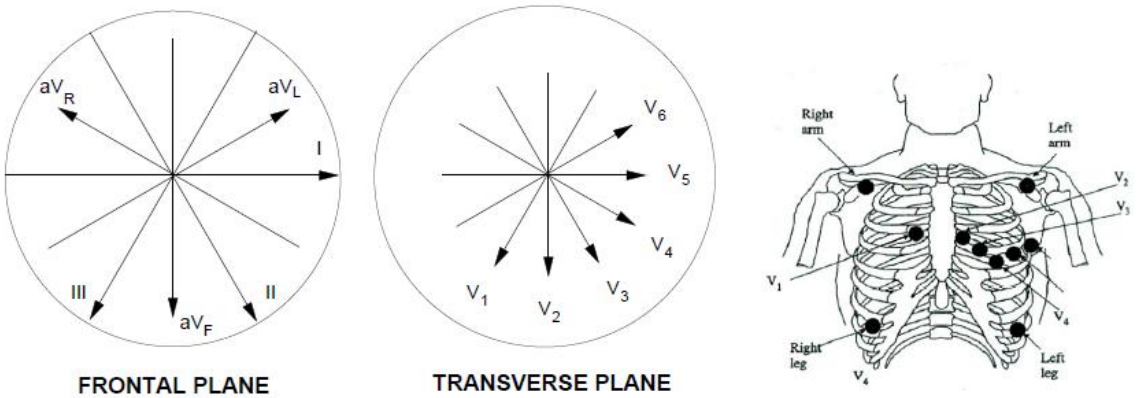
The importance of the ECG derives from the diagnostic information which can be obtained from a detailed analysis of the individual ECG waveforms produced during each heartbeat. In particular the ECG is essential for the identification of disorders of the cardiac rhythm, as well as for the diagnosis of abnormalities of the heart. The ECG can also provide a good indicator of the presence of generalised disorders that affect the rest of the body [57].

2.3.1 ECG recording

The basis of standard clinical electrocardiography is the 12-lead ECG as agreed by the American College of Cardiology and American Heart Association [12]. In ECG, the term 'lead' refers to an electrical viewpoint and not the physical electrodes. Figure 2.3 shows the orientation of the electrical axis of the standard 12 leads in relationship to the body surface (with respect to the frontal and transverse plane of the human body). This type of ECG recording makes use of four limb electrodes and six chest electrodes in order to provide a comprehensive picture of the electrical activity of the heart from 12 different viewpoints around the surface of the body.

Potential differences between the limb electrodes are used by the ECG instrumentation to generate three limb leads and three augmented leads, and similarly potential differences between the chest electrodes are used to generate the six chest leads. The individual leads which make up the 12-lead ECG are referred to as follows:

- Limb leads: I, II, III,
- Augmented lead: aVR, aVL, aVF

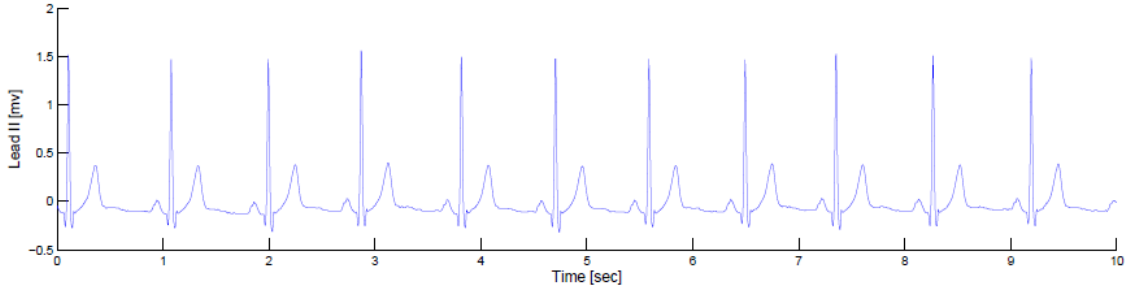


(a) Lead vectors (b) Electrode placement

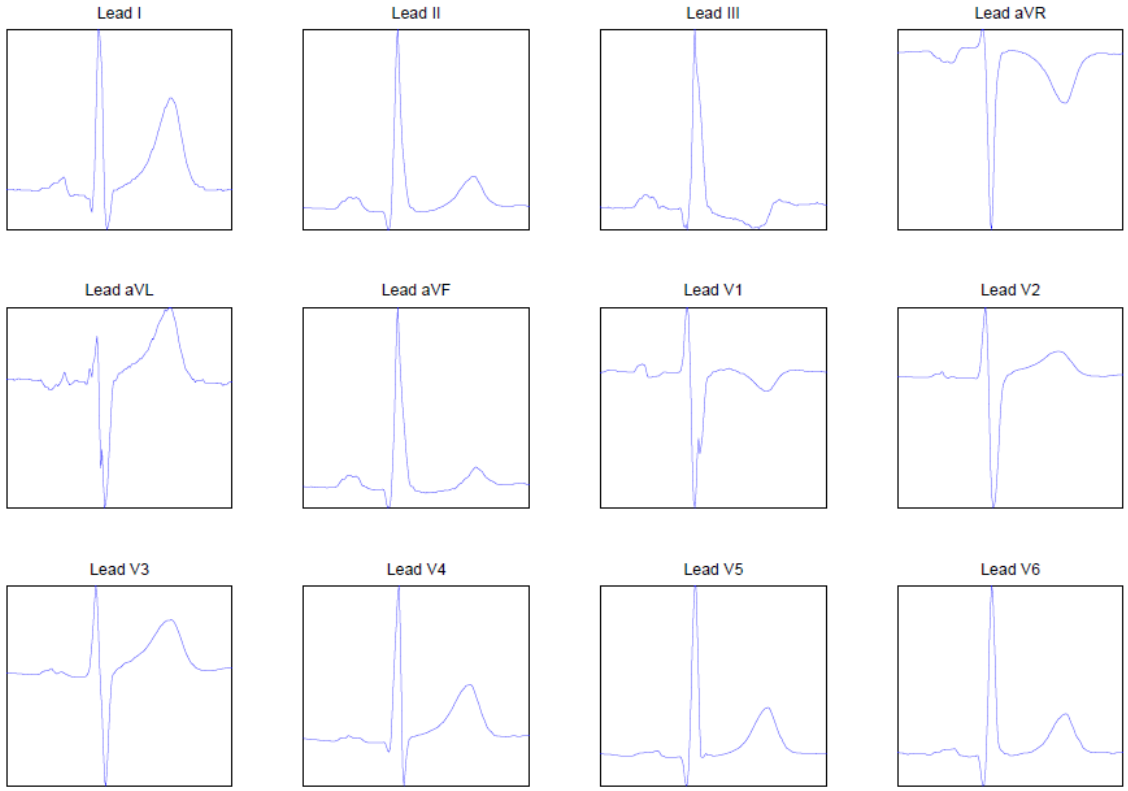
Figure 2.3: (a) The ECG lead vectors in the frontal and transverse plane of the human body. (b) The placement of the ten surface electrodes from which the standard 12-lead ECG is derived [54].

- Precordial leads: V1, V2, V3, V4, V5, V6

The particular viewpoint that each lead has of the heart determines the characteristic form of the corresponding ECG signal [57]. Figure 2.4(a) shows an example of a standard 10-second ECG recording taken from lead II. The periodic nature of the ECG is clearly seen with each heartbeat waveform separated by a period of inactivity (referred to as the baseline or isoelectric line). As the electrical current flows through the heart muscle, it is measured as a positive deflection when it flows towards the positive electrode of any given lead and as a negative deflection when it flows away from the positive electrode. As a result, ECG waveform morphology varies between leads because of their different electrical viewpoints. This is clearly seen in Figure 2.4(b), which shows the same heartbeat recorded with each of the 12 leads. The standard ECG recording typically used in diagnosing STEMI is a 'snapshot' recording of all 12 leads.



(a) 10-second ECG signal from Lead II



(b) ECG waveforms for one heart beat from all 12 leads

Figure 2.4: Examples of standard 12-lead ECG recordings.

2.3.2 The ECG waveform

Figure 2.5 illustrates a short section of a typical single lead from a human ECG waveform and the associated clinical features. The standard features of the ECG waveform are the P wave, the QRS complex and the T wave. Additionally a small U wave (following the T wave) is occasionally present. The origin of the U wave is uncertain but it is believed that small U waves and large U waves have different physiological origins [58]. Typically U waves are less than one third of the amplitude of the preceding T wave and possess the same polarity. The cardiac cycle begins with the P wave which corresponds to the period of atrial depolarisation in the heart. This is followed by the QRS complex, which is generally the most recognisable feature of an ECG waveform and corresponds to the period of ventricular depolarisation. The start and end of the QRS complex are referred to as the Q and J points. The T wave follows the QRS complex and corresponds to the period of ventricular repolarisation.

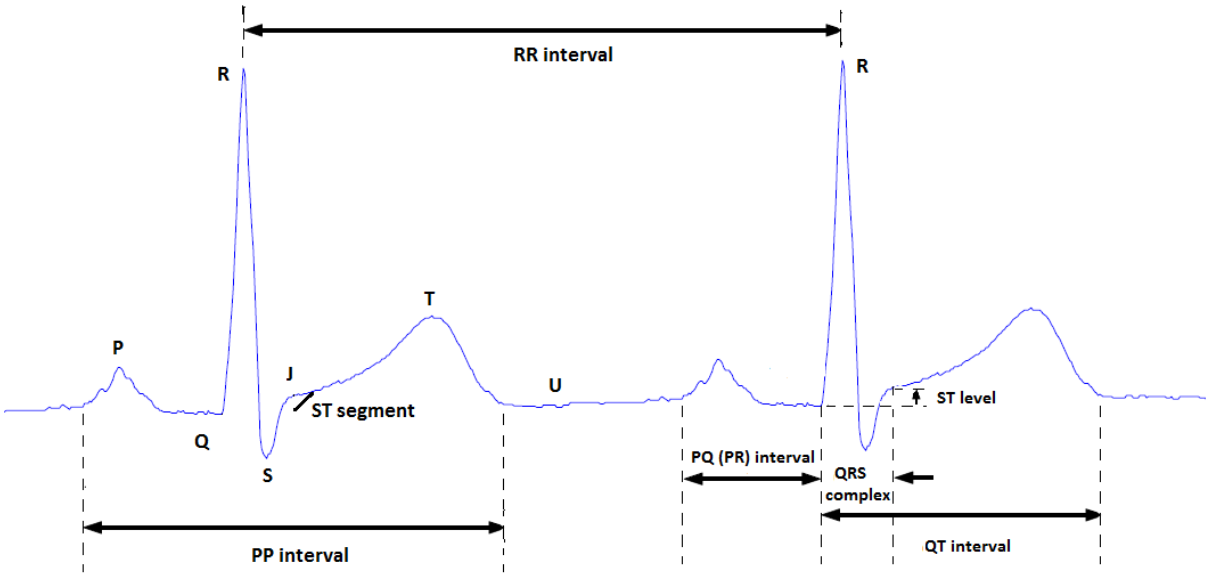


Figure 2.5: Schematic representation of a single cycle of the electrocardiogram signal corresponding to one heart beat. The characteristic features are labelled P, Q, R, S, T and U waves. Of particular interest to this are the J point, ST segment and ST level.

Perhaps the most important segment in the ECG waveform, from the point of view of risk stratification of ACS, is the ST segment. The ST segment is defined from the start of the J point (junction between the QRS complex and ST segment) and ends at the beginning of the T wave.

However, since it is usually difficult to determine exactly where the ST segment ends and the T wave begins, the relationship between the ST-segment and the T wave should be examined together. The typical ST segment duration is usually around 0.08 sec (80 ms). It should be essentially level with the PR and TP segments. The ST segment represents the period when the ventricles are depolarized. ST segment might be either depressed or elevated with respect to the isoelectric line.

The morphology of the various ECG waveform features depends on a number of factors, including the particular ECG lead under consideration, as well as the presence of cardiovascular diseases or cardiac abnormalities in the given subject. The different classes of morphology for P waves and T waves include upright, inverted, and biphasic. The term biphasic is used to refer to a wave which consists of a negative detection followed by a positive detection, or vice versa.

2.3.3 ECG analysis

Clinical ECG analysis is a combination of interval and morphology analysis that links changes of timing intervals and characteristic waveform morphologies with different cardiac pathologies and functional abnormalities. For example, ST segment depression with respect to baseline is linked with myocardial ischaemia, electrolyte abnormalities, structural heart disease and congenital disorders [59]. ECG interval analysis is based on timing intervals, such as the QT interval, that are defined between two fiducial points (e.g. the onset and offset points of particular waveform features) and provides insight into the functionality of different regions of the heart.

QT interval

The QT interval is defined as the time from the start of the QRS complex to the end of the T wave. It corresponds to the total duration of electrical activity (both depolarisation and repolarisation) within the ventricles in a given heartbeat. It is important to recognise that the QT interval varies according to the particular ECG lead selected for analysis. Thus, the QT intervals measured from the same heartbeat on a number of different leads typically have a range of

different values [60].

PR interval

The PR interval is defined as the time from the start of the P wave to the start of the QRS complex. It corresponds to the time from the onset of atrial depolarisation to the onset of ventricular depolarisation. The PR interval has precise time limits in health. In particular, it should be in the region of 0.12 to 0.2 seconds long [60]. Drug-induced prolongation of the PR interval indicates that the drug slows atrioventricular conduction, which can in turn lead to heart block [57].

QRS duration

The QRS duration corresponds to the duration of ventricular depolarisation in each heartbeat. In health individuals its value is normally no longer than 0.12 seconds [60]. Drug-induced prolongation of the QRS duration indicates that the drug delays the time taken for conduction through the ventricles. This effect has the potential to cause arrhythmias.

2.3.4 Sources of noise in ECG waveforms

The ECG is often corrupted by noise and physiological artefacts that overlap with the frequency range of the ECG. Figure 2.6 shows five examples of common noise sources and artefacts found in the ECG, namely [61]:

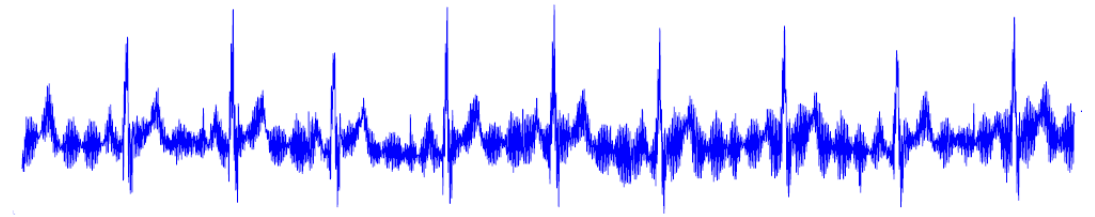
- Mains interference: capacitance effects between mains power supply (50 or 60Hz) and the ECG recording equipment.
- Muscle artefact: contraction of skeletal muscle under the ECG electrode.
- Movement artefacts: movement of the subject or electrode during ECG recording changing the electrode contact impedance.

- Baseline wander: change in electrode contact impedance due to increased perspiration and breathing-related body movements.
- Electrode noise: a sharp change in electrode contact impedance, which results in a spike in the trace coming from that lead.

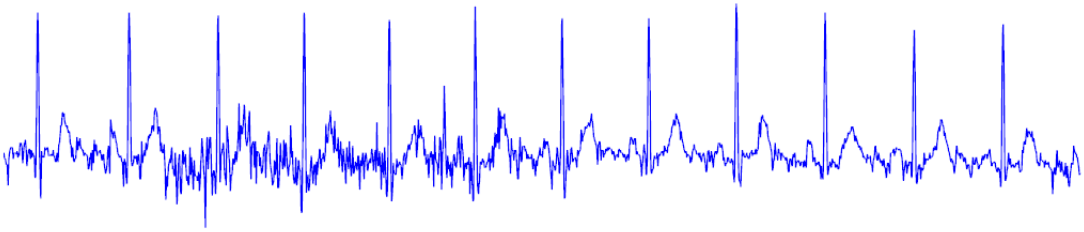
2.3.5 Selection of leads for diagnosing ST segment changes

The ST segment Monitoring Practice Guideline Working Group recommends that if only two leads are available for ST segment monitoring for patients with ACS, leads III and V3 should be used [62]. If information from a patient's prior 12-lead ECG recorded during an ischaemic event indicates another lead is more sensitive, then this should be used instead. The working group also states that the best three-lead combination is III, V3, and V5. However, for bedside cardiac monitoring it is often the case that only a single precordial lead is used because the monitors provide only a single-chest electrode [63]. In addition, the two- and three-lead combinations for myocardial ischaemia exclude lead V1, which is considered the best lead to monitor for detection of cardiac arrhythmias. Furthermore, the use of at least three chest leads (V3, V4, V5) is recommended for ST analysis to allow noise reduction and artefact identification although four- or five-lead configurations are considered to give better results. In particular the addition of V2, which is orthogonal to V5, and V6, is recommended. A six-lead configuration and sometimes just a two-lead configuration, can be substituted for the standard 12-lead ECG in certain limited clinical and research applications.

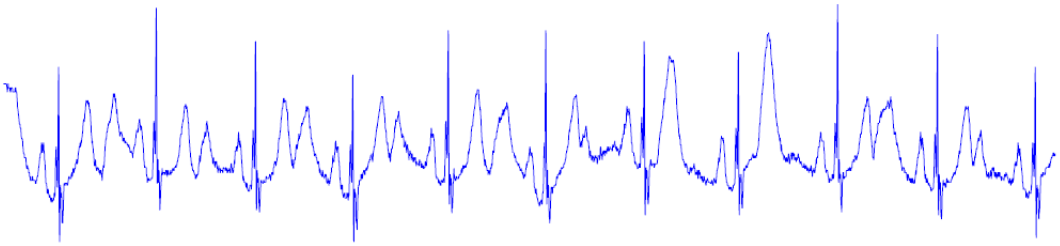
Typically, ST segment elevation in acute MI, measured at the J point, should be found in two contiguous leads and be 250μV in men below the age of 40 years, 200 μV in men over the age of 40 years, or 150μV in women in leads V2V3 and/or 100μV in other leads (in the absence of left ventricular hypertrophy or left bundle branch block)[23].



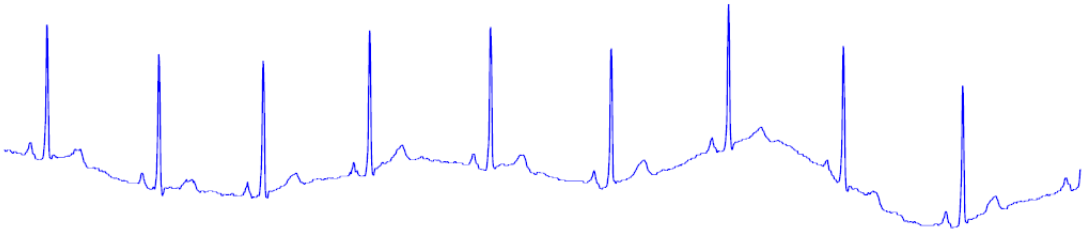
(a) Mains interference



(b) Muscle artefact



(c) Movement artefact



(d) Baseline wander



(e) Electrode noise

Figure 2.6: Examples of different types of ECG noises.

2.4 Causes of ST segment deviation in myocardial ischaemia

The loss of life-sustaining oxygen to cardiac tissue causes changes in the depolarization of the heart's ventricular tissue. Because the oxygen-deprived tissue conducts the depolarizing electrical signal abnormally, the period following depolarization can be disrupted. This normally isoelectric period is represented in the ECG waveform as the ST segment (the time between the QRS and repolarising T wave). Cardiac tissue that is ischaemic or injured does not properly depolarize. This leads to so-called injury current. This current causes a depression in the TQ segment and an elevation in the ST segment, which appears on most medical monitoring equipment as a large ST elevation [64].

Recording a 12-lead ECG is a standard-of-care diagnostic test in any evaluation of possible cardiac ischaemia. Myocardial ischaemia often changes the appearance of the ST segment and T wave. In the early stages of myocardial ischaemia there are classic patterns that are observed in which the ST segment is elevated with a slope which is either straight or positive upwards deflection and wider T waves that are either concave or slope upwards. Leads overlying the normal myocardium situated opposite the infarct location show reciprocal ST segment depression. This is because of an injury current between the ischaemic and non-ischaemic areas, which alters the main cardiac vector. These classic patterns of myocardial ischaemia are seen in about 50% of ischaemic events [65]. In another 45% of cases the ECG shows either ST segment depression or non-diagnostic abnormalities. In the remaining 5% of cases no ECG abnormalities are detected [65].

Under normal conditions the ST segment is relatively isoelectric because all healthy myocardial cells attain about the same potential during repolarisation. Severe acute shortage of oxygen lowers the resting membrane potential, shortens the duration of the action potential and changes the shape of the plateau of the action potential in the ischaemic area. These changes cause a voltage gradient between normal and ischaemic zones, leading to current flow between these regions during both the systolic and diastolic portions of the cardiac cycle [1]. According to current-of-injury theory, ST segment elevation occurs when the injured muscle is loc-

ated between normal muscle and the corresponding precordial electrode. On the other hand, ST segment depression occurs when normal muscle is located between the injured tissue and the corresponding electrode. An ST elevation is considered significant if the vertical distance between the ECG trace and the isoelectric line at a point 0.04 seconds after the J point is at least 100 muV in a limb lead or 200 μV in a precordial lead [66]. Other causes of ST segment elevation, include the following [66]:

- Acute pericarditis: ST elevation in acute pericarditis is generally diffused and does not follow the pattern of blood supply. As a rule, these changes are not accompanied by reciprocal depression of the ST segment in other leads.

- Early repolarisation: In some patients without known heart disease, particularly young patients, early take-off of the ST segment may be seen.

- Ventricular aneurysm: After acute myocardial infarction, the ST segment usually normalizes. However in the presence of a persistent aneurysm in the region of infarction, ST segment elevation may persist indefinitely.

T waves can be peaked, normal, flat, or negative. Flat T wave are defined as < 0.5 mm negative or positive T wave in leads I, II, V3, V4, V5 or V6 [66]. Negative (or inverted) T wave are defined as > 0.5 mm negative T wave in leads I, II, V3, V4, V5 or V6 [66]. Abnormal T waves can be seen in a variety of conditions other than myocardial ischaemia, including; hyperventilation, cerebrovascular disease, mitral valve prolapse, conduction abnormalities, and ventricular pre-excitation [66].

2.4.1 Stages in the development of myocardial ischaemia

Insufficient supply of blood to the myocardium can result in myocardial ischaemia, injury, infarction or all three. Atherosclerosis of the larger coronary arteries is the most common anatomic condition to diminish coronary blood flow. The branches of coronary arteries arising from the root are distributed on the outside of the cardiac epicardium of the heart. These in

turn provide intramural branches that supply the cardiac muscle. Myocardial ischaemia generally appears first and is more extensive in the region between the epicardium and myocardium (subendocardium). Since deeper myocardial layers are farthest from the blood supply they have greater intramural tension and need for oxygen. Myocardial ischaemia in this area prolongs local recovery time, since repolarisation normally proceeds in an epicardial-to-endocardial direction and delayed recovery in the subendocardial region due to myocardial ischaemia does not reverse the direction of repolarisation but merely lengthens it [67].

Transmural ischaemia exists when the ischaemic area extends subepicardially. This process has a more visible effect on recovery of cells situated below the epicardium (subepicardial) compared to subendocardial, resulting in inversion of the T wave in leads overlying the ischaemic regions. Injury to the myocardial cells occurs when the ischaemic area process is more severe [66]. Subepicardial injury is manifested as ST segment elevation; in patients with coronary artery disease, myocardial ischaemia, injury and myocardial infarction of different areas frequently coexist, producing mixed and complex ECG patterns. The direction of the ST segment changes on the epicardium and ECG leads depends on the magnitude and the direction of the injury currents.

An ECG lead which is placed over the site of the infarct might have elevated ST segment reflecting tissue injury and/or T wave inversion reflection tissue myocardial ischaemia; a pathological Q wave reflecting tissue necrosis;. These ECG changes have been described as indicative changes of an MI [67]. An early manifestation of acute myocardial ischaemia is the development of ST segment and T wave changes. ST segment elevation reflects transmural involvement, with greater extent of myocardial injury. ST segment depression is believed to represent subendocardial involvement, with less extensive myocardial injury. ST segment depression is generally induced by factors that increase myocardial demand, such as atrial pacing or exercise stress, whereas ST segment elevation is induced by near-total cessation of coronary blood flow [66–68]. After acute total occlusion of the vessel, myocardial injury is believed to progress from the endocardium to the epicardial layers. Thus, we would expect to observe ST segment depression progressing through an isoelectric point to ST segment elevation. This may

explain why some patients have no significant changes on the ECG when presenting with an acute myocardial infarction [66–68].

Atherosclerotic heart disease is the most common underlying cause of myocardial infarct. A pathological Q wave is defined as an initial downward deflection of a duration of 40ms or more in any lead except III and aVR. The Q wave appears when the injured area leaves unbalanced forces of variable magnitude in the opposite direction from the remote region. The classic changes of necrosis (Q wave), injury (ST elevation), and ischaemia (T wave inversion) may all be seen during acute infarct. In recovery, the earliest change caused by MI can be estimated from the appearance of the ST segment and T wave. The presence of Q wave in the absence of ST and T wave abnormality generally indicates prior infarct. The presence of the indicative ECG changes in certain leads suggest an MI has occurred in specific regions of the heart. The categorizing is usually as follows:

- Lead II, III and aVF usually indicated an inferior infarction.
- Lead V1 to V3 anterospatial infarction.
- Leads V4, V5, V6 , I and aVL anterolateral infarction of the left ventricles.

The conventional 12-lead ECG does not directly record electrical currents from the posterior wall of the left ventricles. Hence, infarction in this region does not manifest the usual indicative ECG changes in any of the 12-leads. However, posterior infarction can be detected in leads V7, V8 and V9.

2.5 Signal processing tools for ECG analysis

The previous sections described the physiological basis of the ECG and how MI manifest itself in the ECG, this section focuses on the signal processing tools that can be applied to the ECG to assist with automated diagnosis of various physiological conditions.

2.5.1 Pre-processing of the ECG

In general, the aim of the preprocessing stage is to improve the signal-to-noise ratio (SNR) for more accurate analysis and measurement. Noise may disturb the ECG to such an extent that measurements from the original signal are unreliable. The two main categories of noise are low frequency baseline wander caused by respiration and body movements, and high-frequency random noise caused by mains interference and muscular activity.

The pre-processing stage consists of digital filtering in order to remove high-frequency mains interference; QRS detection; baseline wander removal to enable accurate identification of the isoelectric line. The main task of QRS detection is to generate a stable fiducial point for each heart beat, a prerequisite for the automatic identification of the isoelectric level. Baseline wander results in erroneous estimates of the ST segment level, thus it is important that it should be removed [69].

Removing high-frequency mains noise

A large number of methods exist in the literature for removal of mains interference from the ECG. The objective of any noise cancellation method for ECG analysis is to produce a noise-suppressed version of the signal without introducing distortion and ringing effects. For the removal of mains interference, a design of linear-phase notch filters is proposed. For this work, we used a two-stage filtering process with notch filters and a low-pass Butterworth digital filter.

Low-pass filtering

In the first stage of removing the mains interference, two notch filters were employed. First, the ECG was preprocessed using 50Hz infinite impulse response (IIR) notch filter with a quality factor of 40. In addition a 60Hz IIR notch filter with a quality factor of 35 was applied to the ECG. The usage of two Notch filter with two different cutoff frequent was done to ensure that the algorithms work with data collected in Europe and America.

In the second stage, a zero-phase filtering was applied using 12th order low pass Butterworth FIR filter with a cutoff frequency of 40Hz to remove the 50 or 60 Hz mains interference.

A linear phase response of the filter in the pass-band and in the cutoff region is desirable. The distortion of the output signal due to the nonlinear phase response of the filter at higher frequencies is not significant, and does not affect ST level measurements. In order to obtain a quantitative estimate of the level of noise reduction achieved, the power spectrum of the ECG after each stage described above was calculated. The Power Spectral Density (PSD) was obtained using the Welch method with Hamming window size of 512 points and overlap of 256 points. The result of applying the filters effectively to remove high-frequency mains noise and its corresponding power density spectrum are shown in Figure 2.7.

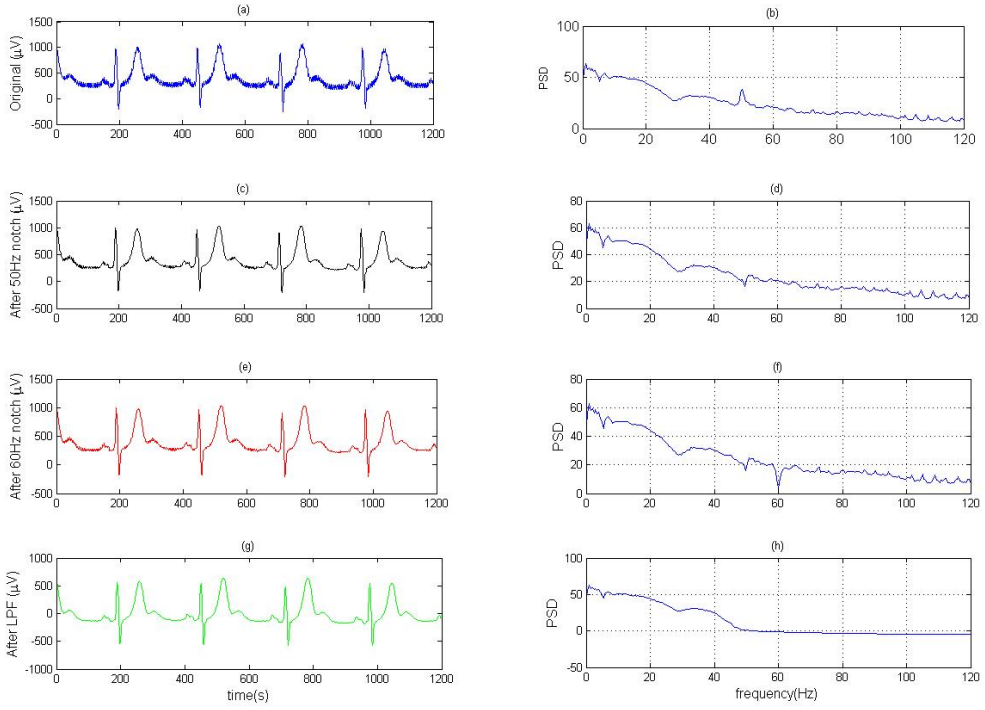


Figure 2.7: Power line removal after applying a two stage filtering procedure using notch filters and low pass filtering. (a) Original ECG and (b) corresponding PSD. (c) ECG after 50 Hz notch filter (d) corresponding PSD. (e) ECG after 50 and 60 Hz (f) corresponding PSD (g) ECG after 50 and 60 Hz and low-pass Butterworth filter (h) corresponding PSD.

2.5.2 QRS detection

Automated QRS detection has been an active research topic for a couple of decades. Many methods have been proposed to identify the R-peak of the QRS complex. Kohler *et al.* presented a comprehensive quantitative review of twenty-seven published R-peak detection algorithms [70]. The methods can be loosely grouped into three main categories: approaches based on signal derivatives and digital filters; time-frequency-based QRS detection; and probabilistic methods. The methods vary in performance and complexity though digital filtering and energy-based methods have become the most widely used, due to their simplicity and low computational complexity. Wavelet-based methods have been shown to perform well but are computationally intensive.

Friesen *et al.* compared the performance of nine algorithms based on signal derivatives and digital filters using idealised test data corrupted by nine different noise conditions [71]. The results suggested that the algorithm based on energy are most immune to noise. However, these algorithms are sensitive to baseline wander. Friesen *et al.* suggested that the QRS detector stage should combine amplitude and slope-based peak detectors with some form of filtering to remove baseline fluctuations. Two methods that adopt this approach and are widely implemented are the adaptive energy-based QRS detector [72, 73] and the Li *et al.* multiscale wavelet analysis R-peak detector [74].

In 1985, Sörnmo *et al.* [72] and Pan and Tompkins [73] independently developed a QRS detector that incorporated band-pass filtering with a peak energy-amplitude detection algorithm. Figure 2.8 illustrates the logic of this type of algorithm which is divided into two stages, a preprocessing or feature extraction stage, followed by a decision stage. The preprocessing stage uses digital filtering techniques and non-linear operations to amplify the QRS complex in the ECG. The decision stage initializes thresholds using peak detection heuristics, which are then used to locate R-peaks in the ECG.

The aim of the preprocessing stage is to isolate the QRS components by increasing their signal-to-noise ratio so as to assist in robust amplitude-based peak detection. The signal is range-normalized before applying a cascade of low- and high-pass filters to achieve a 3 dB pass-

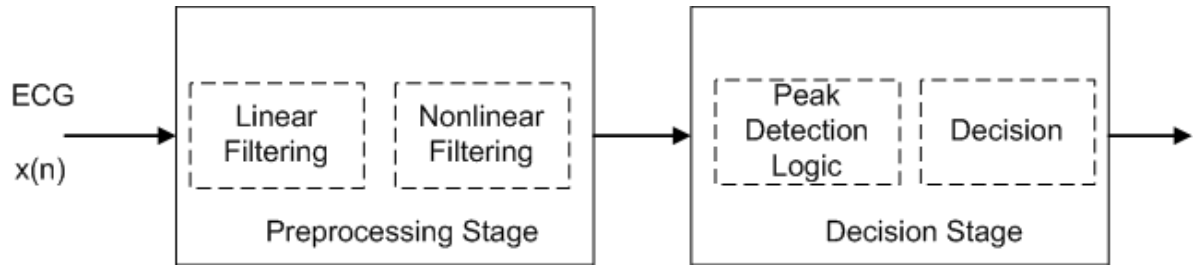


Figure 2.8: The common structure of a QRS detector.

band from 8 to 16 Hz. This is to avoid excessive contamination by other waveform features, such as the P or T wave, and high-frequency noise interference. The filtered signal is then differentiated and squared before applying a sliding window integrator. The squaring processes normalises and amplifies the gradient information captured during the derivative stage so that the energy integration stage creates a large difference between segments with and a without QRS complex. The width of the moving average window is chosen to be roughly the same width of a typical QRS complex.

The decision stage has two stages, namely peak detection, and decision phase. The peak detection phase determines a search region and the second phase detects peaks in the pre-processed signal. The R-peak detection algorithm includes strategies, such as ignoring events during a refractory period (200 ms after the R-peak) and searching back using a lower threshold if no events are detected within 1.6 times the average of the interval from the peak of one QRS complex to the peak of the next QRS complex. The QRS detector used in this research is based on the Pan and Tompkins [73] algorithm which is considered to be a benchmark algorithm for the detection of the QRS complex in ECG signals. A block diagram of the algorithm is shown in Figure 2.9. The code used in this work was obtained from Clifford [61] and tested on data obtained from Physionet [75] and achieved Se and Sp values of 99.5% and 99.8%, respectively on the MIT BH DB.

2.5.3 Beat filtering

Most human beings exhibit a normal cardiac sinus rhythm composed of very similar beats occurring at regular but slightly varying intervals. Beats which occur prematurely in the cycle,

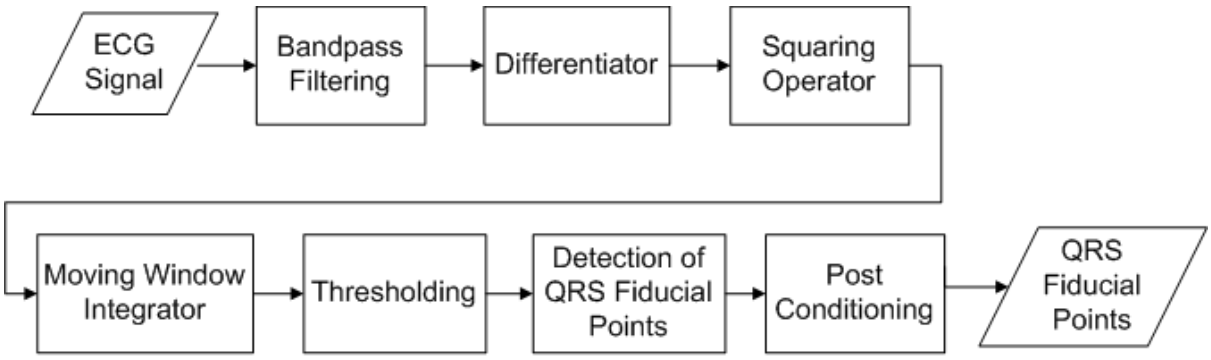


Figure 2.9: Block diagram for Pan and Tompkins Algorithm [54].

often with a different morphology, are known as ectopic beats. An ectopic beat is defined to be of either abnormal morphology or abnormal timing i.e, it arrives earlier or later than would be normally expected for the normal beat-to-beat variations in RR interval in a sequence of normal beats. Although non-sinus beats can arise from any region of the heart an ectopic beat is usually classified as atrial or ventricular.

Ectopic beats were identified by using the percentage change from the average of the last 10 normal previous beats. The percentage change in the n^{th} RR-interval is defined as $\triangle RR$, where;

$$\triangle RR = 100 \times \frac{|RR_n - RR_{n-1}|}{RR_{n-1}} \tag{2.1}$$

If $\triangle RR$ is greater than 20%, the two beats that constitute the current RR interval are defined to be a non-sinus beat pair (abnormal RR interval). If the beat-to-beat variations in the RR intervals are not greater than 20%, the beat is accepted as correct [76].

2.5.4 Baseline wander removal

The presence of baseline wander is a common problem in ECG recordings and is reflected in the ECG as a low frequency signal which does not have a cardiac origin. The frequency content of baseline wander is typically below 0.5 Hz, however increased movements of the body during stress and exercise can lead to a higher frequency content.

There are a number of methods described in the literature for the removal of baseline wander

which can be broadly classified into two groups; linear filtering and polynomial fitting [77].

Filtering

In filter-based approaches, a high-pass filter is designed to remove a slowly-varying baseline from the signal. The cutoff of the filter is selected so as to minimize signal distortion. To achieve this the lowest frequency component is chosen and since minimum heart rates are of the order of 40bpm (0.67 Hz), a cutoff frequency of 0.5Hz is usually selected. However, ST segment changes can occur down to 0.05 Hz, which means there is overlap between the filtered ST segment and the cutoff frequency [78].

Linear phase characteristics are desirable in order to preserve the temporal characteristics in the ECG signal. Linear phase filtering can be achieved by the use of a finite impulse response (FIR) filter but it generally requires a very large filter order (700 to 2000). In order to remove the filter delay, zero-phase filtering is usually implemented by forward-backward filtering. However, backward filtering is not possible in practical applications. Infinite impulse response filters would be more computationally efficient, but have an even longer impulse response and distort the waveform shape because of their non-linear phase response in the pass-band. In addition to traditional linear filtering techniques, more sophisticated forms of filtering such as adaptive filtering have also been tried [78]. An additional problem is that the frequency components of the baseline wander and of the standard features such as the T wave and ST segment can overlap, making the problem of removing noise interference without distorting ECG feature morphology non-trivial [71]. For these reasons, standard filtering approaches are not suitable.

Polynomial fitting

Polynomial fitting based approaches aim at fitting a curve to points from the ECG and then subtracting the trend. A popular approach is to use cubic spline interpolation by taking some representative points, often selected from the PQ-segment region [79]. A cubic spline polynomial is fitted so that it passes through knots at each PQ junction in a smooth manner. The advantage of the approach is that it can adapt automatically to the heart rate as more points

become available with an increase in heart rate. The main disadvantage of this approach is that it requires an accurate identification of each beat and its isoelectric region. In this thesis, baseline wander was removed using cubic spline interpolation and the procedure for finding the PQ junction to fit the cubic spline is described in the next section.

Using the isoelectric values obtained per beat, we generate a cubic spline-interpolated signal of the same sampling frequency as the ECG waveform. Computing a point-by-point subtraction creates a baseline-subtracted ECG waveform that is used in subsequent preprocessing steps.

2.5.5 Locating the PQ junction

The algorithm for locating the PQ junction starts with the R-peak location and traverses 115 ms backwards before using a 100 ms window for finding the PQ position. The 15 ms gap between the R-peak and the end of the 100 ms window is allowed to minimize the effect of the sharp downward slope just immediately before the R-peak. A histogram is fitted to this window and the modal amplitude is calculated. The modal amplitude is taken to be a single knot to be used for cubic spline interpolation [63]. Interpolation between the knots is performed at 5 Hz and the interpolated signal is then resampled back to the ECG sampling frequency of 250 Hz. Figure 2.10 shows the result of applying this algorithm to a typical segment of ECG to remove baseline wander. Firstly, PQ-points are found using the procedure described previously, (a) and then a baseline is constructed by fitting a cubic spline into the PQ-point (b). The reconstructed baseline signal is subsequently subtracted from the de-noised ECG signal, as previously described.

2.6 Dealing with noisy records

The ECG in both hospital and pre-hospital settings is often severely corrupted by noise, artefact and missing data. Therefore it is important to develop a method of assessing its quality. In the case of multi-lead ECGs, the signal quality measurement may be used to identify which ECG leads are of high quality and should therefore be selected for processing. In addition, this

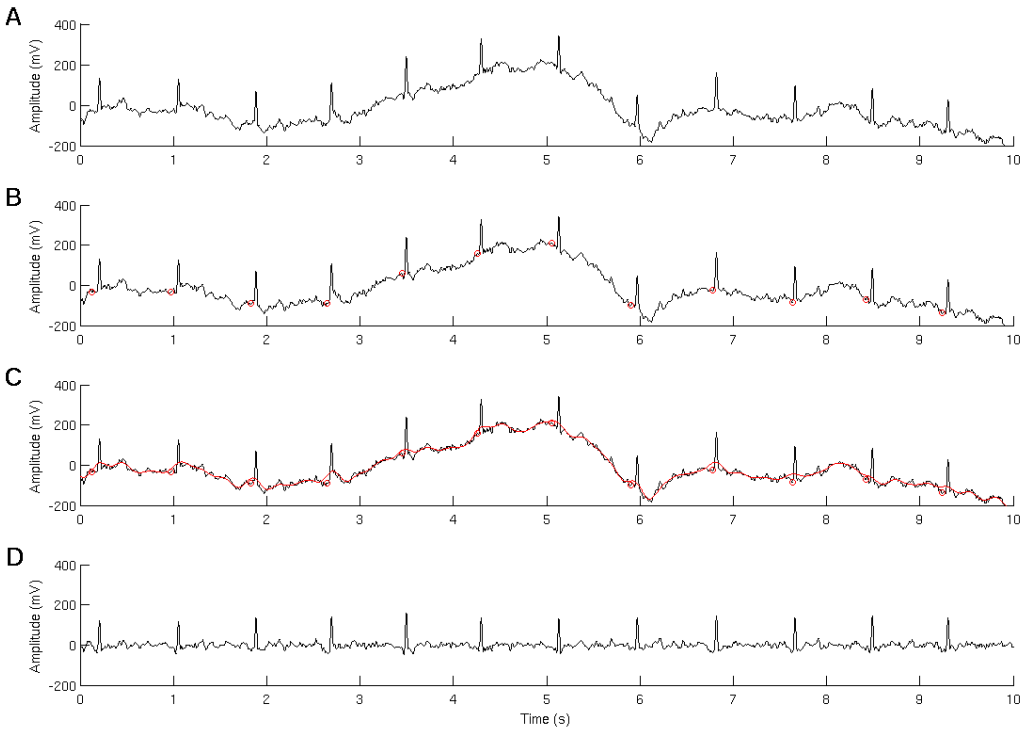


Figure 2.10: Removing baseline wander from a 10-second ECG recording using cubic spline interpolation. Panel A shows the original ECG signal, Panel B shows the original signal with PQ points (red circles), panel C shows the fitting of the cubic spline at 5 Hz, and panel D shows the final ECG signal, constructed by subtracting the baseline from the original signal.

quality measure could also be used to determine the weighting of information from different ECG leads for QRS complex classification.

Clinical experience with current ECG-based monitoring algorithms has shown that noise is the primary source of performance degradation for these algorithms. This includes both non-physiological and physiological noise. Examples of non-physiological noise sources are mains interference, baseline wander, electrode motion artefacts, and muscle artefacts. Examples of physiological noise are axis shift, QRS morphology variation, QRS amplitude variations, and atrial fibrillation flutter.

Moody [80] used the residual after projecting a QRS complex onto the first five principal components (PCs) of an ensemble of QRS complexes. Allen *et al.* [81] investigated the quality of ECG signals in a CCU, based on the number of occurrences that the ECG signal exceeded a predefined threshold (out-of-range events), and the frequency content of the ECG signal in six different bandwidths (0.05-0.25, 0.25-10, 10-20, 20-48, 48-52, and 52-100 Hz). Clifford [82] reviewed standard noise measurement methods for the ECG. These included the root mean square (RMS) power in the isoelectric region, the ratio of R-peak to noise amplitude in the isoelectric region, the Crest factor or peak-to-RMS ratio and the ratio between in-band (5 to 40 Hz) and out-of-band spectral power.

Li *et al.* [83] developed signal quality metrics which included the ratio of power in various bands of the spectrum, the degree of agreement between different QRS detectors, the degree of agreement between beat detection on different leads, the kurtosis, and the Kalman filter. These quality measures were calibrated to provide a mapping between a normalised Signal Quality Index (SQI) and an expected error in heart rate. Redmond *et al.* [84] used signal masking methods to determine artefacts and the degree of missingness in the ECG. Three feature masks were described in their work: 1) a rail contact mask was used to mark the saturation to 0 or rail voltage; 2) a high-frequency mask was obtained by using mainly a 5-order high-pass elliptic forward-backward filter with a cut-off of 40Hz (with a fixed threshold in order to detect muscle and electrode-tissue contact noise), and; 3) a low-power mask was employed by using mainly an infinite impulse response (IIR) filter with a pass-band of 0.7-33 Hz and a fixed threshold

to locate low power sections in the ECG signal. The algorithm gave a sensitivity of 89% and specificity of 98% respectively, although the fixed thresholds had to be tuned manually for different signal sources.

The PhysioNet/Computing in Cardiology (CinC) Challenge 2011 was aimed at detecting algorithms to provide real-time feedback on the diagnostic quality of the ECG and prompt an inexperienced or lay user to make adjustments in the recording of the data until the quality was sufficient that an automated algorithm or medical expert would be able to make a clinical diagnosis, primarily of arrhythmias, but also of more subtle phenomena such as ischaemia. The challenge further specified that the algorithm should be efficient enough to be able to run in near real-time on a mobile phone. At a minimum, the software should be able to indicate within a few seconds, while the patient was still present, if the ECG was of adequate quality for interpretation, or if another recording should be made.

Multiple SQIs and associated classification methods were developed for this challenge. One of the highest scores (93.2%) was achieved by Xia *et al.* [85] who used SQIs such as: at line detection, missing lead identification, auto-correlation and cross-correlation. Clifford *et al.* [86] achieved a comparative score of 92.6% before the competition close and 94% after the close of entries using a neural network approach to combine the SQIs described in their earlier work [83].

In this thesis, a template matching algorithm was used to reject noisy beats and ECG records. This technique was compared with the technique developed by Li *et al.* [83] and the comparison of these algorithms is discussed in Appendix C.

2.6.1 Signal Quality Index

The SQI algorithm developed in this thesis combines the concepts of beat-by-beat analysis and template matching to derive the signal quality index. Figure 2.11 shows the flow diagram of the algorithm.

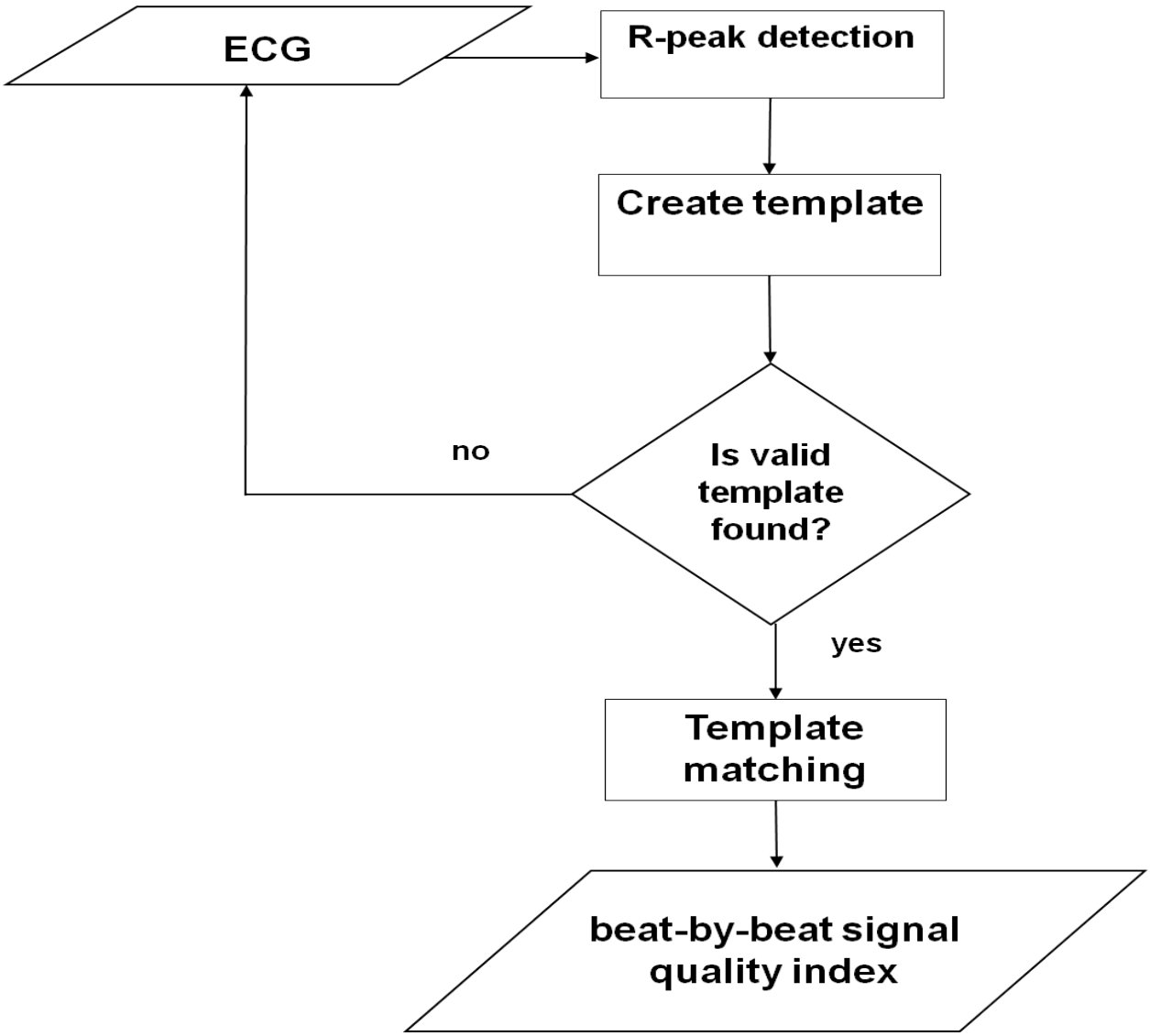


Figure 2.11: Flowchart of the algorithm for computing the Signal Quality Index.

Description of the algorithm

The R-peaks were detected using a QRS detector (see Section 2.5.2). After detecting the R-peak, the onset of the each beat was determined using a thresholding technique. The onset of the segment was defined as 40% of the previous RR-interval from the R-peak. For every window, the first and the last beat were removed because they were likely to be incomplete beats.

Template creation The first minute of a 5-minute window was used to create a template. The template is initialized by taking the mean of all beats from the first minute. The template was updated by performing cross-correlation on each individual beat with the template using

$$CC(t,s) = \frac{\sum_{i=1}^{N}(t_i - \mu_t)(s_i - \mu_s)}{\sqrt{(t_i - \mu_t)^2}\sqrt{(s_i - \mu_s)^2}} \tag{2.2}$$

where t_i is the i^{th} sample of the template, s_i is the i^{th} sample of the beat that is being matched, μ_t is the mean of the template, μ_s is the mean of the beat and N is the total number of samples in the template. A beat was only included in the final template if the correlation coefficient was at least 0.95 [61]. This ensured that all abnormal beats were not included in the template. An example illustration of the creation of the template using a one-minute window is shown in Figure 2.12.

There are instances when a valid template could not be created using the first minute of the five-minute window, in which case the template was created using the first 2 minutes.

Template matching: TSQI Once a valid template is created, each beat in the five-minute window is compared with the template using the cross-correlation function. A beat is considered to be of high quality if the correlation coefficient is at least 0.95. An example illustration of template matching using high- and low-quality beats are shown in Figure 2.13. The high-quality beat has a high correlation of 0.97 while the low-quality beat has a low correlation of 0.25.

2.7 Heart rate variability

The beating of the heart and respiration are two prominent physiological functions which are both modulated by fluctuations of the autonomic nervous system (ANS). Hence, they carry information which may be used to gain insight into the autonomic control of the heart. This section presents, a brief overview of the physiological mechanisms that lead to HRV variations are described in order to demonstrate the relevance of the HRV measures in this work.

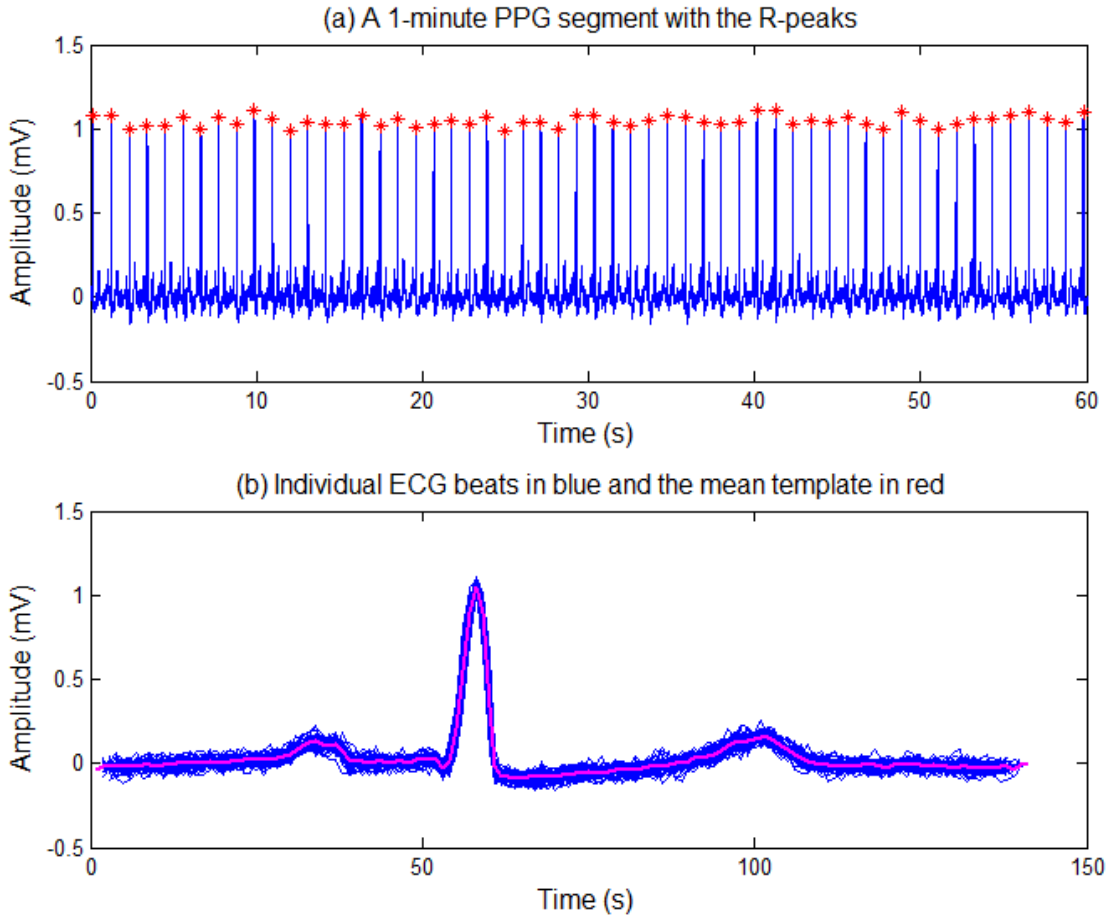
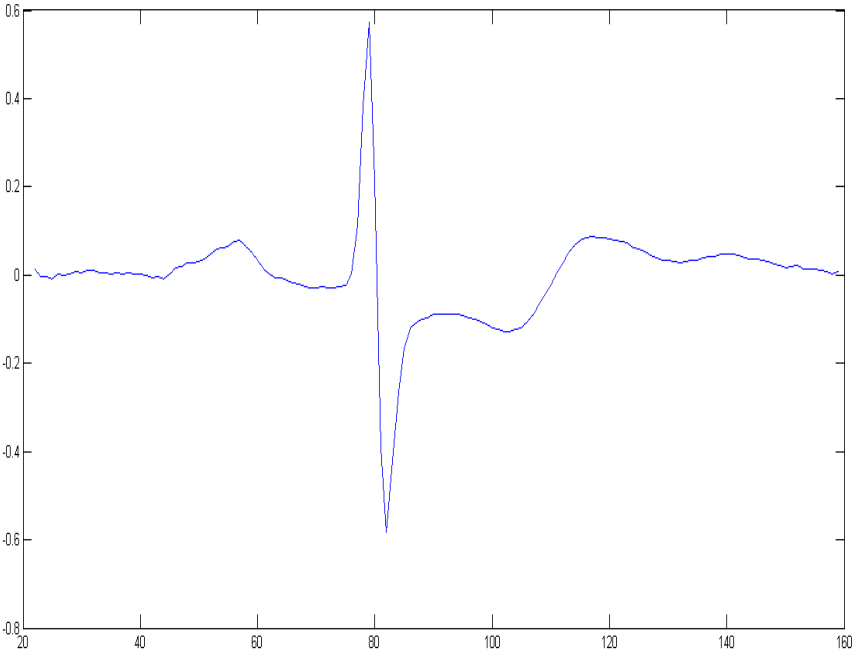


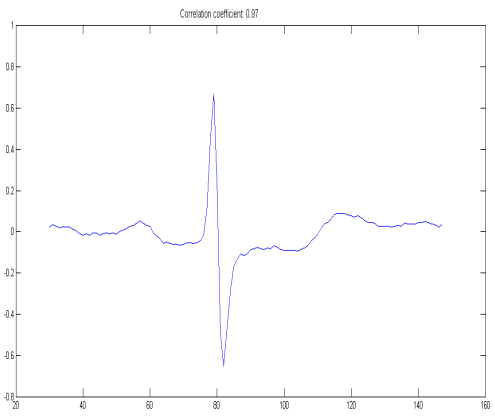
Figure 2.12: Illustration of template creating using one-minute window from patient 0031. The red stars are the R-peak.

The autonomic nervous system is divided into two opposing branches, the sympathetic and the parasympathetic nervous systems, which exert opposing effects on most organs. The parasympathetic nervous system [1] can be thought of as the rest-and-digest mechanism and causes heart rate and blood pressure to drop as well as the pupils to constrict and digestive system activity to increase. The sympathetic nervous system is rapidly activated in physically or mentally stressful situations and is therefore sometimes referred to as the fight or flight response. The sympathetic nervous system causes increases in heart rate, cardiac output, blood flow to the muscles, pupil dilation and a decrease in digestive system activity. Animals lacking a healthy sympathetic nervous system find it difficult to deal with physical and mental stress. The

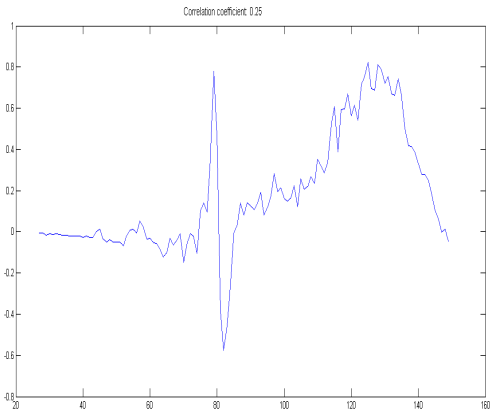
[1] Also known as vagal system



(a) Template beat



(b) High-quality beat



(c) Low-quality beat

Figure 2.13: Illustration of template matching using high-quality beat and the low-quality beats. The high-quality beat has a correlation coefficient of 0.97 and the low-quality beat has a correlation coefficient of 0.25.

complicated interaction between the sympathetic and parasympathetic branches of the ANS, and the overall effect that they have on the autoregulation of the cardiovascular system and the autonomic tone, is known as the sympathovagal balance.

2.7.1 The physiological background of heart rate variability

Heart cells have two types of neuromodulatory receptors, one for acetylcholine and one for norepinephrines corresponding to the parasympathetic and sympathetic nervous systems respectively. Their receptors in turn interact with inhibitory or excitatory proteins which through a series of chemical exchanges, decrease or increase the calcium in the heart cell membrane and inhibit or stimulate heart rate and the strength of contraction of the heart muscle [87]. The heart's intrinsic pacemaker, the sinoatrial node, causes a HR of around 100 to 120 beats/minute (bpm) in the absence of any neurohumoral (nervous and hormonal) influence. However, for a healthy heart with no conduction block, the variation of the heart rate (HR) is a manifestation of both the (antagonistic) effects of the parasympathetic and the sympathetic nerves through changes in acetylcholine and norepinephrine levels, and a resting healthy human is likely to have a heart rate of around 70 to 80 bpm. During rest both autonomic divisions of the sympathetic and parasympathetic system are thought to be tonically active, with the parasympathetic effects achieving dominance [87].

Each set of motor neurons that form the two nerve divisions of the sympathetic and parasympathetic systems interact in a highly complex manner and the modulation of HR cannot simply be interpreted as a linear sum of two opposing effects: a tachycardiac response (i.e. increase in HR) from the sympathetic branch of the ANS and a bradycardiac response (a slowing of the HR) from the parasympathetic branch, since they act over different time scales.

Furthermore, while increased frequency of vagal nerve stimulation tends to decrease the beat-to-beat heart rate and increased frequency of signalling in the sympathetic nerves tends to increase it, at stimulatory frequencies close to that of the sinoatrial node, the cardiac pacemaker can synchronise with the vagal impulses. In such situations small increases in vagal frequency may actually cause the blood pressure (BP) to increase instead of decrease. An increase in the

frequency of vagal stimulation can cause an almost immediate increase in heart rate, the opposite of the normal response. The dynamic balance between parasympathetic and sympathetic activity causes a continuous oscillation of the HR which is called HRV [87].

2.7.2 Measures of heart rate variability

Short-term and long-term variations in HR are known to have different physiological origins and the magnitude of these variations has been shown to be indicative of the autonomic state of a patient [88]. Over the last 40 years, much effort has been put into quantifying these variations with a view to making clinically useful assessments of patient welfare. HRV metrics are calculated from an analysis of the RR tachogram; the time series of RR-intervals. There are many ways of assessing HRV and a comprehensive list of metrics investigated since the 1960s are given by Malik *et al.* [88]. They can be broken down into four basic categories;

- Statistical measures such as moments of a distribution, or approximation of the moments;
- Time domain analysis;
- Frequency domain metrics;
- Nonlinear techniques.

Time domain measures

The time domain measures of HRV are based on statistical or geometric analyses of the lengths of intervals between successive normal complexes [88]. The statistical measures using the length of RR-intervals include the mean RR-interval, the standard deviation of all RR-intervals (SDNN), the standard deviation of the average RR-intervals calculated over short periods (SDANN) and the mean of the 5-minute standard deviations of RR-intervals (SDNNI). SDNN reflects all cyclic components in the analyzed period and thus depends on the length of the period. It is inappropriate to compare SDNN measures obtained from recordings of different durations. The measures derived from differences between RR-intervals (RMSSD, the square root of the

mean squared differences of successive RR-intervals, NN50, the number of interval differences of successive RR-intervals greater than 50 ms, and pNN50, the proportion derived by dividing NN50 by the total number of RR-intervals) estimate the high-frequency variations in heart rate and are correlated closely [89].

Frequency domain measures

Typically, the heart rate variability signal contains several oscillations. These include an oscillation which is synchronous with respiration (known as the respiratory sinus arrhythmia, RSA, and ordinarily found between 0.2 and 0.4 Hz), another oscillation at 0.1 Hz, thought to be due at least in part to blood pressure (BP) regulation, and a variety of oscillations at lower frequencies [90]. Processing the signal in the spectral domain allows these components to be identified and treated separately.

Power spectral density analysis provides basic information about power (variance) distribution as a function of frequency. Power spectral analysis was first introduced into HRV analysis in 1981 by Akselrod *et al.* [91]. The PSD is analyzed by calculating power and peak frequency in different frequency bands. Nonparametric (fast Fourier transform (FFT)) and parametric (autoregressive) methods have been used to compute the power spectral density of the RR-interval time series [91]. The nonparametric methods are simple, fast to compute, and do not require any assumption about model order. The parametric (autoregressive) method produces a smoother spectrum and permits automatic estimation of high frequency (HF) and low frequency (LF) power and their centre frequencies, but results can vary depending on the order of the autoregressive model [91, 92]. Since then, many authors have applied a variety of power spectral estimation techniques. In order to facilitate interstudy comparisons, the frequency spectrum of an RR-interval tachogram has been split into four frequency bands:

- Ultra Low Frequency (ULF): $0.001\,\text{Hz} \leq \text{ULF} < 0.003\,\text{Hz}$
- Very Low Frequency (VLF) : $0.003\,\text{Hz} \leq \text{VLF} < 0.04\,\text{Hz}$
- Low Frequency (LF): $0.04\,\text{Hz} \leq \text{LF} < 0.15\,\text{Hz}$

- High Frequency (HF): $0.15\,\text{Hz} \leq \text{HF} < 0.4\,\text{Hz}$

The motivation for splitting the spectrum into these frequency bands lies in the belief that the distinct biological regulatory mechanisms that contribute to HRV act at frequencies that are confined within these bands. Since the sympathetic and parasympathetic branches of the autonomic nervous system have differing characteristic time constants, it is generally accepted that HF power is a measure of parasympathetic tone [93]. However, the physiological interpretation of the LF band is more controversial and it is believed that it reflects both sympathetic and parasympathetic activity.

The LF component between the frequencies 0.04 Hz and 0.15 Hz is formed in a heart rhythm that is usually observed around 0.1 Hz. It has been suggested that this slow oscillation of the heart rhythm is caused by the mechanisms regulating the BP [94]. The 0.1 Hz peak corresponding to the most dominant of the Mayer waves [2] is mostly mediated by fluctuations of sympathetic nerve activity. Although both sympathetic and parasympathetic mechanisms are involved in the LF band, an increase in LF power has always been observed as a consequence of sympathetic activation such as a mental stress, haemorrhage, and coronary occlusion [95]. An increase in the LF power has therefore been proposed as a marker for sympathetic activation [94, 96].

The HF component of the HRV spectrum is usually identified in the frequency range between 0.15 Hz to 0.4 Hz, which is related to the respiratory frequency. Rhythms within the HF band, synchronous with respiration, are due to the intra-thoracic pressure changes and mechanical variations caused by the action of breathing. As mentioned earlier, the manifestation of the respiration rhythms on the RR tachogram is known as RSA. This higher frequency peak (above 0.15 Hz) is resolved almost exclusively by fluctuations of the vagal-cardiac nerve activity and is generally accepted as a marker of parasympathetic activity [95].

Since physiological interventions produce reciprocal but opposing changes of sympathetic and vagal outflows, it has been suggested that the balance between these opposing neural reg-

[2] Mayer waves are oscillations of arterial pressure occurring spontaneously in conscious subjects at a frequency lower than respiration (≈ 0.1 Hz in humans). Mayer waves are tightly coupled with synchronous oscillations of efferent sympathetic nervous activity and are almost invariably enhanced during states of sympathetic activation.

ulatory mechanisms can be quantified by the ratio of the power in the LF band to the power in the HF band which is then taken as a measure of the sympathovagal balance [96, 97]. Although this metric is generally thought to quantify the relative contributions of the two branches of the central nervous system, it remains a topic of much debate amongst clinicians.

The LF/HF-ratio, when high, is considered to reflect dominance of sympathetic activity, and when low, is thought to reflect dominance of vagal activity, hence it is sometimes cited as an index of sympatho-vagal balance. For instance, clinical studies [95, 96] have presented evidence that the LF/HF-ratio is the best indicator of post-myocardial infarct (MI) mortality up to one year from discharge, although Valkama *et al.* show that only changes in the HF band are relevant for assessment of post-MI convalescence [98]. However, there are two problems with the use of the sympathovagal balance for studying patients with cardiac-related problems. First, their nor-epinephrine levels may not change or they may decrease (rather than the usual increase for healthy subjects) when sitting upright, thus confusing any averages taken over an extended period. Second, these patients may have unusually high levels of muscle sympathetic nerve activity and nor-epinephrine levels, with low standard deviation of RR-intervals and a low LF/HF-ratio [97].

HRV reflects oscillations in the activity of various regulatory systems associated with a variety of factors, including respiration, baroreceptor reflexes, vasomotor control, and thermoregulatory processes. However, the physiological mechanisms behind the different measures of HRV vary. By using the spectral components of HRV, it may be possible to discriminate between the effects of various cardiovascular control mechanisms.

2.7.3 Methodology for computing heart rate variability

In this section, the methodology for performing spectral analysis on the information derived from the ECG is described. The flow chart summarizing the methodology is shown in Figure 6.1. The different stages are now described in detail. QRS complexes were detected using an algorithm based on that of Hamilton and Tompkins [73]. Next the time differences between two consecutive R waves were computed. The resulting time series is an “RR tachogram”,

a sequence of unevenly sampled beat-to-beat intervals. Most human beings exhibit a normal cardiac sinus rhythm composed of very similar beats occurring at regular but slightly varying intervals. Beats which occur prematurely in the cycle, often with a different morphology, are known as ectopic beats. When calculating HRV, there are two main reasons for removing the ectopic beats. Firstly, it is thought that an ectopic beat is not generated by the mechanism that is responsible for the variability in the RR-intervals [99]. Secondly, ectopic beats often occur substantially earlier or later than when one would expect a normal beat to occur and are followed or preceded by a prolonged pause [100]. These unusually short RR-intervals create higher than normal frequency components and lead to a significant rise in the estimation of the HF component which may distort the true measure of an HRV metric.

There are at least two accepted methods for dealing with the effect of ectopic beats on the RR tachogram. If the ectopic or artefactual beats are very occasional, they are removed and interpolation can be used to add a beat where a sinus beat would have been expected to occur [101]. The substitution can take the form of simply replacing the abnormal beats with a local mean or median value but more sophisticated procedures include linear or cubic interpolation or more complicated predictive modelling [101]. Alternatively, if the incidence of ectopic or artefactual beats is high within a given segment, then it is preferable to eliminate the ECG segments that contain such a high occurrence of ectopic beats. However, this may be very restrictive for some patient data and can lead to a great deal of data being discarded. In this thesis, we deal with occasional ectopic beats by replacing them using linear interpolation.

Abnormal beats were identified by using the percentage change from the average of the previous 10 normal beats. If the percentage change was greater than 20%, the two beats that constituted the current RR-interval were defined to be a non-sinus beat pair (abnormal RR-interval). If the beat-to-beat variations in the RR-intervals did not vary by more than 20%, the beat was accepted as correct. Removed beats were replaced using linear interpolation. The result of applying this procedure for abnormal beat removal and replacement is shown in Figure 2.15.

After ectopic removal and replacement, the RR-interval time series was used to estimate

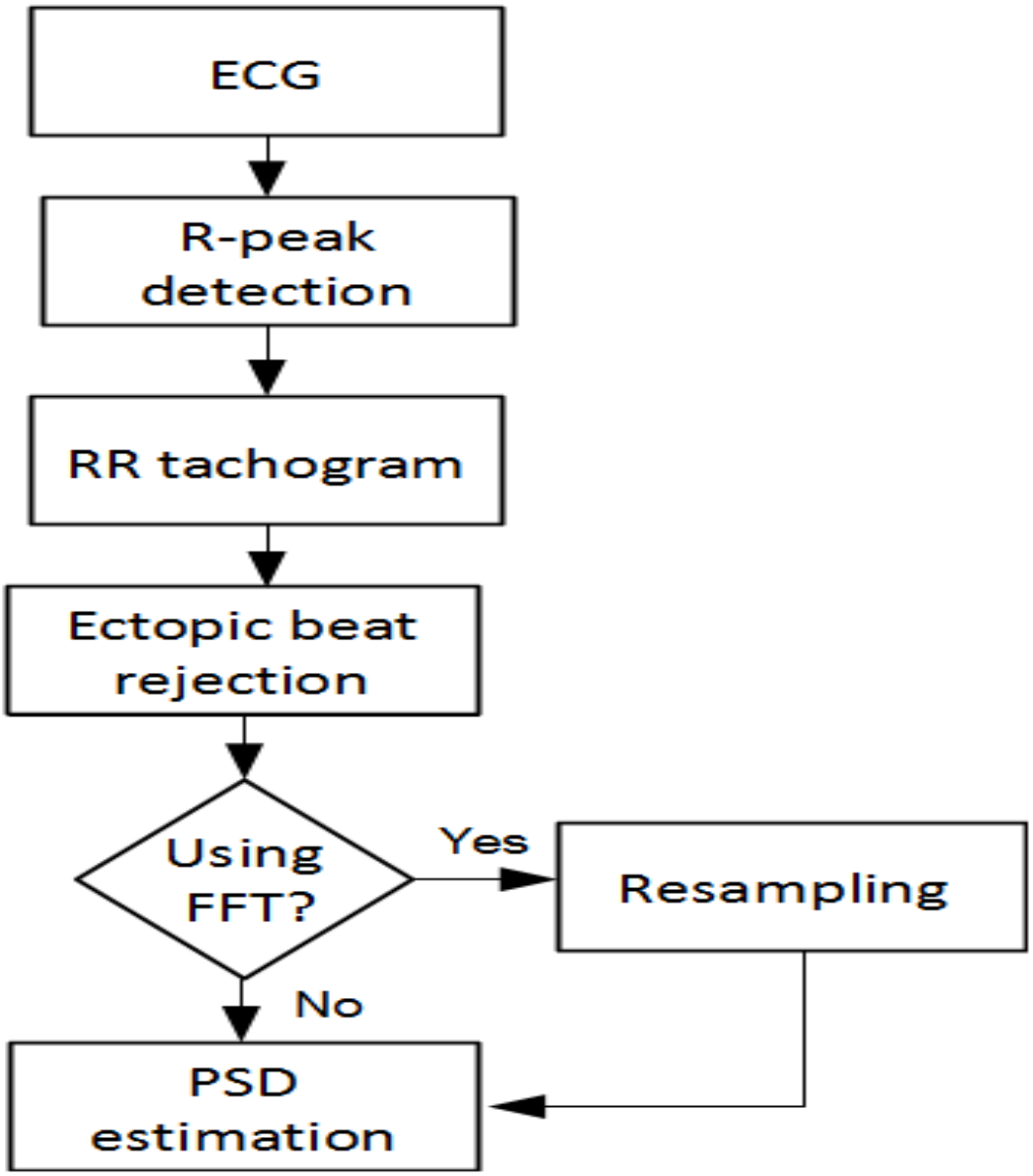


Figure 2.14: Flow diagram of the methodology used for computing HRV using spectral analysis.

the power spectral density (PSD) of heart rate variability. The choice of the number of samples to be used when estimating a PSD and the frequency range over which the estimate is taken determine the frequency resolution. In order to choose a sensible window size, the requirement of stationarity must be balanced against the time required to resolve the information present. The European and North America Task Force on standards of HRV suggested that the shortest time over which HRV should be assessed is 5 minutes [102]. As a result, the lowest frequency that can be resolved is $1/300 = 0.003$Hz, which is just above the lower limit of the VLF band.

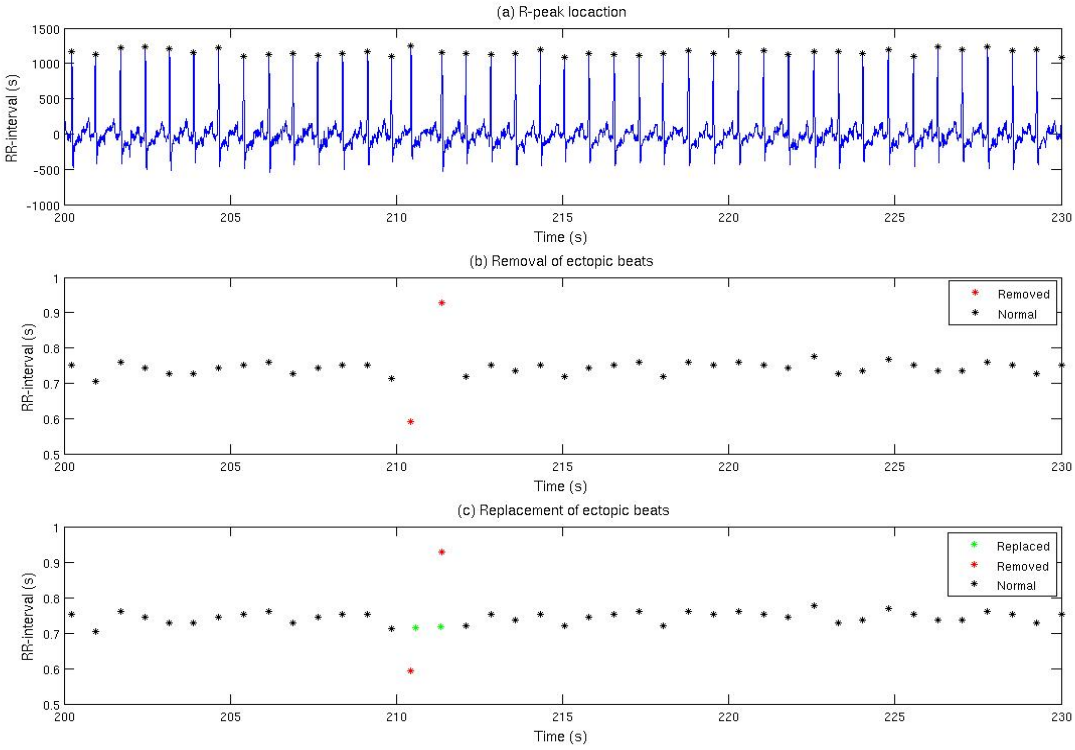


Figure 2.15: Illustration of removal and replacement of ectopic beat. (a) Detection of R-peaks using the Hamilton and Tompkins [73] algorithm; (b) Ectopic beat removal. (c) Replacement with a "phantom" beat using linear interpolation.

This means that only metrics involving the LF and HF bands can be evaluated.

Standard methods for PSD estimation are the Fourier transform (FT) and autoregressive (AR) methods, both of which operate on time series with uniform intervals between samples. Clayton *et al.* [103] demonstrated that FFT and autoregressive (AR) methods provide comparable measures of LF and HF metrics on linearly resampled 5-minute RR tachograms across a patient population with a wide variety of ages and medical conditions (ranging from heart transplant patients who have the lowest known HRV to normals who often exhibit the highest overall HRV). In this thesis, a popular technique for PSD estimation introduced by Lomb-Scargle [104], which does not require evenly sampled RR, was also used to estimate the PSD.

Apart from windowing the data, the only pre-processing performed is the removal of the mean from the data in each one-minute window. All other trends shall be considered as relevant information about the variability of the HR. In particular, no non-linear detrending is

performed.

The PSD was computed using the Lomb-Scargle periodogram, a technique for estimating the frequency content of a signal that is sampled at irregular intervals. The Lomb-Scargle periodogram was shown to produce more robust PSD estimates in the presence of noise and ectopy than the FFT [102]. In the Lomb-Scargle method the data are weighted on a point-by-point basis rather than on per-time interval basis as in conventional FFT analysis. The computation of the Lomb-Scargle periodogram is equivalent to linear least-square fitting a sinusoid of angular frequency (ω) to the data. In Scargle's 1982 paper [105] on unevenly-sampled time-correlated data, he demonstrated that the generalized-point of a time series for arbitrary times (or uneven sampling) with variance (σ^2) and a mean value $\bar{x}$ leads to the expression for the Lomb-Scargle periodogram

$$P_N(\omega) = \frac{1}{2\sigma^2} \frac{[\sum_{n=1}^{N} x(t_n - \bar{x}) \cos \omega(t_n - \tau)]^2}{\sum_{n=1} \cos^2 \omega(t_n - \tau)} + \frac{[\sum_{n=1}^{N} x(t_n - \bar{x}) \sin \omega(t_n - \tau)]^2}{\sum_{n=1} \sin^2 \omega(t_n - \tau)} \quad (2.3)$$

where $\tau \equiv tan^{-1}(\sum_j sin(2\omega t_j)/(2\omega \sum \cos(2\omega t_j))$ is an offset that makes $P_N(\omega)$ completely independent of shifting all the $t_j s$ by any constant. This choice of offset makes Equation 2.3 exactly the solution that one would obtain if the harmonic content of a data set, at a given frequency ω, was estimated by linear least-squares fitting to the model $x(t) = A \sin(\omega t) + B \cos(\omega t)$. Thus, the Lomb-Scargle periodogram weights the data on a per point basis instead of weighting the data on a per-time interval basis.

2.8 Conclusion

This chapter provided a background of cardiac electrophysiology; and signal processing techniques implemented in other chapters to enable automatic ECG analysis. It also described the physiological basis of HRV, and the general methodology used in this thesis to compute HRV.

Chapter 3

Automated ST segment analysis

The ECG is a semi-periodic signal with a combination of high-frequency variations (QRS complex) and low-frequency features (P and T wave). The varying spectral dynamics of the ECG and the wide range of non-stationary noise and artefacts make automated analysis of the ECG a non-trivial problem. This chapter describes a standard implementation for ischaemia detection after a review of current methods is given. A technique for automatic detection of ST segment changes that can be used in the diagnosis of acute coronary syndrome (ACS) using ambulatory ECG recordings is described.

Automated methods for ECG interval analysis offer the potential for a more extensive and reliable evaluation of continuous ECG data for diagnosis and management of ACS. Specifically, automated analysis of ECG intervals offers a number of distinct advantages compared with manual analysis:

- The ability to rapidly analyse large volumes of ECG data
- Cost-effectiveness compared with analysis by human expert
- More-consistent segment measurements

One of the primary advantages of automated approaches is the ability of computer-based systems to process large volumes of ECG data in a short period of time. Perhaps the most significant advantage of the automated approach however is that the resulting ECG segment

measurements are guaranteed to be "self-consistent". Specifically, for a given set of ECG signals, an ECG interval segment algorithm will always produce the same set of measurements for the same set of waveforms. The problem of intra-analyst variability which is the main disadvantage of manual analysis does not exist with automated analysis.

3.1 Available reference databases

This section provides a brief description of the ECG databases used in this research in order to familiarize the reader with the acquisition methodologies and statistical characteristics of the data used to test the methodology implemented for automated ischaemia detection. The two suitable publicly available databases are the European ST-T Database (ESC DB) [106] and the long term ST database (LTST DB) [107] available from PhysioNet [75].

The expert annotators of the European ST-T DB and LTST DB have annotated transient ST segment episodes which satisfy the following clinically defined criteria:

1. An episode begins when the magnitude of the ST deviation first exceeds a lower annotation detection threshold, V_{lower} = 50 μV.

2. The deviation then must reach or exceed an upper annotation detection threshold V_{upper} throughout a continuous interval of at least T_{min} seconds (the minimum duration of an ST episode)

3. The episode ends when the deviation becomes smaller than V_{lower} = 50 μV, provided that it does not exceed V_{lower} in the following $T_{sep} = 30$ seconds (the interval separating consecutive ST episodes).

3.1.1 European ST-T Database

Each of the 90 ECG records in the European ST-T DB database consists of annotated extracts of ambulatory ECG recordings from 79 subjects. Over half (48 of 90 complete records), and reference annotation files for all records of this database was contributed to PhysioNet in 2000,

and the remainder were contributed in November 2009. Each record is two hours in duration and contains two signals, each sampled at 250 Hz with 12-bit resolution over a nominal 20 mV input range. The sample values were rescaled after digitization with reference to calibration signals in the original analogue recordings, in order to obtain a uniform scale of 200 ADC units per millivolt for all signals. Each record is accompanied by a clinical report including information concerning pathology, drug treatment, electrolyte imbalance and additional technical information. For each case, the two leads which were considered most likely to reveal ST-T changes were recorded. Two cardiologists independently annotated QRS complexes, episodes of changes in ST segment or T wave morphology, rhythm changes, and signal quality. Episodes of ST segment and T wave changes were identified in both leads and their onsets, extrema and offsets were annotated. Differences in the annotation by the two cardiologists were resolved by a third cardiologist in the database coordinating group [106].

According to the annotation of the ESC DB, the values of the upper annotation detection thresholds and minimum length of ST episodes are $V_{upper} = 100\,\mu\mathrm{V} and \mathrm{T}_{min} = 30$ seconds.

3.1.2 Long Term ST Database

The LTST DB contains 86 twenty-four hour ambulatory records selected from Holter recordings obtained in routine clinical practice settings in Europe and in the United States between 1994 and 2000. Contributions were obtained from the Beth Israel Medical Center, ICP, Brigham and Women's Hospital (Boston, MA), and Duke University Medical Center (Durham, NC). The records were collected to model real-world clinical conditions as far as possible with or without known coronary artery disease while containing a number of ischaemic and non-ischaemic ST events. Analogue recordings were made using standard ambulatory electrocardiographic recorders.

Since ambulatory electrocardiographic recorders preserve frequency content in the signals typically up to 30Hz (or to 45Hz in best cases) the records were digitized at 128Hz or 250Hz with an amplitude resolution of 12 bits. After resampling the records to the same unique sampling frequency of 250Hz and adjusting the amplitude scale to 200 ADC units per mV, the

records were preprocessed as described in [69]. The LTST DB contains 65 twenty-four hour two-channel ECG records and 15 three-lead ambulatory records with significant ST events annotated by human experts. Each two-channel record contains one of the following pairs: one of the bipolar leads recorded at precordial positions, denoted as pseudo V2-V5, together with modified limb lead III (MLIII); or pseudo-lead V5 and pseudo-lead V2; or modified limb lead L2 (ML2) and modified lead V2 (MV2) [69]. The leads used in the three-channel records included: a combination from leads pseudo V3-V6, II and aVF, or Zymed EASI lead system with the leads E-S, A-S and A-I.

Complete expert annotations have been provided for the database following three different annotation protocols. The ECG waveform on its own is not sufficient for the diagnosis of myocardial ischaemia, so the gold standard for annotating a transient ST segment and ischaemic event was based not only on ECG waveforms but also on detailed clinical information from the subjects including other clinical investigations, the clinical history and the decision of expert annotators of the database. Thus, a classification of a particular episode can be driven by previous knowledge about the patient rather than physiological evidence. This is one of the limitations that should be considered when interpreting the results.

The annotators defined several classes of ST segment changes as follows:

- Non-ischaemic changes in ST segment morphology. These changes are caused by
  - slow or sudden changes due to simultaneous slow or sudden (postural axis shifts) changes in the cardiac QRS electrical axis; these are characterised by a change in the Q-, R- or S-wave amplitude.
  - slow or sudden changes due to paroxysmal or intermittent right or left bundle branch block, or other slow or sudden intraventricular or intermittent QRS conduction changes; these are characterised by bizarre and wider QRS complexes.
  - slow drifts due to heart-rate related diurnal changes or effects of medication on repolarisation; drifts are characterised by slow and persistent typical non-ischaemic changes in ST segment slope and shape within a longer period, and may or may not

be accompanied by a change in heart rate.

- Non-ischaemic heart-rate related change in ST segment morphology: This is characterised by changes in ST segment morphology and by a change in heart rate, when clinical information from the subject does not suggest ischaemia. Typically, and most often, changes in ST segment morphology of this class include: J point depression with positive slope; moving of T wave into ST segment; T wave peaking; or parallel shift of ST segment compared to the reference or basal ST segment.

- Ischaemic change in ST segment morphology: This is characterised by changes in ST segment morphology and may or may not be accompanied by a change in heart rate, when clinical information from the subject suggests ischaemia. Typically, and most often, changes in ST segment morphology of this ischaemic class include: horizontal flattening; down sloping; scooping; or elevation.

- Noisy ST event: This is characterised by consecutive ST segments that cannot be evaluated by annotators because of noise.

Episode annotations of the LTST DB are available in three variant annotation protocols:

1. Protocol A V_{upper} = 75 μV, T_{min} = 30 seconds.

2. Protocol B V_{upper} = 100 μV, T_{min} = 30 seconds, equivalent to the protocol of the ESC DB.

3. Protocol C V_{upper} = 100 μV, T_{min} = 60 seconds.

3.2 Overview of ST segment analysis approaches

Various techniques for the detection of myocardial ischaemia and ST segment episodes have been reported. Each technique can be categorized into one of the following; digital filters, rule-based systems and machine learning techniques. Some of the reported techniques are designed to detect ischaemic episodes related to ST segment deviation only and others to both ST segment deviations and T wave changes.

3.2.1 Performance measures

Three performance measures commonly used to assess performance are; sensitivity (Se), specificity (Sp), and positive predictive accuracy (PPV). Sensitivity, which is the ratio of the number of correctly detected events, true positives (TP), to the total number of events is given by:

$$Se = \frac{TP}{TP + FN} \tag{3.1}$$

where false negatives (FN) denotes the number of missed events.

The specificity, which is the ratio of the number of correctly rejected nonevents, true negatives (TN), to the total number of nonevents events, is given by

$$Sp = \frac{TN}{TN + FP} \tag{3.2}$$

where false positives (FP) denotes the number of falsely detected events. However for most cases the TN values are not available hence...

Positive predictive accuracy (or positive predictive value) is the ratio of the number of correctly detected events, TP, to the total number of events detected and is given by

$$PPV = \frac{TP}{TP + FP} \tag{3.3}$$

In addition, the accuracy (ACC) of an analyser can be calculated using

$$ACC = (TP + TN)/(TP + FP + TN + FN) \tag{3.4}$$

3.2.2 Digital-filter based systems

Digital-filter based systems use filter-based tools such as root mean square (RMS) and Principal Component Analysis (PCA) to detect ischaemic ST episodes.

Senhadji *et al.* [108] used a signal analysis technique based on wavelets. Wavelets are functions, which are both oscillatory and localized in time, used to examine both time and

frequency information of the signal simultaneously. The obtained features from the wavelet transformation were used for beat classification as normal, ischaemic due to ST segment deviation, or premature ventricular contraction. The system was evaluated on a small dataset which is not publicly available containing 20 ischaemic and 20 normal beats and achieved Se and Sp values of 95% and 100%, respectively.

Jager *et al.* [109] developed a system based on PCA which involves a procedure that transforms a number of correlated variables into a smaller number of uncorrelated variables called principal components. The first five principal components for the QRS complex and the first five of the ST segment were computed from the database of 6000 beats from the ESC ST-T database. Their system was evaluated using the ESC-ST-T database and it gave a sensitivity and positive predictive accuracy of 85.2% and 86.2%, respectively.

Garcia *et al.* [110] proposed a method which operates by applying a detection algorithm to the filtered RMS series of differences between the beat segment (ST segment) and an average pattern segment. This method resulted in an average sensitivity and positive predictive value of 85.0% and 86.0%, respectively, for ST segment deviations and 85.0% and 76.0%, respectively, for ST-T complex changes.

3.2.3 Rule-based systems

Rule-based systems employ a set of logical tests that are derived from medical knowledge in order to evaluate the extracted ECG features and detect the ischaemic episodes. Shook *et al.* [111] estimated the average of the ST absolute deviation (maximum ST segment depression from the isoelectric line), the average of the ST segment deviation (ST segment depression at the point J + 80 ms, which is the point that lies 80 milliseconds (ms) after J) and the average of the ST segment slope (slope between the points J and J + 80 ms) in every 30 seconds of the ECG signal. The system was implemented using rules, the rules used were 100 μV for the absolute deviation, 75 μV for the deviation and zero for the slope; in order to classify the ischaemic episodes. The system also used a second set of rules and these are 100 μV for the absolute deviation, 100 μV for the deviation and zero for the slope to classify each ischaemic episode

as definite or probable depending on which set of rules was triggered. The final system's output was the probability of the "definite" and "probable" ischaemic episodes. The system was evaluated using 18 twenty-four hour ambulatory ECGs from a database that is not publicly available and achieved Se and PPV values of 90.0% and 96.0%, respectively.

Taddei *et al.* [106] designed a rule-based system for 2-lead ECG recordings which employed a geometric algorithm that calculated a 2D loop for the ST segment. For each cardiac beat, the ST segment deviations were estimated in the two leads and then each pair of values was graphically represented sequentially in time. The system was tested using the ESC ST-T database and achieved Se and PPV values of 82.0% and 81.0%, respectively.

Papaloukas *et al.* [112] presented a rule-based approach for ST segment and T wave abnormality detection using J + 60 ms or J + 80 ms which is the point at which the ST segment elevation or depression is measured. Application of a set of rules over the slopes and the level of the ST segment and T wave was followed by window characterization for episode detection. The performance measures used in the paper were Se and PPV and the proposed system scored 92% and 94%, respectively for ST segment deviation and 91.1% and 80.1%, respectively in detecting T wave abnormalities on the ESC ST-T database.

Smrdel and Jager [113] used the ST deviation time series for the detection of ST episodes. The algorithm estimates the ST segment level, and constructs the ST segment level function. In addition the algorithm determines the positions of the isoelectric level and the J-point in average heart beats constructed from 16-second windows of normal and non-noisy heart beats. Then the samples of the ST segment level function were derived for each ECG lead. The Se and PPV values for this method on the ESC-ST-T database were 81.3% and 89.2%, respectively.

An ischaemia detection method using genetic algorithms and multi-criteria decision analysis has been proposed by Goletsis *et al.* [114]. This method defined ST deviation at the J + 60 ms or the J + 80 ms point, ST segment slope, T wave amplitude, T wave normal amplitude and polarity along with age. The multi-criteria decision analysis used in their method was based on the comparison between template beats and beats classified using a similarity system. The Se and Sp values for this algorithm for ischaemic beat classification on the ESC ST-T database

were 91% in each case.

Exarchos *et al.* [115] proposed a method using a rule mining approach for ischaemia detection. This method used ECG features such as ST segment deviation, slope, area, T wave deviation from a normal template amplitude along with the patient's age. Their method then used rules obtained from the data for detecting ischaemic ST episodes. The Se and Sp values achieved with this method for ischaemic beat classification over the ESC ST-T database were 87% and 93%, respectively.

Fuzzy logic systems

The rules employed in rule-based systems correspond to inflexible thresholds; this being the main disadvantage of these systems. Fuzzy expert systems are an extension of rule-based systems to deal with this problem. Fuzzy expert systems employ similar sets of rules but their logic is not binary but fuzzy, thus allowing the representation of possibility (called fuzziness) concerning the decision suggested by a rule. This simulates better human-like reasoning and consequently the diagnostic chain of thoughts followed by physicians.

Vila *et al.* [116] developed a system which exploits the rules used by the European Society of Cardiology to construct a fuzzy system for episode identification in the ESC ST-T database using 30 out of the 90 recordings for training. This allowed the determination of the optimum threshold value for the probability associated with the detection of an ischaemic episode. The remaining 60 records were used for testing the algorithm and a Se value of 81.0% and PPV value of 68.0% were achieved. A real-time ischaemia detection method was presented in the paper by Pang *et al.* [117] which used a real time R-peak detector and combined time domain and PCA features along with an adaptive neuro-fuzzy system for classification. This method achieved Se and PPV values of 81.3% and 74.6%, respectively for the ESC ST-T database.

Exarchos *et al.* [118] proposed a fuzzy expert system based on the extraction and application of fuzzy rules and optimization of membership function parameters for ischaemic beat classification. This technique achieved Se and Sp values of 91.0% and 92.0%, respectively, for ischaemic beat detection.

3.2.4 Machine learning techniques

An alternative approach to rule-based systems are machine learning techniques, which do not require any explicit statement of rules. Instead, a classifier is trained to map an input vector into one or more classes using examples contained in a training database. Machine learning techniques that have been used to detect ischaemic episodes include artificial neural networks and hidden Markov models (HMM).

Stamkopoulos *et al.* [119] used an Artificial Neural Network (ANN) model called the multilayer perceptron (MLP) for the detection of myocardial ischaemia using only one lead. The inputs to the MLP were digitized points from the ST segment. This system was trained to classify each beat as normal, ischaemic with ST elevation, ischaemic with ST depression and unclassifiable. This was followed by the identification of ischaemic episodes using 60 out of 90 recordings of the ESC ST-T database and the reported Se and PPV values were 84.4% and 78.8%, respectively.

Silipo *et al.* [120] applied the MLP network to two-channel recordings using information only from the ST segment (ST deviation and slope). This system classified each beat as ischaemic or not and then all the classified beats were examined in groups of 20 seconds. If a group contained only ischaemic beats then it was considered as an ischaemic episode. All the episodes that were closer than five seconds were merged. The system was evaluated using 47 out of 90 recordings of the ESC ST-T database and the reported Se and PPV values were 85.0% and 88.0%, respectively.

Maglaveras *et al.* [121] evaluated a three-layer MLP for the detection of ischaemic episodes and achieved Se and PPV values of 88.6% and 78.4%, respectively for episode detection using average statistics and 85.0% and 68.7% using gross statistics of the European Society of Cardiology Database. The neural network implemented operated on an estimate of the deviation of the baseline-corrected ST segment that starts 40ms after the R-peak with a duration of 160ms.

Frenkel and Nadal [122] proposed an ANN based approach for ST-T segment classification. In this method, ECG data segments with ST-T intervals were extracted and, using PCA, reduced to six components that represented 98.1% of the total data variance. The method gave Se and

PPV values of 84.1% and 72.6%, respectively, on the ESC ST-T database.

Papadimitriou *et al.* [123] trained an ANN to classify each beat as ischaemic or non-ischaemic using information extracted from the ST-T interval. An episode was defined as ischaemic when for at least 15s the beats were ischaemic. The system achieved Se of 82.8% and PPV values of 82.4% when tested on 27 out of 90 recordings from the ESC ST-T database.

Papaloukas *et al.* [124] proposed a technique that uses PCA technique for extracting PCA coefficients that describe the global content of the ST-T complex. The PCA coefficients were used to train the self-organizing map (SOM) with radial basis function (RBF), ANN, and Support Vector Machine (SVM). The SOM, SOM, SOM-RBF and SVM gave Se and PPV values of 74.9% and 73.7%, 79.5% and 77.6%; and 82.8% and 82.4%, respectively.

In other work, Papaloukas *et al.* [125] proposed a technique for the detection of myocardial ischaemia with a neural network trained using Bayesian regularization. They used a 400ms long estimate of the ST segment and five lead-independent principal components of the ST segment estimates were obtained for the entire database for dimensionality reduction. This method gave Se and PPV values of 90.0% and 89.0%, respectively, for aggregate gross statistics and 86% and 87%, respectively for average statistics using the ESC ST-T database.

Andreao *et al.* [126] proposed HMM-based system for automated ECG segmentation and ischaemic detection.The approach was to train a HMM using a data set of ECG waveforms and the corresponding expert annotations. The ECG signal was first encoded using the undecimated wavelet transform (UWT). The UWT coefficients were used for R-peak detection and signal encoding for the HMM. The trained HMM was then applied to a subset of the ECG signal to infer the fiducial points for each heart beat. The second derivative of a Gaussian discrete wavelet was used to encode the ECG for the HMM-based segmentation algorithm. The approach gave values of 83.0% and 85.0%, respectively, for Se and PPV.

3.2.5 Comparison of different systems

The results obtained from each approach cannot always be compared directly since they are not always evaluated on the same dataset or on the same patient subset. Also some of the systems

base their diagnosis only on the ST segment deviation and not the T wave episodes as well. Table 3.1 summarises the systems presented above, giving information concerning the type of the system, the employed techniques, the output of the system (beat classification or ischaemic episode detection) and the dataset used to evaluate the system.

The various ischaemia detection systems that have been proposed so far can be grouped into three main categories; each exhibits certain advantages and disadvantages. The digital-filter analysis techniques are the most common techniques used for medical signals. They are easy to implement and can provide real-time decisions. The rule-based systems are simple to implement and their decision process resembles that of the medical experts. Fuzzy systems provide human-like reasoning allows the expression of doubt concerning the validity of a rule. Machine learning techniques can usually detect ischaemia more reliably than the other systems. Their main disadvantage is that they cannot provide explanation for the diagnosis they provide.

In this section, potential methods, and their advantages and this disadvantages for detection of ST episodes from the ECG were identified from the literature. In this thesis, we chose a rule-based system which uses similar rules to that of doctors as it is able to provide the reason that led to that decision for each ischaemic episode.

3.3 Implementation of an ischaemic detection algorithm

The ECG signal is preprocessed to remove mains interference and baseline wander. To remove the mains interference, a combination of a low-pass Butterworth filter and a notch filter was used and for baseline wander removal, cubic spline interpolation is applied as described in Section 2.5.1. The fundamental component of any ECG-based analysis and decision support system is the segmentation of the ECG into its constituent parts such as the QRS complex and ST segment. The R-peak was found using QRS detector as described in 2.5.2. In this work a rule-based technique was used to find the relevant salient points of the ECG for ST segment analysis. The ST level and deviation were then found and used to identify ST events in the LTST DB. The flowchart describing this process is shown in Figure 3.1.

Type	Ref.	Techniques	Se (%)	PPV (%)	System output	Data
DigitalFilters	[108]	Wavelet	99	100	Beat classification	own database
	[109]	PCA	85.2	86.2	Episode detection	ESC DB
	[110]	RMS	85.0	86.0	Episode detection	ESC DB
Rule-based	[111]	Rule-based	90.0	96.0	Episode detection	own database
	[127]	Geometric method	82.0	81.0	Episode detection (ST changes only)	ESC DB
	[116]	Fuzzy system	81.0	68.0	Episode detection	ESC DB (30/90)
	[112]	4-stage algorithm	92.1	93.8	Episode detection(ST changes only)	ESC DB
	[114]	Multi-criterion	91.0	91.0	Episode detection	
	[113]	Heuristic rules	81.3	89.2	Episode detection	ESC DB
	[117]	Fuzzy system	81.3	74.7	Episode detection	ESC DB
	[115]	Rule-based	87.0	93.0	Beat classification	ESC DB
	[118]	Fuzzy expert	91.0	92.0	Beat classification	ESC DB
Machine learning	[119]	MLP	84.4	78.0	Episode detection (ST changes only)	ESC DB (60/90)
	[120]	MLP with PCA	77.0	86.0	Episode detection (ST changes only)	ESC DB
	[120]	Recurrent neural network	77.0	85.0	Episode detection (ST changes only)	ESC DB
	[120]	Knowledge learning	71.0	66.0	Episode detection (ST changes only)	ESC DB
	[121]	Auto-associative non-linear PCA with RBF	88.6	78.4	Beat classification (ST changes only)	ESC DB (34/90)
	[128]	Auto-associative non-linear PCA with RBF	86.5	76.8	Beat classification (ST changes only)	ESC DB (34/90)
	[122]	ANN with PCA	84.0	72.6	Episode detection (ST changes only)	ESC DB
	[123]	SOM	74.9	73.7	Episode detection	ESC DB (27/90)
	[123]	SVM	82.8	82.4	Episode detection	ESC DB (27/90)
	[123]	SOM and RBF	79.5	77.6	Episode detection	ESC DB (27/90)
	[125]	MLP and Bayesian regularization	91.8	90.4	Episode detection	ESC DB
	[126]	HMM	83.0	85.0	Episodes detection	ESC ST−T

Table 3.1: Comparison of existing methods for ischaemic ST episode detection and beat classification. Beat classification techniques classified individual beats as normal or ST elevated/depressed. Ref. stands for references. Se -Sensitivity, PPV - Positive Predictive Value.

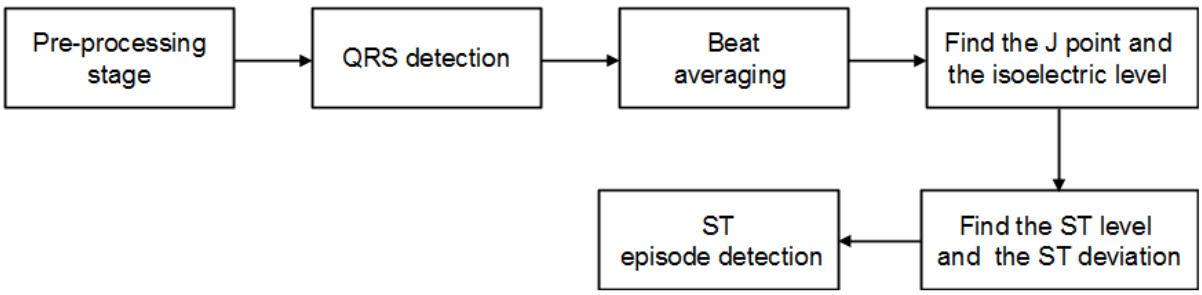


Figure 3.1: Flowchart of the proposed ST analysis algorithm.

The beat averaging and rejection was done using a modified algorithm described in Section 2.6.1. The average beat consists of an R-aligned point-by-point average of the most recently accepted 20 beats. In building the template, the first beat in the recording is used as a template beat. If the cross-correlation between the template and the second QRS exceeds 0.95 at the time instant for the best match, the two beats are averaged to produce a better template. If not, the first beat is discarded and the second one is used as a template beat. This procedure is repeated until 60 consecutive beats have been found with a cross-correlation exceeding 0.95. This initial template is then used to build the average beats.

3.4 Determining the J point and ST level

After QRS detection and baseline wander removal, the instantaneous heart rate, which is defined as $HR(n) = 60/RR(n)$, where $RR(n)$ is the normal beat-to-beat interval, is calculated. The position of the J point is difficult to find in many ECG signals, resulting in errors in ST level measurements.

To find the J point,J , the algorithm developed by Christov and Daskalov [129] was used. The procedure searches forward in each lead from the R-point for up to 32ms for a sample where the slope of the waveform equals zero or changes sign. If such a reference point is not found, the procedure searches forward in each lead from the fiducial point for up to 68ms for a part of the waveform which 'starts to flatten'. The procedure calculates for each signal sample the absolute amplitude difference between the mean of three preceding and three trailing samples. The first of the three consecutive signal samples for which the amplitude difference is

less than 15μV is considered to be the position of the J point for this lead. Figure 3.2 illustrates the result of this procedure on a typical ECG.

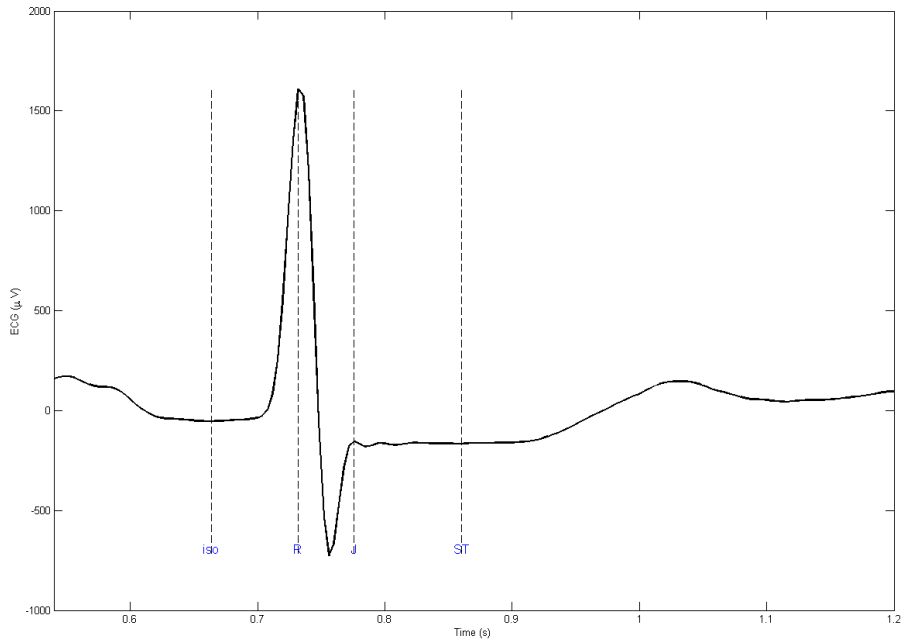


Figure 3.2: Salient points on an ECG beat after QRS detection and determination of the J point and ST amplitude.

The ST segment amplitude, $ST(j,n)$, for lead j, is measured at *J + 80 ms* if the heart rate is less than 120 bpm, or *J + 60 ms* if the heart rate exceeds 120bpm. These rules are given in Equation 3.5.

$$ST_j = \begin{cases} J_n + 80ms & \text{if} : HR_n < 100bpm \\ J_n + 60ms & \text{if} : HR_n \leq 120bpm \end{cases} \tag{3.5}$$

The process of isoelectric point, $ISO(j,n)$, determination is performed twice in pre-processing: first to determine beat-by-beat points to build a spline for baseline subtraction and secondly on the average beat template to determine a reference voltage for repolarisation segment analysis. Whether the beat is a single beat or an average beat template, the process of isoelectric point determination is the same.

ST level function, $ST_{level}(j,n)$, which is defined as the change of ST segment amplitude

over time is measured with respect to the isoelectric level at the selected point in the ST segment. A typical ST level function (as used in this thesis) is defined as;

$$ST_{level}(j,n) = ST(j,n) - ISO(j,n) \tag{3.6}$$

where $ST(j,n)$ is the ST level of an individual heart beat and $ISO(j,n)$ is its isoelectric level.

3.4.1 Building a time series of the ST level function

The monitoring of these features beat-by-beat leads to the corresponding feature time series. As the sampling frequency of these time series varies over time with respect to the heart rate, the resulting time series is further resampled using linear interpolation at a frequency of 2 Hz in order to achieve an evenly sampled time series. Beat filtering is applied in order to delete periods of noisy beats that may distort the ST level measurement, however some noisy values may still remain in the time series along with normal fluctuations. In order to ensure that the time series reflects the normal ST signal of the patient (a 12-point Butterworth low pass filter) was applied to the signal.

After the ST level is extracted, ST level deviation, which is a change in ST level relative to a reference level, is computed. The reference ST level, $ST_{ref}(j,n)$, was computed by searching for a five-minute interval without significant variation in ST level as near as possible to the beginning of the record.

3.4.2 Computation of ST segment deviation

The ST deviation function, $ST_{dev}(j,n)$, for each lead can be derived as the algebraic difference between the ST level function and the ST reference function as follow.

$$ST_{dev}(j,n) = ST_{level}(j,n) - ST_{ref}(j,n) \tag{3.7}$$

3.5 Results of applying the algorithm to LTST DB

The proposed method was tested using the LTST DB and ischaemic episodes were detected according to protocol B (see Section 3.1.2) as this is similar to the rules clinicians use in diagnosing ST elevation [79]. To evaluate the performance of the method two common measures were used for ischaemia detectors, Se and PPV, which can be reported as an average over patients or gross statistic over all episodes. The gross statistic weights each episode equally by pooling all the episodes over all records together, and provides an estimate of how the system behaves on a large number of events. The average statistic weights each record equally, and provides an estimate of how the system behaves on randomly chosen records. The ischaemic episodes in the database were detected separately in each lead and the ECG in each lead was pre-processed as described in Section 3.1.2 in order to obtain the overall detection of ischaemic episodes. Figure 3.3 shows an example of detecting an ST episode in record s20131 of the LTST DB using these techniques.

Using the eighty-six ECG recordings in the LTST DB, the proposed algorithm achieved an aggregate gross statistics of 70.6% and 74.7% for the Se and Sp respectively. The average Se and Sp were 68.1% and 72.2%, respectively. The performance of the proposed algorithm on all records is shown in Table 3.2, while the results per recordings are given in Table 3.3.

	Se			**Sp**		
	Gross		**Average**	**Gross**		**Average**
	%	Episodes	%	%	Episodes	%
All records	70.6	798/1130	68.1	74.7	798/1598	72.2

Table 3.2: Overall performance of the proposed algorithm on the ST episodes annotated according to the annotation protocol B of the LTST DB. The gross and average sensitivity, Se and gross and average specificity, Sp, in determining ST events are used to characterise performance.

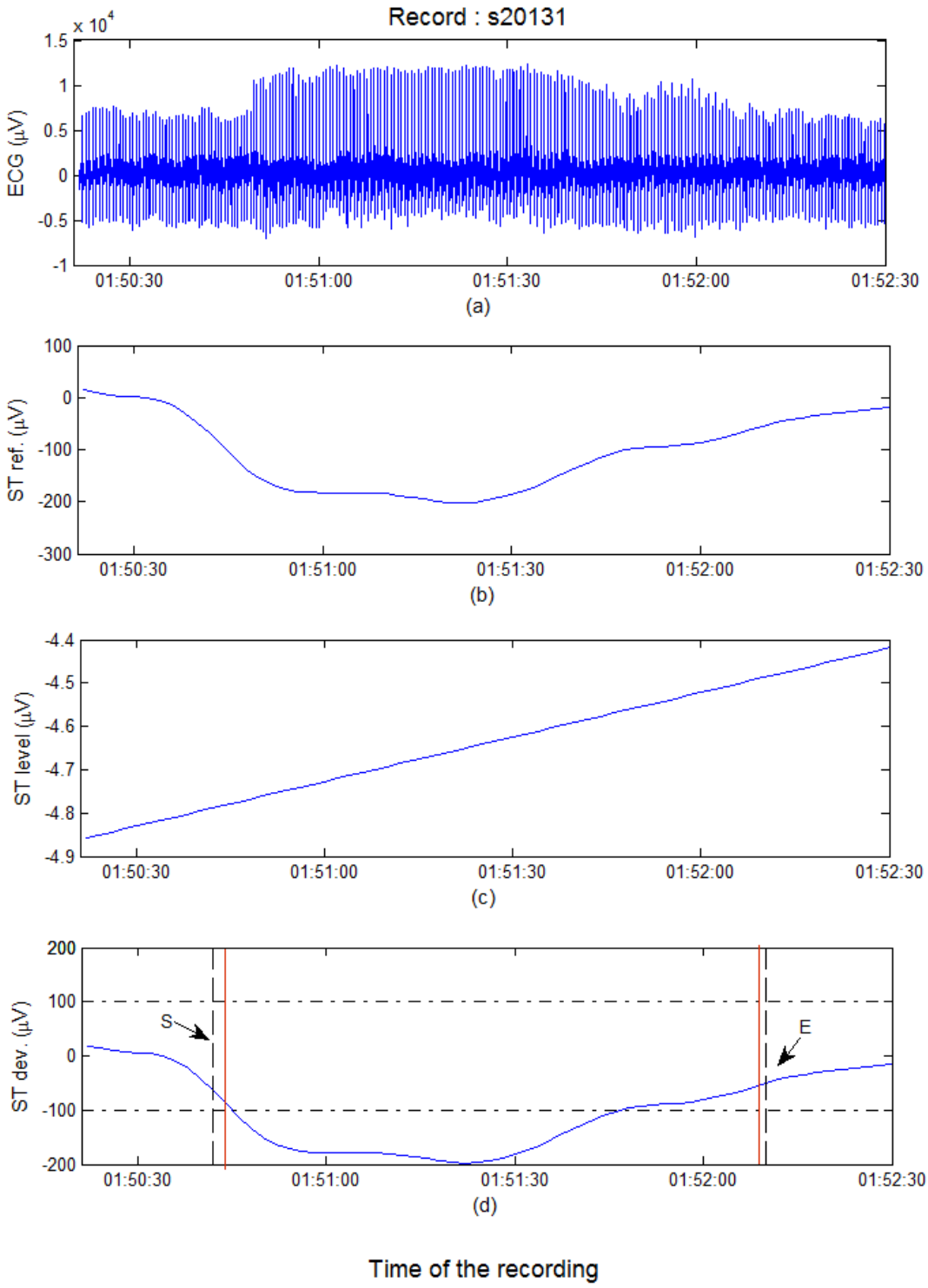


Figure 3.3: An example of a real ischaemic episode of (a) 105 seconds ECG (record s20131 of the LTST DB). The corresponding (b) ST level (c) ST reference (ST ref.), and (d) ST episodes found by our algorithm described in this chapter using the criteria according to protocol B. S and E indicate the start and end of an event as annotated in the database. The solid red lines are the start and end of episode as found by our algorithm. The horizontal dashed lines in (d) indicate the threshold from protocol B used to detect an episode.

Record	ST episodes	Se(%)	Sp(%)
s20011	0/0	-	-
s20021	19/27	73.2	90.5
s20031	4/6	80.0	100.0
s20041	21/29	72.1	61.8
s20051	2/2	100	40.0
s20061	0/0	-	100.0
s20071	0/0	-	-
s20081	26/32	81.3	66.7
s20091	0/0	-	-
s20101	3/3	100.0	100.0
s20111	5/7	71.4	38.4
s20121	4/9	44.4	100.0
s20131	30/31	96.8	76.9
s20141	0/0	-	-
s20151	27/44	61.7	69.2
s20161	37/60	61.7	75.5
s20171	20/26	76.9	71.4
s20181	19/36	61.1	66.7
s20191	5/6	83.3	27.8
s20201	0/0	-	-
s20211	0/0	-	-
s20221	0/0	-	-
s20231	0/0	-	-
s20241	0/0	-	-
s20251	2/6	33.3	16.7
s20261	10/17	58.8	100.0
s20271	41/62	66.1	73.2
s20272	23/25	92.0	85.2
s20273	14/54	53.7	63.1
s20274	53/89	59.6	85.5
s20281	13/15	86.7	81.5
s20291	20/39	51.3	100.0
s20301	28/41	68.3	71.8
s20311	9/10	90.0	50.0
s20321	3/4	75.0	100.0
s20331	6/6	100.0	100.0
s20341	7/7	100.0	100.0
s20351	5/5	100.0	100.0
s20361	2/3	66.7	100.0
s20371	9/9	100.0	100.0
s20381	0/2	0	0
s20391	2/3	66.7	33.3
s20401	5/8	62.5	71.4

Record	ST episodes	Se(%)	Sp(%)
s20411	14/15	93.3	100.0
s20421	11/20	55.0	78.6
s20431	14/15	93.3	87.5
s20441	8/8	100.0	72.7
s20451	5/5	100.0	100.0
s20461	5/5	100.0	100.0
s20471	1/1	100.0	33.3
s20481	7/7	100.0	87.5
s20491	7/7	100.0	100.0
s20501	0/0	-	-
s20511	5/8	62.5	71.4
s20521	0/0	-	-
s20531	0/0	-	-
s20541	0/0	-	-
s20551	4/4	100.0	50.0
s20561	6/8	75.0	75.0
s20571	10/10	100.0	66.7
s20581	3/3	100.0	42.9
s20591	30/55	75.5	85.4
s20601	4/4	100.0	80.0
s20611	25/43	58.1	83.3
s20621	0/0	-	-
s20631	0/0	-	-
s20641	0/0	-	-
s20651	0/0	-	-
s30661	12/22	81.8	81.8
s30671	9/15	60.0	60.0
s30681	23/30	76.7	74.2
s30691	15/23	65.2	93.8
s30701	3/3	100.0	60.0
s30711	14/28	50.0	100.0
s30721	0/2	0	-
s30731	3/7	42.9	100.0
s30732	2/2	100.0	100.0
s30741	9/20	45.0	42.9
s30742	11/19	57.9	61.1
s30751	3/8	37.5	100.0
s30752	4/4	100.0	100.0
s30761	17/23	73.9	100.0
s30771	7/14	50.0	100.0
s30781	0/2	0	-
s30791	0/6	0	-
s30801	0/7	0	-

Table 3.3: Performance of the proposed technique for all ECG recording for the ST episode detection according to the annotation protocol B of the LTST database. The table shows the results of all ST episodes. The second column on the table is correctly detected events / total number of events.

3.6 Results of applying the algorithm to the ESC ST-T database

The proposed technique described in Section 3.3 was tested on the ESC ST-T database (see Section 3.1.1) since most of the ischaemic detection techniques described in the literature have been tested on this database. The results on the ESC DB are given in Table 3.4 which demonstrates that they are comparable with the results obtained by some of the best performing algorithms. The reported Sensitivity for the ESC ST-T database range from 71.0% to 92.1% and the reported specificity ranges from 66.0% to 93.5% as shown in Table 3.1.

	Se			**Sp**		
	Gross		**Average**	**Gross**		**Average**
	%	Episodes	%	%	Episodes	%
All records	87.5	518/592	85.4	74.4	526/707	73.7

Table 3.4: The gross and average sensitivity, Se and gross and average specificity, Sp, of the algorithm proposed in this thesis in determining ST events on the ESC ST-T database.

The thresholds for our algorithm proposed here were optimised on the LTST DB and not re-tuned for the ESC ST-T and which is in contrast to much of the literature and therefore our results should be considered to be similar to performance on the ESC ST-T data. It is also worth mentioning that most of the techniques listed in Table 3.1 are based mainly on neural network and statistical approaches (such as logistic regression). The main disadvantage of these techniques when compared with a knowledge-based approach is their inability to provide explanations for their decisions. This might be a disadvantage from the point of view of the doctor, who expects the decision system to supply explanations for each decision it makes.

In contrast, due to its knowledge-based nature, our proposed algorithm satisfies this important requirement, and it is able to provide the reason that led to that decision for each ischaemic episode. Our algorithm also exhibits the additional desirable features of simplicity and easy and rapid implementation.

3.7 Discussion

This chapter has presented an algorithm for an automated ischaemia detection system. The algorithm uses simple rules, similar to those used by clinicians during the diagnosis of ACS. To remove the mains interference, a low-pass Butterworth filter was applied to the ECG, For baseline wander removal, cubic spline interpolation between isoelectric points on each beat was used to find the baseline which was then subtracted from the ECG. The fundamental component of any ECG based analysis and decision support system is the segmentation of the ECG into its constituent parts such as the QRS complex and ST segment. A rule-based technique was effectively used to find different salient points in the ECG signal. The advantage of the rule-based technique is that it is able to provide for each ischaemic episode, the reason that led to that decision. Therefore, the approach allows for easy addition of rules and provides an institutive explanation of its output.

The performance of the algorithm described in this chapter could be further improved in terms of positive predictive accuracy by further refinement of the noise handling procedure. This can be done by including a signal quality assessment technique to reject regions of the ECG that are too noisy [86]. In addition, extra rules that address the ST slope and T wave inversion as well as the duration and morphology of the QRS complex could be included to increase the sensitivity of the algorithm. Moreover, as will be investigated in the next chapter, both simple and complex classifiers can be used to improve the accuracy of the system and can be introduced to differentiate ischaemic ST events from non-ischaemic ST events.

Chapter 4

Discriminating between ischaemic and non-ischaemic ST changes

As explained in Chapter 2, the changes in the ST segment of the ECG are one of the early markers of transient ischaemia. The ST segment is known to be a highly sensitive but not specific marker, since deviations in the ST segment measurements can result from a wide variety of causes other than ischaemia including changes in heart rate, conduction pattern, position of the subject and noise in the ECG.

Even in subjects who are known to have myocardial ischaemia, ST changes are not considered as a basis for a definitive diagnosis of individual episodes of ischaemia. For example, a previous myocardial infarct may exist and cause permanent distortion in the ST segment, with a persistent abnormal pattern in the frame of reference of the heart. This abnormal pattern appears to change with the subject's body position because of movement of the ECG electrodes relative to the heart's frame of reference. Thus many of those subjects most likely to experience ischaemia are also among those most likely to have non-ischaemic ST changes.

The main focus of this chapter is to describe the design of a system that can distinguish between ischaemic and heart-rate related ST events, which can have very similar ST level pattern. The initial step is to discriminate between ischaemic and heart-rate related ST episodes, using the LTST DB as the test database.

4.1 Existing techniques for discrimination between ischaemic and non-ischaemic ST changes

The dynamics of each type of ST episodes are different. Heart-rate related ST and ischaemic ST episodes are considered to be transient ST segment episodes and are characterized by length and deviation. By contrast, body position and conduction changes are characterized by a sudden shift in the ST level function. Human expert annotators of the LTST DB established a gold standard through manual over-reading. Transient ischaemic and heart-rate related ST segment deviation episodes were annotated based on observation of the ECG morphology and HR trends up to an hour before the event.

Several techniques to automatically detect transient ST segment deviation have been developed using the LTST DB [130–136]. The aim of the 2003 Physionet/Computers in Cardiology (CinC) Challenge [137] was to classify ST changes as either ischaemic episode or non-ischaemic episode (heart-rate related events, body position changes or conduction changes) using a set of freely available annotated records of the LTST DB as a training set and those remaining as a test set. It should be noted that not all annotated ST change episodes from the database were used, but only a selected subset.

The top scoring entry of the CinC 2003 was developed by Langley *et al.* [133] and was based on thresholding. It achieved sensitivity of 99.0% and positive predictivity of 88.8%. The algorithm considered only the change in ST level relative to the baseline ST level (which was provided by the database and manually corrected by experts) within specified time windows. The technique was based on the premise that ischaemic ST changes are large relative to non-ischaemic changes and that they are maintained for a period of time. Langley *et al.* used a threshold to detect ischaemic event and modified the algorithm by using principal component analysis (PCA) to differentiate between ischaemic and non-ischaemic ST episodes.

Smyrnakis and Evans [134] developed a Bayesian inference Multilayer Perceptron (MLP) which was used to classify the episode as ischaemic or non-ischaemic with an accuracy of 89.1%, sensitivity of 82.3% and specificity of 91.2%. The features on which the MLP was

trained included the first four principal components of the ST-T segment. In their paper, they used the automatic relevance determination (ARD) method to identify which of the extracted features used as input in the Bayesian inference MLP were the most important with respect to the model's performance. ARD indicated that a combination of the ST deviation and of the duration of the episode was the most important feature for determining ischaemic episodes, given the data.

Wang *et al.* [130] developed an approach to differentiate between transient ischaemic and non-ischaemic heart-rate related ST segment deviation episodes. Transient ST segment deviation episodes were detected and then classified as ischaemic or heart-rate related using estimates of heart rate variability based on a smoothed Wigner-Ville distribution. The algorithm was developed and tested on a subset of records of the LTST DB. In these records the authors selected specific ST segment deviation episodes and achieved a classification accuracy of 82.2%.

Zimmerman *et al.* [136] used reconstructed phase space as a way of capturing the embedded trajectory of the signal and used the features obtained this way to train a Gaussian mixture model. Using ten-fold cross validation on available training data, they achieved sensitivity and specificity of 81.0% and 88.1% respectively.

Faganeli *et al.* [132] presented a technique that used selected features such as changes of heart rate, changes of time domain, morphologic parameters of the ST segment and changes of the Legendre orthonormal polynomial coefficients of the ST segment for classification using decision trees. The features were obtained at 20-second intervals at the beginning and at the extrema of each ST episode. A sensitivity of 98.1% and a specificity of 85.2% was achieved when classifying ischaemia and heart-rate related episodes using annotation protocol B of the LTST DB.

Dranca *et al.* [131] used time-domain analysis bagging of decision trees. The ST episode detection system achieved sensitivity and positive predictivity of 88.26% and 74.91% respectively using the annotation protocol A of the LTSD database. Minchole *et al.* [135] approached the problem of discrimination between transient ischaemic and artefactual ST segment episodes in Holter recordings by using features such as heart rate changes and several morphology-

change features as well as transient variations in features relating to the QRS complex, the ST segment and the T wave. The proposed technique provided a sensitivity of 84.5% and specificity of 86.6% in discriminating between ischaemic and heart-rate related ST segment deviation episodes.

4.2 Non-linear methodology outline

Although many techniques have been developed to distinguish between ischaemic and heart-rate related ST episodes using a variety of features, there has been little attempt to use non-linear techniques such as neural network and support vector machine algorithms. Ischaemic episodes and heart-rate related episodes have very similar ST level patterns, making them the most problematic events to differentiate using automatic ischaemia detectors. The next section continues by outlining a system developed to overcome this issue.

The technique used to build the system has two stages: feature generation; feature selection and classification. Features are first generated to discriminate between ischaemic and heart-rate related ST events. The feature selection stage is then concerned with finding the best combination of features for discriminating between ischaemic and heart-rate related ST events. The last stage is the training of a classifier to differentiate between ischaemic and heart-rate related ST events. These stages are outlined in the subsections below.

4.3 Feature generation

Using the pre-processing stage described in Section 2.5.1, the high-frequency mains noise was removed, R-peaks were detected using the QRS detector and the baseline wander was removed to enable accurate identification of the isoelectric line. Abnormal beats were removed using a template matching algorithm that only keeps beats when the correlation coefficient between the beats and the template is greater than 0.95 [63]. The ST level was estimated from the beat-averaged ECG, obtained as described in Section 3.4. Additional diagnostic and morphological

features from the ST segment and QRS complex were calculated, including: heart rate; time domain parameters of the ST segment morphology (ST segment, ST slope and root mean square of the sample value from J point to the J point + 120 ms); time domain parameters of the QRS complex morphology such as the duration of the QRS complex; the Mahalanobis distance of the first five PCA coefficients of the QRS complex and ST segment and heart rate variability measures.

To estimate how the values of diagnostic and morphological parameters change during transient episodes, the mean and the standard deviation for each parameter, measured at 20 second intervals, located before the beginning (I_1), right after the beginning (I_2) and around the extrema (I_3), for each ST segment deviation episode were used. A 20-second interval was selected because the length of the shortest episodes is 30 seconds according to the annotation protocols of the LTST DB. 20 seconds is still short enough relative to 30-second episodes to capture the behaviour of the selected parameters along the transient episode. The changes of the mean feature value in interval $\mathrm{I_k}$ with respect to $\mathrm{I_j}$ were computed and included as indices to be used for discriminant analysis. They are given by:

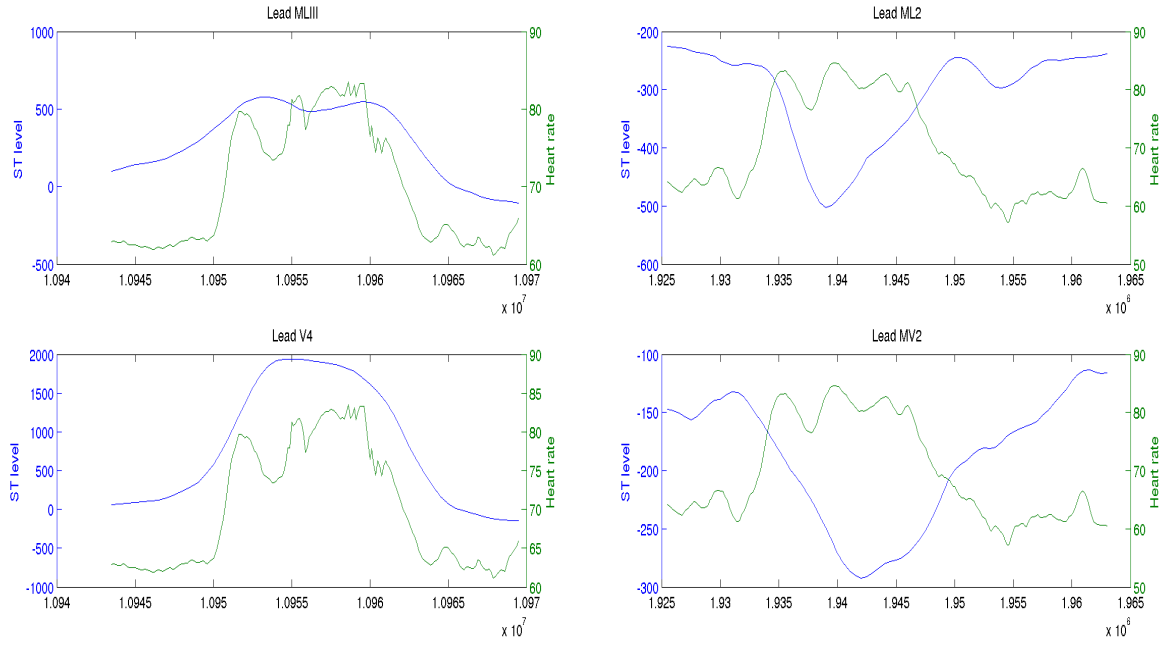
$$\Delta I_{jk} = \frac{\sum_{i \epsilon I_k} I(i)}{N_{I_k}} - \frac{\sum_{i \epsilon I_j} I(i)}{N_{Ij}} \tag{4.1}$$

where i is an integer denoting the i_{th} beat order in intervals I and N_{I_k} and N_{I_j} are the number of beats contained in interval I_k and I_j, respectively.

The subsections below provide some details of the key features.

4.3.1 Heart rate

The selected heart-rate features estimating the heart-rate changes during the ST episodes were, HR_3, $\Delta\mathrm{HR}_{21}$, $\Delta\mathrm{HR}_{31}$ and $\Delta\mathrm{HR}_{32}$, where the subscripts stand for changes in the mean feature value; before the beginning and right after the beginning (21), before the beginning and at the extrema (31) and right after the beginning and the extrema (32) . The change in heart



(a) Ischaemic

(b) Heart-rate related

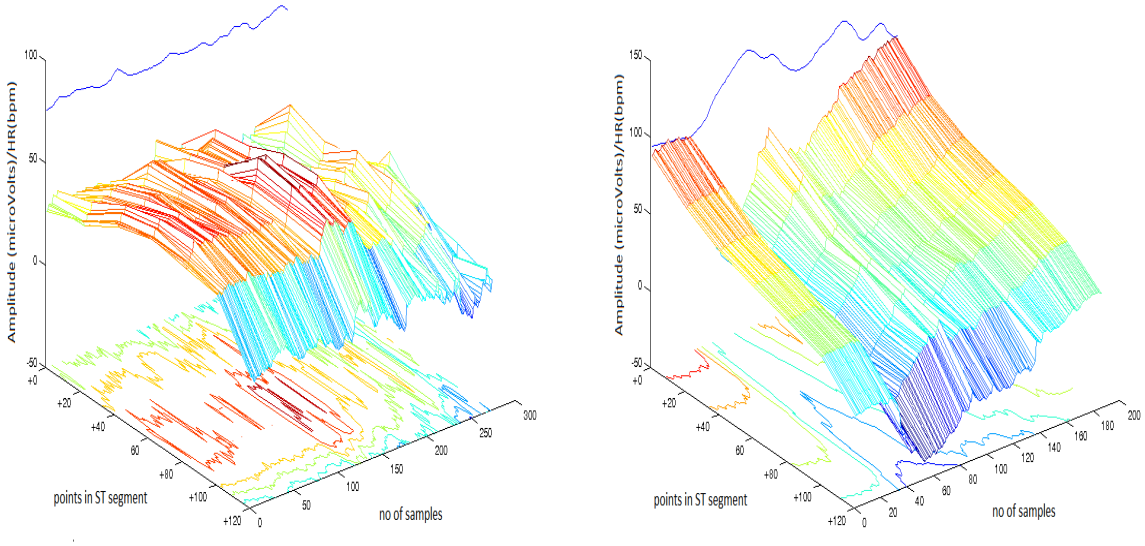
Figure 4.1: Typical transient ischaemic ST segment deviation episode (record, lead, reference), time series of the ST segment deviation (blue) and heart rate, (green). (b) Typical heart-rate related non-ischaemic ST segment deviation (record, lead, reference), time series of the ST segment deviation (blue) and heart rate, (green).

rate in transient ischaemic episodes may or may not be present and the change is usually not simultaneous with the ST segment change as shown by Figure 4.1a. The change may actually precede ischaemia or follow it. In heart-rate related ST segment deviation change, the heart rate change is always simultaneous with the ST segment deviation change, as shown in Figure 4.1b.

Repolarisation indices

As mentioned in Chapter 3, repolarisation for a healthy human ECG typically consists of a characteristic isoelectric segment followed by a T wave. Ischaemia is manifested in repolarisation segment morphology so the ST segment or ST-T segment is generally used to look at changes caused by ischaemia.

The selected-time domain features of the ST segment morphology were the ST segment



(a) Ischaemic

(b) Heart-rate related

Figure 4.2: Evolution of the ST amplitude (J60(80)) with respect to the heart rate for an ischaemic ST segment from record s30651 in the LTST DB (b). Evolution of the ST amplitude with respect to heart rate for heart-rate related non-ischaemic ST segment from record s30651 in the LTST DB.

deviation and the ST segment slope. The ST level, ST, was measured at the point J + 60(80) ms using the procedure described in Section 3.3, while the ST segment slope, SL, was measured from the *J* to the *J + 20 ms* point using $SL_i = J_i + 20\,ms$, where i is the beat number.

These ST segment morphology changes were selected as they are used by clinicians to search for signs of ischaemia and to differentiate ischaemic changes from non-ischaemic changes. Absolute changes in ST level were considered for classification and are represented by $\Delta\mathrm{ST}_{32}$, $\Delta\mathrm{ST}_{21}$ and $\Delta\mathrm{ST}_{31}$. Absolute changes in ST slope were also considered for the classification analysis for each of the intervals and are denoted by $\Delta\mathrm{SL}_{32}$, $\Delta\mathrm{SL}_{21}$ and $\Delta\mathrm{SL}_{31}$.

Figure 4.2 shows the evolution of ST segment amplitude during an ischaemic and heart-rate related ST event respectively. The figure shows that there are no differences in the evolution of the ST segment during ischaemic and heart-rate related ST .

In addition, the root mean square (RMS) of the ST segment shape change, estimating the morphology change of the entire ST segment and was calculated using Equation 4.2. The

hypothesis here is that measuring differences in the area under the ST segment is more robust than measuring the ST level itself, since it includes information about changes in energy for this segment [138].

$$ST_{RMS} = \sqrt{\frac{1}{n} \sum_{n=0,\ldots,120} (x_{I_k}(\overline{st}(i,j,J_{i,j}+n)) - x_{I_j}(\overline{st}(i,j,J_{i,j}+n)))^2} \tag{4.2}$$

where $\overline{st}(i,j,J_{i,j}+n)$ represents the ST segment levels obtained on the average beats composed from non-noisy heart beats in the second window at the selected points $J_{i,j} + 20\,ms$ along the ST segment, where $J_{i,j}$ denotes time in milliseconds of the *J* point of the j^{th} beat in the i^{th} lead and n equals $0, \ldots, 120$. The ST segment was assumed to be from 120 ms long since the duration of ST segment is usually between 80 ms and 120 ms [57]. As with the other measures the absolute difference between the intervals were computed to give the, $\Delta ST_{RMS_{31}}$, $\Delta ST_{RMS_{21}}$ and $\Delta \mathrm{ST}_{\mathrm{RMS}_{32}}$.

4.3.2 Heart rate variability as a feature

The two measures that were computed to be included in the feature vector are; Standard Deviation of the Averages of NN (Normal Sinus to Normal Sinus) (SDANN) intervals in all 5-minutes windows of a recording; and the ratio of the low frequency component to the high frequency component of the power spectral density (PSD), *LF/HF-ratio*. The HF power spectrum is evaluated in the range from 0.15 to 0.4 Hz. while the HF power spectrum is evaluated in the range from 0.04 to 0.15 Hz.

The heart rate variability measures were computed using a five minute window before the start of an episode. The *LF/HF-ratio* was obtained from the PSD that was estimated using the Lomb-Scarlge periodogram which requires no resampling of the unevenly-sampled time series [76]. In Lomb's method the data are weighted on a point by point basis rather than on per time interval basis as in conventional Fast Fourier Transform. The computation of the Lomb periodogram is equivalent to linear least-square fitting a sinusoid of angular frequency (ω) to the data. A detailed explanation on how these measures were computed can be found in Section

2.7.2.

4.3.3 Depolarization Indices

Atrial depolarization is represented by the PR interval (the time from the onset of atrial depolarization to the onset of ventricular depolarization) and the QRS complex (which represents ventricular depolarization). Various measures of the depolarization of the heart have been shown to be effective in detecting ischaemia and hence in this work, some of the measures were included in the attempt to discriminate between ischaemic and heart-rate related ST episodes.

QRS slope

Changes also occur in the depolarization phase (QRS complex) of the ECG during acute ischaemia that could assist in accurate diagnosis. However, these changes are more difficult to characterize and are not used in clinical practice. Some of the changes are considered to represent already necrotic areas (Q waves), but other, potentially reversible changes in the QRS complex also appear. Several studies have reported changes in the depolarization phase both in animals and humans. These include changes in QRS amplitude [139–141] and amplitude changes of the R and S waves [141]. Changes in high-frequency QRS components of the high-resolution signal-averaged ECG have been reported as well [142]. In recent years, changes in the QRS slope have also been reported [143].

Earlier studies on coronary occlusion have considered QRS prolongation amplitude changes of the R and S waves, distortion of the terminal part of the QRS complex and changes in the high-frequency content of the QRS complex. Prolongation of the QRS complex has been described as a marker of more severe ischaemia with slow conduction, both in animal studies and human studies during percutaneous coronary intervention (PCI) and acute myocardial infarction (AMI) [139].

In recent years, Pueyo *et al.* [140] developed a technique for characterising changes in the QRS due to both amplitude and duration changes by measuring the upslope and downslope of the R wave. The method was tested during myocardial ischaemia induced by elective percu-

taneous coronary intervention and this study showed both intra-individual variability and inter-individual variability of the QRS slope. Romero *et al.* [144] using a population of patients undergoing elective PCI, showed that changes of the downward slope are more pronounced than upslope changes regardless of the coronary vessel occluded. The method for computing the QRS slopes is described below.

Computing QRS slopes The QRS slopes were extracted from the ECG using the techniques outlined below. The ECG was pre-processed as before. Abnormal beats were removed using a template matching algorithm that keeps the beats only if the correlation coefficient between the beats and template is greater than 0.95. Beats for which no R-wave peak were present were rejected for analysis.

The procedure for finding the upward and downward slope of the R-wave start by locating the R-peak, $\mathrm{n_R}$. The starting point, $\mathrm{n_U}$, was found by traversing 20 milliseconds backwards from the Rpeak and the end point, $\mathrm{n_D}$, was found by moving forward 20ms from the Rpeak. The 20 milliseconds was chosen empirically. To find the upward slope, $\mathrm{I_{US}}$, a line was fitted using least-square fit between $\mathrm{n_U}$ and $\mathrm{n_R}$+ 0.5 ms. The 0.5 ms was used to ensure that the line is fitted on the correct side of the R-peak. Similarly, to find the downward slope, $\mathrm{I_{DS}}$, a line was fitted between ($\mathrm{n_R}$-0. 5ms) and $\mathrm{n_D}$. The procedure to find the slope is shown graphically in Figure 4.3.

An example of temporal evolution of the $\mathrm{I_{US}}$ and $\mathrm{I_{DS}}$ from record s20031 during an ST episodes is shown in Figure 4.4.

To reduce the influence of noise the QRS slopes were median filtered using a 10 second window. For classification purposes the absolute mean difference between the different intervals was computed for the upslope and downslope. This gave $\Delta\mathrm{QRS_{US_{31}}}$, $\Delta\mathrm{QRS_{US_{21}}}$, $\Delta\mathrm{QRS_{US_{32}}}$ for the upslope and $\Delta\mathrm{QRS_{DS_{31}}}$, $\Delta\mathrm{QRS_{DS_{21}}}$, $\Delta\mathrm{QRS_{DS_{32}}}$ for the downslope.

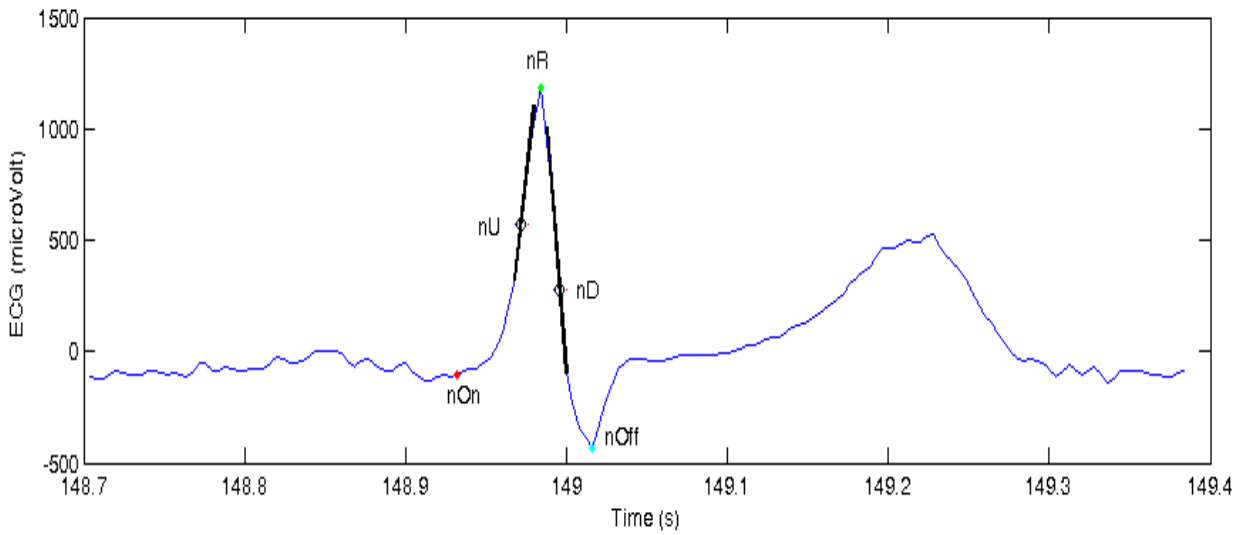


Figure 4.3: Example showing the delineation using the number of samples to evaluate the QRS slopes.

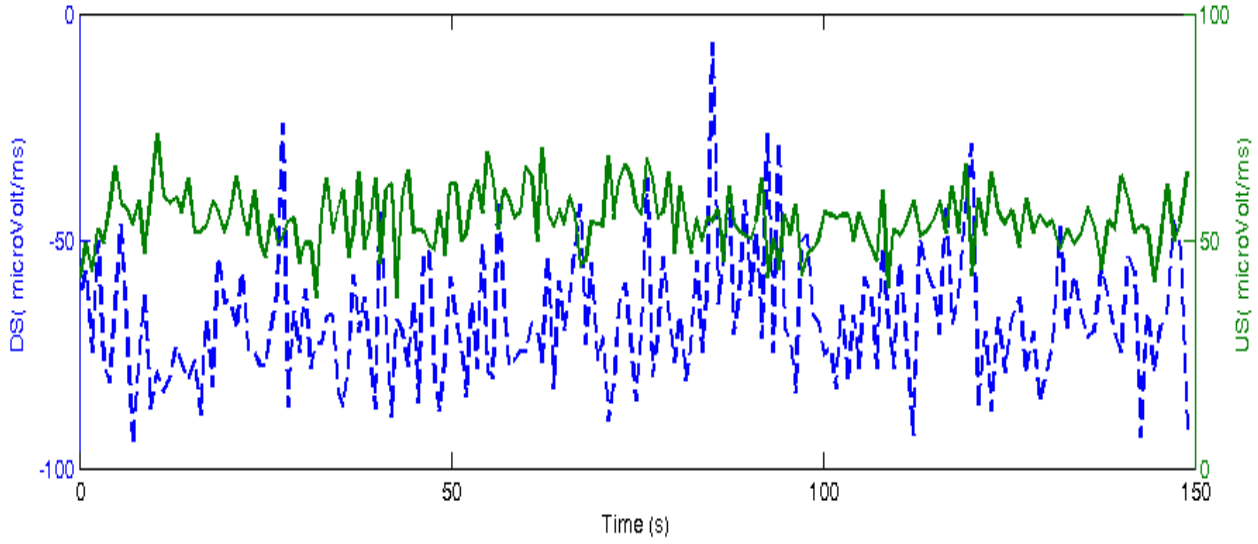


Figure 4.4: An example of temporal evolution of the upslope, I_{US}, and downslope, I_{DS}, during an ST episode.

4.3.4 QRS complex features

In addition to the ST segment morphology features, time-domain features from the QRS complex were also extracted. The features that were selected for estimating QRS morphology changes during the ST episodes were the root mean square of the signal from the onset to the peak of the QRS complex ($\mathrm{QR_{RMS}}$) and the root mean square of the signal from the peak to the offset of the QRS complex, ($\mathrm{RS_{RMS}}$). Also the duration of the QRS complex, $\mathrm{QRS_{DUR}}$ was taken to be from the onset to the offset of the QRS complex . The absolute values of these changes were as classification features and were denoted by $\Delta\mathrm{QRS_{DUR_{32}}}$, $\Delta\mathrm{QRS_{DUR_{21}}}$ and $\Delta\mathrm{QRS_{DUR_{31}}}$. As before, the change in the RMS value of the QR and RS intervals were denoted as $\mathrm{QR_{RMS_1}}$, $\mathrm{QR_{RMS_2}}$, $\Delta\mathrm{QR_{RMS_{32}}}$ and $\mathrm{RS_{RMS_1}}$, $\mathrm{RS_{RMS_2}}$ and $\mathrm{RS_{RMS_3}}$. The absolute values of these changes were also considered as classification features and denoted by $\Delta\mathrm{QR_{RMS_{32}}}$, $\Delta\mathrm{QR_{RMS_{21}}}$, $\Delta\mathrm{QR_{RMS_{31}}}$, $\Delta\mathrm{QR_{RMS_{32}}}$, $\Delta\mathrm{QR_{RMS_{21}}}$ and $\Delta\mathrm{QR_{RMS_{31}}}$.

4.3.5 Feature extraction using Principal Component Analysis

While the time-domain ST segment feature vector described in the previous sections provides a direct measurement of ST segment patterns, principal component analysis (PCA) based on the QRS complex and the ST-T segment morphology vector provides efficient feature extraction with the potential to capture subtle morphology features differentiating between transient ischaemic and heart-rate related non-ischaemic ST segment episodes [109]. Moreover, the principal components of the QRS complex and ST segments have already been used to differentiate between true ischaemic ST segment changes and non-ischaemic ST deviations caused by axis shifts [109]. The other motivation for the use of PCA was dimensionality reduction.

PCA is a statistical technique whose purpose is to condense the information of a large set of correlated variables into a few variables ("principal components"), while not throwing overboard the variability present in the data set [109]. The principal components are derived as a linear combination of the variables of the data set, with weights chosen so that the principal components become mutually uncorrelated. Each component contains new information about

the data set, and is ordered so that the first few components account for most of the variability.

The signal segment of a beat is represented by the column vector

$$x(n) = \begin{pmatrix} x_1 \\ x_2 \\ \vdots \\ x_N \end{pmatrix} \tag{4.3}$$

where N is the number of samples in the segment. The segment is often extracted from several successive beats, thus resulting in an ensemble of M beats. The entire ensemble is compactly represented by the $N \times M$ data matrix,

$$X = [x(1)x(2)\ldots x(M)] \tag{4.4}$$

The beats $x_1, \ldots, x_M$ can be viewed as M observations of the random process x. While this formulation suggests that all beats considered originate from one patient, the beats may alternatively originate from a set of patients depending on the purpose of the analysis. The derivation of principal components is based on the assumption that the signal x is a zero-mean random process being characterized by the correlation $R_x = E[xx^T]$. The principal components of x result from applying an orthonormal linear transformation $\Psi = [\psi_1\psi_2\ldots\psi_N]$ to x is given by, $w = \Psi^T x$, so that the elements of the principal component vector $w = [w_1 w_2 \ldots w_N]^T$ become mutually uncorrelated. The first principal component is obtained as a scalar product $w_1 = \psi_1^T x$ where the vector ψ_1 is chosen so that the variance of w_1 given by,

$$E[w_1^2] = E[\psi_1^T x x^T \psi_1] = \psi_1^T R_x \psi_1 \tag{4.5}$$

is maximized subject to the constraint that $\psi_1^T\psi_1 = 1$. The maximal variance is obtained when ψ_1 is chosen as the normalized eigenvector corresponding to the largest eigenvalue of R_x,

as denoted λ_1; the resulting variance is

$$E[w_1^2] = \psi_1^T R_x \psi_1 = \lambda_1 \psi_1^T \psi_1 = \lambda_1 \tag{4.6}$$

Subject to the constraint that w_1 and the second principal component w_2 should be uncorrelated, w_2 is obtained by choosing ψ_2 as the eigenvector corresponding to the second largest eigenvalue of R_x and so on until the variance of x is completely represented by w. Accordingly, to obtain the whole set of N different principal components, the eigenvector equation for R_x needs to be solved,

$$R_x \Psi = \Psi \Lambda \tag{4.7}$$

where Λ denotes a diagonal matrix with the eigenvalues $\lambda_1, \ldots, \lambda_N$. Since R_x is rarely known in practice, the $N \times N$ sample correlation matrix, defined by

$$\hat{R}_x = \frac{1}{M} X X^T \tag{4.8}$$

replaces R_x when the eigenvectors are calculated in Equation 4.8. Applying PCA to an ensemble of beats X, the associated pattern of principal components reflects the degree of morphologic beat-to-beat variability. When the eigenvalue associated with the first principal component is much larger than those associated with the other components, the ensemble exhibits a low morphologic variability, whereas a slow fall-off of the principal component values indicates a large variability. In most applications, the main goal of PCA is to concentrate the information of x into a subset of components, that is, $w_1, \ldots, w_k$, where $K < N$, while retaining the physiological information. The choice of K may be guided by various statistical performance indices, of which one index is the degree of variation $\Re_K$, reflecting how well the subset of K principal components approximates the ensemble in energy terms,

$$R_K = \frac{\sum_{k=1}^{K} \lambda_k}{\sum_{k=1}^{N} \lambda_k} \tag{4.9}$$

In practice, however, K is usually chosen so that the performance is clinically acceptable and so that no vital signal information is lost. The above derivation results in principal components that characterize intra-beat correlation. However, it is equally useful to define an $M \times M$ sample correlation matrix

$$R_x = \frac{1}{N} X^T X \tag{4.10}$$

in order to characterise interbeat correlation. In this case, the principal components are computed for each sample n rather than for every beat as was done in

$$w(n) = \lambda^T x(n) \tag{4.11}$$

where

$$x(n) = \begin{pmatrix} x_1(n) \\ x_2(n) \\ \vdots \\ x_M(m) \end{pmatrix} \tag{4.12}$$

and Λ^T is the eigenvector matrix of R_x.

Transient non-ischaemic ST segment changes may be efficiently differentiated from real ischaemic ST changes by tracking the QRS complex morphology changes independently of the ST segment morphology changes. It is therefore appropriate to derive two sets of eigenvectors basis functions, one from the data window covering the PQ segment and the QRS complex and the other from the data window covering the ST segment and initial portion of the T wave [109]. In deriving the features, first estimates of the QRS complex amplitudes taken at Rpeak - 96 ms and Rpeak + 24 ms were extracted for each beat after baseline removal. The set for the ST segment was taken from Rpeak + 40 ms to Rpeak + 160 ms.

The distance functions used for each complex (QRS and ST-T) are simply the distance series between each normalized eigenvector (in which only the first five components as they

contain 98% of the variance of the signal are considered) and a mean reference value:

$$I^{e}_{PCA} = \sqrt{\sum_{j=1}^{4} \alpha^{l}_{j}\theta_{i} - \alpha^{l}_{j}r^{2}} \tag{4.13}$$

with α^{l}_{j} and θ_{i} being the j_{th} order eigenvalue and eigenvector respectively at beat i estimated for the lth lead. The Mahalanobis of the first five principal components of the ST segment estimating the ST segment morphology change during the ST episodes and the absolute changes of the ST segment morphology are given by $\Delta\mathrm{ST}_{\mathrm{MD}_{21}}$, $\Delta\mathrm{ST}_{\mathrm{MD}_{31}}$ and $\Delta\mathrm{ST}_{\mathrm{MD}_{32}}$.

The Mahalanobis distance of the first five eigenvectors of the QRS complex, the change during the QRS episodes and the absolute changes of the Mahalanobis distance of the first five principal components of the QRS complex are given $\Delta\mathrm{QRS}_{\mathrm{MD}_{21}}$, $\Delta\mathrm{QRS}_{\mathrm{MD}_{31}}$ and $\Delta\mathrm{QRS}_{\mathrm{MD}_{32}}$, respectively.

4.4 Feature selection

Feature selection, also known as variable selection, feature reduction, attribute selection or variable subset selection, are techniques for selecting a subset of relevant features for building robust learning models. With a limited amount of training data, excessive features will not only significantly slow down the learning process, but also cause the classifier to overfit the training data. Thus removing the most irrelevant and redundant features helps improve the performance of learning models by alleviating the effect of the curse of dimensionality, enhancing generalization capability, speeding up the learning process and improving model interpretability [145].

Feature selection algorithms typically fall into two categories: feature ranking and subset selection. Subset selection evaluates a subset of features as a group for suitability. Subset selection algorithms can be broken into Wrappers, Filters and Embedded [145]. Wrappers use a search algorithm to search through the space of possible features and evaluate each subset by running a model on the subset. Wrappers can be computationally expensive and have a risk of over fitting to the model. Filters are similar to Wrappers in the search approach, but instead of

evaluating against a model, a simpler filter is evaluated. Embedded techniques are embedded in and specific to a model.

Feature ranking sorts the features by a metric and eliminates all features that do not meet the criteria [145]. In statistics the most popular form of feature selection is stepwise regression, which is a greedy algorithm that adds the best feature or deletes the worst feature at each round.

4.4.1 Stepwisefit method

Stepwise regression is a systematic method for adding and removing terms from a multi-linear model based on their statistical significance in a regression [146]. The method begins with an initial model and then compares the explanatory power of incrementally larger and smaller models. At each step, the p-value is computed to test models with and without potential features. If a feature is not currently in the model, the null hypothesis is that the feature would have a zero or nearly zero coefficient if added to the model. If there is sufficient evidence to reject the null hypothesis, the feature is added to the model. Conversely, if a feature is currently in the model, the null hypothesis is that the feature has a zero coefficient. If there is insufficient evidence to reject the null hypothesis, the feature is removed from the model. This technique was used to decide which feature is added to the subset of features to be used for training the classifier.

4.5 Performance measures

In addition to the performance measures described in Chapter 2, additional measures were introduced to assist with model selection and comparison. The first measure investigated at was the receiver operator characteristic (ROC) curve and measures related to it, specifically the area under curve (AUC). The ROC curve is a graphical plot of the sensitivity and false positive rate for a binary classifier system as its discrimination threshold is varied. The AUC is equal to the probability that a classifier will rank a randomly chosen positive instance higher than a randomly chosen negative one [147].

Mapping an output to classes requires the definition of a threshold to be used as the boundary between two classes. The aim is to maintain an adequate balance between low numbers of False Positive (FPs) and False Negatives (FNs), thereby minimizing false diagnosis of ischaemia and missed ischaemic ST episodes simultaneously.

4.6 Classification

There are different machine learning methods that could be used to discriminate between ischaemic and heart-rate related ST episodes. In this chapter, four different types of machine learning tools are investigated. The first technique is linear regression which finds a linear combination of features to separate the two classes. The second technique is the multi-layer perceptron a feedforward artificial neural network with non-linearities. The third classifier is a Support Vector Machine and the last technique is a Bayesian-based system called the Relevance Vector Machine.

4.6.1 Linear regression

A linear regression model for classification can be built by assigning an output value to each of the two classes (e.g. 1 and 0) and modelling this output as a linear sum of the input variables [148]. Equation 4.14 gives a linear regression equation for $n = N$ input variables:

$$y = \beta_o + \beta_1 x_1 + \beta_2 x_2 + \beta_3 x_3, \ldots, + \beta_n x_n \tag{4.14}$$

The $(N + 1)$ regression coefficients β_0 to β_N are typically calculated using a least-squares method on the training set [148], although other methods may be used if the training set is expected to contain outliers which would skew the results. In this work, the least-square fit was used as is less sensitive to outliers in the data[148].

4.6.2 Neural networks

Neural networks are most commonly used as function approximators which map the inputs of a process to a set of outputs. The reason for their wide spread use is that, assuming no restriction on the architecture, neural networks are able to approximate any continuous function of arbitrary complexity [145].

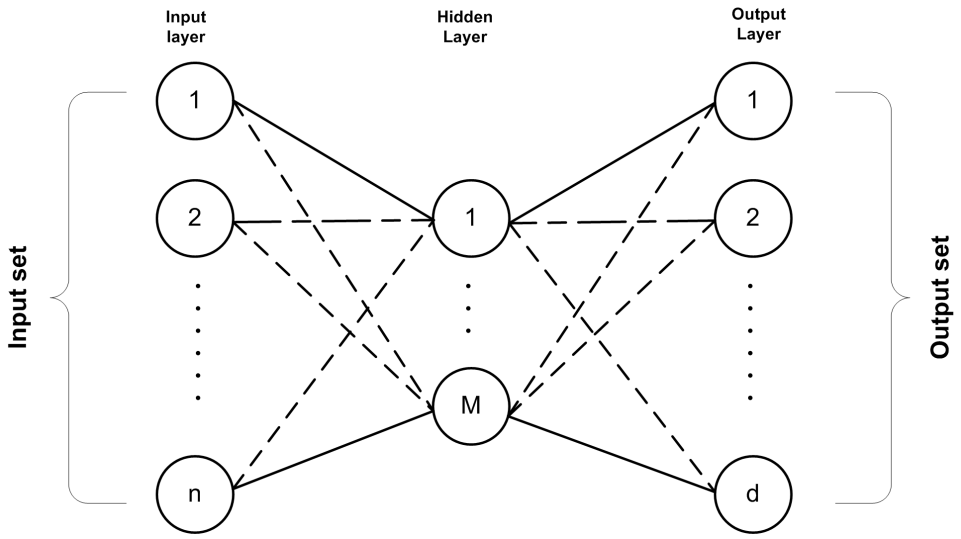


Figure 4.5: Diagram of a generalised neural network model.

The diagram of a generalised neural network model is shown in Figure 4.5. The mapping of the inputs to the outputs using a multilayer perceptron (MLP) neural network can be expressed as follows:

$$y_k = f_{outer}\left(\sum_{j=1}^{M} w_{jk}^{(2)}\left(\sum_{i=1}^{d} w_{ji}^{(1)} x_i + w_{j0}^{(1)}\right) + w_{k0}^{(2)}\right) \tag{4.15}$$

In Equation 4.15, $w_{ji}^{(1)}$ and $w_{jk}^{(2)}$ indicate the weights in the first and second layers, respectively, going from input i to hidden unit j and hidden unit j to output unit k. M is the number of hidden units, d is the number of output units while $w_{j0}^{(1)}$ indicates the bias for hidden unit j and $w_{k0}^{(2)}$ indicates the bias for output unit k. For simplicity the biases have been omitted from the diagram in Figure 4.5.

The weights of the neural network can be 'optimised' via error backpropagation training using, most commonly, scaled conjugate gradient training [148]. The cost function repres-

enting the objective of the training of the neural network can be defined. The objective is to obtain optimal weights which accurately map the inputs to the outputs. If the training set $D = \{x_k, y_k\}_{k=1}^{N}$ is used, the cost function, *E*, may be written using the cross-entropy cost function as follows [148]:

$$E = -\beta \sum_{n}^{N} \sum_{k}^{K} \zeta \ln(y_{nk}) + (1 - t_{nk}) \ln(1 - y_{nk}) + \sum_{j}^{k} \frac{\alpha_j}{2} \gamma_j^2 \tag{4.16}$$

This cross-entropy function has been chosen because it has been found to be more suited to classification problems than the sum-of-square of error cost function [148]. In Equation 4.16, n is the index of the training pattern, hyperparameter β is the data contribution to the error, k is the index for the output units, t_{nk} is the target output corresponding to the n_{th} training pattern and k_{th} output unit and y_{nk} is the corresponding predicted output. The third term (γ) in the expression is the regularisation parameter which penalises weights of large magnitudes. The regularisation parameter coefficient, α, determines the relative contribution of the regularisation term to the training error. The presence of the regularisation parameter gives significant improvements in the generalisation ability of the network [148]. The NETLAB toolbox was used to implement the neural network [149].

The only parameters to be selected are the number of inputs and the number of hidden-layer units. The mean validation cross-entropy and the area under the curve (AUC) were the criteria used to select models.

4.6.3 Support Vector Machine

The Support Vector Machine SVM has been studied extensively for classification, regression and density estimation. Based on the principle of structural risk minimization (SRM), SVM maximizes the expected risk (mean error rate measured on the test set) using the sum of the empirical risk (mean error rate measured on the training set) and a bound, called the Vapnik-Chervonenkis (VC) confidence. In order to construct an optimal decision hypothesis the SVM holds the empirical risk fixed and minimizes the VC confidence by limiting the flexibility of

the set of candidate functions searched by the machine. The minimum of this upper bound is reached by maximizing the margin between the decision hypothesis and the classes as defined using support vectors, thereby enabling the improvement of the classifier generalization ability. The construction of SVMs has been described extensively in the literature [150, 151]. A mathematical formulation for SVM is found in Appendix A.

An SVM is basically a linear learning machine based on the principle of optimal separation of classes and was initially designed to solve classification problems. The aim is to find a linear separating hyperplane that separates classes of interest. The linear separating hyperplane is placed between classes in such a way that it satisfies two conditions. First, all data vectors that belong to the same class are placed on the same side of the hyperplane. Second, the distance between the closest data vectors in the two classes is maximized [150]. In other words, the optimum hyperplane is the one that leaves the maximum margin between the two classes, where margin is defined as the sum of the distances of the hyperplane from the closest data vectors of the two classes. For each class, the data vectors forming the boundary of classes are located on supporting hyperplanes and these data vectors are called the Support Vectors [152]. When a linear separating hyperplane is not able to classify input data without error, the data are transformed to a higher dimensional space using a non-linear transformation function that spreads the data apart such that a linear separating hyperplane may be found in that space. Due to the very large dimensionality of the feature space, it is practically not possible to compute the inner product of two transformed data vectors. This may, however, be achieved by using a kernel function instead of the inner product [150].

Because SVMs do not model the data distribution in their formulation, but instead directly minimise the classification error, the resultant output is a binary decision. Even though a binary decision boundary is sufficient for many applications, it may not be enough when a meaningful, probabilistic interpretation of the decision process is required [153].

4.6.4 Relevance Vector Machine

The Relevance Vector Machine (RVM) has the same functional form as the SVM, but is embedded into a Bayesian framework. That is, an RVM outputs probabilities of class membership rather than point estimates like SVM. This provides a conditional distribution that allows the expression of uncertainty in the prediction [153]. Hence, the RVM, which is a special case of the sparse Bayesian learning algorithm, can be regarded as the Bayesian extension of the support vector machine approach. The mathematical formulation of RVM is found in Appendix B.

A classification problem involving two data classes, namely $\mathcal{C}_1$ and $\mathcal{C}_2$, is considered using the sparse Bayesian learning approach. The posterior probability of the target value of an input variable corresponding to class $\mathcal{C}_1$ is given by $p(y_n = 1|x_n, w) = \sigma(f(x_n))$, $n = 1, \ldots, N$, where $\sigma(\cdot)$ is the logistic sigmoidal function defined by $\sigma(s) \triangleq 1/(1+e^{-s})$. Assuming that the input variables x_n, $n = 1, \ldots, N$ are independent, the likehood function is given by:

$$p(y|x, w) = \prod_{n=1}^{N} \sigma f(x_n)^{y_n} [1 - \sigma(f(x_n))]^{1-y_n} \tag{4.17}$$

$$\sigma(f(x)) = \frac{1}{1 + exp(-y(x))} \tag{4.18}$$

To obtain $p(y|x, w)$, an iterative method is used. Let α_n^* denote the maximum a posteriori estimate of the hyperparameter α_n. The maximum a posteriori estimate of the weights (W_m) can be obtained by maximizing the following objective function:

$$f(w_n) = \sum_{n=1}^{N} logp(y_n/w_n) + \sum_{n=1}^{N} logp(w_n/\alpha_n^*) \tag{4.19}$$

where the first summation term corresponds to the likehood of the class labels and the second term corresponds to the prior on the parameter w_n. In the final solution the gradient of f with respect to w is calculated and the training data have zero coefficients w_n (relevance vectors) contributing to the decision function. The posterior is approximated around W_m by a

Gaussian approximation with covariance $\Sigma = -(H|_{w_m})^{-}$ and mean $\mu = \Sigma \Psi^T Bc$, where H is the Hessian of f, matrix Ψ has elements $\phi = K(x_n, x)$ and B is a diagonal matrix with elements defined by $\sigma(y(x_n))[1 - \sigma(y(x_n))]$. An iterative analysis follows in which the hyperparameters α_n associated with each weight are updated to find the set of weights that maximize Equation B.3. A block diagram illustration of the various steps used by the RVM algorithm is given in Figure 4.6.

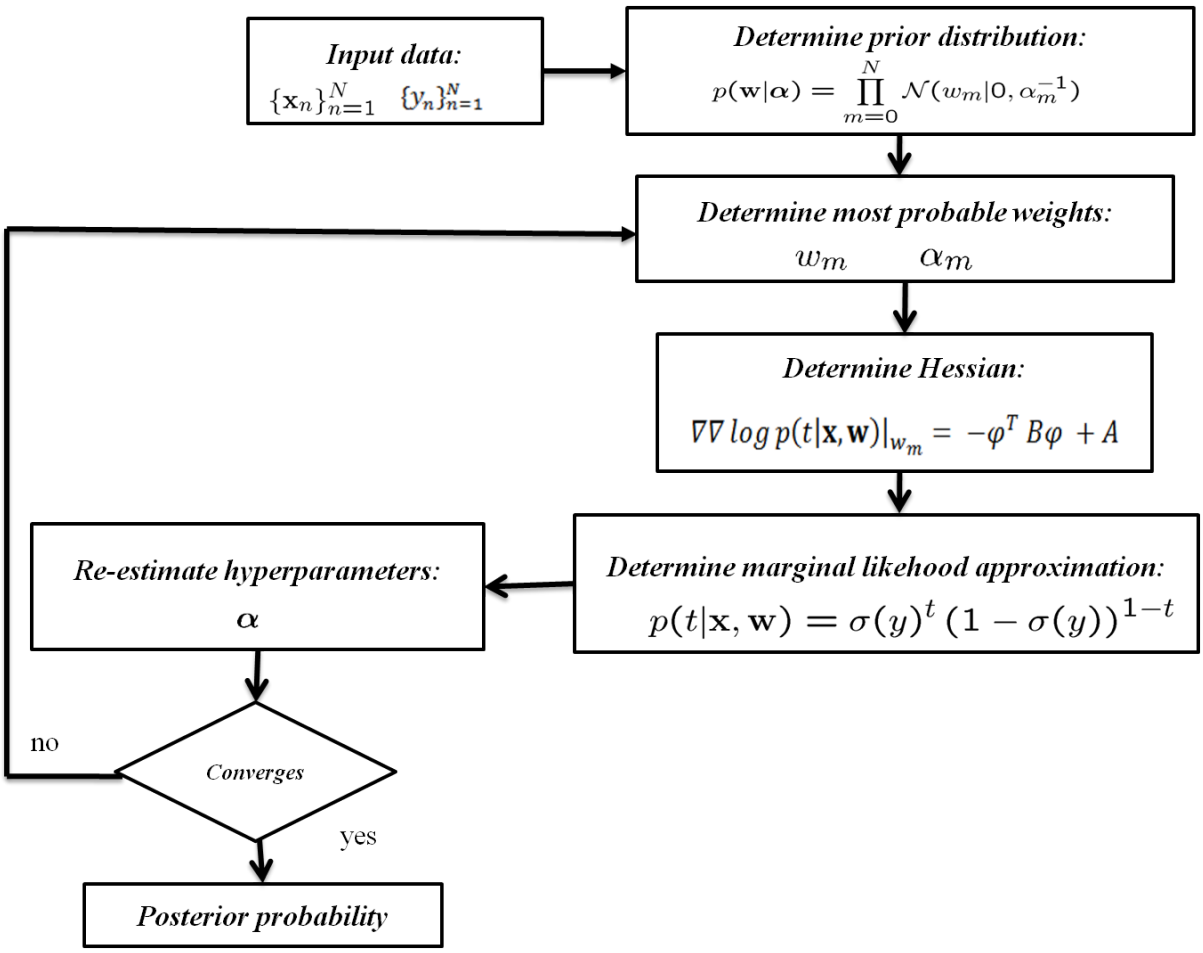


Figure 4.6: Block diagram of the RVM.

4.7 Experimental methods

As shown in Table 4.1, the dataset is unbalanced. In statistics, resampling is any of a variety of methods for either attempting to estimate the precision of sample statistics (medians, variances,

percentiles) by using subsets of available data (jackknifing) or drawing randomly with replacement from a set of data points (bootstrapping) or validating models by using random subsets (bootstrapping, cross validation). The two techniques that were implemented in this thesis are cross-validation and bootstrapping and these are described briefly below.

4.7.1 Cross-validation

Cross-validation is a method for estimating the generalization error and for that reason can be used to compare two or more learning models and estimate which model will perform best on the problem at hand. With *n*-fold cross-validation, the available training data is partitioned into *n* disjoint subsets, the union of which is equal to the original training set. Each learning model is trained on *n-1* of the available subsets and then tested on the one subset that was not used during training. This process is repeated *n* times, each time using a different test set chosen from the n available partitions of the training data, until all possible choices for the test set have been exhausted. The *n* test set scores for each learning model are then averaged (or summed) and the model with the highest average test set score is chosen as the most likely to perform well on unseen data.

4.7.2 Bootstrapping

Bootstrapping is a statistical method for estimating the sampling distribution of an estimator by sampling with replacement from the original sample, most often with the purpose of deriving robust estimates of standard errors and confidence intervals of a population parameter like a mean, median, proportion, odds ratio, correlation coefficient or regression coefficient [148]. It may also be used for constructing hypothesis tests. It is often used as a robust alternative to inference based on parametric assumptions when those assumptions are in doubt, or where parametric inference is impossible or requires very complicated formulas for the calculation of standard errors.

The classifiers were trained using bootstrapping and the procedure used to train and test

the classifier (see Algorithm 1). Firstly N episodes were randomly selected from ischaemic ST episodes and an equal number selected from heart-rate related ST episodes. This formed a new subset of the original data with equal amount of data from both classes within the inner loop, the algorithm starts by separating the data into training and testing sets. Both the testing and training sets contain equal numbers of ischaemic and heart-rate related ST episodes. Once the testing and training sets have been created, the statistics of the training data was used to normalize the patterns both data sets. The classifiers were tested by presenting them with the testing data and the performance metric was calculated.

Algorithm 1 Pseudo-code for Bootstrapping

for $m = 1$ to maximum number of iterations
randomly select N data points from ischaemic and heart rate-related ST episodes dataset
for $n = 1$ to 100
1. use bootstrapping to separate data into training and testing sub-sets
2. normalize all data using coefficients from training set
3. build a classifier
4. test classifier using testing sub-set to get performance measures

end
Create ROC curve and average statistics
end

4.7.3 Data processing

Before applying a machine learning algorithm, the data need to be pre-processed. One of the most common forms of data preprocessing consists of rescaling the input variables. The two most popular normalization techniques are min-max normalization and zero mean unit variance. Min-max normalization performs a linear transformation of the training data and preserves the relationship among features in the training data. The features are usually rescaled to lie between [0,1] or [-1,1]. The main disadvantage of this technique is that if the maximum value in the testing data is greater than in the training data, the normalized testing data falls outside the bounds. In zero mean unit variance normalization the features are normalized based on the mean and standard deviation of the training data. The transformation is carried out by

calculating the sample mean μ and standard deviation σ of the training data and then applying the transformation in Equation 4.20 to the training data:

$$y_t = \frac{y - \sigma}{\mu} \tag{4.20}$$

where y is the original (untransformed) data and y_t is the transformed data.

Although it is only necessary for some learning algorithms, this transformation was carried out in all cases to ensure consistency. When the algorithm is used with testing data, the new inputs should be preprocessed using the mean and standard deviation computed for the training set.

The classification evaluation of this work has been done for the three different sets relative to the annotation protocols. The number of episodes of each type used for the classification analysis in protocols A, B and C is shown in Table 4.1 The number of analysed episodes is slightly lower than in the original database [109] due to the fact that some episodes at the beginning of the record have not got any onset annotations since their onsets start before the beginning of the records and were excluded from the analysis.

	Protocol A	Protocol B	Protocol C
Ischaemic ST episodes	1795(1788)	1126(1126)	857(794)
Heart-rate related ST episodes	516(513)	234(232)	116 (115)
Sudden step changes	2388	2388	2388

Table 4.1: Number of ischaemic, heart-rate related and sudden-step changes used in discrimination for each annotation protocol. The numbers in brackets represent the number of episodes with start and end points.

Annotations are attached to the lead or leads for which the episode is significant, so all analysis was performed using the lead for which the annotated episodes pertains.

4.8 Experimental results

Before applying the stepwise method to select the best combination of features, each feature was evaluated according to its ability to separate the two types of ST episodes using Analysis of

Variance (ANOVA). ANOVA is a standard technique for measuring the statistical significance of a set of independent variables [154]. ANOVA takes a single feature and the class associated with the data samples and measures the significance of the class variables in predicting the means of the feature. The measure that ANOVA produces is a *p-value* for the feature set. The results of applying ANOVA to the set of features are shown in Table 4.2.

There is no significant difference in $\Delta\mathrm{ST}_{21}$ between the two groups because according to the definition of transient ST segment deviation episodes, the change in ST segment level at the beginning of the episode is always 50 μV. However, there is a significant difference in $\Delta\mathrm{ST}_{31}$ for ischaemic and heart-rate related ST episodes as shown by the small *p-value*. This parameter is greater in ischaemic ST episodes than in heart-rate related ST episodes. This feature was chosen by MATLAB routine stepwisefit as one of the most relevant features in creating a discriminator between ischaemic and heart-rate related ST episodes.

There are also statistically significant differences in $\Delta\mathrm{HR}_{21}$, $\Delta\mathrm{HR}_{31}$ and HR_3 between ischaemic and heart-rate related ST episodes. The inclusion of heart rate measures is to be expected as heart rate related ST episodes are mostly associated with a much greater change in heart rate than ischaemic ST episodes.

$\Delta\mathrm{SL}_{21}$ and $\mathrm{ST}_{\mathrm{RMS}_{31}}$ are also significantly different between the two groups as expected, since the ST segment slope in ischaemic episodes may change in the beginning of the episode. The $\Delta\mathrm{ST}_{\mathrm{RMS}_{31}}$ feature associated with changes in ST segment energy for the entire episode was significantly higher in ischaemic episodes than in heart-rate related ST episodes.

In addition, there is a significant difference in the *LF/HF-ratio* as measured five minutes before the start of an episode between ischaemic and heart-rate related ST episodes. However, the QRS slopes are not statistically significant and were not selected by the stepwise fit for inclusion in the model. The *LF/HF-ratio* component is reduced for both classes but much more so in ischaemic ST episodes than in heart-rate related ST episodes.

There is a significant difference in $\Delta\mathrm{RS}_{\mathrm{RMS}_{31}}$ between ischaemic and heart-rate related ST episodes and this parameter was added to the vector of most relevant features. The $\Delta\mathrm{RS}_{\mathrm{RMS}_{32}}$, $\Delta\mathrm{RS}_{\mathrm{RMS}_{21}}$,$\Delta QR_{RMS_{21}}$ seem not to add any discriminatory information to the model as they

Variables	Ischaemic episodes($\mu \pm \sigma$)	HR-related episodes($\mu \pm \sigma$)	*p-value*
HR_3(bpm)	89.6±24.2	110.1±21.0	1.9e-30 ‡
$\Delta\mathrm{HR}_{31}$(bpm)	12.2±12.4	24.0±14.8	2.8e-25 ‡
$\Delta\mathrm{ST}_{31}$ (μV)	223.2±166.6	145.1±109.5	2.2e-24 ‡
$\Delta\mathrm{ST}_{32}$ (μV)	228.5±160.2	180.7±122.1	2.1e-15 ‡
LF/HF-ratio	0.5±0.4	1.1±0.5	2.4e-15 ‡
$\Delta\mathrm{HR}_{21}$(bpm)	5.5±7.7	11.2±11.6	4.9e-14 ‡
$\Delta\mathrm{QRS}_{\mathrm{MD}_{21}}$ (std)	352.3±231.2	259.6±114.8	7.0e-11 ‡
$\Delta\mathrm{ST}_{\mathrm{RMS}_{31}}$($\mu$V)	189.5±126.7	146.6±59.2	9.7e-10 ‡
$\Delta\mathrm{QRS}_{\mathrm{MD}_{31}}$(std)	211.8 ±207.4	139.8±87.5	7.7e-09 ‡
$\Delta\mathrm{SL}_{21}$ (μV)	6.3±46.4	24.6±47.2	3.9e-07 ‡
$\Delta\mathrm{STT}_{\mathrm{MD}_{32}}$ (std)	129.2±97.76	81.0±47.7	2.2e-05 ‡
$\Delta\mathrm{SL}_{31}$ (μV)	99.2±67.3	147.5±76.7	4e-05 ‡
$\Delta\mathrm{RS}_{\mathrm{RMS}_{31}}$ (μV)	57.6±64.2	52.9±55.0	0.004 ‡
$\Delta\mathrm{QR}_{\mathrm{RMS}_{31}}$($\mu$V)	67.0±82.3	56.7±57.3	0.005 ‡
$\Delta\mathrm{QR}_{\mathrm{RMS}_{32}}$ (μV)	545.6±256.0	618.0±253.0	0.01 ‡
$\Delta\mathrm{QRS}_{\mathrm{US}_{21}}$	0.03±9.7	0.9±7.8	0.01 ‡
$\Delta\mathrm{QRS}_{\mathrm{DUR}_{32}}$ (s)	0.1±0.0076	0.1±0.009	0.02 ‡
$\Delta\mathrm{QRS}_{\mathrm{DUR}_{31}}$ (s)	0.004±0.005	0.004±0.004	0.05
$\Delta\mathrm{QRS}_{\mathrm{DUR}_{21}}$ (s)	0.002±0.003	0.002±0.002	0.06
SDANN(ms)	50±5	30±7	0.07
$\Delta\mathrm{QRS}_{\mathrm{DS}_{21}}$	0.4± 3.7	0.04 ±5.8	0.1
$\Delta\mathrm{ST}_{21}$(μV)	118.0±101.0	113.4±101.3	0.1
$\Delta\mathrm{QRS}_{\mathrm{MD}_{32}}$ (std)	48.6 ± 50.2	45.4±46.5	0.27
$\Delta\mathrm{STT}_{\mathrm{MD}_{21}}$ (std)	150.6±180.6	110.5±130.9	0.28
$\Delta\mathrm{STT}_{\mathrm{MD}_{31}}$ (std)	410.1±50.84	35.4±370.6	0.28
$\Delta\mathrm{ST}_{\mathrm{RMS}_{32}}$ (μV)	57.7±277.2	7.6±218.5	0.3
$\Delta\mathrm{QR}_{\mathrm{RMS}_{21}}$ (μV)	29.5±39.3	31.6±37.5	0.3
$\Delta\mathrm{SL}_{32}$ (μV)	92.4±64.9	123.6±74.5	0.3
$\Delta\mathrm{RS}_{\mathrm{RMS}_{21}}$ (μV)	28.8±35.4	30.6±36.3	0.5
$\Delta\mathrm{QRS}_{\mathrm{DS}_{31}}$	0.3 ± 1.3	0.3 ±4.2	0.5
$\Delta\mathrm{ST}_{\mathrm{RMS}_{21}}$ (μV)	53.4±39.0	62.8± 44.6	0.6
$\Delta\mathrm{QRS}_{\mathrm{DS}_{32}}$	0.4±5.9	0.9±4.1	0.7
$\Delta\mathrm{RS}_{\mathrm{RMS}_{32}}$ (μV)	471.1±276.0	546.8±279.4	0.90

Table 4.2: List of the selected features by groups, their means and standard deviations ($\mu \pm \sigma$) for ischaemic and heart-rate related ST episodes annotated according to the annotation protocol B of the LTST DB, *p-value* from the ANOVA. ‡ indicates significance of $p < 0.05$.

Variables	Se (%)	Sp (%)	PPV(%)	NPV (%)	Acc
$\Delta\mathrm{QRS}_{\mathrm{MD}_{21}}$	69.7	66.4	66.7	68.1	67.9
$\Delta\mathrm{QRS}_{\mathrm{MD}_{31}}$	77.9	77.1	71.1	64.23	67.5
$\Delta\mathrm{STT}_{\mathrm{MD}_{31}}$	75.0	73.4	61.3	67.9	70.6
$\Delta\mathrm{HR}_{21}$	81.4	67.6	72.3	60.0	69.1
$\Delta\mathrm{HR}_{31}$	82.7	52.9	55.8	71.1	75.4
HR_3	72.7	55.9	70.8	72.1	57.4
$\Delta\mathrm{ST}_{31}$	79.8	60.2	53.7	59.7	68.1
$\Delta\mathrm{ST}_{\mathrm{RMS}_{31}}$	92.5	68.0	65.0	77.6	74.2
$\Delta\mathrm{SL}_{12}$	83.0	54.6	65.9	56.5	56.3
$\Delta\mathrm{SL}_{31}$	67.8	54.5	57.2	55.6	55.6
$\Delta\mathrm{RS}_{\mathrm{RMS}_{31}}$	50.9	65.5	60.43	57.1	58.3
LF/HF-ratio	67.3	57.6	51.7	52.6	52.3

Table 4.3: List of the selected features identified by stepwise fit with performance measures for ischaemic and heart-rate related ST episodes annotated according to the annotation protocol B of the LTST DB. The results were obtained using linear regression.

were not selected by stepwisefit.

In terms of which interval contained the most discriminatory information, most of the features included in the model are from the interval I_{31}. This is expected as it is the interval that measures the difference in a feature at the beginning of the episode and the extrema, which is where there is the largest change in the ST level.

4.8.1 Feature selection results

The performance of individual features was tested using the bootstrap method described previously in Section 4.7.2. Table 4.3 shows the list of features that were chosen by stepwisefit using linear regression together with the sensitivity, specificity and accuracy obtained using individual features. The median performance of the AUC and RMSE on the training and test sets are shown in Figure 4.7 for a range of input features. This figure shows that each of the performance measures improves monotonically over the first 12 included features. Even though the performance on the test data decreased after, the number of k=12, where k is the number of features, the decrease AUC and increase in RMSE is not .

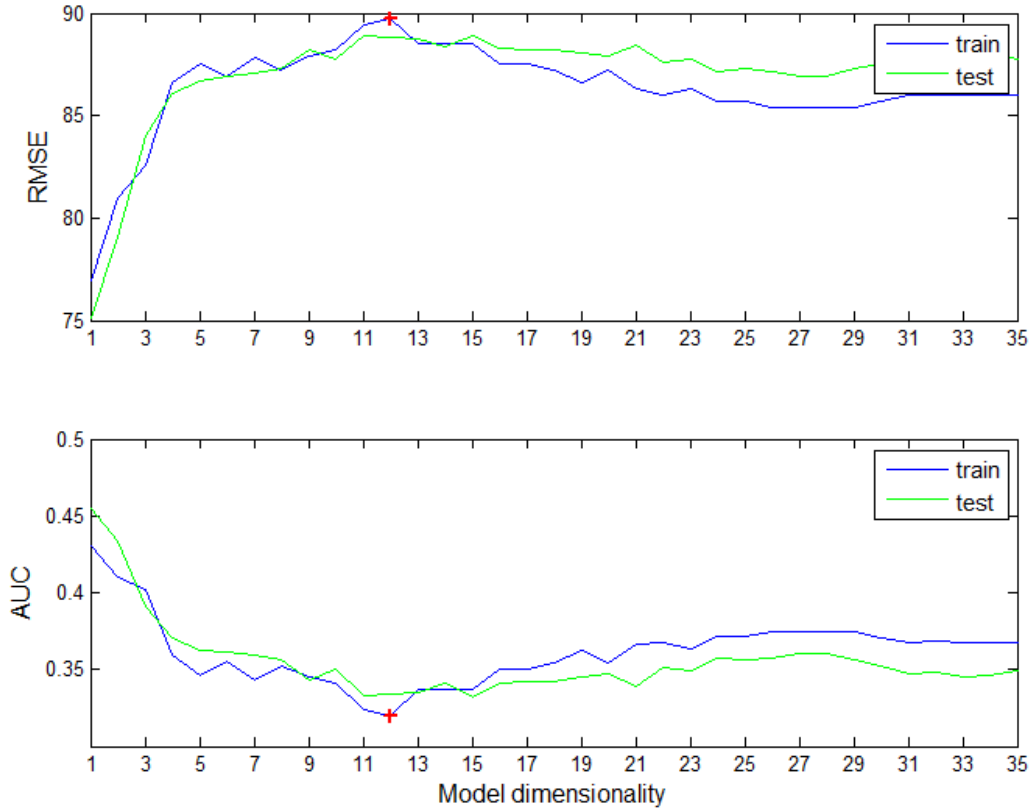
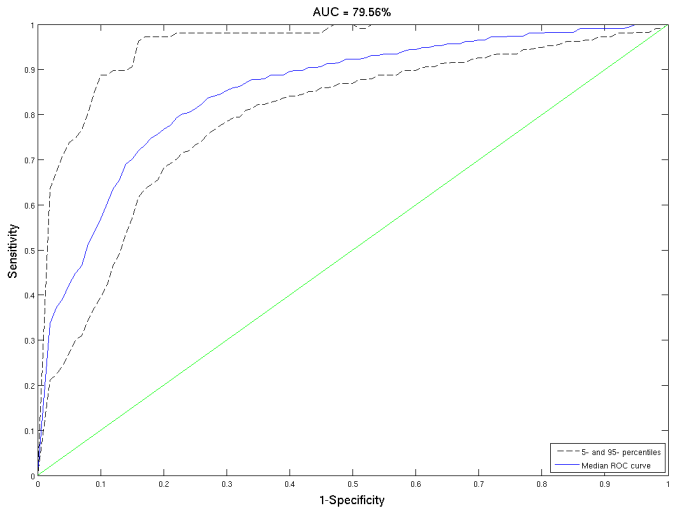


Figure 4.7: Evolution of different metric on the training (blue) and testing (green) for when increasing model dimensionality (k). The selected dimensionality for the model (k=12) is indicated by a red star.

4.8.2 Classification results

Linear regression

The ROC curve together with its 5th and 95th centiles is shown in Figure 4.8 for the linear regression model using the subset of 12 features chosen by ANOVA tested on annotation protocol B. The values for the performance metrics are also shown in the same figure. The optimal threshold point of the ROC curve is generally selected to minimize the distance between the top left corner and the median ROC curve and give an accuracy of 75.89%. The median AUC was 79.56%, indicating acceptable classification performance, with values of 74.32% and 90.26% for the 5th and 95th percentiles respectively. Good performance is observed when classifying the ST episodes defined by the annotation protocol B using linear regression.



Metric	Value(%)
AUC	79.56 ± 10.80
Se	76.93 ± 9.07
Sp	79.68 ± 8.44
Acc	75.87 ± 6.91
PPV	77.36 ± 6.93
NPV	78.09 ± 6.70

Figure 4.8: ROC plot showing the median curve and the 5th and 95th percentiles over the 1000 independent splits of the data for linear regression on annotation protocol B using 12 most relevant features obtained from the stepwise fit.

Figure 4.9 shows the empirical probability distribution functions of the output values from the linear regression model trained using the 12 features. As expected, there was significant overlap between the two distributions, showing that perfect separation of the two classes using linear regression is not possible. This motivates the use of non-linear classifiers.

The classification results of applying linear regression to classify ischaemic and heart-rate related ST episodes for annotation protocols A, B and C using 12 features is shown in Table

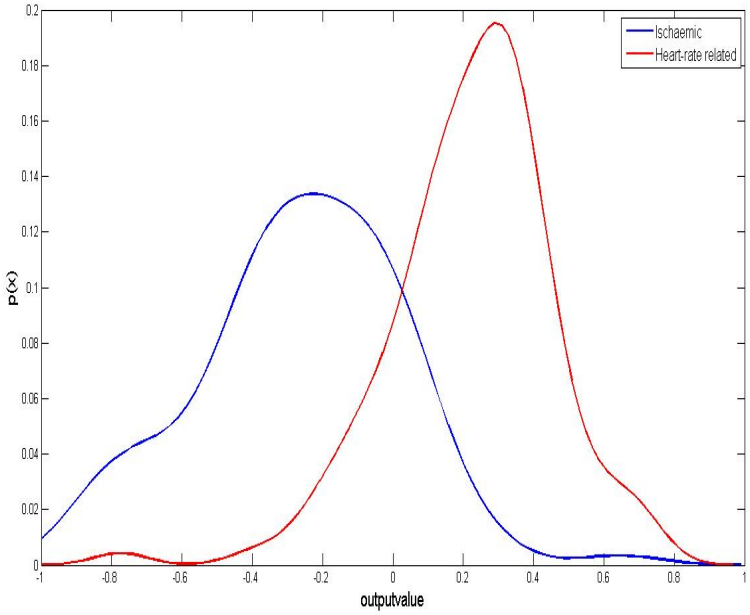


Figure 4.9: Empirical probability distribution of outputs of linear regression for each class.

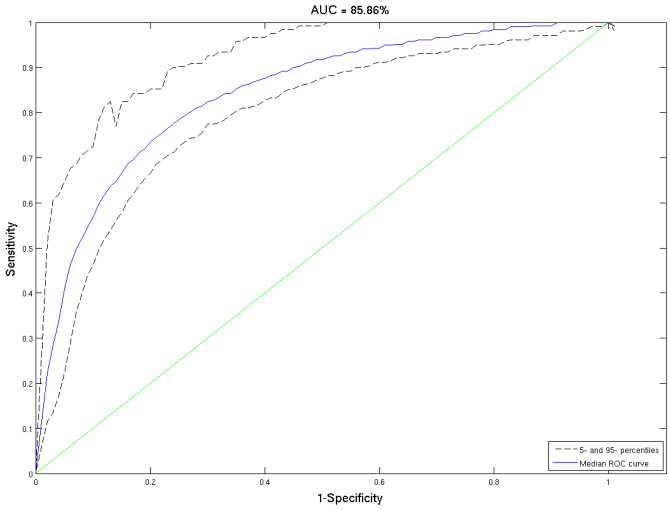
4.4. The use of protocol C, the most restrictive criteria for classifying ST events led to the best classification performance followed by protocol B and then A.

	Se%	Sp %	PPV%	NPV%	ACC%	AUC%
Protocol A	78.37	69.89	75.56	74.09	77.58	77.60
Protocol B	76.93	79.68	77.36	78.09	75.87	79.56
Protocol C	83.33	89.66	83.44	86.66	85.18	84.99

Table 4.4: summary of the classification performance in terms of sensitivity, specificity and accuracy between ischaemic ST and heart-rate related ST episodes using linear regression for annotation protocols A, B and C from the LTST DB database.

Multi-layer perceptron

The MLP was implemented using the NETLAB toolbox [149].The feature vector of 12 features was used as input data and the class as the target. The optimum number of hidden-layer neurons was identified by varying the number of hidden units from 6 to 20 using 5-fold cross validation and found to be 8. The ROC curve together with its 5th and 95th percentiles and the performance metrics are also shown in Figure 4.10.



Metric	Value(%)
AUC	85.86 ± 2.81
Se	82.51 ± 2.84
Sp	82.57 ± 4.42
Acc	82.51 ± 2.84
PPV	82.52 ± 3.37
NPV	82.36± 3.81

Figure 4.10: ROC plot showing the median curve and the 5th and 95th percentiles over the 10000 independent splits of the data for the MLP on protocol B together with corresponding statistics.

The classification results for the annotations in protocols A, B and C of the LTST DB using ANOVA-defined are shown in Table 4.5 . The median AUC for protocol B was 85.86%, providing an increase of over 6% compared to linear classifier, with values of 84.32% and 87.14% for the 5th and 95th percentiles of the AUC respectively.

	Se (%)	Sp (%)	PPV (%)	NPV (%)	ACC (%)	AUC(%)
Protocol A	78.23	76.34	75.58	74.23	75.45	76.14
Protocol B	82.51	82.57	82.52	82.36	82.51	85.86
Protocol C	84.88	82.42	79.72	87.38	83.52	89.72

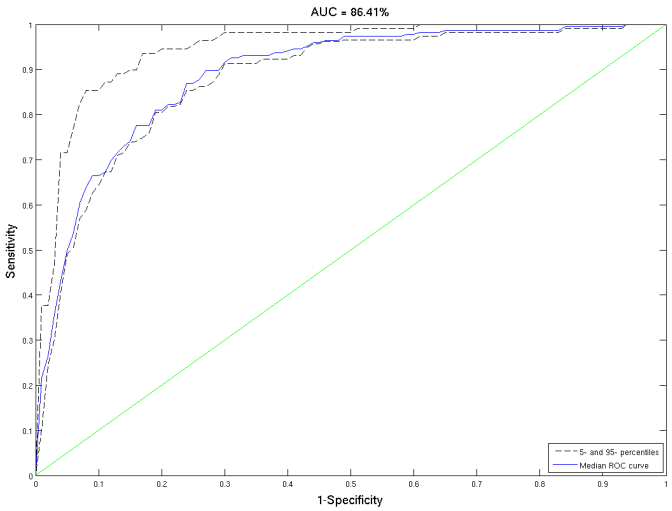
Table 4.5: Summary of the classification performance in terms of sensitivity, specificity and accuracy between ischaemic ST and heart-rate related ST episodes using an MLP for annotation protocols A, B and C from the LTST DB database.

Support Vector Machine

In finding the most suitable kernel function for the LTST DB, three different kernels functions were evaluated; linear kernel, polynomial and radial basis functions. The SVM classifier for discriminating between ischaemic and heart-rate related ST episode was implemented using the LIBSVM toolbox [155]. SVMs having different combinations of kernels and settings of

parameters were evaluated on a partition of the data using a 5-fold cross-validation experiment. The SVM paramors (penalty term , C and width of the kernel width (γ) described in Appendix A were chosen using grid search. The penalty parameter was found to be 8 and the kernel width was chosen to be 0.012. The performance of the model was evaluated using the AUC on the training data. It was found that the RBF kernel that gave the best classification performance (on training protocol B) and hence was used to build the model to discriminate between ischaemic and heart-rate related ST episodes for all three annotation protocols of the LTST DB.

As with previous classifiers, bootstrapping was used to train and evaluate the performance of the SVM using 12 features. The median ROC curve for the test data along with its 5th and 95th centiles are shown in Figure 4.11 for annotation protocol B. The values for the performance metrics on the test data are also shown in Figure 4.11.



Metric	Value(%)
AUC	86.41 $\pm$ 2.54
Sen	82.43 $\pm$ 2.84
Spe	82.76 $\pm$ 4.73
Acc	84.68 $\pm$ 4.43
PPV	83.05 $\pm$ 4.14
NPV	84.40$\pm$ 4.41

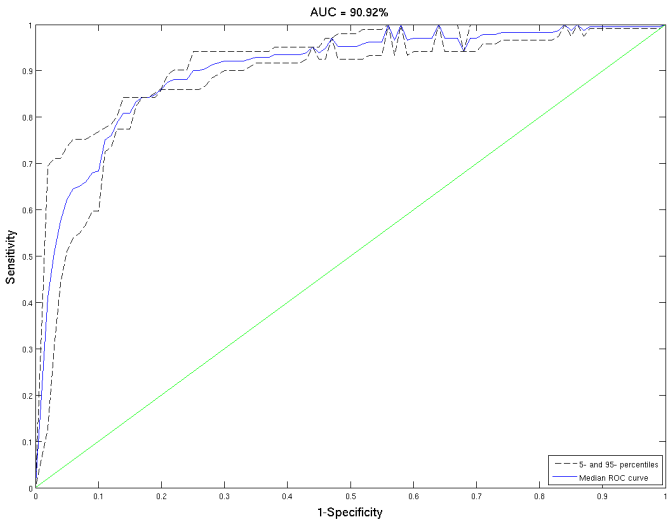
Figure 4.11: ROC plot showing the median curve and the 5th and 95th percentiles over the 1000 independent split of the data for SVM.

	Se (%)	Sp (%)	PPV (%)	NPV (%)	ACC (%)	AUC(%)
Protocol A	79.44	82.76	80.95	81.36	81.67	80.10
Protocol B	82.43	82.76	83.05	84.40	84.40	86.41
Protocol C	85.00	83.33	86.44	81.64	83.26	84.17

Table 4.6: Summary of the classification performance in terms of sensitivity, specificity and accuracy between ischaemic ST and heart-rate related ST episodes using SVM for annotation protocols A, B and C from the LTST DB.

Relevance Vector Machine

As with the previous classifiers, the RVM was trained using the 12 most relevant features to discriminate between ischaemic ST episodes and heart-rate related ST episodes using a Radial Basis Function kernel with a width of 0.9. The width of the RVM was optmised using 5-fold cross-validation on the training data. Bootstrapping was performed as described previously and the resulting ROC curves together with the performance measures are shown in Figure 4.12. The 5th and 95th percentiles of the RVM shows that there is a small variation in the performance of the RVM when the training dataset is changed.



Metric	Value(%)
AUC	90.42 ± 0.35
Se	84.31 ± 0.52
Sp	85.77 ± 0.73
ACC	88.00 ± 0.65
PPV	85.30 ± 0.21
NPV	84.48 ± 0.20

Figure 4.12: ROC plot showing the median curve and the 5th and 95th percentiles over the 1000 independent split of the data achieved using RVM to discriminate between ischaemic and heart-rate related ST episodes.

The RVM was used to differentiate between ischaemic and heart-rate related ST episodes for annotations in protocols A, B and C of the long term ST database and the results achieved for the three protocols are shown in Table 4.7. As with previous classifiers, the RVM achieved the best performance on protocol C. Note that the RVM resulted in the highest AUC on all protocols by at least 4%.

	Se (%)	Sp (%)	PPV (%)	NPV (%)	ACC (%)	AUC(%)
Protocol A	83.45	84.33	84.12	83.12	86.34	86.00
Protocol B	85.77	84.30	85.30	84.48	88.00	90.42
Protocol C	97.80	88.67	86.86	97.75	90.69	91.15

Table 4.7: Summary of the classification performance in terms of sensitivity, specificity and accuracy between ischaemic ST and heart-rate related ST episode using RVM for annotation protocols A, B and C from the LTST DB database.

4.8.3 Comparison of different models

Boxplots of the AUC with the median; edges of the box at 5th and 95th centiles for each of the four classifiers are shown in Figure 4.13. The RVM classifier performed very well, with the largest AUC values, followed by the SVM and then MLP. There was small variation in the AUC of the RVM and the largest variation occurred with the MLP which is known to be more prone to overfitting than the other techniques.

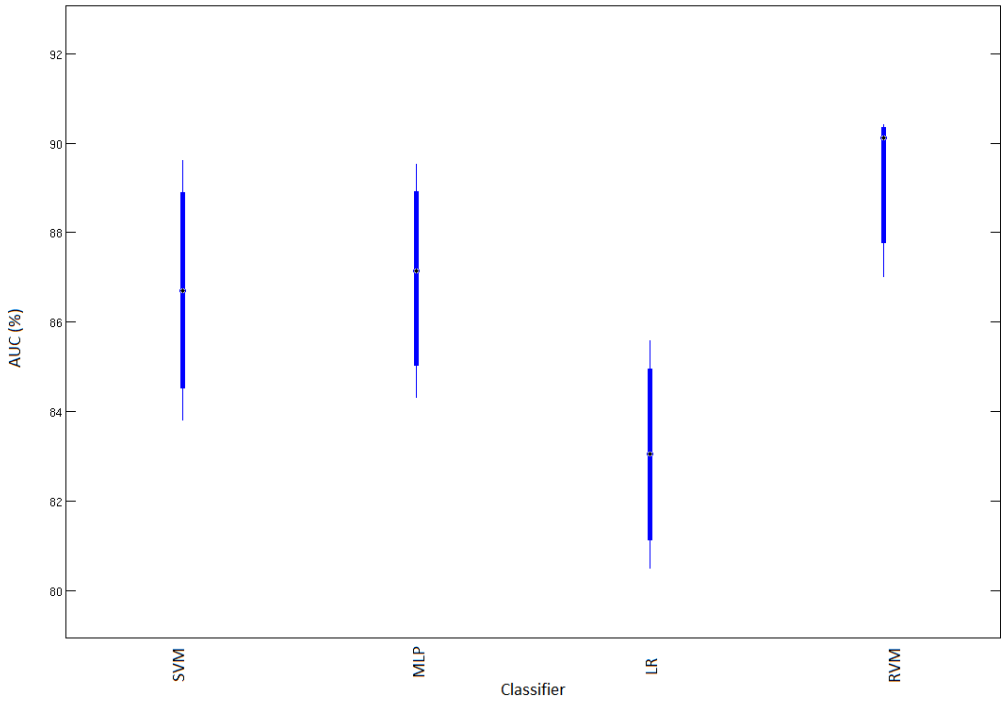


Figure 4.13: Comparison of areas under the ROC curves for the four different classifiers used in this study. Each boxplot has a central mark at the median, while the edges of the box are the 5th and 95th centiles.

In this section, the classification between ischaemic and heart-rate related ST segment deviation episodes only was performed, while most of previous work had mainly focused on discriminating between ischaemic and non-ischaemic ST segment deviation episodes [130–134, 136]. As described in Section 4.1, Minchole *et al.* [135] obtained a sensitivity and specificity of 84.5% and 86.6% on protocol B when discrimination between ischaemic ST event and heart-rate related which is comparable to results achieved in this work. However, our results were not as good as with those by Faganeli and Jager [132], which gave a sensitivity and specificity values of 98.1% and 88.7% on protocol B.

4.8.4 Discrimination between ischaemic and non-ischaemic ST episodes

In addition to distinguishing between ischaemic and heart-rate related ST changes, discrimination between ischaemic and non-ischaemic episodes was performed in order to isolate a true ischaemic event. As before, features to discriminate between ischaemic and non-ischaemic ST episodes were selected using a stepwisefit approach.

When the classification target is ischaemia, it was observed that the two first variables that best distinguish between ischaemic ST and non-ischaemic ST changes are those related to the ST segment: RMS values of ST segment and Mahalabonis distance of ST segment. The reason is that the ischaemic group has a much higher change in the RMS values of the ST segment and also in the ST-T complex than non-ischaemic changes.

Since the RVM achieved the best performance out of all the classifiers in the previous section, it was used to distinguish between ischaemic and non-ischaemic ST episodes. As shown in Table 4.8, it gave a sensitivity and specificity values of 90.1% and 88.4%, respectively on protocol B of the LTST DB.

	Se (%)	Sp (%)	PPV (%)	NPV (%)	ACC (%)	AUC(%)
Protocol B	90.1	88.4	87.3	89.8	90.2	89.6

Table 4.8: Summary of the classification performance in terms of sensitivity, specificity and accuracy between ischaemic and non-ischaemic ST episodes using RVM for annotation protocols B from the LTST DB database.

In relation with the Physionet/Computers in Cardiology Challenge, our results are comparable with Langley *et al.* [133] (Acc=90.7%). However, as mentioned before, their results were achieved using a small subset of representative episodes from the LTST database. Furthermore, the results achieved are also comparable to those achieved by Minchole *et al.* [135], who achieved an accuracy of 87.5% using the full set of data.

4.9 Discussion

Heart-rate related ST events are mostly associated with larger increases in heart rate than ischaemic ST episodes. Therefore, to differentiate between these two classes of episodes, a major parameter that should be considered is the change in heart rate during the episode. However, a change in heart rate is also a key factor associated with ischaemia in patients with coronary occlusion and therefore other indices in addition to the heart rate (such as changes in the ST segment) are needed to increase the separation between the two classes of ST episodes.

Smrderl and Jager [113] stated that a large number of the records of the LTST DB contain demand ischaemic episodes, related to heart rate. However, episodes in the database are not clinically classified as demand or supply episodes. Besides, care should be taken in the sense that not all episodes in heart-rate related classes are associated with an increase in heart rate. In about 10% of the episodes, heart rate is oscillating or even decreasing [132].

For ischaemia detectors based on changes in the ST segment, discrimination between ischaemic event and heart-rate related episodes, both of which have very similar patterns in the ST level function, could prove to be a very useful tool for automatic screening of Holter episodes. In discriminating between ischaemic and heart-rate related ST changes, one of the most significant variables in the model is related to changes in energy of the ST segment. In addition to using the absolute magnitude change of the features to account for the dynamic effect of the ST episode, perhaps including a combination of the raw data might provide more information. The absolute magnitude of the episodes change might actually conceal information such as difference in ST segment due to the type of ischaemia (supply or demand ischaemia) or location

of the ischaemia.

In terms of protocols, protocol C, with the least number of transient ischaemic episodes and the most restrictive in terms of criteria used to define an ST episode, gave the highest accuracy for all classification methods investigated in this chapter, followed by protocol B and then A, the least restrictive. This is in accordance with the fact that protocol C results in most evident episodes.

This chapter has demonstrated that ST level estimation algorithm developed for this thesis is as accurate as state-of-the-art algorithm in the literature. It has been validated on both the ESC ST-T database and the LTST database which gives us confidence that it can be used on the patient data collected during the ambulance transport in the next three chapters.

Chapter 5

Pre-hospital monitoring of acute coronary syndrome patients

5.1 Introduction

The current state of the art for emergency diagnosis and management of ACS in the UK is a 12-lead ECG. The ambulance crew generally take a "snapshot" 12-lead ECG for patients presenting with signs and symptoms of ACS and transmit it to hospital for diagnosis and risk stratification. If the patient has ST elevated ACS, preparations are made to initiate treatment upon the patient's arrival at the hospital. However, if the patient's 12-lead ECG is normal, they are taken to the Accident and Emergency Department for further risk stratification.

As described in Section 1.1, the ECG has remained the main tool for defining treatment strategy; ST segment elevation ACS (STEACS) initiates an immediate invasive strategy, whereas non-ST segment elevation ACS (NSTEACS) requires further risk stratification. However, the basis of this distinction is based on a 'snapshot' ECG, which may not reflect dynamic changes in the clinical conditions of the patient. Furthermore, the ECG is only one tool which may assist in risk stratification of this high-risk group. Early diagnosis and stratification of patients allows for re-evaluation and early initiation of interventions. Thus, developing additional tools to identify high-risk ACS patients and target appropriate emergency therapy would be clinically

valuable.

Effective risk stratification is integral to the management of patients with acute coronary syndromes. Even among patients with STEMI, for whom initial therapeutic options are well-defined, patient risk characteristics have an impact on early therapeutic decision making. In addition, increasing economic pressures have intensified the need for appropriate triage and clinical resource utilization, including decisions regarding transfer to tertiary centres. In particular, the capacity to reliably identify patients at very low risk for fatal recurrent events may offer the opportunity to select low-risk patients for early hospital discharge.

A range of physiological parameters are recorded during the routine clinical care of ACS patients, and are used to monitor patient progress and status. The parameters that are generally measured are the ECG, heart rate, blood pressure, oxygen saturation and respiration rate. These parameters are usually displayed continuously on the patient's monitor in the ambulance using a portable monitoring system. Although these parameters are routinely measured, the information provided during the monitoring is typically used as an addition to the periodic clinical assessment by the medical staff, rather than as a basis for more quantitative patient monitoring. One of the reasons for the under-usage of the continuous patient monitoring data is that changes in a single parameter are not generally an accurate predicator of a change in patient condition.

At present, the wealth of patient monitoring data acquired during ambulance transport and early hospital management is recorded through separate systems, often on paper, with no integration of individual monitoring data or datasets from different clinical environment. These snapshot recordings have limited value because they rely on clinical indicators derived from single parameters that have very limited diagnostic specificity, and because they cannot evaluate trends with time across different clinical environments. Using patient monitoring data to generate an integrated dataset from pre-hospital monitoring of vital signs has the potential to assist in the diagnosis and management of patients with ACS.

In order to achieve this, a study was conducted to evaluate the feasibility of developing a system to identify high-risk patient from pre-hospital monitoring data in patients transported by ambulance with possible ACS.

An observational pilot study was undertaken during the pre-hospital management of patients at the John Radcliffe (JR) Hospital, Oxford, which had the aim of collecting continuous vital-sign data and electrocardiogram (ECG) for patients presenting with indication for an ECG to be taken as described by National Institute for Health and Clinical Excellence (NICE) [156]. The study was carried out between December 2010 and December 2011. The research was approved by the Central Office of Research Ethics Committees and funded by the Oxford Biomedical Research Centre. This chapter describes the study in detail and gives a summary of the data collected. In addition, a signal quality index was computed on each ECG record to exclude records with unacceptable noise levels.

5.2 The protocol

When the ambulance crew take a pre-hospital ECG as per NICE guidelines, the crew sends the 12-lead ECG to the Coronary Care Unit (CCU) for advice. The 12-lead ECG data is also sent remotely to a Medtronic (Lifenet) server at the JR Hospital where the data is forwarded to the Catherization Laboratory (CathLab) and CCU. If the patient has ST elevation in two or more leads, the patient is taken to the CathLab to be treated immediately. If the patient does not have any changes in the ECG that are indicative of a myocardial infarction (MI), the patient is taken to the Emergency Department (ED) for further tests. If the patient has risk factors for cardiovascular disease, a troponin test is done on arrival in the ED to rule him or her as a patient with ACS. The troponin test is usually repeated every four or six hours.

According to the protocol of the clinical study, if a patient was being taken to hospital and a 12-lead ECG had been recorded, then the data should be transmitted to the Lifenet server. Upon completing the job involving the current patient, the ambulance crew sent all data to the Lifenet server which then forwards the data to the clinical study server. This involved turning off the LIFEPAK 12/15 to save the data, which saved a patient session, and turning it on and selecting the option of sending the patient's data.

The research nurse was informed when a new patient arrived using an automatically gen-

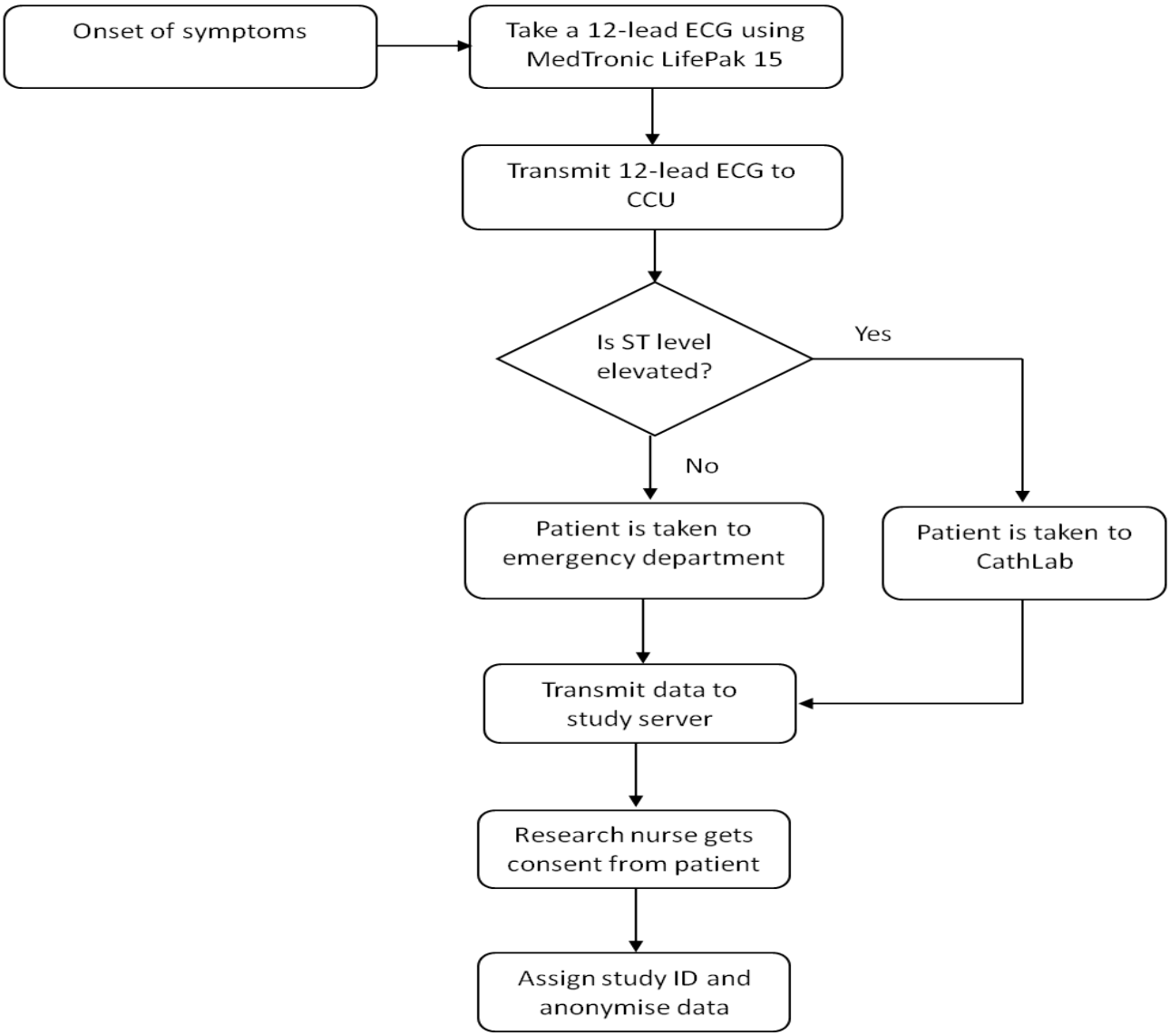


Figure 5.1: Flowchart for the clinical study.

erated email which was sent to a study-specific email address. The email contained patient identifiers such as date of birth. Eligible patients were consented to the study. Once a patient was consented, an email was sent to the Oxford University research team so that a patient could then be assigned a study ID. The data was anonymised and transferred to the study server. The flow diagram of the procedure for collecting data is shown in Figure 5.1.

5.3 Software and hardware

Continuous vital-sign data and ECG were recorded using a Medtronic LIFEPAK 12/15 monitor [157].. An example of a LIFEPAK 15 is shown in Figure 5.2. The data collected during the ambulance transport included: heart rate (HR); systolic (SBP), diastolic (DBP) and mean arterial blood pressure (MAP); peripheral oxygen saturation $\mathrm{SpO_2}$; and continuous 12-lead ECG using Medtronic algorithm. The ECG was recorded using standard chest electrodes. HR was derived using the RR-interval in the heartbeat waveform. The $\mathrm{SpO_2}$ was measured using a pulse oximeter attached to the patient's finger. SBP, DBP and MAP were measured using a standard blood pressure cuff. The HR and $\mathrm{SpO_2}$ were measured every 30 seconds while the SBP, DBP and MAP were measured every 10 minutes.



Figure 5.2: The Medtronic Lifepak 12/15 used for recording the data in the study

5.3.1 Heart rate

The heart rate is the rate at which the heart beats, and may also be referred to as the pulse rate, although this term is usually only used when the heart rate is measured by manual palpation. It is measured in beats per minute (bpm). In order to calculate heart rate, one of the components of the ECG must be detected each time it occurs. The QRS complex corresponds to the ventricular de-polarization current that drives the contraction of the left and right ventricles and causes the largest changes in surface potential; hence it is easiest to detect. The ECG was sampled at a 30 second interval.

5.3.2 Blood pressure

The heart exerts pressure on the blood in order to force it round the body. The blood exerts this pressure on the walls of the arteries. When the ventricles contract (systole), there is a peak in blood pressure (systolic blood pressure, SBP) and on relaxing (diastole) there is a minimum (diastolic blood pressure, DBP).

Blood pressure can be measured non-invasively using an oscillometric method. An inflatable cuff is placed around the upper arm and inflated using an electric pump until blood flow through the artery is completely occluded. The air is then released and the oscillations in cuff pressure caused by the cyclic expansion of the artery due to the in-rushing blood are measured.

When blood starts to flow through the artery as the cuff is deflated in steps, the increasing blood flow causes the amplitude of the pressure pulses in the cuff to increase. As the blood pressure monitor steps the pressure down, the pulses reach a peak amplitude and then start to decrease. The rising and falling amplitude values form a curve that is analysed to yield systolic pressure, diastolic pressure, and mean arterial pressure (MAP).

The blood pressure is generally sampled at 10 minute interval, however, the user can preselect the sampling rate when required.

5.3.3 Peripheral oxygen saturation

Peripheral oxygen saturation is measured using pulse oximetry which exploits the fact that oxygenated haemoglobin has a different absorption spectrum to deoxygenated haemoglobin [158]. Two different wavelengths of light are shone through either a fingertip or an earlobe and the pulsatile variation in absorption of the two wavelengths allows the arterial oxygen saturation to be estimated. Pulse oximetry assumes that the attenuation of light by the body segment can be split into three independent components: that are due to arterial blood, that due to venous blood and that due to tissues. The light transmitted varies with the amount of arterial blood, giving a cardiac-synchronous pulsatile component to the received light signal. It is assumed that the increase of attenuation of light is caused only by the inflow of arterial blood into the fingertip (or earlobe). This means that the oxygen saturation of arterial blood can be calculated by subtracting the DC component of the attenuation from the total attenuation, leaving only the cardiac-synchronous pulsatile component for the dual-wavelength determination of oxygen saturation [158]. $\mathrm{SpO_2}$ is normally between 95% and 100%.

5.3.4 ECG and ST level

The Medtronic Lifepak 12/15 measures the ECG with a sampling frequency of 125 Hz. The ST monitoring is initiated with the patient's first 12-lead ECG. The ST median measurement is derived from the GE Medical Systems 12SL ECG analysis program. Instead of analyzing a single QRS complex, the General Electric Marquette 12SL Program generates a median complex. In other words, all QRSs of the same shape are aligned in time. Next, the algorithm generates a representative QRS complex from the median voltages that are found at each successive sample time. The major wave onsets and offsets are delineated by an analysis of the slopes in all 12 simultaneous leads. After finding the J point, this is used to find the ST point which is then used to find the ST level.

After analysing the 12-lead ECG, the monitor identifies the lead with the most ST median displacement, either negative or positive. This first ST median measurement for each lead

becomes the baseline. All subsequent ST median measurements are compared against this baseline.

The Lifepak 12/15 transmits only one continuous lead and this is normally lead II. However, if lead II is too noisy another lead with a lower signal-noise ratio is transmitted.

5.4 Summary of the data

The total number of patients recruited in the Pre-hospital Monitoring Study from December 2010 to December 2011 was 687. Out of the 687, 8 patients refused to participate. Out of the 679 patients who consented, 179 patients were excluded due to incomplete records. At the end, 500 patients remained for analysis. A summary of the study enrollment is shown in Figure 5.3.

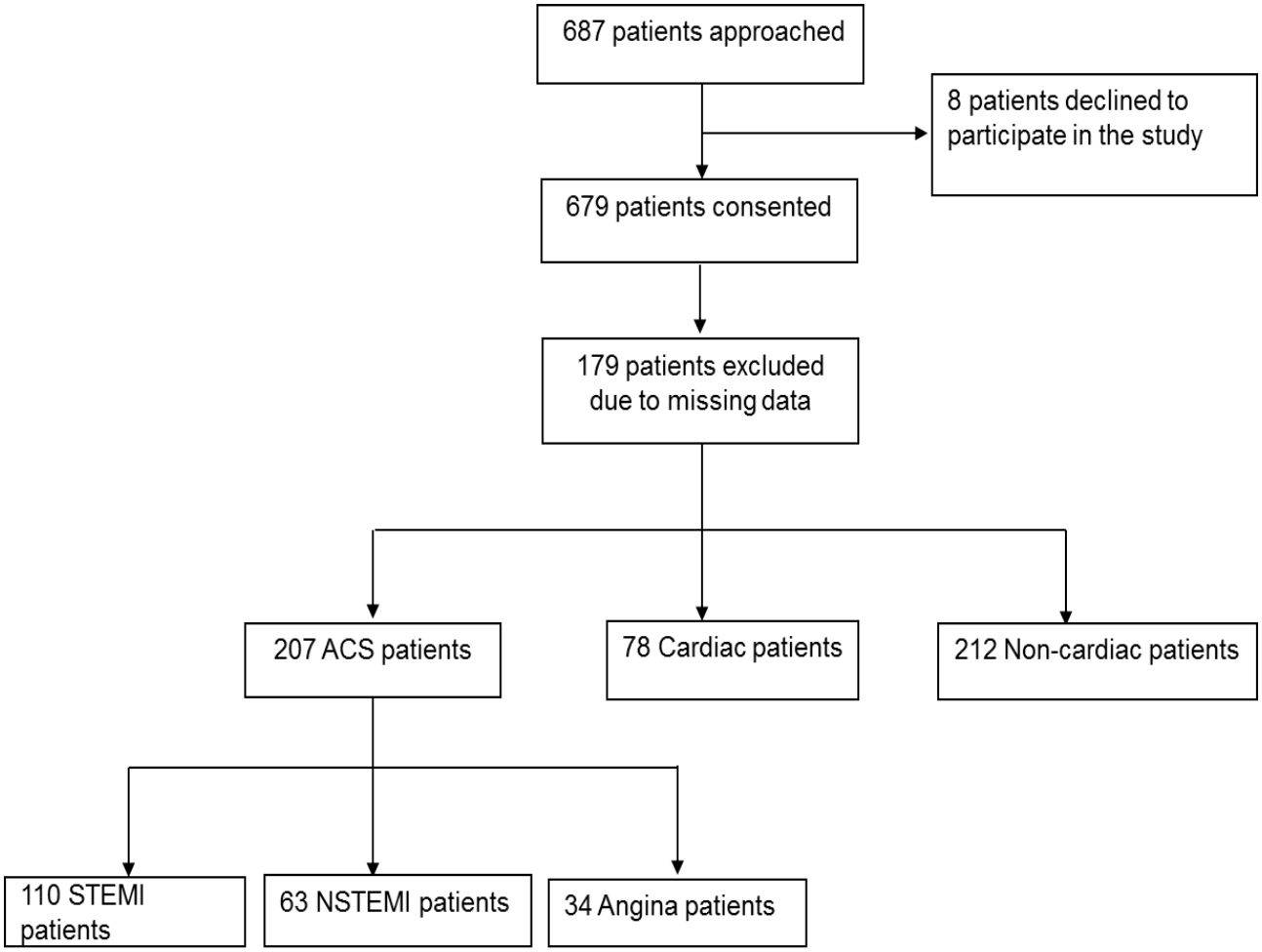


Figure 5.3: Flowchart of the study.

5.4.1 Demographic and clinical data

The study cohort comprised a sample of 500 patients (325 males and 175 females), that were transported by ambulance to the JR hospital and had a 12-lead ECG taken, over a period of 12 months. The age of the patients ranged from 20 to 96 years old, with a mean age of 67 years (standard deviation of 18.5 years). In terms of cardiac risk factors, 58.53% of patients were over the age of 65 years (n = 289), 64.23% of patients smoked or used to smoke (n = 334), and another 48.26% had a past or current medical history of hypertension (n =249). 26.16% of patients had a family history of ischaemic heart disease (n = 135), and 20.74% of patients had a medical history of diabetes mellitus (n = 107).

5.4.2 Classification of patients into groups based on diagnosis

The study cohort was divided into three groups based on the final diagnosis by clinical staff as shown in Figure 5.3. The three groups were: ACS, cardiac, and non-cardiac. The cardiac group consisted of patients with other cardiac-related illnesses such pericarditis and congestive heart failure beside ACS. The non-cardiac group consisted of all patients without any cardiac-related diseases. The ACS group was further divided into three subgroups as per the definition of ACS, ST elevated myocardial infarct (STEMI); non-ST elevated myocardial infarct (NSTEMI); and unstable angina (UA). The summary of the patient cardiovascular risk factors for the main groups are shown in Table 5.1. The ACS group consisted of 207 patients, the cardiac group had 78 patients and the non-cardiac group had 212 patients.

In order to investigate whether there is a difference in the various variables of the ACS group and non-cardiac group, a statistical significant test was conducted. For variables with normal distribution, the Student's t-test for unpaired values was performed to compare the continuous variables such as age between the groups. Student's t-test (for unequal variances) is applied to calculate the probability that the means each variable are significantly different between the two groups. The Chi-square test was performed to calculate the differences in discrete variables between the groups. The assumptions of these statistical tests are that the samples are drawn

from normal distributions and the variances of each data set are homogeneous [154].

There is no significant difference ($p>0.05$) in the age between the ACS group (67.05 ± 13.65) and the non-cardiac group (67.04 ± 18.53). Also, sex was not significantly different between the groups ($p>0.05$). Family history of heart disease is the only risk factor that is significantly different ($p<0.05$) between the two groups.

Variables	All patients (n=500)	ACS (n=207)	Non-cardiac (n=212)	*p-value*
Age	66.97 ± 15.03	67.05 ± 13.65	67.04 ± 18.53	0.67
Male	335	146 (68.54%)	138 (63.29%)	0.52
Smokers	334	154 (72.30%)	127 (58.53%)	0.51
Diabetes mellitus	107	39 (17.97%)	48 (22.54%)	0.24
Hypertension	249	114 (52.53%)	97 (45.54%)	0.15
Family history	135	70 (32.26%)	49 (23.00%)	0.03
Previous MI	94	46 (21.20%)	33 (15.49%)	0.13
Previous Angiogram	78	62 (28.57%)	49 (23.00%)	0.19
Previous PCI	38	40 (18.43)	26 (12.21%)	0.07
Previous CABG	95	11 (5.10%)	19 (8.92%)	0.11

Table 5.1: Demographic and risk factors of the overall population along with the ACS group and non-cardiac group. n represents the number of patients.

Although there was no statistical significant difference in the ages of the ACS and non-cardiac groups, age is still one of the major risk factors for ACS [15]. Age was categorized as younger than 40 years, 40 to 65 years, and older than 65 years according to previous work [159]. For the age group younger than 40 years, there were no patients with ACS. Although there was a small number of patients in this age group, this is still in line with the literature that state that coronary artery disease is generally a disease of the elderly [160]. The other risk factors of ACS for the various age categories are also shown in Table 5.2.

The patient characteristics of the ACS subgroups are shown in Table 5.3. A total of 207 patients had a final diagnosis of ACS. Of these 110 were STEMI (50.23%), 63 were NSTEMI (29.94%) and 34 were UA (15.67%). For simplicity, the NSTEMI and UA were grouped into NSTEACS, thus there were 97 NSTEACS patients (44%). Hence, the occurrence of NSTEACS was similar to that of STEMI for this study population.

In the ACS group, 41.54% of these patients were former or current smokers; 18.43% were

Variables	<40 (n=22)	40-65 (n=165)	>65 (n=313)
Male	14	130	191
Smokers	5(22.72%)	53 (53.11%)	168 (53.00%)
Diabetes mellitus	0 (0%)	27 (24.92%)	80 (24.36%)
Hypertension	3(13.64%)	61 (58.36%)	165 (20.66%)
Family history	4 (18.18%)	63 (21.31%)	68 (21.31%)
ACS	0 (0%)	87	130

Table 5.2: Patient demographics and cardiac risk factors for each age category. n represent stands for the number of patients.

diabetic; 33.18% had hypertension; 21.77% had family history of ACS and 32.26% had previous heart diseases.

Pharmacological treatments for ACS such as aspirin, beta-blockers and nitrates were administered in the ambulance. In the ACS group, 34, 157 and 156 patients were given beta-blockers, aspirin and nitrates, respectively. It should be noted that some patients were given a combination of these treatments.

As described in Section 1.1, STEMI is diagnosed based on persistent ST segment elevation. On the other hand, NSTEACS patients can have transient ST segment depression or T wave inversion, or no ECG changes at presentation. The following ECG characteristics were computed from the pre-hospital 12-lead ECG; (1) ST elevation, (2) ST depression with or without T wave inversion, (3) isolated T wave inversion and (4) ECG confounders (bundle branch block, left ventricular hypertrophy). It should be noted that these ECG characteristics do not occur independently of each other. Some patients have more than one occurrence of these ECG characteristics. Eighty-six percent of patients with ST elevation had simultaneous ST segment depression in other leads.

Table 5.3 shows that the prevalence of NSTEACS (49.23%) is similar to that of STEMI (50.23%). Our analysis show that a significant proportion (49.23%) of ACS patients who develop transient myocardial ischaemia with continuous ST segment monitoring do not have evidence for ischaemia on their initial ECG. It further shows that 25.71% of STEMI patients were diabetic while 32.20% of NSTEACS are diabetic. Furthermore, 65.14% of the STEMI patients and 67.31% NSTEACS were male.

Variables	ACS (n=207)	STEMI (n=120)	NSTEMI (n=63)	UA (n=34)
		Risk factors		
Age	66.94 $\pm$ 12.78	64.79 $\pm$ 12.15	69.77 $\pm$ 13.21	69.72 $\pm$ 13.49
Male	146	71 (65.14%)	51 (72.86%)	21 (61.74%)
Smokers	39	35 (55.71%)	39(31.82%)	17 (50.0%)
Diabetes mellitus	91	16 (25.71%)	18 (14.55%)	6 (17.65%)
Hypertension	114	51 (32.86%)	44 (46.36%)	17 (50.00%)
Family history	70	14 (44.29%)	25 (25.45%)	8 (32.35%)
		Drugs administered in the ambulance		
Beta-blockers	34	16	16	11
Aspirin	165	94	48	23
Nitrate	155	91	45	19
		ECG characteristic		
ST elevation	126	105	20	1
ST depression	142	92	38	11
isolated T wave inversion	34	15	14	2
Bundle block branch	28	9	4	13

Table 5.3: Patient demographics, risk factors and pharmacological factors for subgroups of acute coronary syndrome (ACS). The subgroup are ST elevation Myocardial Infarction (STEMI), non-ST elevation Myocardial Infarction (NSTEMI) and unstable angina (UA). n stands for the number of patients in that subgroup.

5.5 Vital-sign data

In addition to collecting the data, an investigating was conducted into whether the vital-sign data could be collected reliably during the ambulance transportation. The patient data was grouped into groups of 100 patients. For each vital-sign parameter in each group, the percentage of missing data was calculated. As can be seen in Figure 5.4, the pulse rate and the ECG were collected 97% of the time while blood pressure was collected 78% of the time. The reason for the lower collection rate of the blood pressure is that it was measured every 10 minutes. The $\mathrm{SpO_2}$ was collected less than 20% of the time at the beginning of the study (the first 100 patients) this improved to about 49% in the middle of the study and almost 50% for the last 100 patients. The reason for this is that the $\mathrm{SpO_2}$ probes were initially faulty and recalled by the manufacturer.

Figure 5.5 shows the number of records with all vital-sign data. The first 100 records had

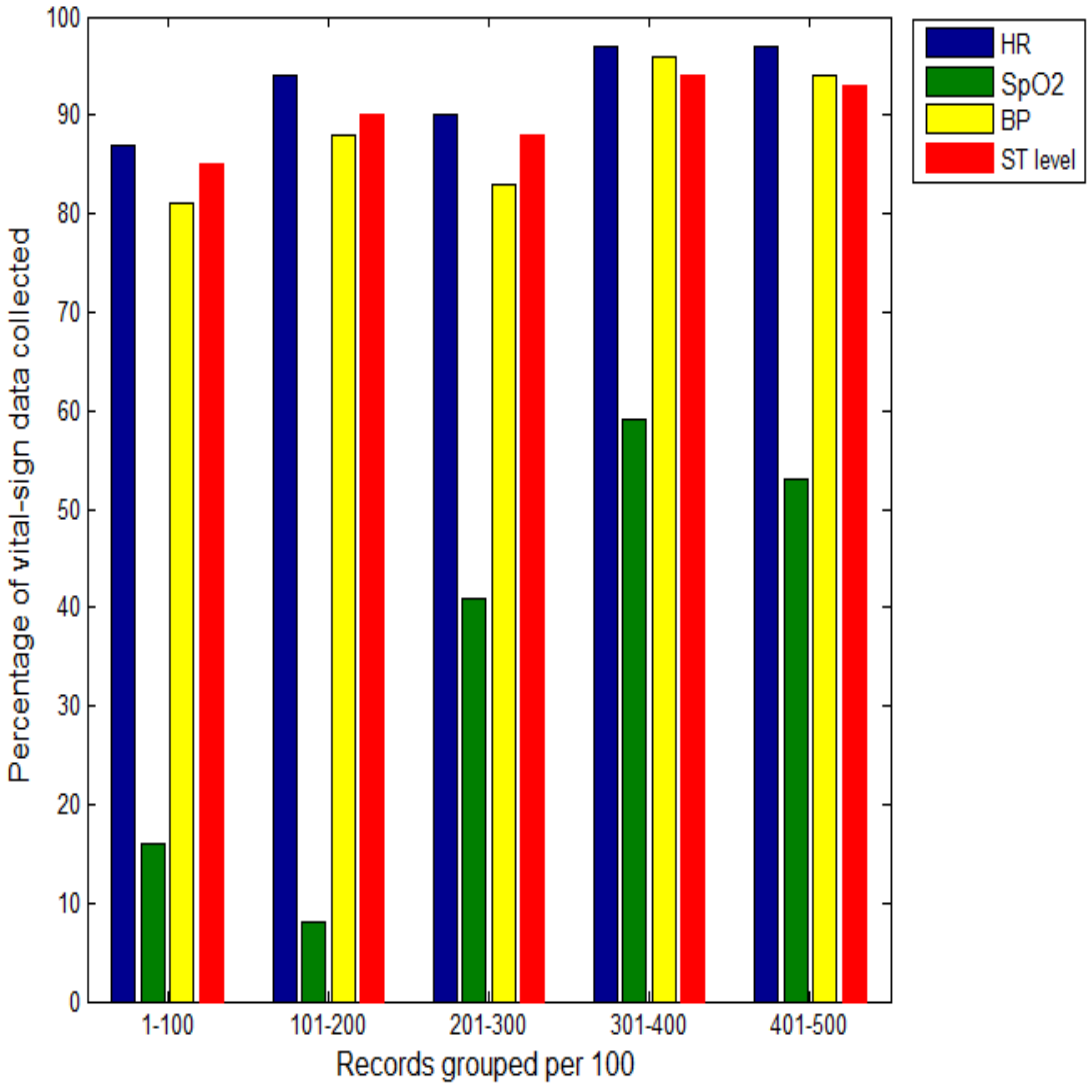


Figure 5.4: Percentage of collected vital-sign data grouped per 100 patients. The blue is the heart rate, green represent SpO_2, yellow represent BP and red is the ST level.

just over 10% of complete data but this figure increased to over 50% for the last 100 patients. In total, the number of complete records was 173. 37 of the patients with complete vital-sign data were on beta-blockers while 136 patients were not on beta-blockers.

Physiological time-series data collected in the pre-hospital setting are noisy. The determination of signal data quality is a primary challenge in developing automated decision-support systems. The next section discusses the implementation of signal-processing techniques described in Section 2.6.1 to rigorously and systematically analyse pre-hospital ECG.

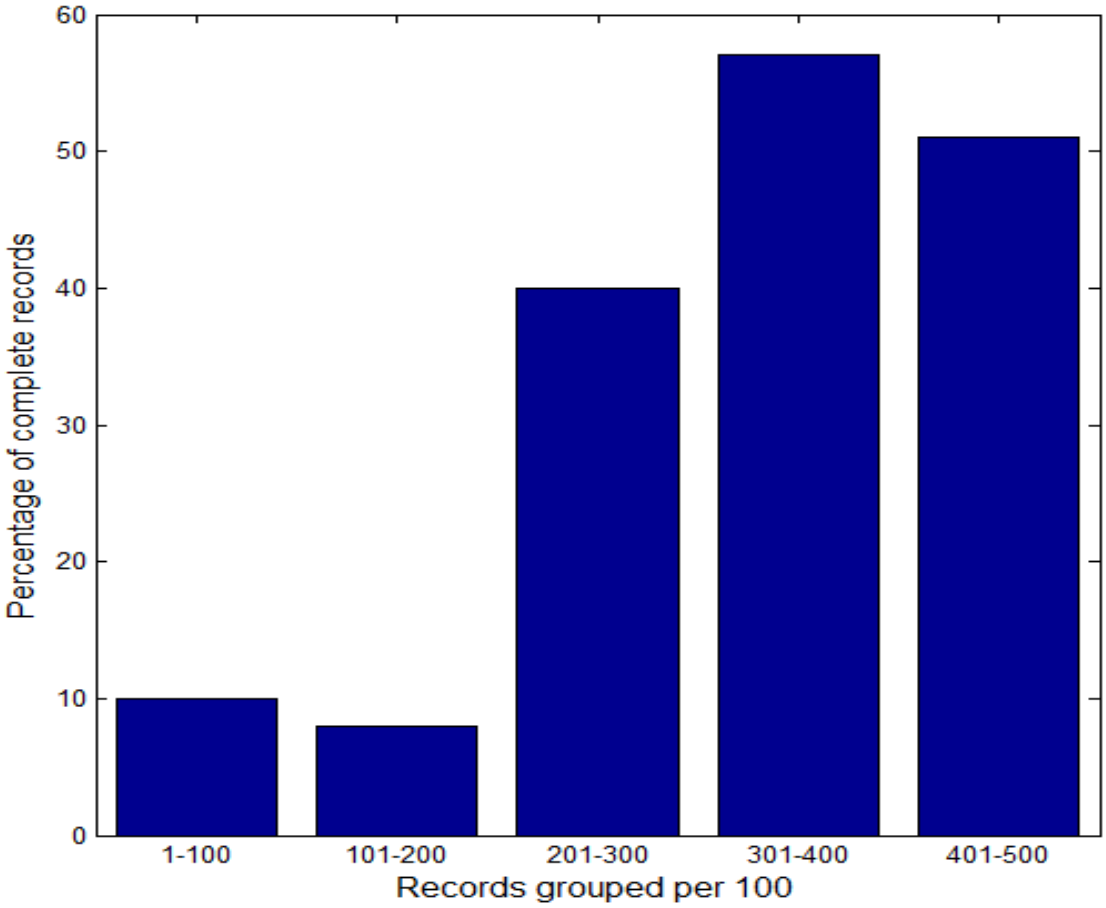


Figure 5.5: Percentage of complete records grouped per 100 patients for all 500.

5.5.1 Signal Quality Index of records in the pre-hospital monitoring study

Figure C.2 shows the performance of the SQI algorithm on a single patient for a 40-second window. The raw ECG is shown in blue. The beat-by-beat quality index has a value of +1 for a high-quality beat and -1 for a low-quality beat.

The SQI algorithm was used on the data from the 500 patients in the database to calculate how many beats in the records were high-quality beats (+1). The distribution of this percentage for the 500 patient records is given by the histogram shown in Figure 5.7. Over 79% of the records have more than 50% of high-quality beats. Approximately 35% of the records have more than 90% high-quality beats.

Of the latter, there are 61 records with complete vital-sign data as shown in Table 5.4. The

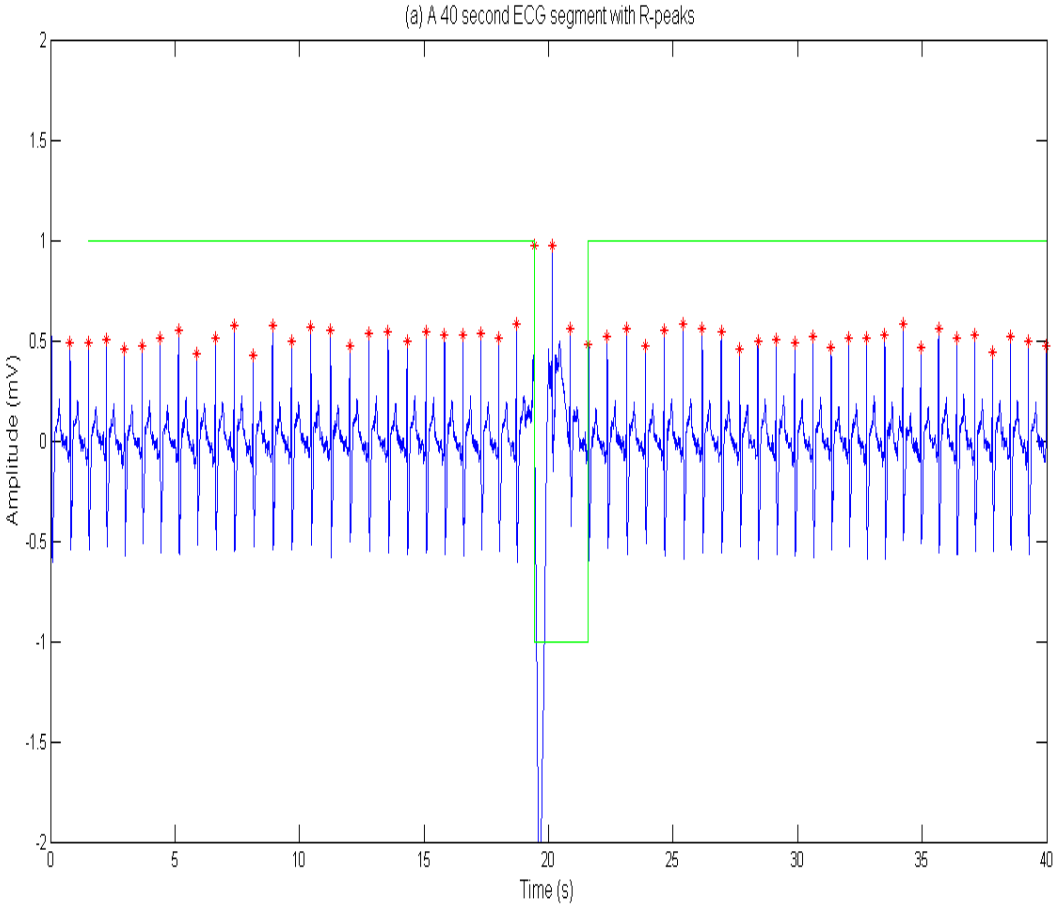


Figure 5.6: Signal Quality Index for patient 0031 for a 40-second window shown in green, with the ECG signal shown in blue.

patients with fewer than 60% high quality beats were excluded from the heart rate variability analysis (see Chapter 5)

Percentage of records with high-quality beats	no of records
>90	61
80-90	43
70-80	25
60-70	12
<60	32

Table 5.4: Percentage of records with high-quality beats for records with all vital-sign parameters (heart rate, blood pressure, oxygen saturation and ST level.)

The main disadvantage of the algorithm is that it requires a template to estimate the quality

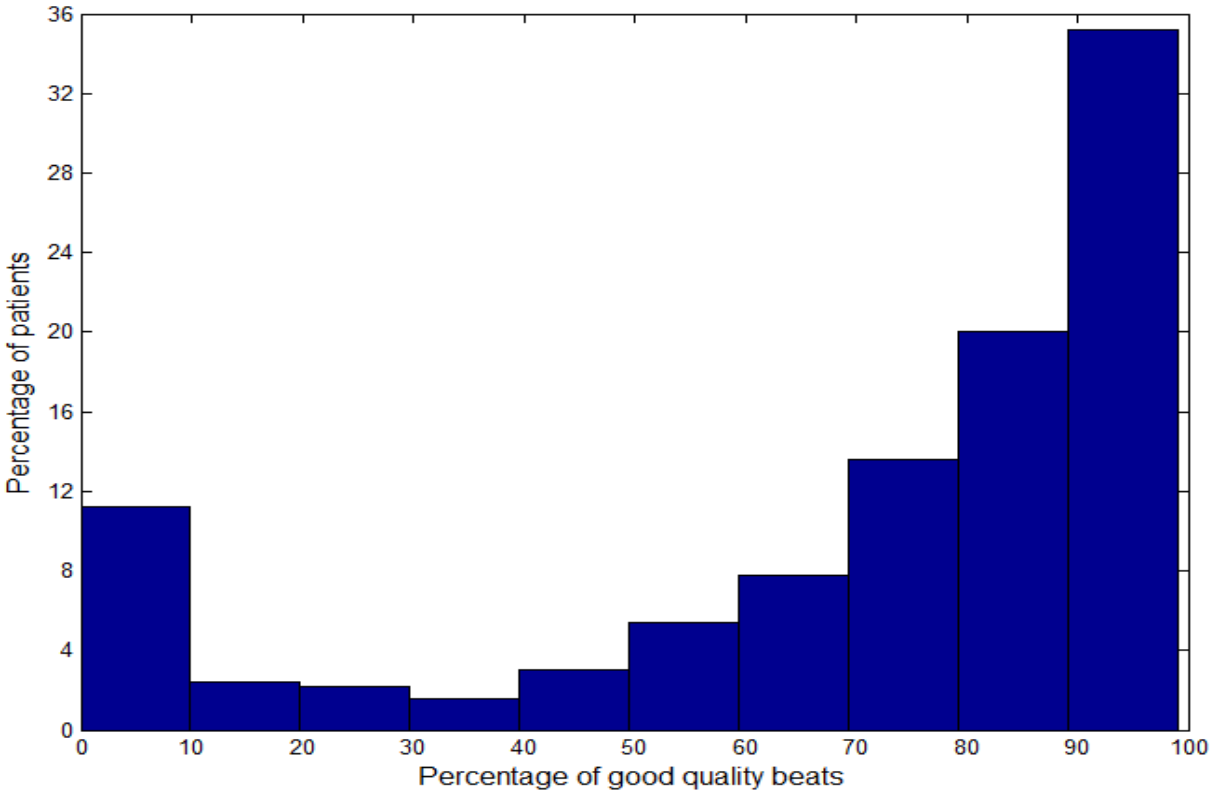


Figure 5.7: Histogram of the SQIs for the 500 patients in the database.

of ECG which makes it unsuitable for real-time analysis. However, this limitation does not affect the analysis in this thesis since the rejection of records is carried out retrospectively.

5.6 Summary

In this ambulance population, there was an almost equal number of patients with STEMI and NSTEACS. Earlier pre-hospital studies have shown that only about 5 to 10% of all patients with chest pain in the pre-hospital field have an acute coronary syndrome. The inclusion criteria in the current study were the usual sending criteria for a pre-hospital ECG among UK ambulance crew. The high percentage of patients with ST elevation may be a selection bias or may simply reflect the fact that the ambulance crew had a greater potential to select chest pain patients in whom there was a clinical suspicion of an acute coronary syndrome.

Out of the 500 patients, just over 50% had complete records. The parameter that was

collected the least reliably was oxygen saturation, while heart rate and ST level were the most reliably collected vital signs. The ECG in the pre-hospital setting is corrupted with noise and for this reason a Signal Quality Index which uses template matching was developed to reject low-quality ECGs. Sixty-one ECG records with an SQI of above 90% were complete.

There were few challenges in the early phase of the data collection process. Firstly, the ambulance crew were forgetting to transmit the data to the Medtronic server, mainly due to cumbersome process of transmitting the data. Secondly, the ambulance crew used different probes to measure oxygen saturation since the Medtronic oxygen saturation probes were recalled by the manufacturer. Lastly, as the data was transmitted using 3G connection, there were many instances where the network was too congested and data could not be transmitted successfully. For the study to be successful, it was critical to engage with the ambulance crew on a regular basis and explain the importance of the study. In order to do this, training workshops were arranged to explain the study and to understand the challenges faced by the ambulance crew in transmitting the data.

The next chapter is concerned with assessing which parameters can be extracted from the ECG to allow distinguishing of non-cardiac groups from ACS group, particularly the NSTEACS group.

Chapter 6

Spectral analysis of ECG-derived information as a diagnostic tool for acute coronary syndrome

6.1 Introduction

The main purpose of this chapter is to investigate the clinical importance of heart rate variability (HRV) in patients with acute coronary syndrome (ACS) in the pre-hospital setting. The chapter also assess whether measures of heart rate variability, as detected during the ambulance transportation, add useful information for the early identification of patients who have non-ST elevated acute coronary syndrome (NSTEACS).

6.1.1 Changes of HRV related to myocardial infarct

This section provides an overview of the HRV metrics and their relevance to autonomic function which have been found to be the most useful. The connection between decreased HRV and mortality in patients suffering acute MI was first reported in 1978 by Wolf *et al.* [161]. Since then, numerous studies have been performed and they have confirmed the reduction of the HRV with time or frequency domain analysis in MI patients, measured a short time after MI

[162–170].

In particular, frequency-domain HRV analysis has been widely investigated in post-MI patients. Valkama *et al.* [98] described a significant decrease in the parasympathetic activity influenced high-frequency power of HRV from the early phase of MI, 12 hours to one week after MI, which was also more striking in patients with inferior MI. Lombardi *et al.* [171], who studied 33 patients with acute MI three hours after the onset of symptoms and one week after hospital admission, found a lower HRV in patients with anterior MI during the acute phase and a significant increase in the LF component one week after the acute event in inferior MI reaching the values of patients with anterior MI. According to these findings it can be hypothesized that the initial vagal hyperactivity of an inferior MI is short-lasting but capable of reducing sympathetic excitation, and is rapidly followed by sympathetic activation still detectable four weeks and several months after acute MI [172].

The first large study to show the usefulness of HRV for predicting long-term outcome after a MI, the Multi-Center Post-Infarction Program (MPIP), involved 808 patients who underwent ambulatory monitoring within 11 days of an acute MI [162]. After a mean 31-month follow-up, the mortality rate of patients with SDNN $<$50 ms was 34% compared to 12% in those with an SDNN $>$100 ms. SDNN predicted mortality independently of other risk predictors such as left ventricular ejection fraction or ventricular arrhythmias.

A re-analysis of the MPIP data comparing the predictive value of all time domain HRV indices found that SDANN $<$40 ms had the strongest univariate association with all-cause and both cardiac and arrhythmic mortality. This association persisted after adjustment for covariates. Measures of high frequency fluctuations in NN intervals, such as rMSSD or pNN50, were not significantly associated with outcome [173].

The majority of the studies described above examined changes in HRV and correlation to outcome of death and coronary events in post-MI patients. There are very few studies that investigated the changes in HRV in the early stages of MI. The results of Goseki *et al.* [174] indicated significant decreases in HF power before ischaemia (of most relevance in this thesis). Although the majority of patients in that study (12 out the 19) were monitored without discon-

tinuation of beta-blocking agents, which are known to affect HRV parameters.

Kop *et al.* [175] investigated the role of autonomic changes in the onset of ischaemic events using spectral analysis of HRV. HRV was assessed 60, 20, 10, 4 and 2 minutes before each ischaemic event and 2, 10, 20 and 60 minutes after ischaemic events. A significant decrease in HF and LF components was observed in the period preceding the ischaemic event. HF decreased in the 60-to-10-minute interval before the ischaemic event. The study demonstrated that decreases in HRV precede myocardial ischaemia and that the decreases occur as early as 10 minutes before the event and are most pronounced in the 4 minutes before ischaemic ST-segment depression. These findings suggest that vagal withdrawal precedes the onset of transient myocardial ischaemia and may help explain the phenomenon of mental stress-induced ischaemia, which typically occurs at low heart rates.

In 2003, Manfrini *et al.* [168] assessed vagal and sympathetic activities using time domain measures of HRV in 172 consecutive patient. Twenty-four hour ECG monitoring for HRV analysis was performed during the early phase of the acute coronary syndrome (recording started within 12 hours of admission). The primary events (outcome) were define as cardiac death, MI, urgent revascularization, and hospital readmission, due to unstable angina. PNN50 $<3\%$ was used as a marker of low parasympathetic activity. Extremely low values of parasympathetic activity (pNN50 $<3\%$) were strongly related to subsequent events ($P<0.001$).

The mechanism by which HRV is transiently reduced after MI and by which a depressed HRV is predictive of the neural response to acute MI is not yet defined, but it is hypothesised to involve derangements in the neural activity of cardiac origin [176]. One hypothesis involves cardiac sympathetic and sympathovagal reflexes and suggests that the changes in the geometry of a beating heart due to necrotic and non-contracting segments may abnormally increase the firing of sympathetic afferent fibers by mechanical distortion of the sensory endings. This sympathetic excitation attenuates the activity of vagal fibres directed to the sinoatrial node. Another explanation, especially applicable to marked reduction of HRV, is the reduced responsiveness of sinus nodal cells to neural modulations [162].

6.2 Computation of heart rate variability

Respiratory information is known to be present in the ECG in three forms; Respiratory Sinus Arrhythmia (RSA); R-S amplitude modulation and baseline wander. RSA can be thought of as "frequency modulation" as characterised by variations in the period between consecutive R-peaks in the ECG waveform. The R-S amplitude and baseline wander can be thought as "amplitude modulation" of the ECG.

In this section, we describe the methodology developed for computing HRV measures for the patients in our clinical study. The aim is to understand whether the spectral characteristics of HRV could help identify high-risk ACS patients. In this section, the methodology for performing spectral analysis on the information derived from the ECG is described.

The flow chart summarising the methodology is shown in Figure 6.1. The left hand side of the flowchart shows the technique for extraction the RSA from the ECG while the right hand side shows how to extract respiratory information from the baseline wander signal. The two process are described in details in following sections.

In this thesis, a sliding window of one-minute length with 50-second overlap was used to extract respiratory information from the baseline wander (see Section 6.2.2) and parasympathetic activity from the HRV (see Section 6.2.1). This means the lowest frequency that can be resolved is 1/60 = 0.0167Hz.

6.2.1 Respiratory sinus arrhythmia as an index of vagal tone control

Respiration modulates the heart rate such that it increases during inspiration and decreases during expiration. Heart rate changes synchronously with respiration via two different mechanisms: the mechanical effects of respiration (mainly changes in venous return which directly modulates the sinoatrial node) and through the autonomic nervous system [177]. RSA is affected by conditions that suppress or enhance HRV. Hence RSA decreases with age, but can also be reduced by the presence of cardiac and neurological conditions, as well as medication such as beta-blockers and sedatives.

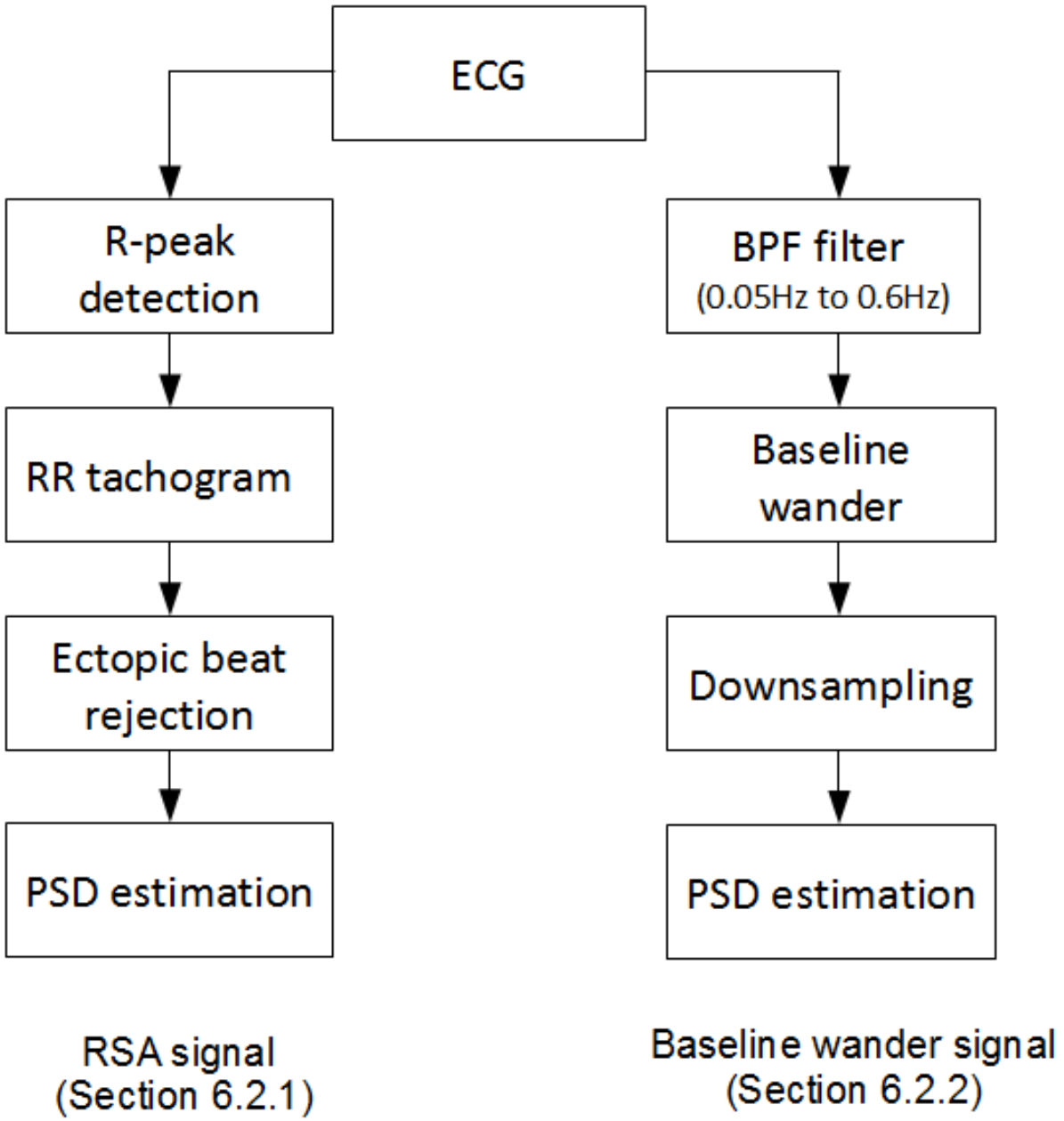


Figure 6.1: Flow diagram of the methodology used for computing heart rate variability from RSA and extraction respiratory information from baseline wander.

The RR-interval was obtained from subject 0196, and a example record belonging to an 84 year old male who was diagnosed with NSTEMI towards the end of his hospital stay. This example is used throughout this section to demonstrate the methodology for computing HRV. The RR-interval time series was band-pass filtered after resampling. This was achieved using a bandpass least-square FIR filter with a pass band extending from 0.05 to 0.5Hz (corresponding to 3 to 30 breaths per minute), 5% ripple in the pass-band, and 60dB of attenuation in the stop-

band. An example of applying the technique described in Section 2.7.3 to obtain the RSA prior to computing the Lomb-Scargle periodograms is shown in Figure 6.2.

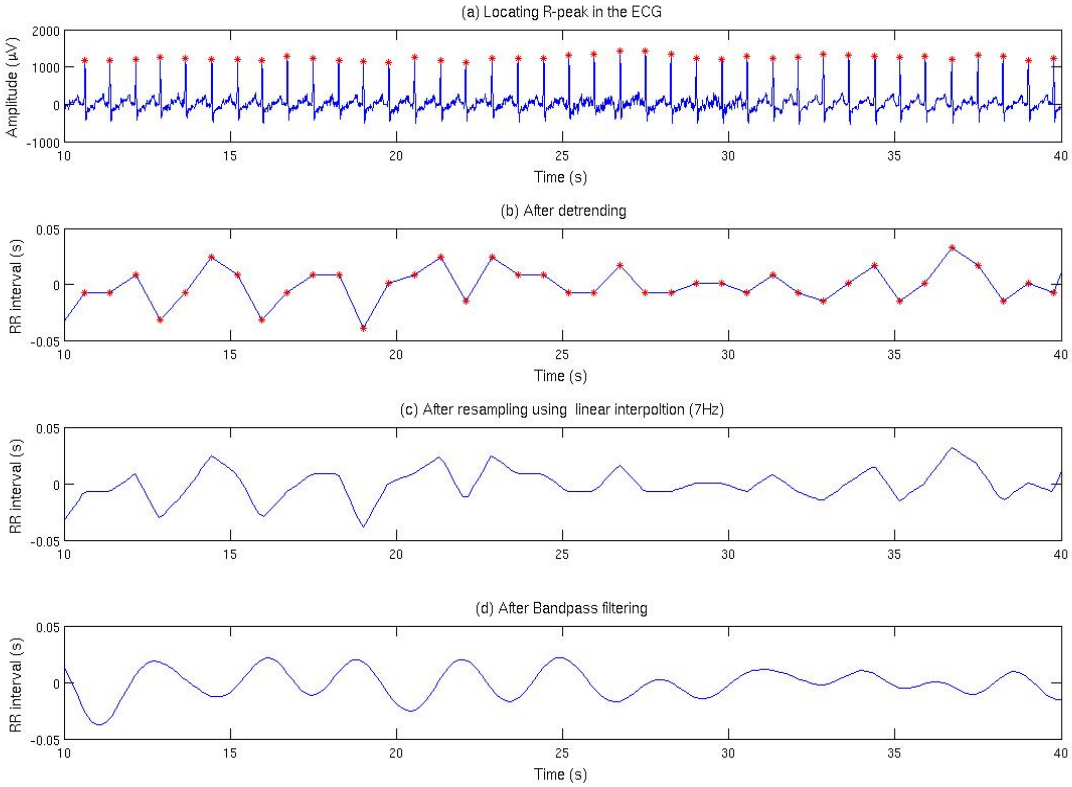


Figure 6.2: Illustration of the steps involved in processing the ECG to extract the RSA signal. (a) R-peak detection. (b) After detrending the RR-interval (c) After band-pass filtering (d) After resampling at 7Hz.

The PSD of the RSA was computed using the Lomb-Scargle periodogram, as shown in the example in Figure 6.3 where it can be seen that the Lomb-Scargle periodograms gives a dominant peak at the same location of 0.33Hz (20 breaths per minutes).

Each PSD was normalized individually using the square of the magnitude of the signal (the total energy), to scale the PSDs [178]. The evolution of the normalised PSD for the entire duration of the recording is shown in Figure 6.4. The dominant peak remains close to 0.37Hz for the first two-thirds of the recording.

As described in Section 2.7.2, the frequency content of HRV may be split up into bands. These include VLF fluctuations (at frequencies below 0.05Hz), which are thought to be related

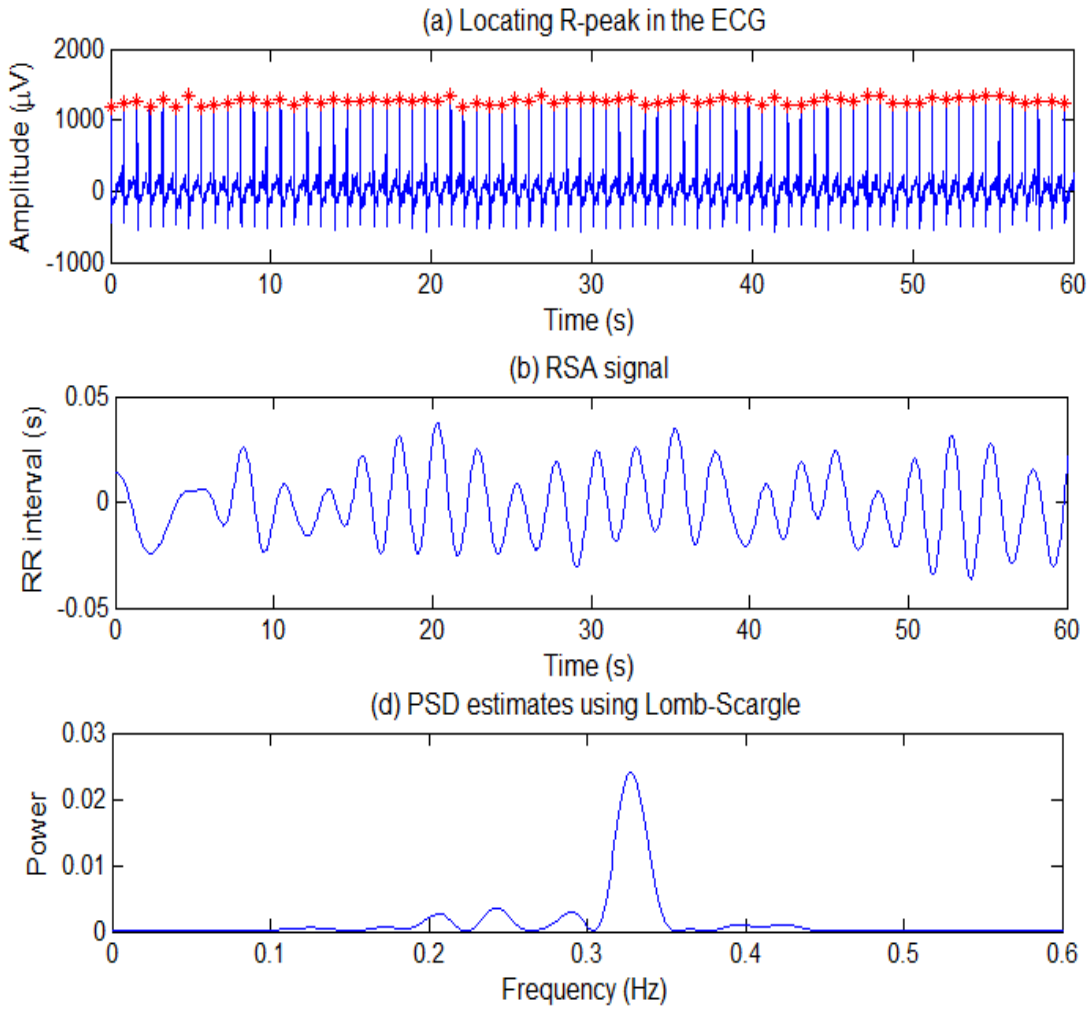


Figure 6.3: Illustration for estimating the power spectral density of the HRV for a one-minute window using the Lomb-Scargle periodogram. (a) Extraction of RR interval (b) The RSA signal. (c) Power spectral estimated from the Lomb-Scargle periodogram. In this example the dominant peak is at 0.33Hz.

to thermoregulation; LF fluctuations (around 0.1Hz) related to baroreflexes; and HF fluctuations due to RSA [177]. The HF component is resolved almost exclusively by fluctuations of the vagal-cardiac nerve activity and is generally accepted as a marker of parasympathetic activity [95]. Therefore, "a priori" information about respiration can be included in the estimation of the HF component to enable proper tracking of this component.

In the past decade, there has been great interest in the development of algorithms to enable reliable quantification of the energy in the LF and HF bands during nonstationary events [179–181]. Different time-frequency and time-varying approaches have been proposed to track the

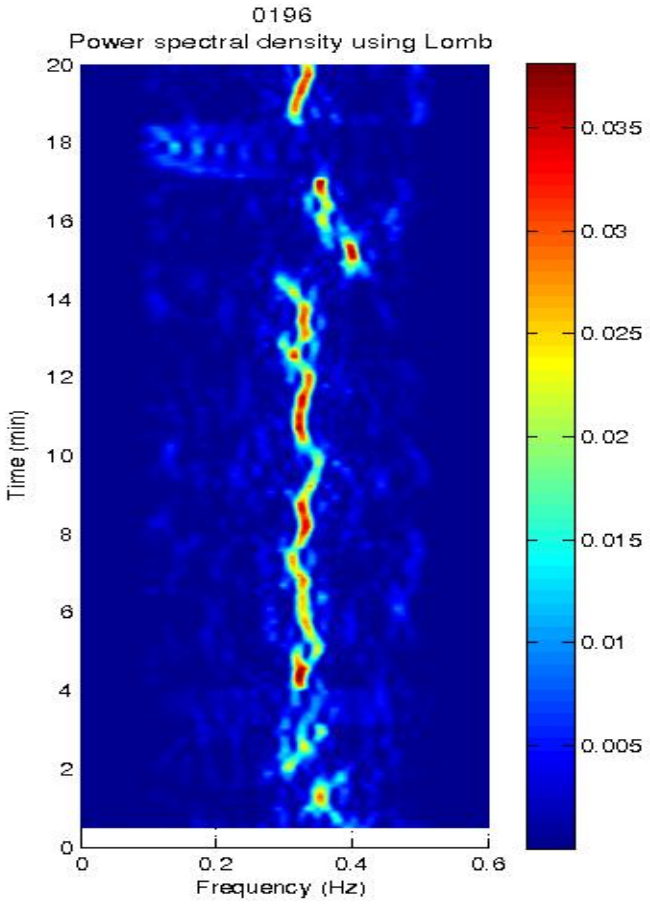


Figure 6.4: Evolution of the energy normalised power spectral density for the RSA signal for the duration of the recording. The dominant peak remained around the same region of about 0.38Hz for the first two-thirds of the recording.

changes in HRV during nonstationary events such as ischaemic attacks. There has been interest in selecting the most appropriate frequency band for the computation of the LF and HF power. In traditional spectral analysis, these bands are fixed, but this choice is obviously suboptimal when dynamical tracking is required. Goren *et al.* [180] outlined the four main limitations of using constant boundaries for analyzing physiological signals. Firstly, the choice of a suitable set of constant boundaries is usually made without reference to the data or sometimes by examining the data of all the subjects, and choosing a set of frequency limits which best suits most of the data. Secondly, the location of the peaks and the limits of the frequency ranges may change significantly with time, as a result of autonomic manoenvres. Standard frequency ranges do not take this into account. Thirdly, there may be a lack of selectivity as additional peaks may sometimes occur in the higher frequency ranges (such as very high-frequency peaks

in transplant patients [181]). Lastly, the frequency bands depend strongly on the individual, their age and health.

Algorithms for tracking the time-varying changes in HRV taking into account the definitions of the LF and HF regions have been proposed [180, 182]. Goren *et al.* [180] developed an algorithm to track changes in the frequency bands using the continuous wavelet transform. The algorithm works by finding the maximum value within a predefined frequency region. Then it locates the two minima surrounding this peak. Bailón *et al.* [181] proposed two techniques for defining the LF and HF bands. The first method used half the mean of the heart rate to set the upper bound of the HF band. The motivation for using half the mean HR is that the intrinsic sampling frequency of HRV is defined by heart rate. Hence, the maximum frequency that can be resolved is half of the heart rate (Nyquist criteria). The second method used the respiratory information to set the upper limit of the HF band. In both techniques the LF band was defined from its lower limit to the lower limit of the HF [181].

The main limitation of this approach is that it requires the direct recording of respiratory signal, which is not always suitable. If the bandwidth would be estimated from the power spectrum of the HRV signal itself, the much higher variability may yield inaccurate estimates. However this limitation was overcome in this thesis by estimating the respiratory information from the baseline wander signal.

6.2.2 Extraction of respiratory rate from amplitude modulation of the ECG

Baseline wander is caused by the patient's breathing or movements during recording. The expansion and contraction of the chest that accompanies respiration results in the motion of chest electrodes with respect to the heart. This can cause baseline wander in the ECG, clearly seen in deep or exaggerated breathing. During inspiration, the apex of the heart is stretched towards the abdomen because of the filling of the lungs, helped by the shifting down of the diaphragm. During expiration the elevation of the diaphragm, that helps the emptying of the lungs, com-

presses the apex of the heart towards the breast. Thus respiration changes the angle that the electric cardiac vector makes with a reference vector and this modulates the R-S amplitude of the ECG waveform [93]. There are various techniques for extracting respiratory information from the amplitude modulation of the ECG. In this thesis, we use spectral analysis of the baseline wander signal to extract information.

Baseline wander was extracted from the same ECG as in Section 6.2.1, by band-pass filtering using the filter with the characteristics given in Section 6.2.1. After band-pass filtering, the frequency content of the baseline wander in a 1-minute window was estimated as follows. First the output of the band-pass filter was downsampled from 125Hz to 25Hz. A decimation algorithm, which filters the signal prior to resampling, was used to reduce the effect of aliasing in the downsampled signal. Figure 6.5 shows the baseline wander extracted using these signal processing steps.

Figure 6.6 shows an example of the PSD estimated from the baseline wander signal using the Lomb-Scargle periodogram. As can be seen from the lower plot (c), there is a dominant peak at 0.33Hz corresponding to a respiratory rate of 20 breaths per minute.

As with the RSA signal, the PSDs were energy normalized for each one-minute window. The evolution of the normalised PSDs over the entire duration of the recording are shown in Figure 6.7. It can be seen from the plot that the respiratory frequency remains close to 0.38Hz for the first two-thirds of the recording.

The dominant peak of each PSD was found by locating the largest peak in the spectrum. Estimation of the respiratory frequency from the largest peak comes with the risk of selecting the location of a spurious peak. This risk can be reduced by narrowing down the search interval to include only the frequencies which are physiologically plausible. The search interval for the dominant peak was defined to be between 0.15 and 0.5Hz (between 9 and 30 breaths per minute) [178].

The dominant peaks were extracted from each PSD obtained from the baseline wander signal in successive one-minute windows. To reduce the effect of noise the extracted respiratory rates from each window were median filtered using a 5-point median filter. The respiratory

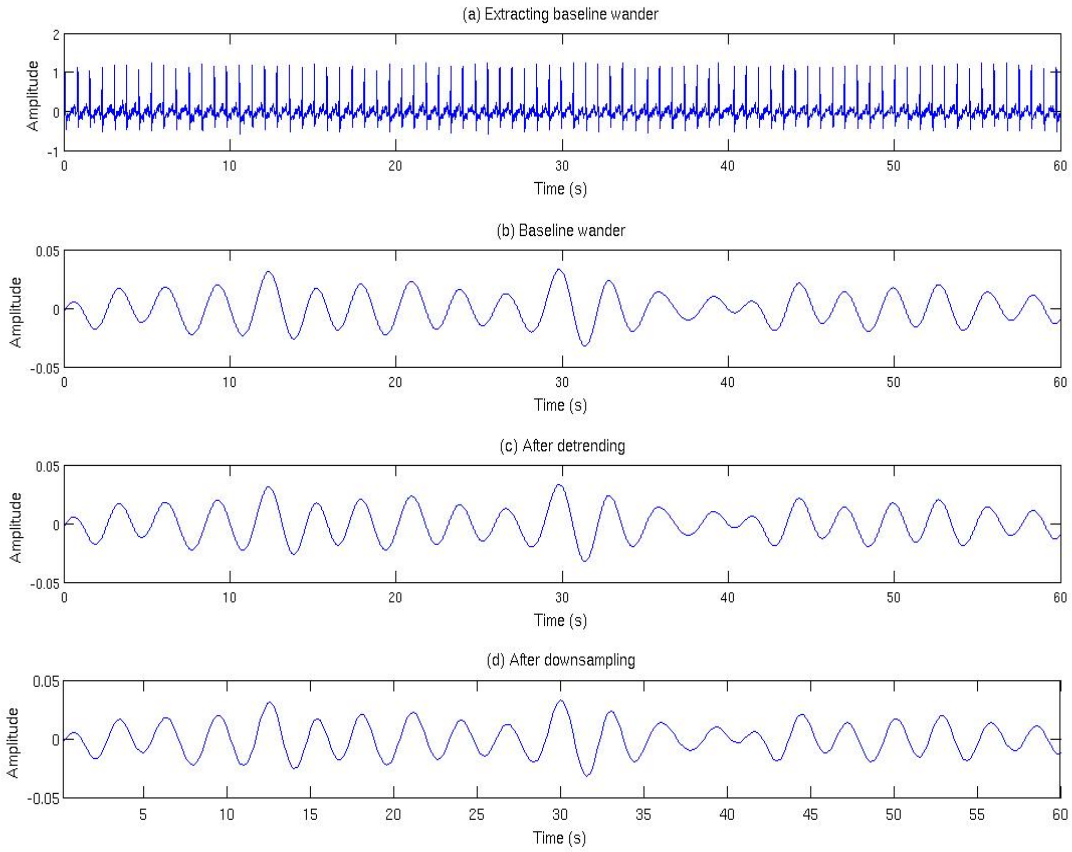


Figure 6.5: Extracting the baseline wander signal using a bandpass filter. (a) The ECG waveform. (b) The extracted baseline wander signal using the band-pass FIR filter described in the text. (c) The baseline wander signal after detrending. (d) The baseline wander signal after downsampling from 125Hz to 25Hz.

frequencies were band-limited to ± 3 breaths per minute and this is shown by the black solid lines in Figure 6.8.

6.2.3 Tracking changes in parasympathetic activity

In this thesis, we investigate the two techniques proposed by [181] to track changes in parasympathetic activity. For the first method, half the mean HR is calculated for each window and used to define an upper limit for the HF band. The second method uses the dynamic respiratory information extracted from the baseline wander signal and the bandwidth is set to 0.1Hz (as discussed in Section 6.2.2). With the example shown in Figure 6.9, the band set using the res-

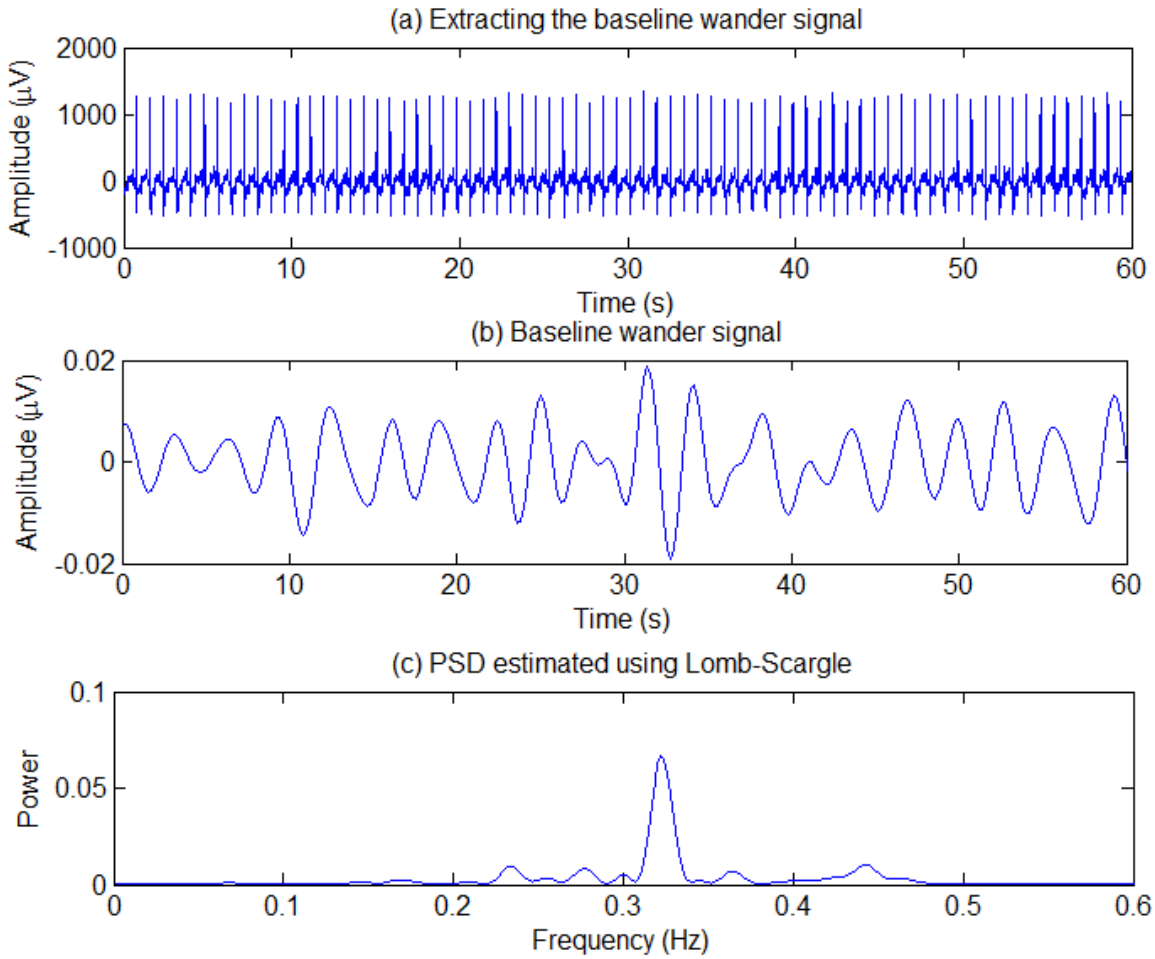


Figure 6.6: Power spectral density of the baseline wander for a one-minute window of the same subject as in Figure 6.5. (a) Extraction of baseline wander signal from the ECG (b) The baseline wander signal. (c) Power spectral estimated from the Lomb-Scargle periodogram. For this example the dominant peak is at 0.33Hz.

piratory frequency lies slightly outside the limit of the standard band of 0.15 and 0.4 Hz. Thus analysis of HRV using the standard frequency band may have yielded an inaccurate interpretation of the evolution of the vagal tone activity. The new definition of the HF band allows the tracking of the parasympathetic activity changes.

The power in the LF and HF bands was calculated by integrating the power spectral density over the specified frequency range. In addition to the power in the LF and HF band. To ensure a smooth signal the ECG was median filtered using a 7-point median filter. Figure 6.10 shows the trends of the normalised LF and HF components and the LF/HF-ratio obtained using the dynamic band (upper cut-off set by respiratory frequency). As can be seen, the power in the

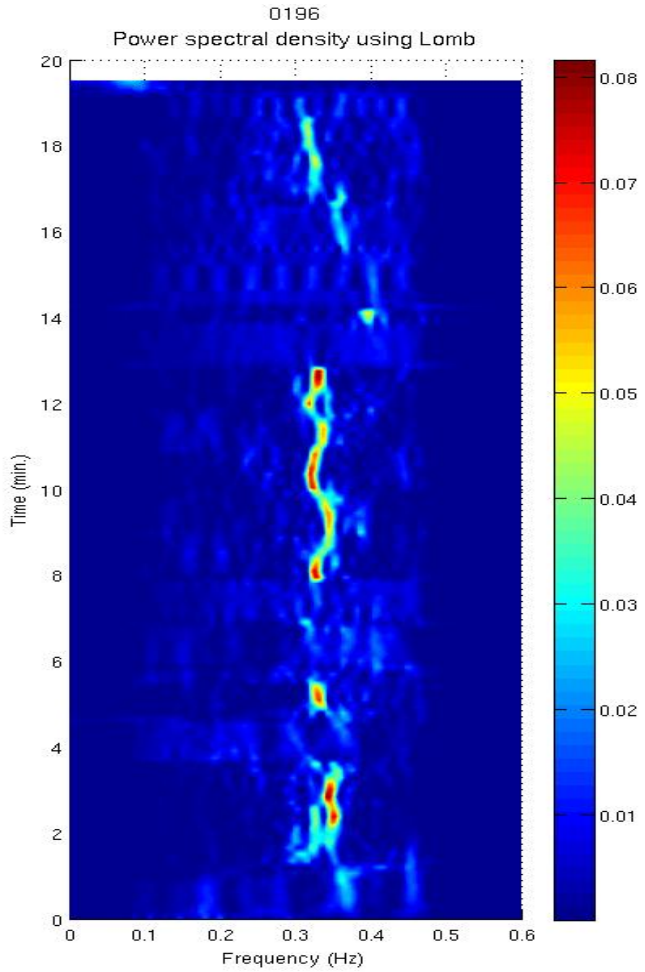


Figure 6.7: Evolution of the normalised power spectral density (PSD) computed using Lomb-Scargle periodogram for the duration of the recording. The dominant peak remains close to 0.38Hz for the first two-thirds of the recording.

HF band is higher than the power in the LF band. The high HF power implies that there is an increase in parasympathetic activity while the low value of LF/HF-ratio suggests depressed HRV which is expected since this patient is elderly and was diagnosed with NSTEMI.

6.3 Vagal tone control in acute coronary syndrome patients

Patients who were given beta-blockers or have diabetes were excluded from the analysis, as both affect the cardiovascular system. In addition poor quality ECG recordings which prohibited reliable R-peak detection were excluded. This includes those with weak and barely recognizable cardiac pulses, severe baseline drifting causing the signal to go out of recording

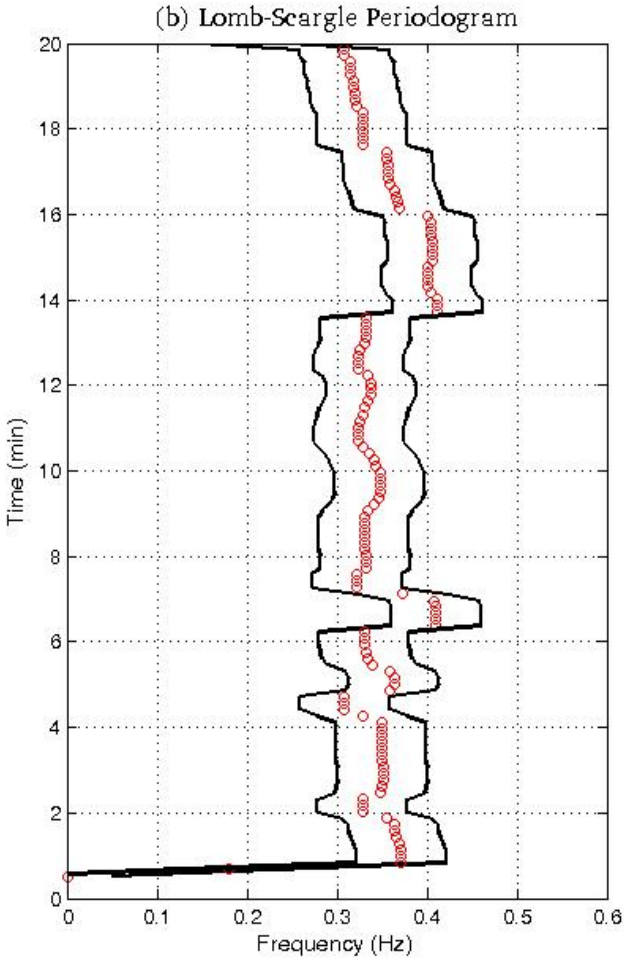


Figure 6.8: Extracting the respiratory frequencies from baseline wander signal using the Lomb-Scargle periodogram. The red circles are respiratory frequencies after median filtering. The black solid lines are the respiratory frequencies $\pm$ 0.05Hz ($\pm$ 3 breaths per minute).

range, severe motion artefacts and frequent occurrence of abnormal beats as determined by the use of the signal quality index technique described in Chapter 4. The study consisted of 500 patients of which 107 were diabetic, 109 were on beta-blockers and 125 had noisy ECG. In the non-cardiac group, 22.5% of the patients were diabetic, 27.6% were on beta-blocker and 18.4% had noisy ECG. In the ACS group, 18.0% of the patients were diabetic, 16% were on beta-blockers and 27.6% had noisy ECG.

A subset of 20 patients from the ACS group and 20 from the non-cardiac group were selected for HRV analysis. The aim was to investigate whether HRV spectral analysis can offer some discrimination between non-cardiac and ACS patients during the pre-hospital phase of

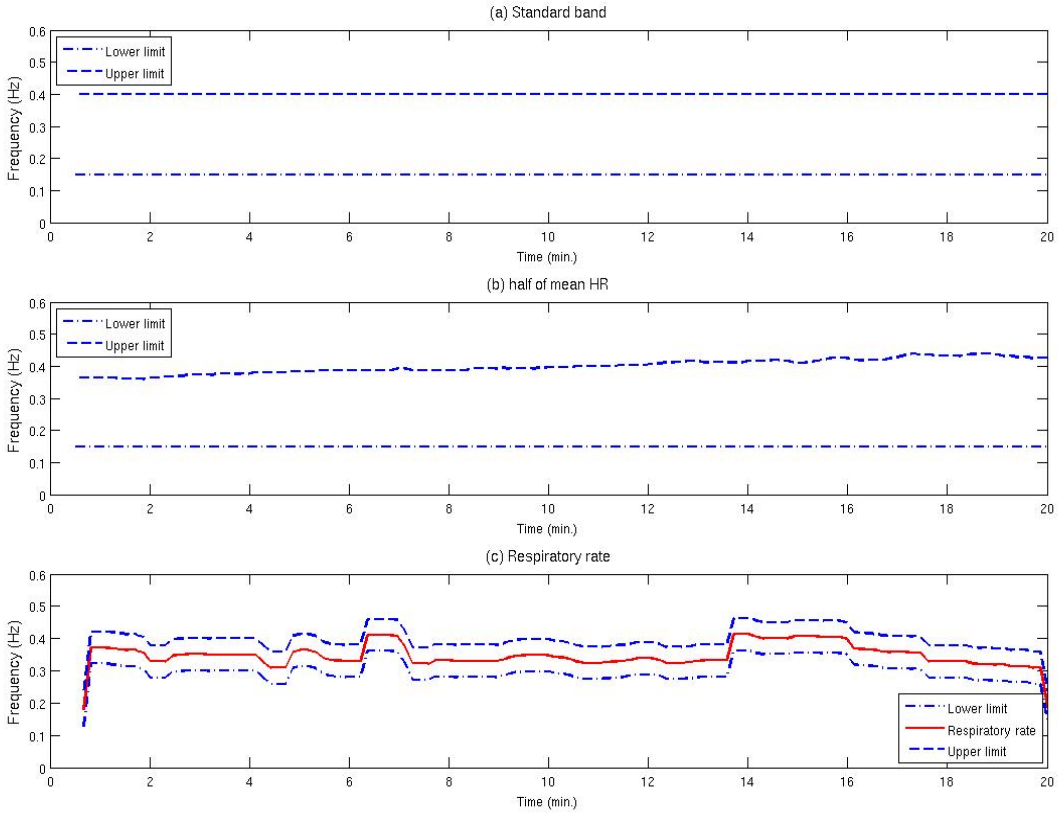


Figure 6.9: Illustration of the three methods used for defining the bands to compute the HF component of the HRV from the ECG recording in Figure 6.6 (baseline wander signal). (a) Standard band (0.15Hz and 0.4Hz). (b) Half the mean HR. (c) Limits set using the ECG-derived respiratory sinus arrhythmia (RSA).

their care. Table 6.1 shows a list of patients from the non-cardiac and ACS groups which were selected for comparison. As previously stated, aging leads to a decline in autonomic nervous system function. Research shows that the LF power decreases with age and there is no association with age for the LF/HF-ratio [183–185]. As the ages of the patients in the two groups fall within the same range of ≥ 65 (with only three patients from non-cardiac group and four from ACS group falling outside this range). Therefore, age correction for heart rate variability was deemed unnecessary. A statistical significance using the Mann-Whitney rank-sum test showed that there is no statistical significant difference (*p-value* = 0.09) in the median of these two patient groups.

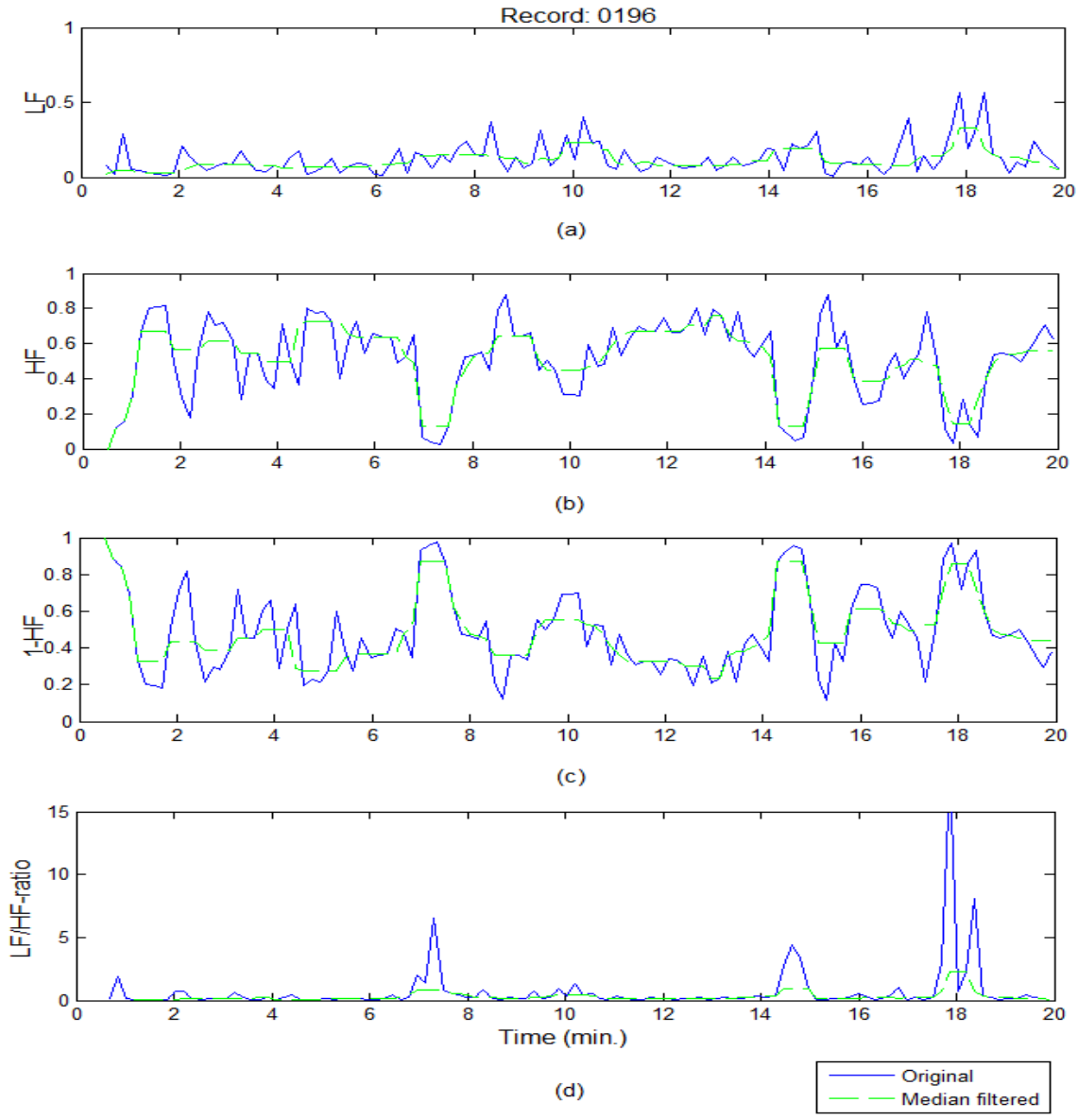


Figure 6.10: The frequency trends of the power in LF and HF using dynamics bands set using respiratory frequency. The components were computed from the PSD estimated using the Lomb-Scargle periodogram. The red graphs are the median filtered plots.

6.3.1 Analysis of results from the two patient groups

The power in the LF and HF bands was calculated by integrating the power spectrum over the specified frequency range (found using the standard bands), and expressed in normalized units (nu) after dividing by the total power in the range 0.04-0.45 Hz (i.e. excluding the very low-frequency range at < 0.04 Hz), then multiplied by 100 (denoted as LFnu and HFnu). The LF/HF-ratio of the RR-interval was also computed. In some of the patients it was difficult

Record ID	Age	Gender
0014	82	Female
0020	80	Female
0021	68	Male
0033	75	Female
0036	73	Male
0039	85	Female
0041	88	Female
0044	73	Female
0045	58	Male
0080	84	Male
0110	90	Female
0114	53	Female
0120	56	Female
0279	78	Male
0280	71	Male
0334	75	Female
0345	92	Female
0367	89	Male
0451	82	Female
0478	71	Female

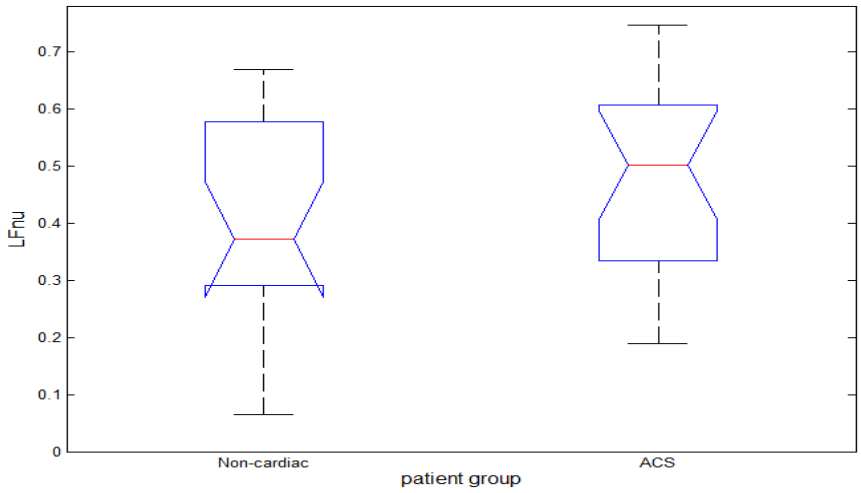
Record ID	Age	Gender
0008	52	Male
0010	71	Male
0011	68	Male
0019	66	Male
0022	55	Male
0030	79	Female
0031	57	Male
0035	73	Male
0048	60	Male
0049	66	Female
0057	80	Female
0086	72	Female
0134	86	Male
0255	89	Male
0302	77	Female
0351	73	Male
0453	57	Male
0502	69	Female
0503	69	Female
0505	75	Female

Table 6.1: A list of patients included in non-cardiac and ACS subsets for analysis.

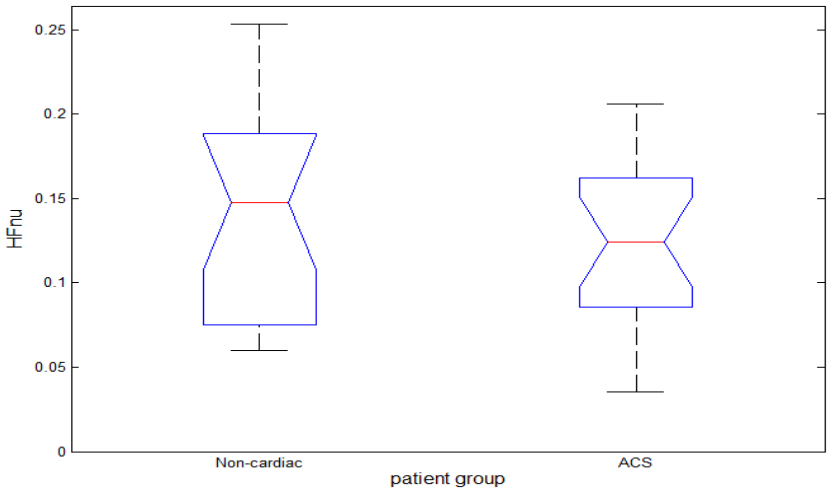
to extract the respiratory information from baseline wander signal. Therefore, standard bands were used for the analysis of HRV.

Boxplots of each parameter were plotted for easier comparison between the different groups and subgroups (see Figure 6.11 and Table 6.2). Each boxplot has a central mark at the median, while the edges of the box are the 25th and 75th percentiles. The whiskers extend to the most extreme data points not considered outliers, and outliers are plotted individually. The spectral analysis showed a dominance of the LF power (symphathetic activity) in both ACS and non-cardiac groups. The median of the LF/HF-ratio is non-cardiac group is 3.89 while that of ACS is 6.89. The median of the LF-power for the ACS group is 0.53 which is higher than that of the non-cardiac. The median of the HF power is lower in the ACS group than in the non-cardiac group, this implies that there is a greater vagal tone withdrawal for patients in the ACS group.

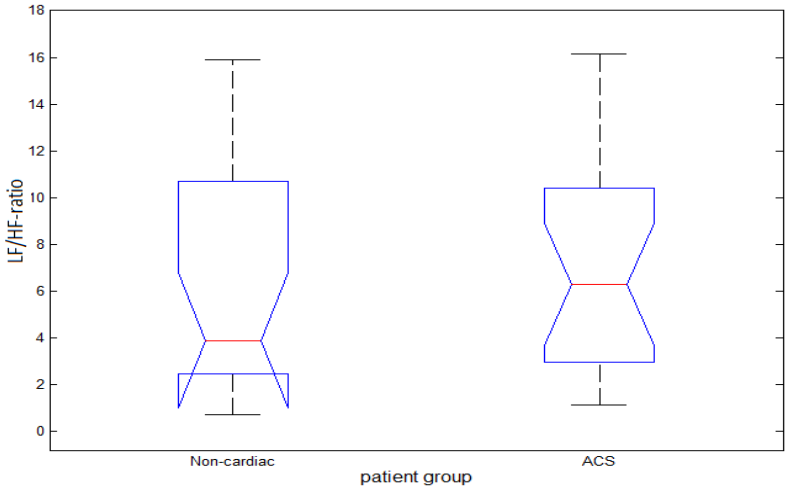
In addition, statistical significance differences in LF, HF and LF/HF-ratio between these two groups is calculated using the F-test, the Kolmogorov-Smirnov (K-S) test, Mann-Whitney rank-



(a) LFnu



(b) HFnu



(c) LF/HF-ratio

Figure 6.11: Boxplots showing low- (LF) and high frequency (HF) components of RR-interval in normalized units and their LF/HF-ratio between non-cardiac and ACS groups (both STEMI and NSTEACS). The boxplot is placed around the median (50%), represents centile 25-75%.

Variables	Non-cardiac (median ± IQR)	ACS (median ± IQR)
LF	0.37 ±0.29	0.53 ±0.26
HF	0.15 ±0.11	0.12 ±0.08
LF/HF-ratio	3.89 ±8.42	6.39 ±9.44

Table 6.2: The ACS subset has 20 patients and the non-cardiac subset also has 20 patients. The values given are median and interquartile range (IQR).

sum test ,and Student's t-test for unequal variances [154]. The F-test evaluates the probability that the variances in each distribution are significantly different (and hence one variance is significantly less than another). The K-S statistic is used for calculating the significance level of two data sets being drawn from different distributions functions. It is therefore useful for testing whether the distributions of the frequency measures in each group are significantly different. In particular, the K-S test is a robust method of finding shifts (rather than spreads) in a probability distribution (especially changes in the median value). Spreading of the distribution affects the tails of the probability distribution and may leave the median value unchanged. The K-S statistic is therefore insensitive to outliers and changes in the distribution's tails. Student's t-test (for unequal variances) is applied to calculate the probability that the means of LF, HF and LF/HF-ratio are significantly different between the two groups. The assumptions of these statistical tests are that the samples are drawn from normal distributions and the variances of each data set are homogeneous [154]. In addition, the distribution of the two patient groups can be compared using the Mann-Whitney rank-sum test, which tests whether the median are statistically different. The advantage of this test is that it does not assume any knowledge about the shape of the distribution.

Table 6.3 presents the results of testing the significance between the non-cardiac and the ACS group along with the mean(μ) and standard deviation (σ). Where the F-test gives a low probability, ($p < 0.05$), this indicates that the variance (and hence the mean) of the LF, HF or LF/HF-ratio between these two groups is significantly different. Where the K-S test results in a low probability, the distributions of the LF, HF or LF/HF-ratio can be said to be different between the two groups. If the Student's t-test results in a low probability, then there exists a

significant difference in the LF, HF or LF/HF-ratio between these two groups. The results in Table 6.3 show that none of the parameters are statistically different between the two groups. Finally, if the Mann-Whitney test give a low probability, this indicate that the medians of the LF, HF or LF/HF-ratio between the two groups is statistically significant.

Variables	Non-cardiac ($\mu \pm \sigma$)	ACS ($\mu \pm \sigma$)	F-test	K-S test	Student's t-test	Mann-Whitney test
LF	0.40 $\pm$0.17	0.48 $\pm$0.17	0.98	0.77	0.19	0.29
HF	0.15 $\pm$0.11	0.12 $\pm$0.08	0.97	0.77	0.24	0.34
LF/HF-ratio	5.98 $\pm$4.82	8.56 $\pm$4.82	0.08	0.28	0.25	0.34

Table 6.3: Results of statistical significance test between the ACS and the non-cardiac group using frequency domain measures of heart rate variability. The ACS subset has 20 patients and the non-cardiac subset also has 20 patients. The values given are mean (μ) and standard deviation (σ). The *p-values* of F-test, K-S test unequal t-test and Mann-Whitney test are shown. The statistical significance level was set at < 0.05.

The results of statistical significance test using F-test, K-S test, Student's t-test and the Mann-Whitney rank-sum test for LF, HF and LF/HF-ratio are shown in Table 6.3. The results in Table 6.3 further show that there is no statistical difference between the mean and variance of the non-cardiac and the ACS group. Furthermore, there is no statistical significant difference in median of the non-cardiac and NSTEACS groups.

Few studies are available about the prognostic role of changes in HRV in NSTEACS patients (unstable angina and non-ST-segment elevation myocardial infarction (NSTEMI) particularly in the early phases. In the section below, we attempt to see if there is any autonomic changes that are caused by NSTEACS. Using a subset of seven non-cardiac patients and seven NSTEACS patients from Table 6.1.

Variables	Non-cardiac (median $\pm$ IQR)	NSTEACS (median $\pm$ IQR)
LF	0.37 $\pm$0.28	0.41 $\pm$0.20
HF	0.15 $\pm$0.11	0.12 $\pm$0.07
LF/HF-ratio	3.99 $\pm$8.25	6.21 $\pm$6.48

Table 6.4: Results of the non-cardiac and the NSTEACS group using frequency domain measures of heart rate variability. The non-cardiac group had a subset of 7 patients and the NSTEACS subset had 7 patients. The values given are median and interquartile range (IQR).

Rimoldi *et al.* [186] experimentally documented that regional myocardial ischaemia provoked a powerful sympathoexcitatory response with a marked increase of the LF component of RR-interval and arterial pressure variability. In clinical settings, ischaemia-induced sympathetic over-activity was first described by Webb *et al.* [187] who found tachycardia and hypertension in the early phase of myocardial infarction. Lombardi *et al.* [163] applied autoregressive power spectral analysis of heart rate variability to detect autonomic disturbance within the first few hours of acute myocardial infarction in humans. They found a relative predominance of LF component independently from the infarct localization. In our study, the dominance of the LF power was observed in both non-cardiac and NSTEACS group. The possible mechanisms for the dominance of the LF component in NSTEACS involve a complex neural, metabolic and mechanical interaction during myocardial ischaemia. Generally, acute myocardial ischaemia affects both excitatory reflexes mediated by sympathetic afferent fibers and inhibitory reflexes mediated by vagal afferent fibers [187]. The relative magnitude of these opposing reflexes was shown to be related to the site and severity of myocardial ischaemia and the grade of ischaemia-induced cardiac deterioration [187]. The causes of the dominance of the LF components in the non-cardiac group might be due to the fact that the chosen patients are elderly and have illnesses that might affect the automatic nervous system.

6.4 Discussion

Changes in the respiratory rate are known to have an effect on HRV. Respiratory rate is inversely correlated with the power of the HF peak. Therefore a decrease in the HF peak while breathing rate increases indicates a decrease in vagal activity, which is smaller than estimated if one disregards the change in respiratory rate. Breathing rate was not measured in this study but was computed from using amplitude modulation of the ECG signal. However, for many of the records respiratory rate could not be computed due to noisy ECG.

Many drugs and illnesses such as diabetes and beta-blockers influence the activity of the autonomic nervous system. We addressed this limitation by excluding all patient with known

conditions or drugs that affect the automatic nervous system. This is a large portion of the patient population, which resulted in a small sub-group for analysis. This limitation may be further addressed by considering changes in HRV in a patient relative to the baseline condition of that specific patient (intrapatient evaluation).

The study was designed to help in the process of risk stratifying patients with ACS. Although the finding seems to indicate that heart rate variability does not have any diagnostic value, it is not possible to draw firm conclusion about the diagnostic value of HRV. Additional studies of more stringent design are needed to measure the clinical impact of the assessment of heart rate variability in early phases of ACS.

The next chapter investigate whether data fusion of vital-sign data may be effective in differentiation between the non-cardiac and NSTEACS groups.

Chapter 7

Data fusion for pre-hospital patient monitoring

Data fusion techniques may help to identify NSTEACS patients from the vital-sign data. This chapter discusses the implementation of different data fusion methods using the vital-sign data acquired from the pre-hospital monitoring described in Chapter 4 as inputs.

In an acute setting, vital signs are considered a marker of underlying pathology (sensitivity) and can alert the physician to a disease process and severity, but they do not define which disease process is ongoing (specificity). For example, an abnormal temperature signifies an underlying process which needs additional investigation, but not the type of process, location, or cause. Using established normal ranges for each vital sign can help clinicians quantify abnormal findings. When measured serially, vital signs are a monitoring tool which can signify both the progression of a disease process and the effectiveness of treatment. For example, a change in systolic blood pressure from 120 mmHg to 90 mmHg might mark increasing sepsis or the effect of a treatment.

NSTEACS can cause directional changes in vital signs, such as progressive hypertension and tachycardia [2]. These temporal trends may be of diagnostic value. There are also changes in vital signs that do not change with time, such as variability caused by discrete events (e.g., sympathetic activation due to painful manipulation of an injured extremity or changes due to a

dose of pain medication). If such non-directional variability is large enough, it can mask subtle temporal trends. Thus it is important to find features that can be used to distinguish NSTEACS patients from non-cardiac patients and may be able to take these changes into account.

A feature may be as simple as a moving average or the maximum value of a continually monitored vital-sign. Other features can be computationally more sophisticated, such as the variability of a signal or its signal power at a specific frequency. In this work, parameters related to temporal patterns that might have diagnostic value such as means and standard deviations were explored.

The process of building a data fusion model involves two stages; firstly, to determine which combination of automatically collected vital-sign features offers the best discrimination between non-cardiac and NSTEACS patients; secondly, to determine whether nonlinear classifiers provide improved discrimination over simpler linear classifiers. The chapter begins by providing an overview of existing data fusion techniques and discusses their suitability in the pre-hospital setting.

7.1 Overview of data fusion techniques

Most of the previous work on providing early warning of in-hospital patient deterioration can be separated into two groups: methods that rely on single parameters, such as single channel-alarms and those based on a combination of multiple parameters such as early warning scores [188].

Data can be collected from different single-channel, and then fused together to obtain an indication of patient's health status. An example of a simple data fusion system is the Early Warning Score (EWS) reported by Morgan *et al.* [189]. The EWS is a tool for bedside evaluation based on five physiological parameters: systolic blood pressure, pulse rate, respiratory rate, temperature and AVPU [1] score. Early warning scores allocate an increasing number of points to worsening physiological values until a trigger score is reached. The scores are usually

[1]This is a scale to assess level of consciousness. A=alert V = Responding to voice P= Responding to pain U = Unconscious

calculated by nursing staff during their regular observations of patients on general wards and surgical wards. Most aggregate scoring systems are based on the work of Morgan *et al.* [189] or later modifications produced by Stenhouse *et al.* [190]. The choice of score values and thresholds in these systems are based on clinical experience alone.

Various researchers have also attempted to use expert systems to build data fusion systems for early warning of patient deterioration [191–195]. There are many limitations to the use of knowledge based systems to identify patient deterioration: Rule-based systems generally only use very simple relationships to link measured values to generated alerts. Rule formation requires medical knowledge that is often difficult to capture and difficult to translate into rules. Formation of the rules is labour intensive for clinicians and after the initial design stage, the systems have to be repetitively evaluated in the clinical context to obtain acceptable levels of performance. Small changes in rules such as the thresholds or relations between variables can have a significant effect on the timing and number of alarms generated, and re-evaluation is therefore required. Rule-based systems have therefore had limited success even if the rules are evaluated continuously and automatically.

An alternative approach to expert systems is machine learning, which does not require any explicit statement of rules. Instead, a classifier is trained to map an input vector into one or more classes using examples contained from the training data. Various machine learning techniques have been used to build early warning systems; these include Factorial Switching Kalman Filter [196], Parzen windows [197], Support Vector Machine [198]. Almost all of these systems mentioned have been developed to identify deterioration in patients in the hospital setting particularly in the ICU. There are several major differences between the in-hospital and pre-hospital settings. In the ICU, therapy is much more intensive depending on the level of care: there are frequent inputs to the system, such as drug infusions or changes in treatment therapy, and so the vital signs are only part of the information. The function of alerts in the ICU is to attract a clinician's attention to an abnormality in one parameter, or in a subset of the parameters being monitored.

As described in Chapter 4, it was demonstrated that continuous vital-sign data could be

Parameter	Lower	Upper
HR(bpm)	30	300
$SpO_2(\%)$	85	100
SBP (mmHg)	20	200
DBP (mmHg)	20	200
MAP (mmHg)	20	200
ST level(μV)	-1000	1000

Table 7.1: Physiological upper and lower bounds for the vital-sign parameters.

collected during ambulance transport. The early warning scores mentioned above mostly use six vital-sign parameters: HR, RR, oxygen saturation, temperature, SBP and DBP. In our ambulance transport study, temperature and respiratory rate were not collected but the ST level could be computed from the ECG.

The Medtronic Lifepak 12/15 monitor saves only one continuous lead to be transmitted to a server and this is normally lead II. However, if lead II is too noisy another lead with a lower signal-noise ratio is saved. Thus ST level in this study were derived mainly from lead II.

To be able to see if there is any difference in the individual vital-sign data between the non-cardiac and NSTEACS, a univariate analysis is initially performed on each vital-sign parameter.

7.2 Data statistics

As there are physiological limits to the vital-sign values, rejection of data outside of these limits was performed prior to training the data fusion models. When calculating the mean and the standard deviation to be used for normalisation, it is necessary to remove artefacts, so that artefactual values do not influence the normalisation. The limits for artefact rejection are based on physiological knowledge, with the exception of blood oxygen saturation, for which the lower limit is set at 85%, as the pulse oximetry finger probe is increasingly inaccurate below this point [199]. The artefact rejection limits are given in Table 7.1.

The mean, μ, and standard deviation, σ, of the vital-sign data for all three groups are also calculated and shown in Table 7.2. The means of the vital signs of the ACS, non-cardiac and cardiac groups are very close, the largest differences being in heart rate and diastolic blood

pressure. The standard deviations themselves are also very similar for all groups.

Variables	ACS ($\mu \pm \sigma$)	Non-cardiac ($\mu \pm \sigma$)	Cardiac ($\mu \pm \sigma$)
HR (bpm)	81.02±10.4	84.71±13.17	97.27±16.48
SpO_2 (%)	96.56±2.0	94.38±2.0	94.78±2.34
SBP (mmHg)	139.13±7.8	139.6±8.95	138.39±11.06
DBP (mmHg)	86.75±8.5	83.6.61±7.83	86.26±11.82
MAP (mmHg)	103.07±8.7	104.93±8.95	103.00±12.08

Table 7.2: Mean and standard deviation of vital-sign parameters for the ACS, cardiac and non-cardiac groups.

Since we are mainly interested in distinguishing between the non-cardiac group and the NSTEACS group, which is a subgroup of the ACS, the means and the standard deviations of these two groups are also calculated and shown in Table 7.3. There is no difference in the means and standard deviation between these two groups. The ST level has a negative mean which is very close to zero; this implies that most of the values are clustered around zero. This is expected since most of these patients in these two groups do not have any ST elevation.

Variables	Non-cardiac ($\mu \pm \sigma$)	NSTEACS ($\mu \pm \sigma$)
HR(bpm)	84.71±13.17	84.25±12.60
SpO_2 (%)	95.38±2.0	95.59±1.70
SBP (mmHg)	139.60±8.95	140.55±8.29
DBP (mmHg)	83.61±7.83	83.11±5.79
MAP (mmHg)	104.93±8.95	102.66±7.75
ST level (μV)	-7.15 ± 69.41	-0.3± 53.98

Table 7.3: Mean and standard deviation of vital-sign data for non-cardiac and NSTEACS groups.

In addition to the means and standard deviations, the histograms for the vital-sign parameters from the non-cardiac and NSTEACS groups are shown in Figure 7.1. These histograms are very similar for both groups.

Figure 7.2 shows an example of vital-sign data from a patient in the NSTEACS group. The example is from patient 0297 who is a 37-year old male who was eventually diagnosed with unstable angina towards the end of his hospital stay. The vital-sign parameters recorded for these patients were SpO_2 , HR, SBP, DBP, MAP and the ST level. The heart rate for this

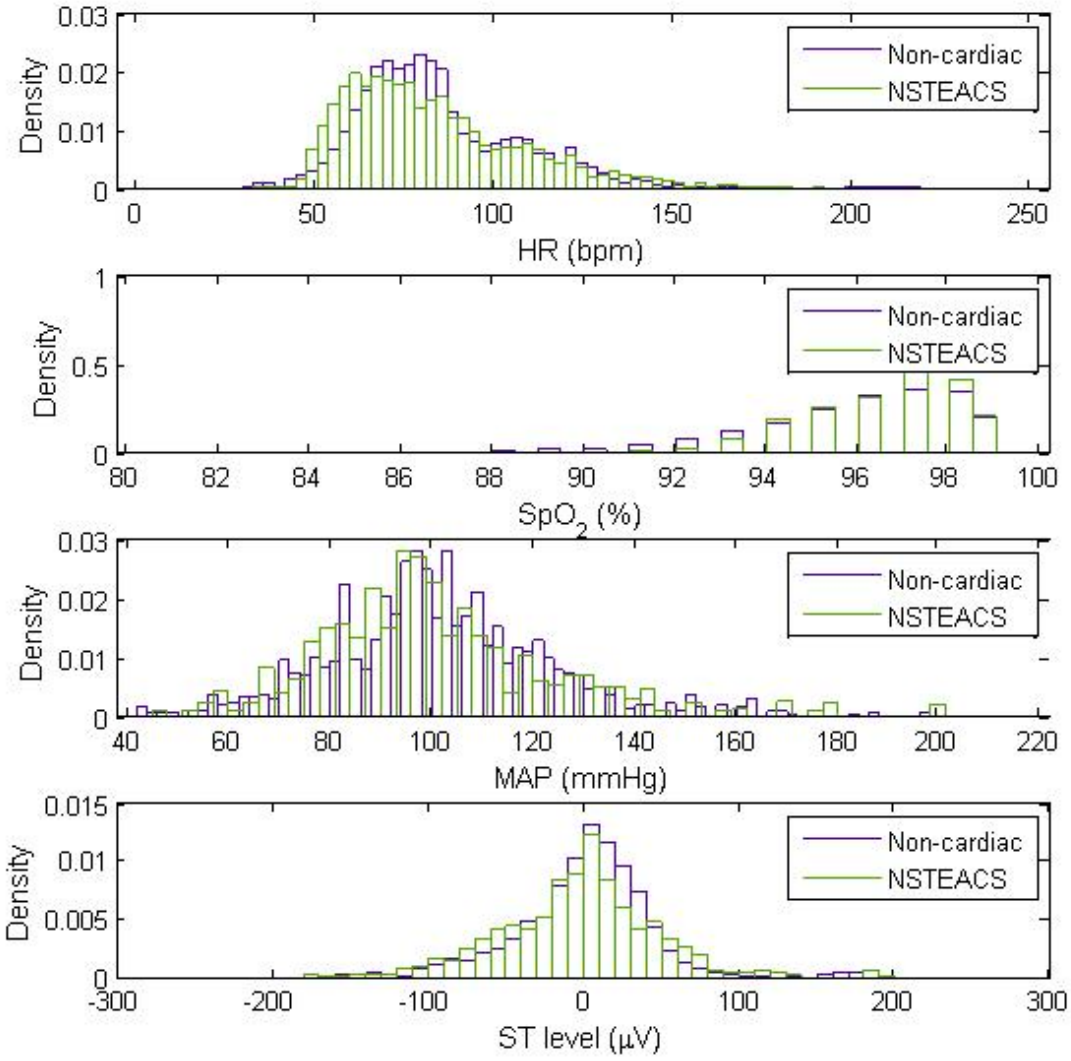


Figure 7.1: Distribution of vital-sign data for the non-cardiac group (blue) and the NSTEACS group (green).

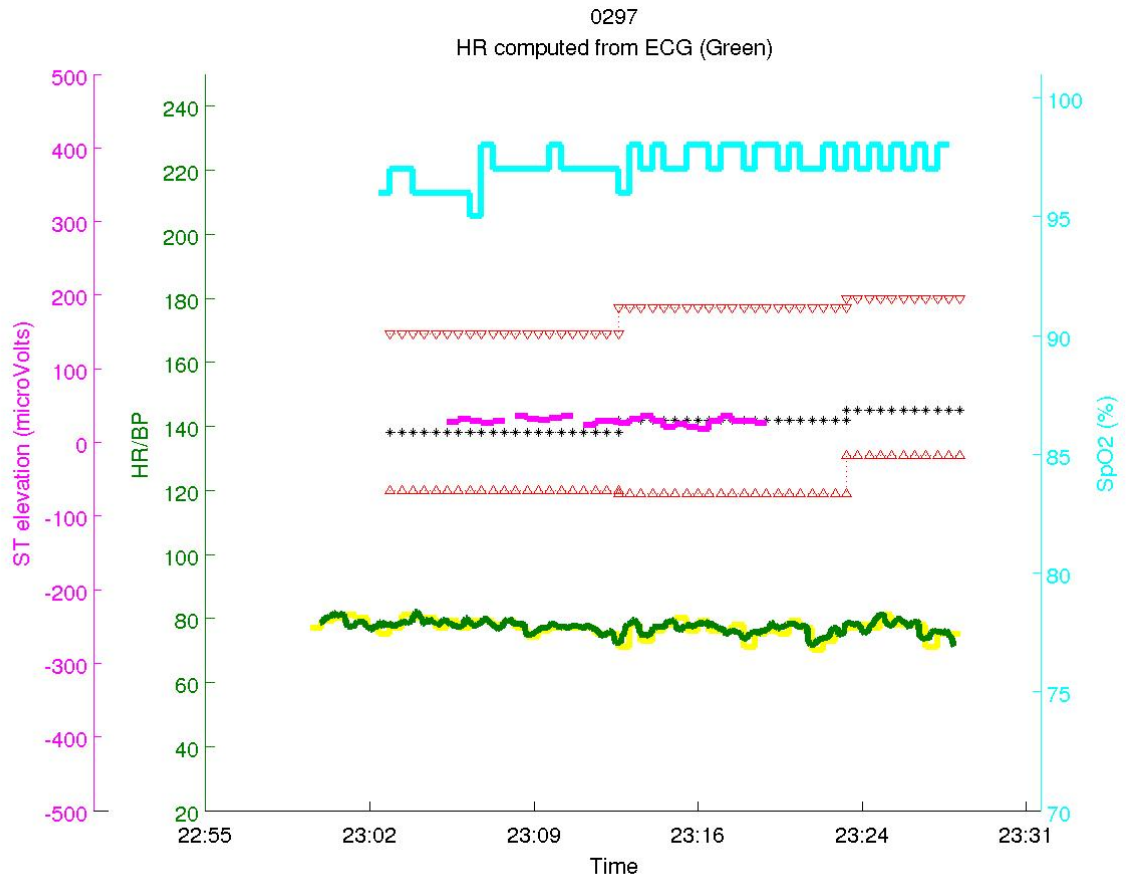


Figure 7.2: Vital sign record for patient 0297 from the NSTEACS group. The HR, SpO_2 , ST level are recorded in yellow, pink and blue respectively. The Systolic BP and Diastolic BP are indicated by the upper and lower red line, while the mean arterial pressure is shown as a dashed black line.

patient falls within the healthy range of 60 -120 bpm. The blood pressure indicates that the patient was hypertensive. The SpO_2 also falls within the normal range of 95% - 100%. The patient did not experience any ST level elevation during the ambulance journey.

The aim of this chapter is to investigate the feasibility of using these vital-sign parameters (and other relevant parameters) to identify as early as possible patients with NSTEACS.

Data fusion techniques may help to discriminate between the NSTEACS and the non-cardiac groups from multiple sources of vital-sign data. There are both advantages and disadvantages to assessing data fusion methods using data collected in the pre-hospital setting. Pre-hospital data represent the spectrum of vital signs (both NSTEACS and non-cardiac) that are encountered in this setting, and will also contain a mix of unrelated illness such as cancer

and diarrhoea. In addition, the vital-data collected in this setting are prone to having a lot of gaps and tend to be noisy.

7.3 Comparison of data fusion techniques

7.3.1 Data pre-preprocessing

Heart rate and SpO_2 were recorded every 30 seconds with the exception of the Mean Arterial Pressure, which was recorded approximately once every 10 minutes and held at that point until the next measurement. The ST level was estimated every 10 seconds using the ST analysis algorithm derived in the first half of this thesis. As the vital signs are sampled at different rates, it is important that they are resampled at the same rate. To achieve this, a linear time vector was created with each element representing a 30-second window. Each measurement was then associated with the nearest element in the vector. If two or more measurements were recorded within a 30-second window the median of the readings was used.

Normalisation of each parameter was carried out by calculating the sample mean μ and standard deviation σ of the training data, and then applying the transformation in Equation 4.20. Missing variables were replaced by the mean of that parameter from the group to which that record belonged.

7.4 Experimental results

The experimental methods used to build the models to differentiate between non-cardiac and NSTEACS group were described in Section 4.6. When training a data fusion model, it is not necessarily helpful to use the full dataset to build the model, if the number of data points in one class is much larger than the number in the other class. If this is the case, the model is likely to be biased towards the more frequently occurring class, and may not accurately model the behaviour of the class with fewer examples. This can be avoided by generating training sets with equal amounts of data from each class. The data fusion models in this chapter were

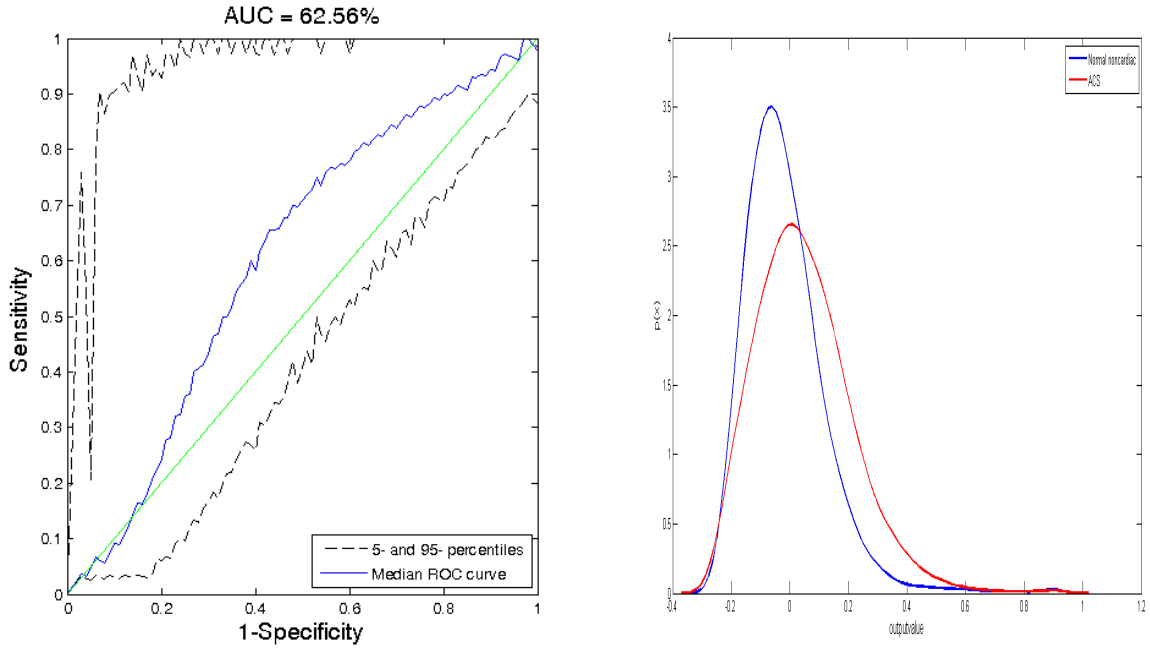
created with equal numbers of records from the NSTEACS group and from the non-cardiac group. From Table 5.3, it can been seen that the non-cardiac group consists of 212 records while the NSTEACS group has 97 patients. The classes were balanced using bootstrapping where for the non-cardiac group, 97 records were randomly selected from the main group. Since we have a small amount of data, bootstrapping as described in Algorithm 1 was used to improve the assessment of classification performance. At end of this process, there are two sets of 97 4-dimensional vectors to train the data fusion models.

The data from each set was divided into equal amounts of training and test sets (48 and 49 in each feature vectors). Once the training and testing sets have been created using bootstrapping, the statistics of the non-cardiac group in the training set are used to transform all the data in both data sets. The data from the training set is then used to train the data fusion model and set any free parameters in the model. The data fusion model was tested by presenting it with the data from the testing set and recording the outputs of the model. The performance measures used in this chapter are; area under the curve (AUC) of the Receiver Operating Curve (ROC), sensitivity and specificity, which are the same as those used in Chapter 3. The next section presents the results obtained using the different classification techniques when using the mean of each parameter (HR, MAP, $\mathrm{SpO_2}$, ST-level) during the ambulance transport as the input four-dimensional feature vector.

7.4.1 Linear regression

The graph in Figure 7.3 shows the summary ROC curves for linear regression. The figure shows the median, and 5th and 95th percentiles of the ROC curves. The graph shows acceptable performance when classifying the dataset using linear regression, but also shows that the shape of the ROC curve varies greatly between tests, as these are only 48 or 49 of feature vectors in the training set and hence classification performance will depend on the choice of these feature vectors.

The area under each ROC curve was calculated, and the summary statistics were calculated from these values. The median AUC was 62.56%, with values of 60.55% and 71.00% for



(a) ROC curve

(b) Empirical probability

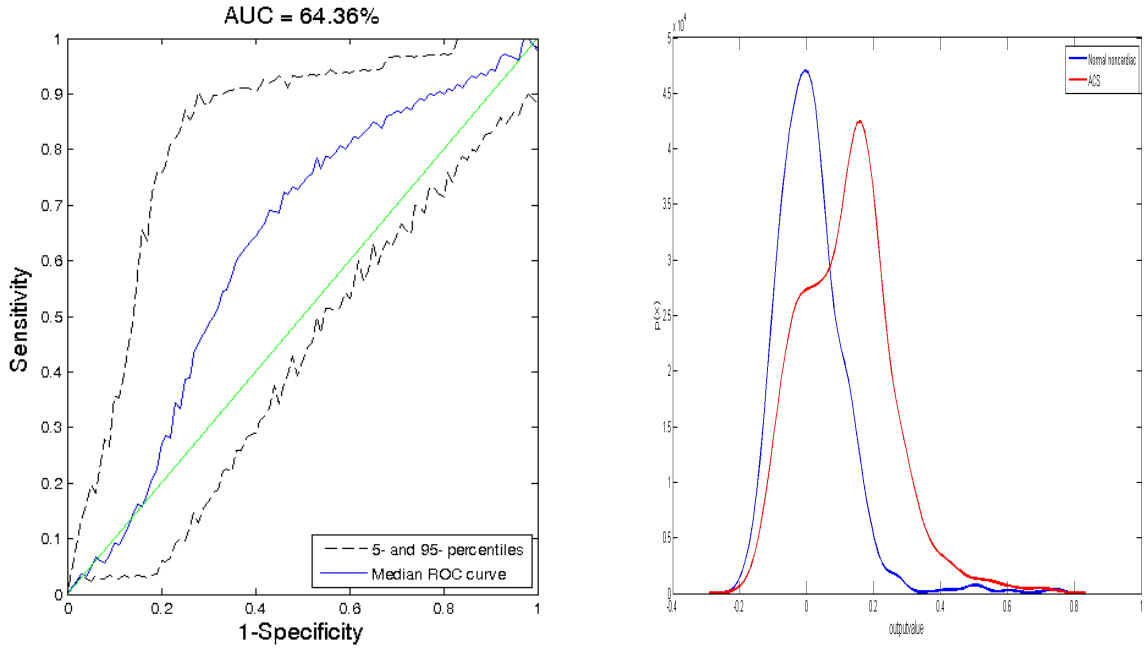
Figure 7.3: ROC curve and empirical probability for linear regression.

the 5th and 95th centiles respectively. The sensitivity and specificity were calculated for each ROC curve at the point with the minimum distance to the (0, 1) point. The median (5%-95%) sensitivity for linear regression was 58.01% (53.49% - 73.51%), and the median specificity was 66.47% (64.35%- 70.37%). Figure 7.3b shows the empirical probability density function of the output values from the linear regression model. As expected, there is significant overlap between the two functions, showing that separation between two classes using linear regression is minimal.

7.4.2 Logistic regression

Figure 7.4 shows the summary ROC curves for logistic regression, which are similar to those in the previous section for linear regression.

There was also a difference between the empirical probability density functions produced by linear and logistic regression. As previously discussed, the output of logistic regression is limited to the range (0, 1), and this can be seen in Figure 7.4b. The median (5%-95%) AUC for



(a) ROC curve

(b) Empirical probability

Figure 7.4: ROC curves for logistic regression. (a) The median curve is in blue and the 5th and 95th centile as shown as dashed lines. (b) Empirical probability of the NSTEACS group and normal non-cardiac group.

logistic regression is 64.36% (49.94%- 78.69%), showing that this technique classifies this data marginally more accurately than linear regression. The sensitivity is 68.75% (47.06%-70.12%), and the equivalent specificity is 64.28% (44.44% - 82.35%).

7.4.3 Multi-layer perceptron

As described in Section 4.6.2, the most important parameter that needs to be set for the MLP is the number of hidden-layer units and this was chosen empirically to be three after exhaustive search. Figure 7.5 shows the summary ROC curves for the multi-layer perceptron classifier. The curves for the MLP tend to lie closer to the (0, 1) point than the curves for linear and logistic regression, indicating better separation of the two classes. The median AUC is 84.22%, indicating near-acceptable classification performance, with values of 60.12% and 94.14% for the 5th and 95th percentiles respectively. The median (5% -95%) sensitivity for the MLP is 83.87% (62.85%- 93.75%) , and the specificity was 86.11% (60.99% - 89.11%) .

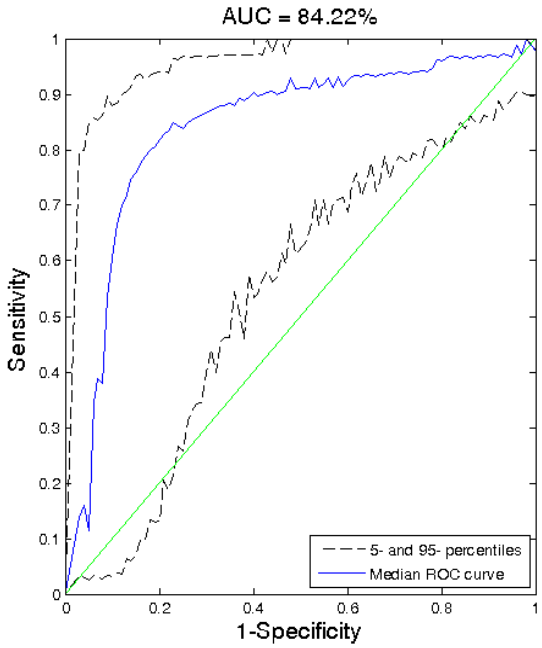


Figure 7.5: ROC curves of multi-layer perceptron. The median curve is in blue and the 5th and 95th centiles as shown as dashed lines.

MLP gave good performance and performed much better than both linear and logistic regression. This suggests that there might be some underlying non-linear relationship between the different vital-sign parameters which could not be captured by the linear regression techniques.

7.4.4 Support Vector Machine

Model selection for SVM involves setting two hyperparameters: the penalty parameter and the kernel width. The width of the RBF kernel and the penalty term were selected using grid search and 5-fold cross-validation to be 0.25 and 8, respectively. As can be seen in Figure 7.6, the median AUC is 77.17%, indicating acceptable classification performance, with values of 56.68% and 87.50% for the 5th and 95th centiles respectively. The median (5% -95%) sensitivity for support vector machine is 78.79% (51.42%- 86.53%), and the specificity was 76.47% (75.32% - 92.59%).

The SVM performs slightly worse than the MLP but performs better than both linear and logistic regression.

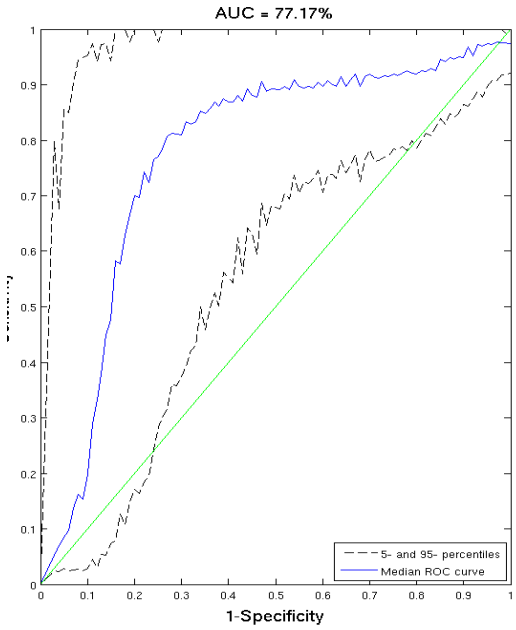
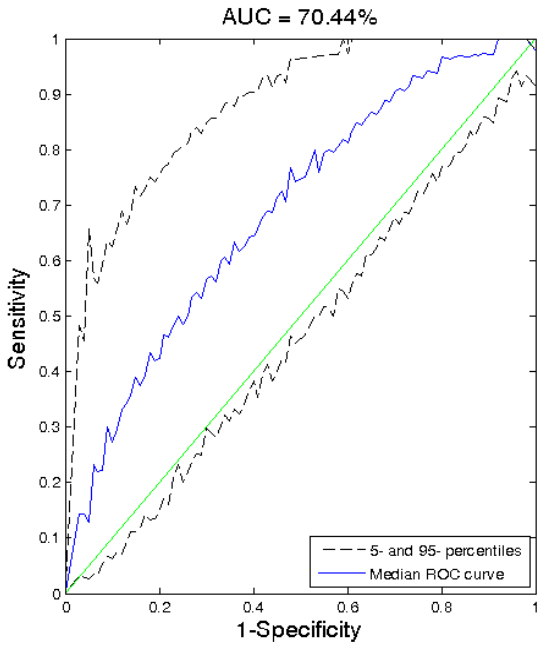


Figure 7.6: ROC curves for SVM. The median curve is in blue and the 5th and 95th centile as shown as dashed lines.

7.4.5 Relevance Vector Machine

As can be seen from Figure 7.7, the median AUC for the RVM is 70.44%, indicating acceptable classification performance, with values of 51.20% and 87.29% for the 5th and 95th percentiles respectively. The median sensitivity for the RVM was 70.43% (51.20%- 85.71%), and the specificity is 69.44% (48.38% - 87.50%).

The RVM provides a slightly lower AUC when compared to the SVM. The main reason is likely to be the fact that the RVM classifier uses a significantly lower number of relevance vectors compared with the number of support vectors used in SVM, resulting in a more sparse representation.



(a) ROC curve

Figure 7.7: ROC curves for Relevance Vector Machine. The median curve is in blue and the 5th and 95th centile as shown as dashed lines.

7.5 Using additional features to discriminate between non-cardiac and NSTEACS

7.5.1 Variability indices

We wish to assess whether there is a difference in classification performance when additional parameters which give some information about the variability of that parameter during the period of monitoring are added to the input feature vector. Variability here is encoded using the standard deviation of HR, $\mathrm{SpO_2}$ and ST level during the period of monitoring. The variability of blood pressure was not considered as on average there are only three measurements during the ambulance transport. The addition of three standard deviations to the four vital-sign parameters resulted in as in a 7-dimensional feature vector.

Figure 7.8 shows the ROC curves for using the four models identified in the previous section. Since the linear regression and logistic regression achieved very similar performance when the 4-dimensional feature vector, in this section only logistic regression is considered for

the regression techniques. As before, the number of hidden layer units was chosen to be six using 5-fold cross-validation. For the SVM, the RBF kernel was used and the width of the kernel and penalty term were found to be 4 and 0.125.

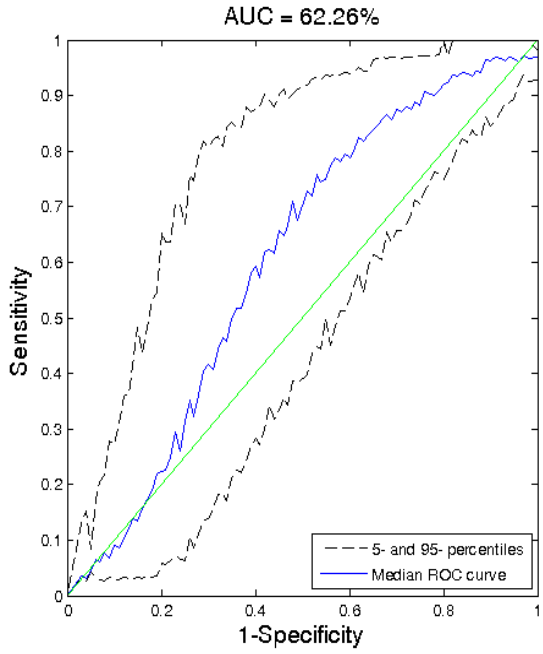
The values in Table 7.4 and the graphs in Figure 7.8 show that there was a decrease in classification performance when using the 7-dimensional vector instead of the 4-dimensional vector. The biggest drop in classification performance was observed with the MLP. The reason for the decline in performance might be due to the increase in the number of free parameters (42 input to hidden weights of 6 hidden-to-output weights) with only input vectors in the training set. This increase results in an increase in model complexity which causes the model to overfit the training data.

Model	AUC (%)	Sensitivity (%)	Specificity (%)
Logistic regression	62.26 (47.72 -75.92)	70.58 (50.00 - 87.88)	61.76 (41.93 -78.78)
MLP	75.90 (59.25 - 88.75)	79.41 (60.91 - 100.00)	76.66 (69.57 -91.17)
SVM	77.24 (62.03-86.03)	72.22 (54.54-100.00)	80.00(60.00-93.93)
RVM	71.94 (54.59 - 87.65)	67.67 (48.34 - 96.30)	73.52 (55.52 - 87.43)

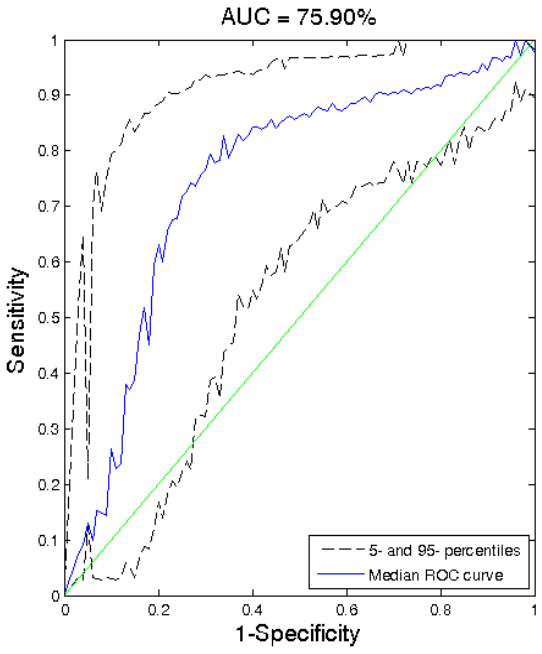
Table 7.4: Median (5%-95%) of AUC, sensitivity and specificity of logistic regression, MLP, SVM and RVM using 7-dimensional vector with the means and standard deviations of the four vital signs.

7.5.2 Demographic information

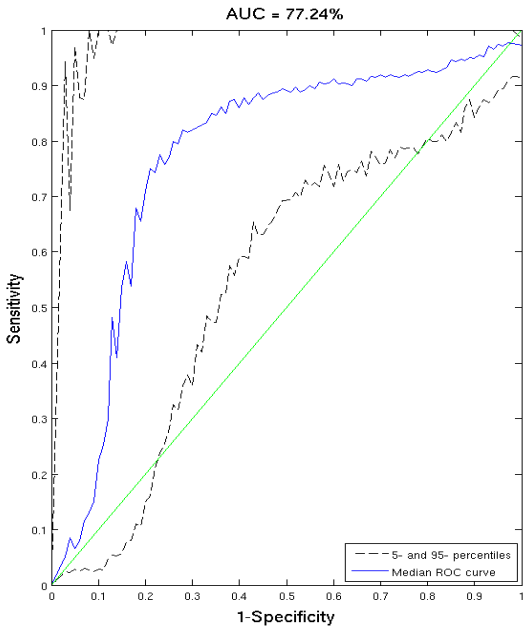
As discussed in Section 1.4.1, demographic factors such as age, smoking and previous MI are associated with increase risk of an MI. These demographic factors are easy to ascertain prior to or during ambulance transport. Therefore their effect on the classification performance of the data fusion models was evaluated. If a patient was a smoker, this was coded as 1 in the feature vector otherwise it was coded to be 0. The previous MI categorical factor was also coded in the same way. These parameters along with the means of the four vital signs were then used to build a 7-dimensional vector to train the data fusion models. Since we are dealing with categorical data, the SVM and RVM are not included in this analysis. The reason is that the SVM and RVM used in this thesis do not support categorical data.



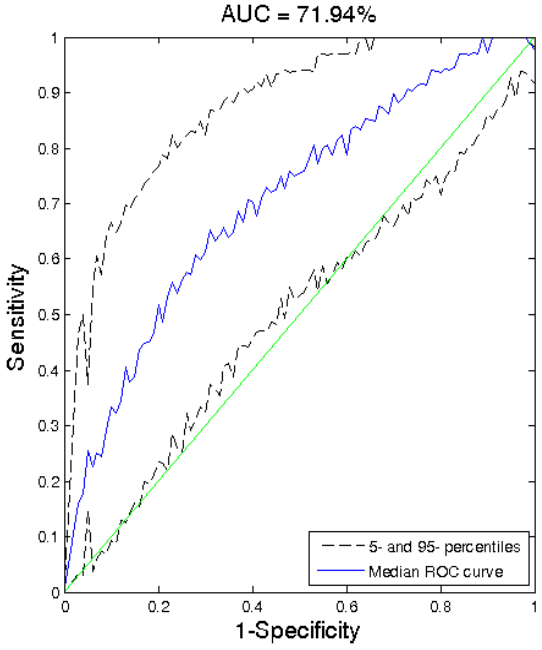
(a) Linear regression



(b) MLP



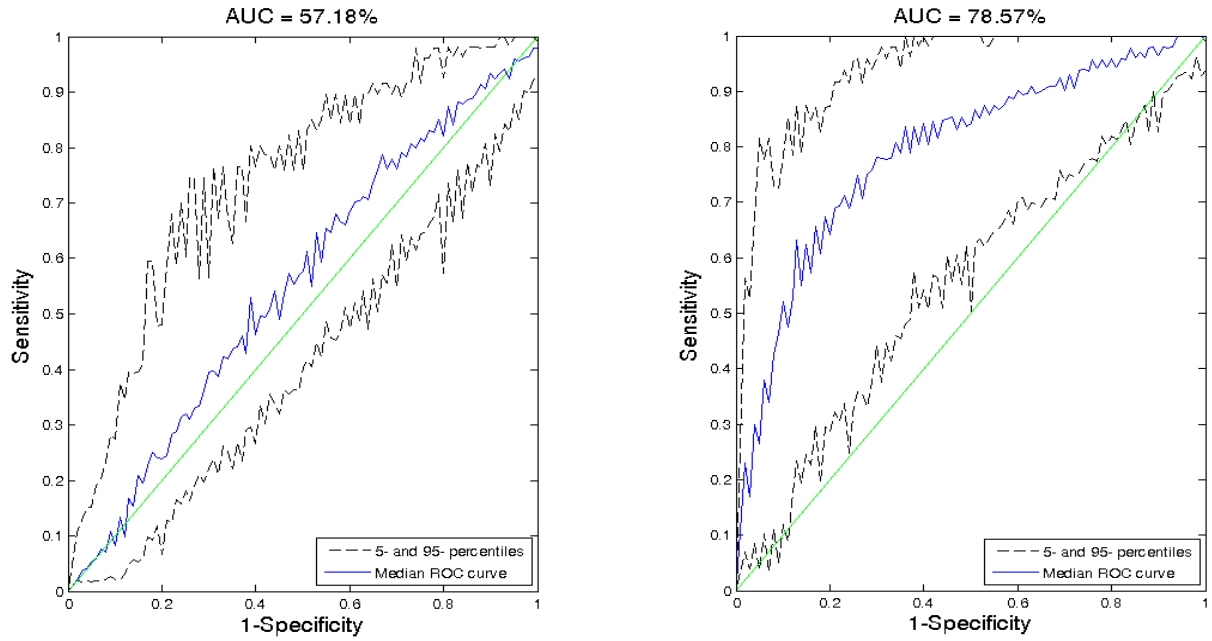
(c) SVM



(d) RVM

Figure 7.8: ROC curves using means and standard deviations as features (7-dimensional feature vector) for (a) Logistic regression, (b)Multi-layer perceptron (MLP), (c) Support Vector Machine(SVM), (d) Relevance Vector Machine (RVM).

Figure 7.9 and Table 7.5 show that both the logistic regression and MLP provided suboptimal results when tested on the means of the vital signs together with the demographic information. The 7-dimensional vector with demographic information as features performed worse than the 7-dimensional vector with standard deviations of the vital sign when using logistic regression. However, the MLP showed a marginal improvement in classification performance. In each case, however, performance was worse than for the model with 4-dimensional input vectors indicating that there are two few training patterns to cope with the increased dimensionality of the input vector.



(a) Linear regression

(b) MLP

Figure 7.9: ROC curves using means and demographic information as features for (a) Logistic regression, (b)Multi-layer perceptron (MLP).

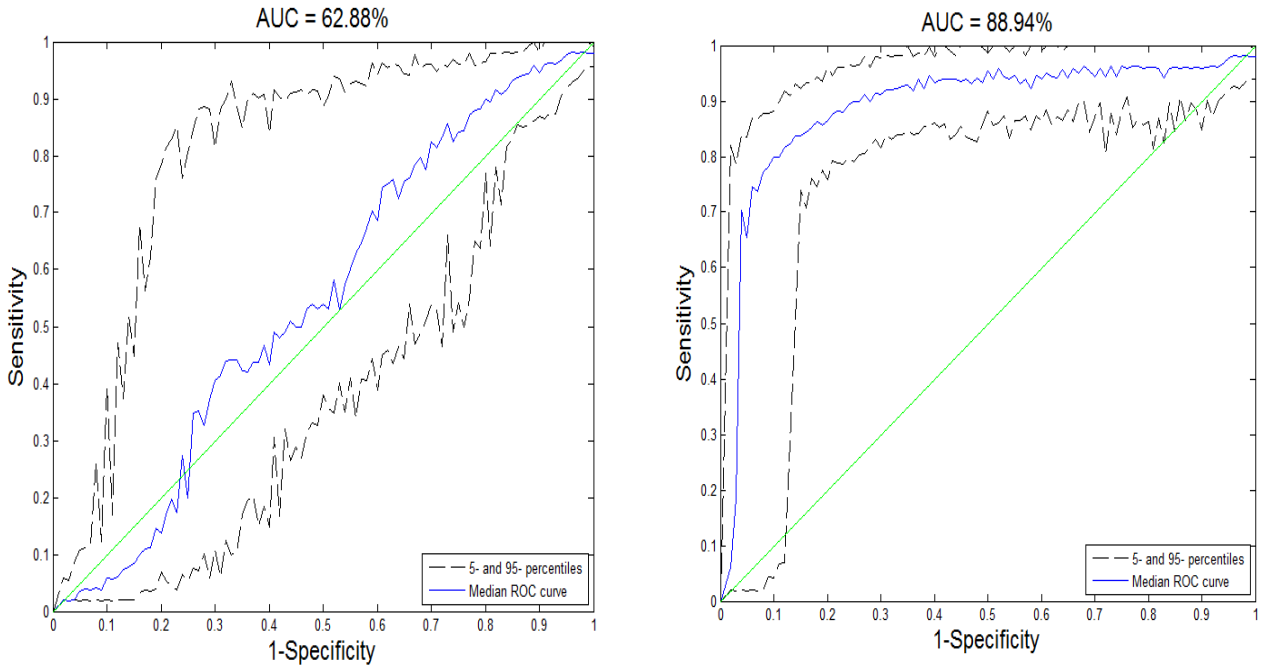
Model	AUC (%)	Sensitivity (%)	Specificity (%)
Logistic regression	57.72(42.12 -78.43)	61.40 (41.34 - 75.93)	57.62 (46.84 -69.97)
MLP	78.75(54.58 - 86.60)	77.56 (57.38 - 90.64)	79.42 (55.78 -89.54)

Table 7.5: Median (5%-95%) AUC, sensitivity and specificity of logistic regression and MLP using the means of the HR, SpO_2, MAP and ST level and the demographic factors; age, previous MI and smoker or not.

7.5.3 Feature selection and classification

As with Section 4.4.1, feature selection was performed using stepwisefit. Stepwisefit was done using 5-fold cross-validation and the features selected to be included in the final feature vectors. From the vital-sign information, the mean value of the SpO_2 and the variability of the SpO_2 were selected. From the demographic information, the smoker and previous MI were also selected to be included in the subset of features.

The selected features were used to train logistic regression and MLP. Figure 7.10 and Table 7.6 show that both the logistic regression and MLP provided gave the best performance when using a selected subset of features. The MLP gave the best classification performance with median AUC, Sensitivity and Specificity of 88.94%, 85.18% and 90.18% respectively.



(a) Linear regression

(b) MLP

Figure 7.10: ROC curves using the subset of selected features (a) Logistic regression, (b)Multi-layer perceptron (MLP).

Model	AUC (%)	Sensitivity (%)	Specificity (%)
Logistic regression	62.88(44.54-79.18)	77.68(43.13-93.81)	68.51(41.96-87.97)
MLP	88.94(80.19-94.71)	85.18(85.19-92.73)	90.18(81.13-97.94)

Table 7.6: Median (5%-95%) AUC, sensitivity and specificity of logistic regression and MLP using the subset of selected features, mean values of SpO_2, standard deviation values of SpO_2, previous MI and smoker or not.

7.6 Discussion

In this chapter, a number of different data fusion methods have been compared using the data collected in the pre-hospital setting. The MLP achieved the largest area under the ROC curve when using the 4-dimensional input feature vector. Demographic information of the patient did not seem to add any value when attempting to distinguish between the non-cardiac and NSTEACS groups. Although, the RVM gave lower classification performance when compared to both the SVM and the MLP, the advantage of the RVM is that it provides the posterior probability of the membership of a patient to a class. Using a Bayesian interpretation of probability, the probability of a patient belonging to NSTEACS group could can be interpreted as the degree of the uncertainty associated with such a prediction.

Given the limited data available for the work described in this chapter, it is not possible to draw firm conclusion about the data fusion methods. More accurate results will be possible if data is collected in the Emergency Department following arrival at the hospital where it is likely that data collected in such settings would have fewer missing variables, such as $\mathrm{SpO2}$ and respiratory rate.

Very accurate prediction of NSTEACS using only vital signs is unlikely. Even if a patient has normal or near-normal vital signs, they may have symptoms, such as chest pain or a concerning clinical history, which should inform clinical decision-making. The output of a data fusion system as developed in this chapter could only be an aid to the identification of patients with NSTEACS, rather than replacing a clinician's detailed assessment.

Chapter 8

Conclusions

The work in this thesis has been divided into two main sections. The first section explored two topics; the development and validation of an automated ST segment analysis tool using post-myocardial infarct patients; and a technique to discriminate between ischaemic ST episodes and non-ischaemic ST episodes. The second section of the work reported in this thesis has concentrated on the analysis of vital signs recorded continuously in the pre-hospital setting (ambulance transport). The major areas of research explored as part of this thesis:

- Development and validation of an automated ST segment analysis tool;
- Discrimination between ischaemic ST episodes and non-ischaemic ST episodes;
- Development and validation of spectral analysis method for the estimation of heart rate variability;
- Assessment of the diagnostic potential of data fusion methods for discriminating between NSTEACS and non-cardiac patients in a pre-hospital setting.

8.1 Overview of the thesis

In Chapter 3, an automated ST segment analysis tool was developed and validated on the existing databases of post-MI patients. The results achieved using these techniques were comparable

with results obtained by other techniques on one of the two databases used.

The ST segment is known to be a highly sensitive but not specific marker, since deviations in the ST segment measurements can result from a wide variety of causes other than ischaemia including changes in heart rate, conduction pattern, position of the subject and noise in the ECG. Even in subjects known to have myocardial ischaemia, ST changes are not considered as a basis for a definitive diagnosis of individual episodes of ischaemia. Thus it was important to be able to discriminate between 'true' ischaemic ST episodes and artefactual ones.

In Chapter 4 it was shown that ST episodes can be classified into ischaemic and non-ischaemic ST episodes using features extracted from the ECG and non-linear classifiers. The results achieved showed that the RVM gave the best performance followed by the SVM, MLP and then linear regression. The additional benefit of using the RVM over other classifiers is that it provides the posterior probability of the membership of a class. Using a Bayesian interpretation, the probability of an event can be interpreted as the degree of associated uncertainty. The results achieved using these techniques were comparable with results in the literature.

At the outset of this research there was no available database with continuous vital-sign data for recorded during the ambulance transport. Chapter 5 described the observational pilot study that was undertaken during pre-hospital management of patients at the John Radcliffe Hospital, Oxford. The aim of the study was to collect continuous vital signs and the electrocardiogram (ECG) for any patient presenting with an indication for an ECG to be taken. The final study cohort consisted of 500 patients with various illnesses. For analysis, the data was classified into three groups; the non-cardiac, cardiac and ACS groups. Since the data was collected in a pre-hospital setting it was expected that some of the ECG signal would be of low quality. The noise in the ECG was caused by sensor issues such as movement artefacts and poor electrode placement as well physiological factors. A template-based Signal Quality Index technique was used to reject noisy ECG records.

In Chapter 4, the data collected in Chapter 5 was used for spectral analysis of heart rate variability to investigate the feasibility of distinguishing between ACS patients and non-cardiac patients. More importantly, the measures of HRV were used to investigate the feasibility of

identifying NSTEACS patients. The technique used prior respiratory information also derived from the ECG (extraction of baseline wander) to define the frequency bands for spectral analysis. However, in some of the patients it was difficult to extract the respiratory information from baseline wander signal. Therefore, standard bands were used for the final analysis of HRV. The results achieved indicate that there is no statistically significant difference in the various frequency measures of heart rate variability between the non-cardiac and ACS patients. It should however be taken into consideration that the data from only 40 patients could be used for this analysis.

Chapter 6 attempted to show that a variety of data fusion methods can be used to identify NSTEACS patients in the pre-hospital setting. The results of the analysis showed that with further work this can be done in clinical setting. An MLP classifier was shown to produce the best results using a set of features derived from the vital-sign data. Very accurate prediction of NSTEACS using only vital signs is unlikely. The output of a data fusion system as developed in this chapter could only be an aid to the identification of patients with NSTEACS, rather than replacing a clinician's detailed assessment.

8.2 Future work

8.2.1 Heart rate variability measures

As many conditions are known to affect the autonomous nervous system, the assessment of heart rate variability in the early phases of ACS needs to be carried out in a larger groups of patients. Respiratory information to define the HF band also needs to be investigated properly, for example by extracting the respiratory rate using accelerometers to track chest wall movement or from the PPG waveform recorded with the pulse oximeter finger probe [200].

Further sub-group analysis could also be carried out on the data for patients with diabetes or on beta-blockers. These would increase the population size of the study while the patients with fairly homogeneous characteristics that allow comparison of sympathetic-parasympathetic balance in the setting of different modalities of ischaemia.

An investigation into prognostic factor that could have been useful to identify those patients who were going to have adverse events after in-hospital and after discharge. The events that could be considered are; composite of cardiac death, myocardial infarction, urgent revascularization, and hospital readmission. Adverse events should not be measured only by the incidence of cardiac death and myocardial infarction, but must include the inability to stabilise an unstable condition, which implies further coronary care unit management and, often immediate urgent mechanical support by coronary angioplasty or by-pass surgery.

Only one algorithm for signal quality quantification for ECG was investigated in this thesis to reject noisy records. It would be beneficial to investigate the ability of other algorithms, and also to consider the application of multiple signal quality indices, which could potentially be combined to obtain a more accurate estimation of signal quality.

8.2.2 Data fusion models

Further work is required to build on the initial data fusion investigations reported in this thesis. These should include larger populations of ACS patients to remove the need for bootstrapping techniques in order to construct an ROC curve. Since it is unlikely that a dataset containing complete sets of vital signs for all patients could be obtained, different methods for inputting missing data could be investigated and their effect on the resulting data fusion models assessed. Furthermore, techniques which look at temporal information of the vital sign data should be investigated. This will ensure that historical data is incorporated into the data fusion model.

Finally, the data fusion methods developed in the previous chapter should be applied to the vital-sign data recorded in the Emergency Department while the patients are having troponin test to determine whether they belong to the non-cardiac group or the NSTEACS group. The ultimate aim of the data fusion will be earliest possible ruling out of an NSTEACS.

Appendix A

Support Vector Machine

SVMs involve sparse kernel algorithms used in classification and regression problems, and have their origin in statistical learning theory. Here, we consider the classification problem involving two data classes, namely, $\mathcal{C}_1$ and $\mathcal{C}_2$.

Let the training set be given by $x_1, x_2, \ldots, x_N$, with target values given by $y_1, y_2, \ldots, y_N$, respectively, where $x_n \in \mathbb{R}^{\mathrm{D}}$ and $y_n \in \{\mathbb{R}^D\}$ and with $x_n \in \mathcal{C}_1$ if $y_n = -1$, and $x_n \in \mathcal{C}_2$ if $y_n = 1$. To classify a new data point $x \in \mathbb{R}^{\mathrm{D}}$, define the classifier function

$$f(x) \triangleq w^T \phi(x) + b \tag{A.1}$$

where $\phi : \mathbb{R}^{\mathrm{D}} \to \mathbb{R}^{\mathrm{M}}$ is a continuous fixed feature-space, $w \in \mathbb{R}^{\mathrm{M}}$ is a weight vector, and $b \in \mathrm{R}$ is a bias parameter. The sign of the classifier function $f(x)$ determines the class of x. More specifically, for a new input variable x, the target value is given by $y = sgn(f(x))$, where $sgnf \triangleq f/|f|$, $f \neq$ and $sgn(0) \triangleq 0$.

Next, assume that the training set is linearly separable in the feature space $\mathbb{R}^{\mathrm{M}}$, that is, there exist a weight vector $w \in \mathbb{R}^{\mathrm{M}}$ and a bias parameter $b \in \mathrm{R}$, such that $f(x_n) > 0$ for $x_n \in \mathbb{R}^{\mathrm{M}}$ and $y_n = 1$, and $f(x_n) < 0$ for $x_n \in \mathbb{R}^{\mathrm{D}}$ and $y_n = -1$, or equivalently, $y_n f(x_n) > 0$ for all $x_n \in \mathbb{R}^{\mathrm{D}}$ and $y_n \in -1, 1$. Later, we relax the linear separability assumption and consider the more general case of overlapping classes.

Note that the classifier function $f(\cdot)$ separates the feature space $\mathbb{R}^{\mathrm{M}}$ into two disjoint regions

characterized by $f(x) > 0$ and $f(x) < 0$ for $x \in \mathbb{R}^{\mathrm{D}}$. The affine hyperplane separating the two disjoint regions, namely $f(x) = 0$, is called the decision boundary and is denoted by $\mathcal{D}$. Note that $\phi(\cdot)$ can be a nonlinear transformation, which would correspond to a nonlinear decision boundary in the original input space $\mathbb{R}_{\mathrm{D}}$. The minimum distance between the training set and the decision boundary $\mathcal{D}$ is called the margin. The distance of a point $x_n \epsilon \mathbb{R}^{\mathrm{D}}$ to the decision boundary $\mathcal{D}$ is given by

$$dist(\phi(x_N), \mathcal{D}) = \frac{|f(x_n)|}{\|w\|} = \frac{y_n f(x_n)}{\|w\|} \tag{A.2}$$

where $\|\cdot\|$ denotes the Euclidean norm on $\mathbb{R}^{\mathrm{M}}$ and $dist(x, \mathcal{D}) \triangleq inf_{s \in \mathcal{D}} \|x - s\|$. Hence, the margin is given by

$$\min_{n \in \{1,\ldots,N\}} dist(\phi(x_N), \mathcal{D}) = \min_{n \in 1,\ldots,N} \frac{y_n f(x_n)}{\|w\|} \tag{A.3}$$

As in all classification methods, the goal of the SVM algorithm is to classify a new input variable $x \in \mathbb{R}^{\mathrm{D}}$ based on the information provided by the training set and the target values. The SVM framework addresses this problem by choosing the decision boundary in such a way so that the margin is maximized. The following problem presents the SVM algorithm as an optimization problem.

Consider the training set given by $x_1, x_2, \ldots, x_N \subset \mathbb{R}^{\mathrm{D}}$ and let the classifier function $f : \mathbb{R}^{\mathrm{D}} \to \mathbb{R}$ be given by Equation A.1. Find the weight vector $w \epsilon \mathbb{R}^{\mathrm{M}}$ and the bias parameter $b \epsilon \mathbb{R}$ such that Equation A.3 is maximized.

When $w^* \in \mathbb{R}^{\mathrm{M}}$ and $b^* \in \mathbb{R}$ solve the maximum margin classification problem if and only if w^* and b^* are the solutions to the optimization problem

$$\max_{w \in \mathbb{R}^{\mathrm{M}} b, \in \mathbb{R}} \{\frac{1}{\|w\|} \min_{w \in 1,\ldots,N} [y_n(w^T \phi(x_n) + b)]\} \tag{A.4}$$

The solution to the nonconvex optimization problem Equation A.4 is not unique. To see this, note that scaling the weight vector $w \in \mathbb{R}_{\mathrm{M}}$ and the bias parameter $b \in \mathbb{R}$ by a positive scalar does not change the value of the function to be maximized. The following theorem presents

an alternative characterization to the maximum margin classification problem. $w^* \in \mathbb{R}_{\mathrm{M}}$ and $b^* \in \mathbb{R}$ solve the maximum margin classification problem if and only if w^* and b^* are the solutions to the optimization problem

$$\min_{w \in \mathbb{R}^{\mathrm{M}}, b \in \mathbb{R}} \frac{1}{2}\|w\|^2 \tag{A.5}$$

subject to

$$y_n(w^T\phi(x_n) + b) \geq 1 \tag{A.6}$$

where $x_n \in \mathbb{R}^{\mathrm{D}}$, $y_n \in \{-1, 1\}$, and $n = 1, \ldots, N$. Since rescaling the weight vector $w \in \mathbb{R}_{\mathrm{M}}$ and the bias parameter $b \in \mathbb{R}$ in Equation A.4 by a positive scalar does not change the value of the function to be maximized, the optimization problem Equation A.5has a continuum of solutions corresponding to the same optimal value. Hence, introducing the new constraint

$$y_{n*}(w^T\phi(x_{n*}) + b) = 1 \tag{A.7}$$

where $n^* = argmin_{n \in \{1,\ldots,N\}} dist(\phi(x_n), \mathcal{D})$ does not change the optimal value of the optimization problem Equation A.4. Thus, the inequality constraint holds for all $x_n \epsilon \mathbb{R}_{\mathrm{D}}$,$y_n \in \{-1, 1\}$, and $n = 1, \ldots, N$. The proof now follows by noting that the optimization problem Equation A.4 subject to Equation A.7 is equivalent to the optimization problem Equation A.5 subject to Equation A.6.

The constrained optimization problem given by Equation A.5 and Equation A.6 is convex and can be solved using Lagrange multiplier methods. Specifically, introducing the Lagrange multipliers $\lambda_n \in \mathbb{R}$, $n = 1, \ldots, N$, and forming the Lagrangian

$$\mathcal{L}(w, b, \lambda) = \frac{1}{2}\|w\|^2 - \sum_{n=1}^{N} \lambda_n[(y_n(w^T\phi(x_n) + b) - 1] \tag{A.8}$$

where $\lambda = [\lambda_1, \lambda_2, \ldots, \lambda_N]^T$, it follows from the first-order necessary conditions for optim-

ality that

$$w = \sum_{n=1}^{N} \lambda_n y_n \phi(x_n) \tag{A.9}$$

$$0 = \sum_{n=1}^{N} \lambda_n y_n \tag{A.10}$$

Note that Equation A.9 and Equation A.10 can be used to eliminate w and b from the Lagrangian Equation A.8 leading to a dual representation of the optimization problem Equation A.4. Namely,

$$\max_{\lambda \in \mathbb{R}_N} \mathcal{L}(\lambda) \tag{A.11}$$

subject to

$$\sum_{n}^{N} \lambda_n y_n = 0 \tag{A.12}$$

$$\lambda_n \geq 0, n = 1, \ldots, N \tag{A.13}$$

where

$$\mathcal{L}(\lambda) \triangleq \sum_{n=1}^{N} \lambda_n - \frac{1}{2} \sum_{n=1}^{N} \sum_{m=1}^{N} \lambda_n \lambda_m y_n y_m k(x_n, x_m) \tag{A.14}$$

and

$$k(x, x') = \phi^T(x)\phi(x') \tag{A.15}$$

is the kernel function. Here, we introduced an alternative formulation of the optimization problem Equation A.4 in terms of the kernel function $k : \mathbb{R}^{\mathrm{D}} \times \mathbb{R}^{\mathrm{D}} \to \mathbb{R}$, which allows us to avoid working explicitly in the feature space. Note that the classifier function Equation A.1 can

be rewritten using the kernel function as follows:

$$f(x) = \sum_{n=1}^{N} \lambda_n y_n k(x, x_n) + b \tag{A.16}$$

The KuhnTucker (KT) necessary conditions for optimality for the constrained optimization problem Equation A.11-A.13 are given by

$$\lambda_n \geq 0 \tag{A.17}$$

$$y_n f(x_n) - 1 \geq 0 \tag{A.18}$$

$$\lambda_n (y_n f(x_n) - 1) = 0 \tag{A.19}$$

where $n = 1, \ldots, N$. Now, it follows from Equation A.19 that either $\lambda_n = 0$ or $y_n f(x_n) = 1$. The input variables $x_n \in \mathbb{R}^{\mathcal{D}}$, $n = 1, \ldots, N$, for which the corresponding Lagrange multiplier $\lambda_n \in \mathbb{R}$ vanishes, do not contribute to the classifier function, and hence, can be omitted. The remaining input variables are called support vectors, and by definition, lie on the maximum margin affine hyperplanes $w^{*T}\phi(x_n) + b^* = \pm 1$,$n = 1, \ldots, N$. Hence, only the support vectors play a role in the classification of the new input variables and the rest of the training set can be discarded.

Next, we consider the case of overlapping classes. For this case, the SVM algorithm considered earlier identifies the decision boundary so that the training set is separated into two data classes with no input variables being misclassified. This results in poor class assignments for new input variables. The SVM algorithm, however, can be modified by allowing input variables in the training set to lie on the wrong side of the margin boundary and penalizing such constraint violations. Specifically, for every input variable $x_n \in \mathbb{R}_{\mathrm{D}}$, $n = 1, \ldots, N$, define the slack variable $\xi_n \geq 0$ such that $\xi_n = 0$ if Equation A.6 is satisfied, that is, for $n \in \{1, \ldots, N\}$, x_n is on or inside the correct margin boundary, and $\xi_n = |y_n - f(x_n)|$ otherwise. The modified

SVM algorithm is given by the following optimization problem:

$$\min_{w\in\mathbb{R}^{\mathrm{M}},b\in\mathbb{R},\xi\in\mathbb{R}^{\mathrm{N}}} C\sum_{N}^{n=1}\xi_n + \frac{1}{2}\|w\|^2 \tag{A.20}$$

subject to

$$y_n f(x_n) \geq 1-\xi_n, n=1,\ldots,N \tag{A.21}$$

$$\xi_n \geq 0, n=1,\ldots,N \tag{A.22}$$

where $\xi_n = [\xi_1,\xi_2,\ldots,\xi_N]^T$ and $C>0$ is a complexity parameter controlling the tradeoff between the margin and the slack variable penalty. It can be shown that if $\xi_n = 0$, then Equation A.21 reduces to Equation A.22 and the corresponding input variable $x_n \epsilon \mathbb{R}_{\mathbb{D}}$ will be correctly classified. Moreover, if $0 < \xi_n - 1$, then the input variable is correctly classified while lying inside the margin boundary, whereas if $\xi_n > 1$, then the input variable is misclassified.

Lagrange multiplier methods can be used to solve the optimization problem Equation A.20 by introducing the Lagrange multipliers $\lambda_n \in \mathbb{R}$ and $\mu \in \mathbb{R}$, $R, n=1,\ldots,N$, corresponding to the constraints Equation A.20 and A.21, respectively. In this case, the Lagrangian is given by

$$\mathcal{L}(w,b,\lambda,\xi) = \frac{1}{2}|w|^2 + C\sum_{N}^{n=1}\xi_n - \sum_{n=1}^{N}\lambda_n(y_n(f(x_n))) - 1 + \xi_n - \sum_{N}^{n=1}\mu_n\xi_n \tag{A.23}$$

where $\lambda = [\lambda_1,\lambda_2,\ldots,\lambda_N]^T$. It follows from the first order necessary conditions for optimality that

$$w = \sum_{n=1}^{N}\lambda_n y_n \phi(x_n) \tag{A.24}$$

$$0 = \sum_{n=1}^{N} \lambda_n y_n \tag{A.25}$$

$$\alpha_n = C - \mu_n, n = 1, \ldots, N \tag{A.26}$$

and the KT necessary conditions give

$$\alpha_n \geq 0 \tag{A.27}$$

$$y_n f(x_n) - 1 + \xi_n \geq 0 \tag{A.28}$$

$$y_n(y_n f(x_n) - 1 + \xi_n) = 0 \tag{A.29}$$

$$\mu_n \geq 0 \tag{A.30}$$

$$\xi_n \geq 0 \tag{A.31}$$

$$\mu_n \xi_n = 0 \tag{A.32}$$

where $n = 1, \ldots, N$.

The dual representation of the optimization problem Equation A.20 subject to Equation A.21 and Equation A.22 given by

$$\min_{\lambda in \mathbb{R}_N} \mathcal{L}^{-}(\lambda) \tag{A.33}$$

subject to

$$0 \leq \alpha_n \leq C, n = 1, \ldots, N \tag{A.34}$$

$$\sum_{n=1}^{N} \lambda_n y_n = 0; \tag{A.35}$$

where $\mathcal{L}^{-}(\lambda)$ is given by Equation A.14, the kernel function is given by Equation A.15, and where we have used Equation A.24- A.32.

Appendix B

Relevance Vector Machine

Tipping *et al.* [153] introduced the Relevance Vector Machine which makes probabilistic predictions and yet retains the good predictive performance of the support vector machines. Although the SVM framework generally yields good predictive performance for a broad range of practical applications.

Such methods not only classify a new input variable, but can also provide a degree of uncertainty (in terms of posterior probabilities) for such a classification. The RVM, which is a special case of the sparse Bayesian learning algorithm, can be regarded as the Bayesian extension of the support vector machine approach.

Consider the Laplace approximation given method involving the random variable $\upsilon \in \mathbb{R}^{\mathrm{M}}$ with associated probability density function given by $(p : \mathbb{R}^{\mathrm{M}} \rightarrow \mathbb{R})$. Assume that $p(\upsilon) = \frac{f(\upsilon)}{/}V$, where $f : \mathbb{R}^{\mathrm{M}} \rightarrow \mathbb{R}$ is a function defined on $\upsilon \in \mathbb{R}^{\mathrm{M}}$ and $V = \int_{\mathbb{R}^{\mathrm{M}}} f(\upsilon)d\upsilon$ is the normalization coefficient. The probability density function $p(\upsilon)$ is approximated by a multivariate Gaussian distribution $\mathcal{N}(\upsilon, \upsilon_0, \Sigma)$ with mean $\upsilon_0 \in \mathbb{R}^{\mathrm{M}}$ and covariance matrix $\Sigma \in \mathbb{R}^{\mathrm{M}\times\mathrm{M}}$, where $\upsilon_0 = argmax_{\upsilon|\in\mathbb{R}^{\mathrm{M}}} p(\upsilon)$ and $\Sigma = \partial^2/\partial\upsilon^2 Inf(\upsilon)|_{\upsilon=\upsilon_0}$. The normalization coefficient V can be approximated by [153].

$$V \backsimeq f(\upsilon_0)\frac{(2\phi)^{M/2}}{(det\Sigma)^{1/2}} \tag{B.1}$$

where $det(\cdot)$ denotes the determinant factor. The training set is given by $x_1, x_2, \ldots, x_N \subset$

$\mathbb{R}^{\mathrm{D}}$ with target values given $y_1, y_2, \ldots, y_N$, where $x_n \in \mathbb{R}^{\mathrm{D}}$ and $y_n \in 0, 1$, $n = 1, \ldots, N$ and with $x_n \in \mathcal{C}_1$ if $y_n = 0$, and $x_n \in \mathcal{C}_2$ if $y_n = 0$. For a new input variable $x \in \mathbb{R}^{\mathrm{D}}$, we predict the associated class membership posterior probability distribution $p(\mathcal{C}_{\mathrm{k}}|\mathrm{x}, \mathrm{X}, \mathrm{Y}|)$, $k = 1, 2$ where $p(\mathcal{C}_1|\mathrm{x}, \mathrm{X}, \mathrm{Y}|)$ is the class membership conditional probability distribution of the data class $\mathcal{C}^{\mathrm{k}}$ given $x \in \mathbb{R}^{\mathrm{D}}, \mathrm{X} = [\mathrm{x}_1, \mathrm{x}_2, \ldots, \mathrm{x}_{\mathrm{N}}]$, and $Y = [y_1, y_2, \ldots, y_N]^T$. RVM method separates the prediction stage (i.e., finding the posterior class membership probabilities for the new input variables) from the decision making stage (i.e., assigning the new input variable x to the appropriate class). This separation is particularly useful when dealing with asymmetric classification costs, where misclassification of input variables belonging to a certain class is more costly. Now we define the classifier function

$$f(x) \triangleq w^T \phi(x) \tag{B.2}$$

where $\phi : \mathbb{R}^{\mathrm{D}} \to \mathbb{R}^{\mathrm{M}}$ is a continuous feature-space transformation and $w = [w_1, w_2, \ldots, w_M]^T \in \mathbb{R}^{\mathrm{M}}$ is a weight factor. Specifically, in the RVM, $w^T \phi(x)$ has a special form given by $\Sigma_{n=1}^{N} w_n k(x, x_n) + b$ where $k(\cdot, \cdot)$ is the kernel function.

The posterior probability of the target value of an input variable corresponding to the class $\mathcal{C}_1$ is given by $p(y_n = 1|x_n, w) = \sigma(f(x_n))$, $n = 1, \ldots, N$, where $\sigma(\cdot)$ is the logistic sigmoidal function defined by $\sigma(s) \triangleq 1/(1 + e^{-s})$. Assuming that the input variables x_n, $n = 1, \ldots, N$ are independent, the likehood function is given by:

$$p(Y|X, w) = \prod_{n=1}^{N} p(y|x_n, w) = \prod \sigma(f(x_n))^{y_n} (1 - \sigma(f(x_n)))^{1-y_n} \tag{B.3}$$

Each weight parameter w_n, $n = 1, \ldots, M$ is assumed to have a zero-mean Gaussian distribution, and hence, the weight prior distribution is given by

$$p(w|\alpha) = \prod_{n=1}^{M} \mathcal{N}(w_n, 0, \alpha_n^{-1}) \tag{B.4}$$

where α_n, $n = 1, \ldots, M$ is the precision corresponding to w_n and $\alpha = [\alpha_1, \alpha_2, \ldots, \alpha_M] \in \mathbb{R}^{\mathrm{M}}$. The parameters α_n, $n = 1, \ldots, M$ in the prior distribution are called hyperparameters.

Each weight w_n, $n = 1, \ldots, M$ has a separate hyperparameter α_n. Given a new input variable $x \in \mathbb{R}^{\mathrm{D}}$, the corresponding target value $y \in 0, 1$ can be predicted using the predictive distribution $p(y|x, X, y)$. The predictive distribution is given by

$$p(y|x, X, Y) = \int_{-\infty}^{\infty} \int_{-\infty}^{\infty} p(y|x, X, Y, w, \alpha) \times p(w|x, X, Y, \alpha) p(\alpha|x, X, Y) dw d\alpha \qquad \text{(B.5)}$$

where the distribution is marginalized with respect to the weight vector $w \in \mathbb{R}^{\mathrm{M}}$ and the hyperparameter $\alpha \in \mathbb{R}^{\mathrm{M}}$. Since $\sigma(\cdot)$ is nonlinear, no closed-form solution exist for B.5. The type-2 maximum likehood also known as the evidence approximation is used to approximate Eq. B.5 by replacing $\alpha \in \mathbb{R}^{\mathrm{M}}$ with a constant value $\alpha^* \in \mathbb{R}^{\mathrm{M}}$ corresponding to the mode of the marginal likehood function $p(Y|X, \alpha)$. In particular, an approximation to the predictive distribution $p(Y|x, X, Y)$ is given by

$$p(Y|x, X, Y) \backsimeq p(y|x, X, Y, \alpha^*) = \int_{-\infty}^{\infty} p(y|x, X, Y, w, \alpha^*) p(w|x, X, Y, \alpha^*) dw \qquad \text{(B.6)}$$

The value of α^* is found via an iterative process, After initializing α, the posterior probability distribution $p(w|x, X, Y, \alpha)$ is approximated by a Gaussian distribution using the Laplace approximation method. The maximizer is found using the iterative reweighted least square method, which uses sequential quadratic approximation to find the maximizer. Taking the log of identity.

$$p(w|x, X, Y, \alpha) = \frac{p(Y, x, X, w, \alpha) p(w|x, X, \alpha)}{p(Y|x, X, \alpha)} = \frac{p(Y|X, w) p(w|\alpha)}{p(Y|X, \alpha)} \qquad \text{(B.7)}$$

the maximization problem is equivalent to

$$\max_{w \in \mathbb{R}_{\mathrm{M}}} \ln(p(Y|X, w) p(w|\alpha) - \ln p(Y|X, \alpha)) \qquad \text{(B.8)}$$

or equivalently

$$\max_{w\in\mathbb{R}^{\mathrm{M}}}\{\Sigma(f_n \ln f_n + (1-f_n)\ln(1-f_n)) - \frac{1}{2}w^T Aw + c\} \tag{B.9}$$

where $f_n = \sigma(f(x_n)) \in \mathbb{R}$, $A = diag[\alpha] \in \mathbb{R}^{\mathrm{M}\times\mathrm{M}}, c \in \mathbb{R}$ is a variable independent of y (and hence, plays no role in the optimization), and where we have used Eq. B.9. Note that the covariance matrix of the Gaussian approximation to the posterior distribution $p(w|x, X, Y, \alpha)$ is equal to the negative Hessian of $lnp(w|x, X, Y, \alpha)$ evaluated at the maximizer w^* The mean and covariance of the Gaussian approximation are given by

$$w* = A^{-1}\Phi^T(Y - F) \tag{B.10}$$

$$\sum = (\Phi^T B\Phi + A)^{-1} \tag{B.11}$$

where $\Phi = [\Phi_{i,j}] \in \mathbb{R}^{\mathrm{N}\times\mathrm{M}}$ with $\Phi_(i, j) = \phi_j(x_i)$ for $i = 1, ldots, N$ and $j = 1, \ldots, M$, $B = diag[b_1, b_2, b_N] \in \mathbb{R}^{N\times N}$ with $b_n = f_n(1 - f_n) \in \mathbb{R}$, $n = 1, \ldots, N$ and $F = [f_1, f_2, \ldots, fN]^T \in \mathbb{R}^{\mathrm{N}}$. Now, using the updated estimate $\alpha^{new} = [\alpha_1^{new}, \alpha_2^{new}, \ldots, \alpha_M^{new}]^T \in \mathbb{R}_{\mathrm{M}}$ for α, the above steps are repeated until a given convergence criterion is met.

As a result of the maximization of the marginal likelihood function, a number of hyperparameters α_n approach infinity, and hence, the corresponding weight parameter w_n will be centered at zero with zero variance. Therefore, the corresponding component of the feature-space transformation $\phi_n(\cdot)$ plays no role in the prediction, resulting in a sparse predictive model. In the case of the RVM, the input variables x_n belonging to the training set $x_1, x_2, \ldots, x_N$, which have a nonzero weight w_n , are called relevance vectors. Only the relevance vectors play a role in the classification of new input variables and the rest of the training set can be discarded. Finally, we note that the posterior probability for the membership of a new input variable x to the class C_1 represented by $p(\mathcal{C}_1|x, X, Y)$ can be approximated by the logistic sigmoidal function $(f(x))$ using the calculated value of the weight vector w. This approximations becomes exact as the number of input variables in the training set approaches infinity.

Table B.1: Sparse Bayesian Learning Algorithm

Step 1.	Initial parameter
a.	Set $\Phi_(i,j) = \phi_j(x_i),\ i = 1,\ldots,N,\ j = 1,\ldots,M$
b.	Set $\Phi = [\Phi_(i,j) \in \mathbb{R}^{\mathrm{N}\times\mathrm{M}}]$
c.	Set $b_n = y_n(1-y_n), n = 1,\ldots,N$
d.	Set $B = diag[b_1, b_2, \ldots, b_N]$
Step 2.	Initialize the hyperparameters $\alpha = [\alpha_1, \alpha_2, \ldots, \alpha_M]$
Step 3.	Find the Gaussian approximation $\mathcal{N}(w; w^*, \sum)$ to the posterior distribution $p(w\|x, X, Y, \alpha)$
a.	Set $A = diag[\alpha]$
b.	Set $w^* = A^{-1}\Phi T(Y-F)$
c.	Set $\sum = (\Phi^T B\Phi + A)^{-1}$
Step 4	Compute the approximate marginal likehood function using $p(Y\|X,\alpha) \backsimeq$
Step 5	Set $\gamma_n = 1 - \alpha\sum_{nn}, n = 1,\ldots,M.$
Step 6	Update α using $\alpha_n \leftarrow \frac{\gamma_n}{(w^*)^2}, n = 1,\ldots,M$
Step 7	If $\|\delta\alpha\| >$ or If $\|\delta w^*\| >$, where $\delta\alpha$ and δw^* are the changes in the values of α and w^* in the iteration, respectively and Tol_1 and Tol_2 are specified tolerances, then go to Step 3.
Step 8	Set $\alpha^* = \alpha$

Appendix C

Signal quality index assessment

This appendix compares the signal quality index (SQI) assessment technique implemented in Section 2.6.1, based on template matching (TSQI) with an established ECG SQI technique (ECGSQI).

C.1 Established signal quality assessment techniques

Several ECG signal quality techniques have been described, ranging from early work of Moody and Mark [201] to more recent developments in ICU monitoring by Li *et al.* [83] and subsequently in ambulatory monitoring, an overview of which can be found in Silva *et al.* [202]. However, in contrast to the works of Moody and Mark [201] and Li *et al.* [83], the more recent works did not address quality estimation during ischemic episodes.

In particular, Li *et al.* [83] evaluated their algorithm for tracking tachycardia and bradycardia. Their technique combines the following four basic algorithms on 10 second windows of ECG centered around each beat:

- A comparison of multiple beat detection algorithms on a single lead.
- Comparison of the same beat detection algorithm on different simultaneously recorded ECG leads.
- Evaluation of the non-Gaussianity of the segment of ECG.

- Calculating the proportion of the spectral distribution of a given ECG segment found to be within a certain physiological frequency band, compared to a wider spectral band.

A short description of the the various analysis technique is given below.

C.1.1 Comparison of multiple beat detection algorithms on a single lead: bSQI

Different ECG algorithms are sensitive to different types of noise [71], and therefore the comparison of how accurately multiple QRS detectors isolate each event provides some estimate of the level of noise in the ECG. In their approach, Li and colleagues [83] used two well-documented open-source QRS detection algorithms with different noise sensitivities. The noise-resistant detector is based on digital filtering (DF) and integration [73] and the noise sensitive detector is based on a length transform (LT) after filtering [203]. The signal quality for a given segment of ECG was defined to be the ratio of beats detected synchronously (within a tolerance interval of 50 ms to account for different responses) by both algorithms, to all the detected beats (by the most robust algorithm) within the window.

C.1.2 Beat detection comparison using different ECG leads: iSQI

The second analysis method was motivated by the fact that in theory, when synchronous ECG leads are available, comparison between different leads can provide more accurate estimates of signal quality, since more information is present. Although , a signal quality can be calculated for different leads separately, if one QRS detection algorithm misses one or more beats (due to low QRS amplitudes) or registers extra beats (due to artifact or high amplitude T waves), a single lead signal quality index may fail to give a good signal quality measure. Thus, beat detection comparison between different leads, using the same QRS detection algorithm may reveal such anomalies. An inter-channel signal quality index (iSQI) was calculated as the ratio of the number of matched beats in both leads to all detected beats in both leads. Note that only the noise-resistant QRS detector of Hamilton, Pan and Tompkins [73] was used.

C.1.3 Kurtosis of the ECG: kSQI

From the central limit theorem we know that random uncorrelated processes, such as thermal noise, tend to have Gaussian distributions. Conversely, correlated signals tend to have non-Gaussian distributions. A simple measure of the Gaussianity of a signal is *kurtosis*, the empirical estimate of the fourth standardized moment of a distribution. Kurtosis measures the relative peakedness of a distribution with respect to a Gaussian distribution with large values indicating highly peaked distributions, with large outliers, such as we might observe in an ECG, which is mostly baseline values with infrequent large excursions from the mean (the QRS complex). The kurtosis, K, of signal x with mean μ_x and standard deviation σ is defined as $K = E(x - \mu_x)^4\sigma^4$ where E is the mathematical expectation operator. The empirical estimate of kurtosis, $\hat{K}$, of a discrete signal x_i is given by

$$\hat{K} = \frac{1}{M}\sum_{i=1}^{M}\left[\frac{x_i - \hat{\mu}_x}{\hat{\sigma}}\right] \tag{C.1}$$

where $\hat{\mu}_x$ $\hat{\sigma}$ are the empirical estimate of the mean and standard deviation of x_i respectively, and M is the number of samples in the signal.

The kurtosis of a Gaussian distribution is equal to 3 and clean, sinus rhythm ECG generally has a kurtosis larger than 5 [204]. Muscle artifact has a kurtosis around 5 and baseline wander and power-line interference have kurtosis lower than 5 [204]. The signal quality index, for each kth beat, using kurtosis (kSQI) was therefore defined as:

$$kSQI(k) = \begin{cases} 1 & \text{if kurtosis (k,w)} > 5 \\ 0 & \text{if kurtosis (k,w)} \leq 5 \end{cases}$$

Low kSQI usually indicates low frequency noise such as baseline wander. low or negative values indicate high frequency sinusoidal noise (such as mains interference).

C.1.4 Spectral distribution of ECG: sSQI

The third component of the SQI algorithm was motivated by the fact that the QRS energy is mainly concentrated in a 10 Hz wide frequency band, centered around 10 Hz [205], the ratio of the power spectral density (PSD) in this band compared to the PSD in the overall signal above 5 hz (to exclude low frequency behaviour) provides a measure of the signal quality of the ECG with respect ot high frequency contamination. The spectral distribution ratio (SDR) of an ECG segment was then defined to be the ratio of the sum of the power of a given ECG segment between frequencies of 5 Hz and 14 Hz to the power in the same segment between 5 Hz and 50 Hz.

When the SDR is low, high frequency noise contamination in the ECG, such as muscle artifact, is likely. When the SDR is extremely high, an increased presence of QRS-like artifact, such as electrode motion, is likely. Moderate values of SDR indicate good ECG quality. Thus, the spectral distribution signal quality index (sSQI) was defined as

$$sSQI(k) = \begin{cases} 1 & \text{if SDR} \geq 5 \text{ and SDR} \leq 0.8 \\ 0 & \text{if SDR} < 5 \text{ or SDR} > 0.8 \end{cases}$$

These thresholds were empirically determined through repeated observations and can be adjusted slightly with little effect.

C.1.5 Combined ECG SQI

The combined ECG signal quality index was derived by combining the four SQI metrics detailed above as follows:

$$ECGSQI(k) = \begin{cases} max(bSQI(k), iSQI(k)) & \text{if kSQI(k) =1 and sSQI(k)=1} \\ bSQI(k) & \text{if kSQI(k) = 1 and sSQI(k)=0} \\ max(bSQI(k), iSQI(k)) * \eta & \text{if kSQI(k) = 0 and sSQI(k)=1} \\ bSQI(k) * \eta & \text{if kSQI(k) = 0 and sSQI(k)=0} \end{cases}$$

where η is a positive coefficient less than unity that indicates the presence of spectral or statistical noise and can be thought as the boundary between moderate and high quality data.

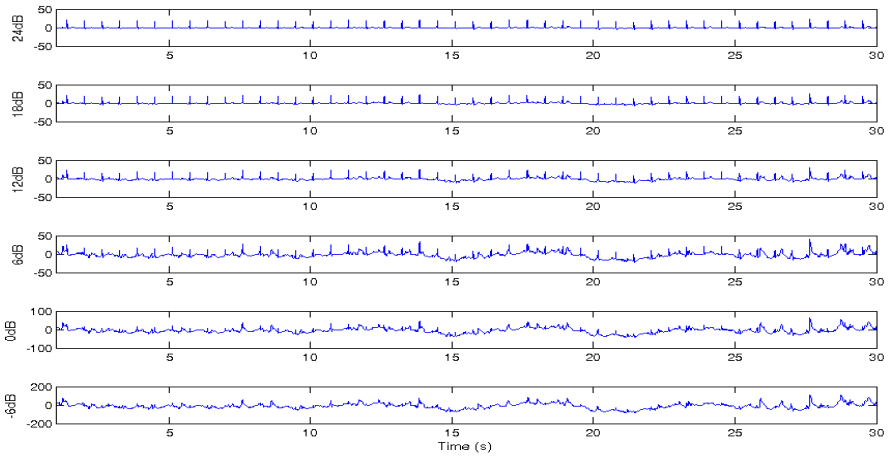
C.1.6 Database

The ECG signal quality metric ECGSQI was evaluated in Li *et al.* [83] on a large subset of the Physionet MIMIC II database [75, 206] which represented low-noise regions of the database. After experimenting to determine a suitable quality level, the authors chose segments where the ECGSQI was greater than or equal to 0.95 for at least one hour (to identify continuous segments). From the 2500 patients available at the time, comprising a total of 150 000 h of simultaneous ECG and ABP data, the resultant clean dataset included 437 subjects, comprising 3762 1 hour or longer (1.62 ± 0.69 hours) data segments, and a total of 6084 hours.

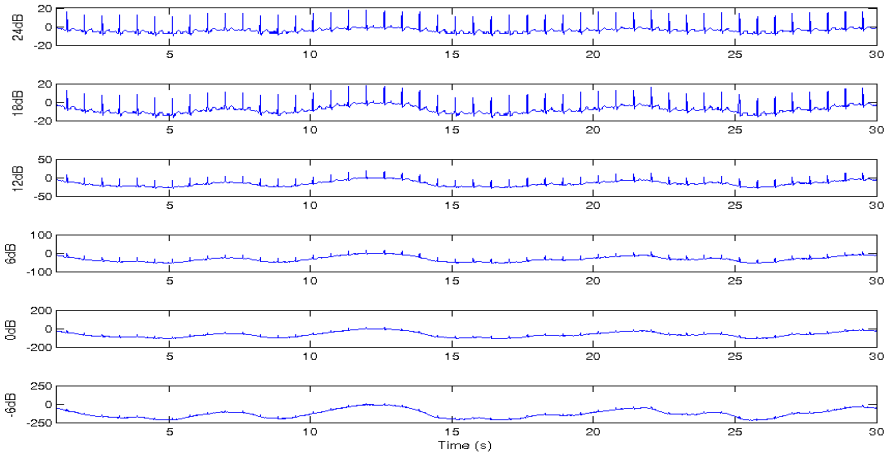
For the work in this thesis 16 subjects were chosen at random from the data used by Li *et al.* [83] (for computational simplicity) resulting in a total of approximately 150 hours of ECG data.

C.1.7 Additive noise

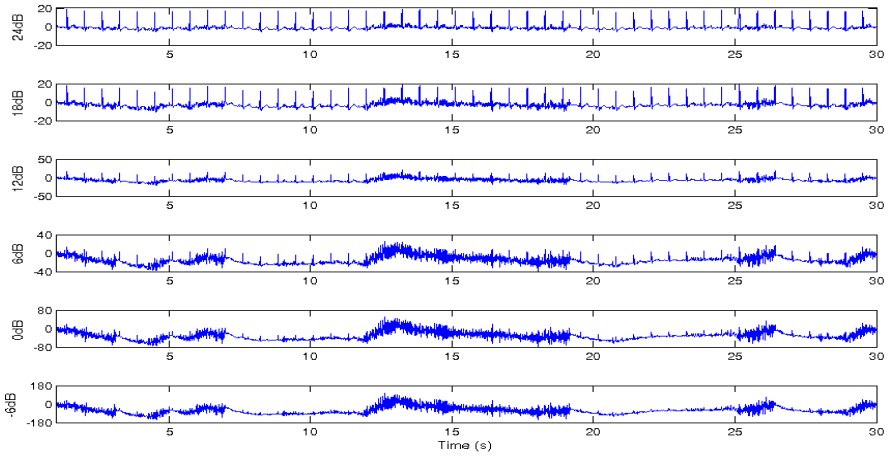
In order to evaluate the response of TSQI, real noise from PhysioNet's NSTDB database [75, 207] was introduced to the ECG. The ECG noise included electrode motion artifact (EM), baseline wander (BW) and muscle artifact (MA), each with two channels of simultaneously recorded data recorded from real humans and designed not to include any cardiac sources. Each of the three ECG noise types (MA, BW, EM) were added separately to each ECG lead of the clean dataset with varying signal to noise ratios (SNRs), starting five minutes into the recording, and then for every other 2 min window in the clean data. Noise segments were added with SNR = 24, 18, 12, 6, 0 and -6 dB for each noise type - see figure C.1.



(a) Electrode movement



(b) Baseline wander



(c) Muscular artefacts

Figure C.1: An example of 30 s of evaluation data. (a) EM noise at different SNRs, (a) BW noise at different SNRs (a) MA noise at different SNRS (SNR = 24, 18, 12, 6, 0 and -6 dB)

C.2 Comparison of ECGSQI with a template-based method, TSQI

In this section, results of application of the signal quality algorithm (TSQI) developed in Section 2.6.1 are presented and compared to those of the SQI algorithm developed by Li *et al.* [83]. For the comparison reported in this appendix, noise at a -6dB SNR level was added to the database of clean ECGs. The SQI indices were computed for each (non-overlapping) 60 s window of ECG signal.

Low quality ECG signals were labelled as 0 while high quality signals were labelled as 1.

Figure C.2 show examples of how the two algorithms performed on an ECG with -6dB SNR MA noise (this is before thresholds are chosen for both algorithms).

As can be seen in Figure C.2, the SQI metrics range continuously between 0 and 1, while the human annotation is a binary 0 or 1, forming a square wave with a 2 minute period (except for the 5 minute beginning segment). Li *et al* [83] demonstrated that there are two interesting discontinuities in the metric. First, ECGSQI is defined to have a boundary (at ECGSQI=0.7) between extremely high quality ECG, which are perhaps useful for diagnostic purposes and beat classification, and moderate quality ECG, which can still be used for HR estimation. However, if the SQI drops too low (ECGSQI< 0.5), the ECG becomes untrustworthy, even for heart rate estimation. Therefore, the EGSQI metric allows for three levels of ECG quality, which can be used for three different purposes. For this analysis we used ECGSQI≥ 0.7 as the criterion for acceptable ECG from the method of Li *et al* [83]. For the template-based SQI (TSQI), the SQIth was set to be 0.65 and this was obtained empirically for this database.

To compare the performance of the algorithms over all records in the evaluation database, the following measures were used; sensitivity; specificity and accuracy. The TP was defined to be number high SQI beats classified correctly while TN was defined to be low SQI beat classified correctly. From this it follows that FP is the number of low SQI beats classified as high SQI beats and FN is the number of high SQI beats classified as low SQI beats.

Table C.1 provides sensitivity, specificity and accuracy of the three different types of noises,

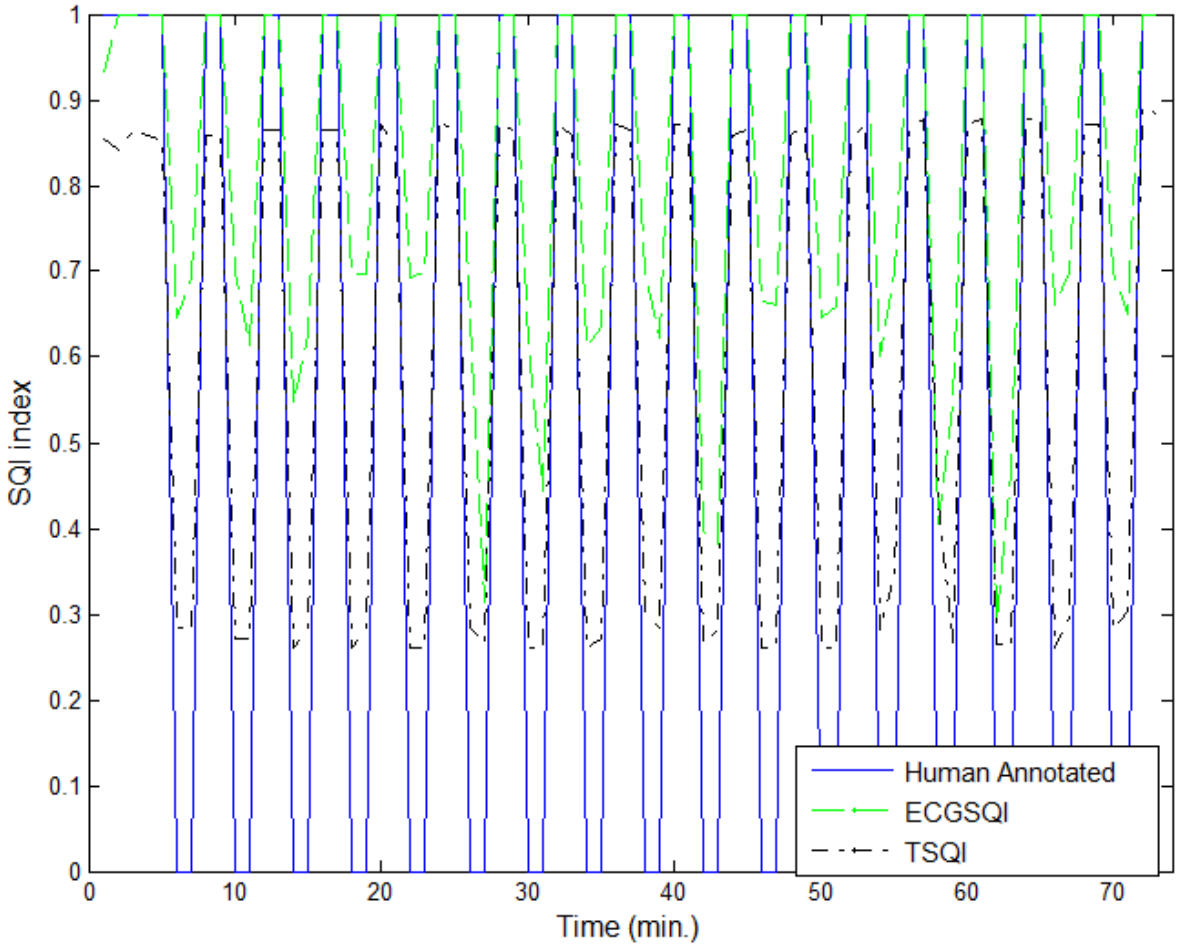


Figure C.2: An example of a comparison of the two SQI algorithms on a ECG signal added with -6dB movement artefacts (MA) noise. The SQI were computed for 1-minute window with no overlaps. Gold standard human annotated SQI in blue. Template-based SQI (this work) in black. ECGSQI in green)

averaged over the datasets.

Variables	Sensitivity (%)	Specificity (%)	Accuracy (%)
EM noise			
TSQI	91.11	97.25	94.38
ECGSQI	91.39	87.32	89.46
MA noise			
TSQI	90.72	96.76	93.57
ECGSQI	96.67	94.68	95.72
BW noise			
TSQI	97.44	97.92	97.67
ECGSQI	99.67	99.68	99.68

Table C.1: Performance of ECGSQI and TSQI on the entire subset of data selected from the MIMIC II database in this study, with three different types of noise added; electrode motion (EM), muscle artifact (MA) and and baseline wander (BW) .

Although marginally inferior to ECGSQI on baseline wander and muscle artifact, TSQI provides superior performance on electrode motion noise for the data subset selected at the 6bB noise level. This is expected since before template matching is performed, baseline wander was removed from the ECG signal using the technique described in Chapter 2.

The slightly higher performance on EM noise indicates that ECGSQI might be slightly undersensitive to electrode motion, in favour of other noises. Since TSQI relies heavily on correctly detected QRS complexes, the presence of MA noise might makes it challenging to correctly locate the QRS complexes and consequently explain the slightly lower performance on MA type noise.

In conclusion, we have validate that the TSQI index implemented for this thesis provides a suitable (and simple) method for excluding noisy segments of ECG prior to ST-segment analysis.

Bibliography

[1] L. Gettes and W. Cascio, *The Heart and Cardiovascular System*, ch. Effect of acute ischemia on cardiac electrophysiology, pp. 2021–2054. New York: Raven Press Ltd, 2 ed., 1992.

[2] J. L. Anderson, C. D. Adams, E. Antman, C. R. Bridges, R. M. Califf, and D. Casey, "ACC/AHA 2007 guidelines for the management of patients with unstable angina/non-ST-elevation myocardial infarction: a report of the American College of Cardiology/American Heart Association Task Force on Practice Guidelines.," *J Am Coll Cardiol*, vol. 50, pp. e1–e157, Aug 2007.

[3] WHO, "Global atlas on cardiovascular disease prevention and control," tech. rep., Wolrd Health Organization, 2011.

[4] P. Scarborough, P. Bhatnagar, K. Wickramasinghe, K. Smolina, C. Mitchell, and M. Rayner, "Coronary heart disease statistics," tech. rep., British Heart Foundation Research, 2011.

[5] C. Hamm, B. Goldmann, C. Heeschen, G. Kreymann, J. Berger, and T. Meinertz, "Emergency room triage of patients with acute chest pain by means of rapid testing for cardiac troponin T or troponin I," *N Engl J Med*, vol. 337, pp. 1648–1653, 1997.

[6] E. Ohman, P. Armstrong, R. Christenson, C. B. Granger, H. Katus, C. Hamm, M. O'Hanesian, G. S. Wagner, N. Kleiman, and F. Harrell, "Cardiac troponin T levels for risk stratification in acute myocardial ischemia. GUSTO IIA investigators," *The New England Journal of Medicine*, vol. 335, no. 18, pp. 1333–1341, 1996.

[7] J. Lima, "Myocardial viability assessment by contrast-enhanced magnetic resonance imaging," *Am J Cardiol*, vol. 42, pp. 902–904, 2003.

[8] G. Korosoglou, N. Labadze, A. Hansen, C. Selter, E. Giannitsis, H. Katus, and H. Kuecherer, "Usefulness of real-time myocardial perfusion imaging in the evaluation of patients with first time chest pain," *Am J Cardiol*, vol. 94, pp. 1225–1231, 2004.

[9] S. W. Goodacre, K. Angelini, J. Arnold, S. Revill, and F. Morris, "Clinical predictors of acute coronary syndromes in patients with undifferentiated chest pain," *QJM*, vol. 96, pp. 893–898, Dec 2003.

[10] M. Roe, R. Christenson, E. Ohman, R. Bahr, F. Fesmire, and A. Storrow, "A randomized, placebo-controlled trial of early eptifibatide for non-ST-segment elevation acute coronary syndromes," *Am Heart J*, vol. 146, pp. 993–998, Dec 2003.

[11] K. A. A. Fox, S. G. Goodman, W. Klein, D. Brieger, P. G. Steg, O. Dabbous, and A. Avezum, "Management of acute coronary syndromes. variations in practice and outcome;

findings from the Global Registry of Acute Coronary Events (GRACE)," *Eur Heart J*, vol. 23, pp. 1177–1189, Aug 2002.

[12] E. Antman, D. Anbe, and P. Armstrong, "ACC/AHA guidelines for the management of patients with ST-elevation myocardial infarction: a report of the American College of Cardiology/American Heart Association Task force on Practice Guidelines," *J Am Coll Cardiol*, vol. 44, p. 1211, 2004.

[13] E. Antman, M. Hand, P. Armstrong, E. Bates, L. Green, L. Halasyamani, and J. Hochman, "2007 Focused update of the ACC/AHA 2004 guidelines for the management of Patients with ST-elevation Myocardial Infarction: a report of the American College of Cardiology/American Heart Association Task Force on Practice Guidelines," *Circulation*, vol. 117, pp. 296–329, Jan 2008.

[14] D. Patel, G. Holdright, and K. D.R., "Early continuous ST segment monitoring in unstable angina: prognostic value additional to the clinical characteristics and the admission electrocardiogram," *Heart*, vol. 75, pp. 222–228, 1996.

[15] K. Eagle, M. Lim, O. Dabbous, K. Pieper, R. Goldberg, F. Van de Werf, and S. Goodman, "A validated prediction model for all forms of acute coronary syndrome: estimating the risk of 6-month postdischarge death in an international registry," *The Journal of the American Medical Association*, vol. 291, pp. 2727–2733, Jun 2004.

[16] D. Hasdai, S. Behar, L. Wallentin, N. Danchin, A. K. Gitt, E. Boersma, P. Fioretti, M. L. Simoons, and A. Battler, "A prospective survey of the characteristics, treatments and outcomes of patients with acute coronary syndromes in Europe and the Mediterranean basin; the Euro Heart Survey of Acute Coronary Syndromes (Euro Heart Survey ACS)," *European Heart Journal*, vol. 23, pp. 1190–1201, Aug 2002.

[17] D. Hasdai, E. Lev, S. Behar, V. Boyko, N. Danchin, A. Vahanian, and A. Battler, "Acute coronary syndromes in patients with pre-existing moderate to severe valvular disease of the heart: lessons from the Euro-Heart Survey of acute coronary syndromes," *Eur. Heart J.*, vol. 24, pp. 623–629, Apr 2003.

[18] J. Hoekstra, C. V. Pollack, M. Roe, E. Peterson, R. Brindis, R. Harrington, R. Christenson, S. Smith, E. Ohman, and W. Gibler, "Improving the care of patients with non-ST-elevation acute coronary syndromes in the emergency department: the CRUSADE initiative," *Acad Emerg Med*, vol. 9, pp. 1146–1155, Nov 2002.

[19] E. Lev, A. Battler, S. Behar, A. Porter, M. Haim, V. Boyko, and D. Hasdai, "Frequency, characteristics, and outcome of patients hospitalized with acute coronary syndromes with undetermined electrocardiographic patterns.," *Am J Cardiol*, vol. 91, pp. 224–227, Jan 2003.

[20] U. Stenestrand, L. Wallentin, and Swedish Register of Cardiac Intensive Care (RIKS-HIA), "Early statin treatment following acute myocardial infarction and 1-year survival," *The Journal of the American Medical Association*, vol. 285, no. 4, pp. 430–436, 2001.

[21] U. Stenestrand and L. Wallentin, "Early revascularisation and 1-year survival in 14-day survivors of acute myocardial infarction: a prospective cohort study.," *Lancet*, vol. 359, pp. 1805–1811, May 2002.

[22] D. Cox, G. Stone, C. Grines, T. Stuckey, P. Zimetbaum, and J. Tcheng, "Comparative early and late outcomes after primary percutaneous coronary intervention in ST-segment elevation and non-ST-segment elevation acute myocardial infarction (from the CADILLAC trial)," *Am J Cardiol*, vol. 98, pp. 331–337, Aug 2006.

[23] F. Van de Werf, J. Bax, A. Betriu, C. Blomstrom-Lundqvist, F. Crea, V. Falk, G. Filippatos, K. Fox, K. Huber, A. Kastrati, A. Rosengren, P. Steg, M. Tubaro, F. Verheugt, F. Weidinger, and M. Weis, "Management of acute myocardial infarction in patients presenting with persistent ST-segment elevation," *G Ital Cardiol (Rome)*, vol. 10, pp. 450–489, Jul 2009.

[24] J. G. Canto, M. G. Shlipak, W. J. Rogers, J. A. Malmgren, P. D. Frederick, C. T. Lambrew, J. P. Ornato, H. V. Barron, and C. I. Kiefe, "Prevalence, clinical characteristics, and mortality among patients with myocardial infarction presenting without chest pain," *The Journal of the American Medical Association*, vol. 283, pp. 3223–3229, Jun 2000.

[25] D. A. Morrow, E. M. Antman, S. M. Snapinn, C. H. McCabe, P. Theroux, and E. Braunwald, "An integrated clinical approach to predicting the benefit of tirofiban in non-ST elevation acute coronary syndromes. application of the TIMI risk score for UA/NSTEMI in PRISM-PLUS.," *Eur Heart J*, vol. 23, pp. 223–229, Feb 2002.

[26] J. P. Curtis, E. L. Portnay, Y. Wang, R. L. McNamara, J. Herrin, E. H. Bradley, D. J. Magid, M. E. Blaney, J. G. Canto, and H. M. Krumholz, "The pre-hospital electrocardiogram and time to reperfusion in patients with acute myocardial infarction, 2000-2002: findings from the national registry of myocardial infarction-4.," *Am J Cardiol*, vol. 47, pp. 1544–1552, Apr 2006.

[27] C. Terkelsen, J. Lassen, B. Nrgaard, J. Gerdes, S. Poulsen, K. Bendix, J. Ankersen, L. B.-H. Gtzsche, F. Rmer, T. Nielsen, and H. Andersen, "Reduction of treatment delay in patients with ST-elevation myocardial infarction: impact of pre-hospital diagnosis and direct referral to primary percutanous coronary intervention," *Eur Heart J*, vol. 26, pp. 770–777, Apr 2005.

[28] N. Albert, "Non-ST segment elevation acute coronary syndromes: treatment guidelines for the nurse practitioner.," *J Am Acad Nurse Pract*, vol. 19, pp. 277–289, Jun 2007.

[29] J. P. Brown, E. Mahmud, J. V. Dunford, and O. Ben-Yehuda, "Effect of prehospital 12-lead electrocardiogram on activation of the cardiac catheterization laboratory and door-to-balloon time in ST-segment elevation acute myocardial infarction," *Am J Cardiol*, vol. 101, pp. 158–161, Jan 2008.

[30] E. Bradley, S. Roumanis, M. Radford, T. Webster, R. McNamara, J. Mattera, B. Barton, D. Berg, E. Portnay, H. Moscovitz, J. Parkosewich, E. Holmboe, M. Blaney, and H. Krumholz, "Achieving door-to-balloon times that meet quality guidelines: how do successful hospitals do it?," *Am J Cardiol*, vol. 46, pp. 1236–1241, Oct 2005.

[31] E. H. Bradley, L. A. Curry, T. R. Webster, J. A. Mattera, S. A. Roumanis, M. J. Radford, R. L. McNamara, B. A. Barton, D. N. Berg, and H. M. Krumholz, "Achieving rapid door-to-balloon times: how top hospitals improve complex clinical systems.," *Circulation*, vol. 113, pp. 1079–1085, Feb 2006.

[32] R. Swor, S. Hegerberg, A. McHugh-McNally, M. Goldstein, and C. McEachin, "Prehospital 12-lead ECG: efficacy or effectiveness?," *Prehosp Emerg Care*, vol. 10, no. 3, pp. 374–377, 2006.

[33] V. N. Dhruva, S. I. Abdelhadi, A. Anis, W. Gluckman, D. Hom, W. Dougan, E. Kaluski, B. Haider, and M. Klapholz, "ST-segment analysis using wireless technology in acute myocardial infarction (STAT-MI) trial," *J Am Coll Cardiol*, vol. 50, pp. 509–513, Aug 2007.

[34] H. Ting, H. Krumholz, S. FaHa, E. Bradley, D. Cone, J. Curtis, and B. Drew, "Implementation and integration of prehospital ECGs into systems of care for acute coronary syndrome," *Circulation*, vol. 118, pp. 1066–1079, 2008.

[35] K. Scholz, R. Hilgers, D. Ahlersmann, H. Duwald, R. Nitsche, G. von Knobelsdorff, B. Volger, K. Mller, and F. Keating, "Contact-to-balloon time and door-to-balloon time after initiation of a formalized data feedback in patients with acute ST-elevation myocardial infarction," *Am J Cardiol*, vol. 101, pp. 46–52, Jan 2008.

[36] K. M. Akkerhuis, P. A. Klootwijk, W. Lindeboom, V. A. Umans, S. Meij, P. P. Kint, and M. L. Simoons, "Recurrent ischaemia during continuous multilead ST-segment monitoring identifies patients with acute coronary syndromes at high risk of adverse cardiac events; meta-analysis of three studies involving 995 patients.," *Eur Heart J*, vol. 22, pp. 1997–2006, Nov 2001.

[37] T. Jernberg, B. Lindahl, and L. Wallentin, "ST-segment monitoring with continuous 12-lead ECG improves early risk stratification in patients with chest pain and ECG nondiagnostic of acute myocardial infarction," *American College of Cardiologiost*, vol. 34, p. 14131419, 1999.

[38] P. Klootwijk, S. Meij, G. A. von Es, E. J. Mller, V. A. Umans, T. Lenderink, and M. L. Simoons, "Comparison of usefulness of computer assisted continuous 48-h 3-lead with 12-lead ECG ischaemia monitoring for detection and quantitation of ischaemia in patients with unstable angina," *European Heart Journal*, vol. 18, pp. 931–940, Jun 1997.

[39] M. Zairis, J. Ambrose, O. Papadaki, S. Manousakis, A. Stefanidis, M. DeVoe, S. Handanis, C. Olympios, and S. Foussas, "C-reactive protein and ST-segment monitoring by continuous 12-lead electrocardiogram in patients with primary unstable angina pectoris.," *Am J Cardiol*, vol. 91, pp. 600–603, Mar 2003.

[40] G. Landesberg, Y. Vesselov, S. Einav, S. Goodman, C. L. Sprung, and C. Weissman, "Myocardial ischemia, cardiac troponin, and long-term survival of high-cardiac risk critically ill intensive care unit patients.," *Crit Care Med*, vol. 33, pp. 1281–1287, Jun 2005.

[41] J. Kress, A. Vinayak, J. Levitt, W. Schweickert, B. Gehlbach, F. Zimmerman, A. Pohlman, and J. Hall, "Daily sedative interruption in mechanically ventilated patients at risk for coronary artery disease," *Crit Care Med*, vol. 35, pp. 365–371, Feb 2007.

[42] T. Jernberg, P. Abrahamsson, B. Lindahl, P. Johanson, L. Wallentin, and M. Dellborg, "Continuous multilead ST-monitoring identifies patients with unstable coronary artery disease who benefit from extended antithrombotic treatment," *Eur Heart J*, vol. 23, pp. 1093–1101, Jul 2002.

[43] K. L. Lee, L. H. Woodlief, E. J. Topol, W. D. Weaver, A. Betriu, J. Col, M. Simoons, P. Aylward, F. Van de Werf, and R. M. Califf, "Predictors of 30-day mortality in the era of reperfusion for acute myocardial infarction. results from an international trial of 41,021 patients. GUSTO-I investigators.," *Circulation*, vol. 91, pp. 1659–1668, Mar 1995.

[44] A. Maas, C. Wyatt, C. Green, G. Wagner, K. Trollinger, J. Pope, A. Langer, P. Armstrong, R. Califf, M. Simoons, and M. Krucoff, "Combining baseline clinical descriptors and real-time response to therapy: the incremental prognostic value of continuous ST-segment monitoring in acute myocardial infarction," *Am Heart J*, vol. 147, pp. 698–704, Apr 2004.

[45] A. Yan, R. Yan, M. Tan, M. Senaratne, D. Fitchett, A. Langer, and S. Goodman, "Long-term prognostic value and therapeutic implications of continuous ST-segment monitoring in acute coronary syndrome," *Am Heart J*, vol. 153, pp. 500–506, Apr 2007.

[46] M. Pelter, M. Adams, and B. Drew, "Transient myocardial ischemia is an independent predictor of adverse in-hospital outcomes in patients with acute coronary syndromes treated in the telemetry unit," *Journal of Acute and Critical Care*, vol. 32, no. 2, pp. 71–78, 2003.

[47] E. Braunwald, E. M. Antman, J. W. Beasley, R. M. Califf, M. D. Cheitlin, J. S. Hochman, and et al., "ACC/AHA 2002 guideline update for the management of patients with unstable angina and non-ST-segment elevation myocardial infarction–summary article: a report of the American College of Cardiology/American Heart Association task force on practice guidelines (committee on the management of patients with unstable angina)," *Am J Cardiol*, vol. 40, pp. 1366–1374, Oct 2002.

[48] E. Antman, M. Cohen, and P. Bernink, "The TIMI risk score for unstable angina/non-ST elevation MI: a method for prognostication and therapeutic decision making," *The Journal of the American Medical Association*, vol. 284, pp. 835–842, 2000.

[49] E. Boersma, K. S. Pieper, E. W. Steyerberg, R. G. Wilcox, W. C. Chang, K. L. Lee, K. M. Akkerhuis, R. A. Harrington, J. W. Deckers, P. W. Armstrong, A. M. Lincoff, R. M. Califf, E. J. Topol, and M. L. Simoons, "Predictors of outcome in patients with acute coronary syndromes without persistent ST-segment elevation. results from an international trial of 9461 patients. The PURSUIT Investigators.," *Circulation*, vol. 101, pp. 2557–2567, Jun 2000.

[50] D. A. Morrow, N. Rifai, E. M. Antman, D. L. Weiner, C. H. McCabe, C. P. Cannon, and E. Braunwald, "Serum amyloid A predicts early mortality in acute coronary syndromes: A TIMI 11A substudy," *J Am Coll Cardiol*, vol. 35, pp. 358–362, Feb 2000.

[51] T. Killip III and J. Kimball, "Treatment of myocardial infarction in a coronary care unit: A two year experience with 250 patients," *Am J Cardiol*, vol. 20, no. 4, pp. 457–464, 1967.

[52] C. Hamm, J. Bassand, and S. Agewall, "ESC guidelines for the management of acute coronary syndromes in patients presenting without persistent ST-segment elevation: The Task Force for the management of acute coronary syndromes (ACS) in patients presenting without persistent ST-segment elevation of the European Society of Cardiology (ESC)," *Eur. Heart J.*, vol. 32, no. 23, pp. 2999–3054, 2011.

[53] F. Van de Werf, J. Bax, A. Betriu, C. Blomstrom-Lundqvist, F. Crea, V. Falk, G. Filippatos, K. Fox, K. Huber, A. Kastrati, A. Rosengren, P. Steg, M. Tubaro, F. Verheugt, F. Weidinger, and M. Weis, "Management of acute myocardial infarction in patients presenting with persistent ST-segment elevation: the task force on the management of ST-segment elevation acute myocardial infarction of the European Society of Cardiology," *Eur Heart J*, vol. 29, pp. 2909–2945, Dec 2008.

[54] J. Venegas and R. Mark, "HST.542J Quantitative Physiology:Organ Transport Systems." http://ocw.mit.edu, Spring 2004 (Accessed 15 Apr 2010). License: Creative Commons BY-NC-SA.

[55] R. Rangayyan, *Biomedical Signal Analysis: A Case-Study Approach*, ch. Effect of acute ischemia on cardiac electrophysiology, pp. 20–21. IEEE Press, 2002.

[56] J. K. Cooper, "Electrocardiography 100 years ago, origins, pioneers, and contributors," *The New England Journal of Medicine*, vol. 315, pp. 461–464, July 1986.

[57] A. Houghton and D. Gray, *Making sense of the ECG*. Oxford: Oxford University Press, 1997.

[58] R. Fenichel, M. Malik, C. Antzelevitch, M. Sanguinetti, D. Roden, S. Priori, J. Ruskin, R. Lipicky, and L. Cantilena, "Drug-induced torsades de pointes and implications for drug development," *Journal of Cardiovascular Electrophysiology*, vol. 15, pp. 475–495, July 2004.

[59] G. Yan and C. Antzelevitch, "Cellular basis for the brugada syndrome and other mechanisms of arrhythmogenesis associated with ST-segment elevation," *Circulation*, vol. 100, pp. 1660–1666, Oct 1999.

[60] J. C. Cowan, K. Yusoff, M. Moore, P. A. Amos, A. E. Gold, J. P. Bourke, S. Tansuphaswadikul, and R. W. Campbell, "Importance of lead selection in QT interval measurement.," *Am J Cardiol*, vol. 61, pp. 83–87, Jan 1988.

[61] G. Clifford, *Signal Processing of Heart Rate Variability*. PhD thesis, University of Oxford, 2003.

[62] B. Drew, S. Wung, M. Adams, and M. Pelter, "Bedside diagnosis of myocardial ischemia with ST-segment monitoring technology: measurement issues for real-time clinical decision making and trial designs," *J Electrocardiol*, vol. 30 Suppl, pp. 157–165, 1998.

[63] G. Clifford, A. Aboukhalil, X. SunJ, W. Zong, B. Janz, G. Moody, and R. Mark, "Using the blood pressure waveform to reduce critical false ECG alarms," in *Proc. Computers in Cardiology 2006*, vol. 33, pp. 829–832, 2006.

[64] B. Drew, R. Califf, M. Funk, E. Kaufman, M. W. Krucoff, M. Laks, P. Macfarlane, C. Sommargren, S. Swiryn, G. Van Hare, A. H. Association, C. C. Councils on Cardiovascular Nursing, and C. D. in the Young, "Practice standards for electrocardiographic monitoring in hospital settings: an American Heart Association scientific statement from the Councils on Cardiovascular Nursing, Clinical Cardiology, and Cardiovascular Disease in the Young: endorsed by the International Society of Computerized Electrocardiology and the American Association of Critical-Care Nurses," *Circulation*, vol. 110, pp. 2721–2746, Oct 2004.

[65] B. L. Chia, J. W. Yip, H. C. Tan, and Y. T. Lim, "Usefulness of st elevation II/III ratio and ST deviation in lead I for identifying the culprit artery in inferior wall acute myocardial infarction," *Am J Cardiol*, vol. 86, pp. 341–343, Aug 2000.

[66] H. Yasue, S. Omote, A. Takizawa, N. Masao, H. Hyon, S. Nishida, and M. Horie, "Comparison of coronary arteriographic findings during angina pectoris associated with ST elevation or depression," *American Journal of Cardiology*, vol. 47, pp. 539–546, 1981.

[67] R. Holland and M. Arnsdorf, "Solid angle theory and the electrocardiogram: physiologic and quantitative interpretations," *Cardiooasc Dis*, vol. 19, pp. 431–452, 1977.

[68] G. Timogiannakis, I. Amende, E. Martinez, and M. Thomas, "ST segment deviation and regional myocardial blood bow during experimental partial coronary artery occlusion," *Cardiowsc Res*, vol. 8, pp. 469–477, 1974.

[69] F. Jager, *Introduction to feature extraction*, ch. Advanced Methods and Tools for ECG Data Analysis, pp. 246–269. Artech House, 2006.

[70] B. Kohler, C. Hennig, and R. Orglmeister, "The principles of software QRS detection," *IEEE Engineering in Medicine and Biology Magazine*, vol. 21, pp. 42–45, 2002.

[71] G. Friesen, T. Jannett, M. Jadallah, S. Yates, S. Quint, and H. Nagle, "A comparison of the noise sensitivity of nine QRS detection algorithms," *IEEE Transactions on Biomedical Engineering*, vol. 37, no. 1, pp. 85–98, 1990.

[72] L. Sörnmo, O. Paklm, and M. Nygards, "Adaptive QRS detection: A study of performance," *IEEE Transactions on Biomedical Engineering*, vol. 32, no. 6, pp. 392–401, 1985.

[73] J. Pan and W. Tompkins, "A real-time QRS detection algorithm," *IEEE Transactions on Biomedical Engineering*, vol. 3, pp. 230–236, 1985.

[74] C. Li, C. Zheng, and C. Tai, "Detection of ECG characteristic points using wavelet transforms," *IEEE Transactions on Biomedical Engineering*, vol. 42, no. 1, pp. 21–28, 1995.

[75] A. Goldberger, L. Amaral, L. Glass, J. Hausdorff, P. Ivanov, R. Mark, J. Mietus, G. Moody, C. Peng, and H. Stanley, "Physiobank, Physiotoolkit, and Physionet: Components of a new research resource for complex physiologic signals," *Circulation*, vol. 101, no. 23, pp. 215–220, 2000.

[76] G. Clifford, L. F. Zapanta, B. Janz, J. E. Mietus, C. Y. Youn, and R. Mark, "Segmentation of 24-hour cardiovascular activity using ECG-based sleep/sedation and noise metrics," in *Proc. Computers in Cardiology*, pp. 595–598, 2005.

[77] C. Meyer and H. Kelser, "Electrocardiogram baseline noise estimation and removal using cubic splines and state-space computation techniques," *Computers and Biomedical Research*, vol. 10, pp. 459–470, 1977.

[78] L. Sörnmo, "Time varying digital filtering of ECG baseline wander," *Med Biol Eng Comput*, vol. 31, no. 5, pp. 503–508, 1993.

[79] F. Jager, *Advanced Methods and Tools for ECG Data Analysis*, ch. ST Analysis, pp. 270–290. Artech House, 2006.

[80] G. Moody and R. Mark, "A new method for detecting atrial fibrillation using RR intervals," *Computers in Cardiology*, vol. 10, pp. 227–230, 1983.

[81] J. Allen and A. Murray, "Assessing ECG signal quality on a coronary care unit," *Physiol Meas*, vol. 17, pp. 249–258, Nov 1996.

[82] G. Clifford, A. Shoeb, P. McSharry, and B. Janz, "Model-based filtering, compression and classification of the ECG," *Intern J Bioelectromagnetism*, vol. 7, no. 1, pp. 158–161, 2005.

[83] Q. Li, R. G. Mark, and G. D. Clifford, "Robust heart rate estimation from multiple asynchronous noisy sources using signal quality indices and a Kalman filter," *Physiol Meas*, vol. 29, pp. 15–32, Jan 2008.

[84] J. A. Sukor, S. J. Redmond, G. S. H. Chan, and N. H. Lovell, "Signal quality measures for unsupervised blood pressure measurement.," *Physiol Meas*, vol. 33, pp. 465–486, Mar 2012.

[85] H. Xia, G. A. Garcia, J. McBride, A. Sullivan, T. D. Bock, J. Bains, D. Wortham, and X. Zhao, "Computer algorithms for evaluating the quality of ECGs in real time," pp. 10–11, 2011.

[86] G. Clifford, D. Lopez, Q. Li, and I. Rezek, "Signal quality indices and data fusion for determining acceptability of electrocardiograms collected in noisy ambulatory environments," pp. 1–5, 2011.

[87] M. Levy, "Sympathetic-parasympathetic interactions in the heart," *Circulation Res*, vol. 29, pp. 437–445, 1971.

[88] M. Malik, "Graphical representation of circadian patterns of heart rate variability components.," *Pacing Clin Electrophysiol*, vol. 18, pp. 1575–1580, Aug 1995.

[89] R. E. Kleiger, P. K. Stein, M. S. Bosner, and J. N. Rottman, "Time domain measurements of heart rate variability.," *Cardiol Clin*, vol. 10, pp. 487–498, Aug 1992.

[90] M. Moser, M. Lehofer, A. Sedminek, M. Lux, H. Zapotoczky, T. Kenner, and A. Noordergraaf, "Heart rate variability as a prognostic tool in cardiology. A contribution to the problem from a theoretical point of view," *Circulation*, vol. 90, pp. 1078–1082, 1994.

[91] S. Akselrod, D. Gordon, F. Ubel, D. Shannon, A. Berger, and R. Cohen, "Power spectrum analysis of heart rate fluctuation: a quantitative probe of beat-to-beat cardiovascular control.," *Science*, vol. 213, pp. 220–222, Jul 1981.

[92] R. L. Burr and M. J. Cowan, "Autoregressive spectral models of heart rate variability," *J Electrocardiology*, vol. 25, pp. 224–233, 1992.

[93] S. Akselrod, D. Gordon, J. B. Madwed, N. C. Snidman, D. C. Shannon, and R. J. Cohen, "Hemodynamic regulation: investigation by spectral analysis.," *Am J Physiol*, vol. 249, pp. H867–H875, Oct 1985.

[94] M. Kamath and E. Fallen, "Power spectral analysis of HRV: a noninasive signature of cardiac autonomic functions," *Crit. Rev. Biomed. Eng*, vol. 21, no. 3, pp. 245–311, 1993.

[95] M. Pagani, F. Lombardi, S. Guzzetti, O. Rimoldi, R. Furlan, P. Pizzinelli, G. Sandrone, G. Malfatto, S. Dell'Orto, and E. Piccaluga, "Power spectral analysis of heart rate and arterial pressure variabilities as a marker of sympatho-vagal interaction in man and conscious dog," *Circ Res*, vol. 59, pp. 178–193, Aug 1986.

[96] A. Malliani, N. Montano, and M. Pagani, "Physiological background of heart rate variability," *Physiology*, pp. 343–346, 1997.

[97] M. Malik, "Heart rate variability: Standards of measurement, physiological interpretation, and clinical use," *Circulation*, vol. 17, no. 3, pp. 1043–1065, 1996.

[98] J. Valkama, H. Huikuri, K. Airaksinen, M. Linnaluoto, and J. Takkunen, "Determinants of frequency domain measures of heart rate variability in the acute and convalesccent phases of myocardial infarction," *Cardiovasc-Res.*, vol. 28, pp. 1273–1276, 1994.

[99] P. Haji-Michael, V. Vincent, J. Degaute, and P. van de Borne, "Power spectral analysis of cardiovascular variability in critically ill neurosurgical patients," *Critical Care Medicine*, vol. 28, no. 7, pp. 2578–2583, 2000.

[100] B. Acar, I. Savelieva, H. Hemingway, and M. Malik, "Automatic ectopic beat elimination in short-term heart rate variability measurement," *Comput Methods Programs Biomed*, vol. 63, pp. 123–131, Oct 2000.

[101] N. Lippman, K. Stein, and B. Lerman, "Comparison of methods for removal of ectopy in measurement of heart rate variability," *American Journal of Physiology*, vol. 267, no. 36, pp. 411–418, 1994.

[102] G. Clifford and L. Tarassenko, "Quantifying errors in spectral estimates of HRV due to beat replacement and resampling," vol. 52, no. 4, pp. 630–638, 2005.

[103] R. H. Clayton, S. W. Lord, J. M. McComb, and A. Murray, "Comparison of autoregressive and fourier transform based techniques for estimating rr interval spectra," in *Proc. Computers in Cardiology 1997*, pp. 379–382, 1997.

[104] N. R. Lomb, "Least-squares frequency analysis of unequally spaced data," *Astrophysics and Space Science*, vol. 39, pp. 447–462, 1976.

[105] J. Scargle, "Studies in astronomical time series analysis. II. ,Statistical aspects of spectral analysis of unevenly spaced data," *Astrophysical Journal*, vol. 263, pp. 835–853, 1982.

[106] A. Taddei, G. Distante, M. Emdin, P. Pisani, G. Moody, C. Zeelenberg, , and C. Marchesi, "The European ST-T database: standard for evaluating systems for the analysis of ST-T changes in ambulatory electrocardiography," *European Heart Journal*, vol. 13, no. 9, pp. 1164–1172, 1992.

[107] F. Jager, A. Taddei, G. Moody, M. Emdin, G. Antolic, R. Dorn, A. Smrdel, C. Marchesi, and R. Mark, "Long-term ST database: a reference for the development and evaluation of automated ischemia detectors and for the study of the dynamics of myocardial ischemia," *Medical and Biological Engineering and Computing*, vol. 41, pp. 172–183, 2003.

[108] L. Senhadji, G. Carrault, and J. Bellanger, "Comparing wavelet transforms for recognizing cardiac patterns," *IEEE Eng Med Biol.*, vol. 14, no. 2, pp. 167–173, 1995.

[109] F. Jager, G. Moody, and R. Mark, "Detection of transient ST segment episodes during ambulatory ECG monitoring," *Computers and Biomedical Research*, vol. 31, no. 5, pp. 305–322, 1998.

[110] J. García, L. Sörnmo, S. Olmos, and P. Laguna, "Automatic detection of ST-T complex changes on the ECG using filtered RMS difference series: application to ambulatory ischemia monitoring," *IEEE Transactions on Biomedical Engineering*, vol. 47, no. 9, pp. 1195–1201, 2000.

[111] T. Shook, V. Valvo, and M. Hubelbank, "Validation of a new algorithm for detection and quantification of ischemic ST-segment changes during ambulatory elctrocardiography," *Computers in cardiology*, pp. 57–62, 1989.

[112] C. Papaloukas, D. Fotiadis, A. Likas, C. Stroumbis, and L. Michalis, "Use of a novel rule-based expert system in the detection of changes in the ST segment and the T-wave in long duration ECGs," *Journal of Electrocardiology*, vol. 35, no. 1, pp. 27–34, 2002.

[113] A. Smrdel and F. Jager, "Automated detection of transient ST-segment episodes in 24h electrocardiograms," *Medical and Biological Engineering and Computing*, vol. 42, no. 3, pp. 303–311, 2004.

[114] Y. Goletsis, C. Papaloukas, D. Fotiadis, A. Likas, and L. Michalis, "Automated ischemic beat classification using genetic algorithms and multicriteria decision analysis," *IEEE Transactions on Biomedical Engineering*, vol. 51, no. 10, pp. 1717 –1725, 2004.

[115] T. Exarchos, C. Papaloukas, D. Fotiadis, and L. Michalis, "An association rule mining-based methodology for automated detection of ischemic ECG beats," *IEEE Transactions on Biomedical Engineering*, vol. 53, no. 8, pp. 1531–1540, 2006.

[116] J. Vila, J. Presedo, M. Delgado, S. Barro, R. Ruiz, and F. Palacios, "SUTIL: Intelligent ischemia monitoring system," *International Journal of Medical Informatics*, vol. 47, no. 3, pp. 193–214, 1997.

[117] L. Pang, I. Tchoudovski, M. Braecklein, K. Egorouchkina, W. Kellermann, and A. Bolz, "Real time heart ischemia detection in the smart home care system," pp. 3703–3706, 2005.

[118] T. Exarchos, M. Tsipouras, C. Exarchos, C. Papaloukas, D. Fotiadis, and L. Michalis, "A methodology for the automated creation of fuzzy expert systems for ischaemic and arrhythmic beat classification based on a set of rules obtained by a decision tree," *Artif. Intell. Med.*, vol. 40, no. 3, pp. 187–200, 2007.

[119] T. Stamkopoulos, M. Strintzis, C. Pappas, and N. Maglaveras, "One-lead ischemia detection using a new backpropagation algorithm and the European ST-T database," in *Proc. Computers in Cardiology*, pp. 663–666, Oct 1992.

[120] R. Silipo and C. Marchesi, "Articifial neural networks for automatic ECG analysis," *IEEE Transaction on Signal Processing*, vol. 46, pp. 1417–1425, 1998.

[121] N. Maglaveras, T. Stamkopoulos, C. Pappas, and M. Gerassimos Strintzis, "An adaptive backpropagation neural network for real-time ischemia episodes detection: development and performance analysis using the european ST-T database," *IEEE Transactions on Biomedical Engineering*, vol. 45, no. 7, pp. 805–813, 1998.

[122] D. Frenkel and J. Nadal, "Ischemic episode detection using an artificial neural network trained with isolated ST-T segments," in *Computers in Cardiology*, pp. 53–56, 1999.

[123] S. Papadimitriou, S. Mavroudi, L. Vladutu, and A. Bezerianos, "Ischemia detection with a self-organizing map supplemented by supervised learning," *IEEE Transactions on Neural Networks*, vol. 12, no. 3, pp. 503–515, 2001.

[124] C. Papaloukas, D. Fotiadis, A. Likas, A. Liavas, and L. Michalis, "A knowledge-based technique for automated detection of ischaemic episodes in long duration electrocardiograms," *Medical and Biological Engineering and Computing*, vol. 39, no. 1, pp. 105–112, 2000.

[125] C. Papaloukas, D. Fotiadis, A. Likas, and L. Michalis, "An ischemia detection method based on artificial neural networks," *Artificial Intellegence in Medicine*, vol. 24, no. 1, pp. 167–178, 2002.

[126] R. Andreao, B. Dorizzi, J. Boudy, and J. Mota, "ST-segment analysis using hidden Markov Model beat segmentation: application to ischemia detection," in *Computers in Cardiology*, pp. 381–384, Sept. 2004.

[127] A. Taddei, G. Costantino, R. Silipo, M. Emdin, and C. Marchesi, "A system for the detection of ischemic episodes in ambulatory ECG," *Computers of Cardiology*, pp. 705–708, 1995.

[128] T. Stamkopoulos, K. Diamantaras, N. Maglaveras, and M. Strintzis, "ECG analysis using nonlinear PCA neural networks for ischemia detection," *IEEE Transactions on Signal Processing*, vol. 46, no. 11, pp. 3058–3067, 1998.

[129] I. Christov and I. Daskalov, "Filtering of electromyogram artifacts from the electrocardiogram," *Med Eng Phys*, vol. 21, pp. 731–736, 1999.

[130] X. Wang, L. Xu, Z. Sun, Z. Yang, and Y. Peng, "Heart rate variability analysis of ischemic and heart rate related ST-segment deviation episodes based on time-frequency method," in *Proc. Joint Meeting of the 6th Int. Symp. Noninvasive Functional Source Imaging of the Brain and Heart and the Int. Conf. Functional Biomedical Imaging NFSI-ICFBI 2007*, pp. 162–164, 2007.

[131] L. Dranca, A. Goai, and A. Illarramendi, "Real-time detection of transient cardiac ischemic episodes from ecg signals," *Physiological Measurement*, vol. 30, no. 9, p. 983, 2009.

[132] J. Faganeli and F. Jager, "Automatic classification between transient ischaemic and transient non-ischaemic heart-rate related ST segment episodes in ambulatory ECG records," *Physiological Measurement*, vol. 5, pp. 323–337, 2010.

[133] P. Langley, E. J. Bowers, J. Wild, M. J. Drinnan, J. Allen, A. J. Sims, N. Brown, and A. Murray, "An algorithm to distinguish ischaemic and non-ischaemic ST changes in the holter ECG," in *Proc. Computers in Cardiology*, pp. 239–242, 2003.

[134] M. Smyrnakis and D. Evans, "Classifying ischemic events using a Bayesian inference Multilayer perceptron and input variable evaluation using automatic relevance determination," in *in Proc.Computers in Cardiology*, pp. 305–308, 2007.

[135] A. Minchole, F. Jager, and P. Laguna, "Discrimination between ischemic and artifactual st segments events in holter recordings," *Biomedical Signal Processing and Control*, vol. 5, pp. 21–31, 2010.

[136] M. W. Zimmerman, R. J. Povinelli, M. T. Johnson, and K. M. Ropella, "A reconstructed phase space approach for distinguishing ischemic from non-ischemic ST changes using holter ECG data," in *Proc. Computers in Cardiology*, pp. 243–246, 2003.

[137] G. B. Moody and F. Jager, "Distinguishing ischemic from non-ischemic ST changes: the PhysioNet/Computers in Cardiology Challenge 2003," in *Proc. Computers in Cardiology*, pp. 235–237, 2003.

[138] J. Faganeli and F. Jager, "Automatic classification between transient ischaemic and transient non-ischaemic heart-rate related ST segment episodes in ambulatory ECG records," in *Proc. Computers in Cardiology*, pp. 381–384, 2008.

[139] A. Wagner, H. Mahrholdt, T. Holly, M. Elliott, M. Regenfus, F. Parker M, Klocke, R. Bonow, R. Kim, and R. Judd, "Contrast-enhanced MRI and routine single photon emission computed tomography (SPECT) perfusion imaging for detection of subendocardial myocardial infarcts: an imaging study," *Lancet*, vol. 361, p. 374379, 2003.

[140] E. Pueyo, L. Sornmo, and P. Laguna, "QRS slopes for detection and characterization of myocardial ischemia," *IEEE Transaction in Biomedical Eng.*, vol. 55, no. 2, pp. 468–477, 2008.

[141] B. Surawicz, "Reversible QRS changes during acute myocardial ischemia," *J Electrocardiol*, vol. 31, pp. 209–220, Jul 1998.

[142] P. Lander, P. Gomis, G. Hartman, K. Gates, J. Petterson, and G. Wagner, "Analysis of high-resolution ECG changes during percutaneous transluminal coronary angioplasty," *Journal of Electrocardiology*, vol. 28 Suppl, pp. 39–40, 1995.

[143] G. Dori, A. Rosenthal, S. Fishman, Y. Denekamp, B. Lewis, and H. Bitterman, "Changes in the slope of the first major deflection of the ECG complex during acute coronary occlusion," *Comput Biol Med*, vol. 35, pp. 299–309, May 2005.

[144] D. Romero, M. Ringborn, P. Laguna, O. Pahlm, and E. Pueyo, "A vectorial approach for evaluation of depolarization changes during acute myocardial ischemia," in *Proc. Computers in Cardiology*, pp. 265–268, 2010.

[145] S. Theodoridis and K. Koutroumbas, *Pattern Recognition*. Orlando, FL, USA: Academic Press, Inc., third ed., 2006.

[146] K. Fukunaga, *Introduction to Statistical Pattern Recognition*. Academic Press, 1972.

[147] T. Fawcett, "ROC graphs: Notes and practical considerations for researchers," Tech. Rep. HPL-2003-4, HP Labs, 2003.

[148] C. M. Bishop, *Pattern Recognition and Machine Learning*, ch. 1, p. 45. Springer, 2006.

[149] I. Nabney, *NETLAB: algorithms for pattern recognition*. Springer-Verlag New York, Inc, 2002.

[150] V. Vapnik, *The nature of statistical learning theory*. New York, NY, USA: Springer-Verlag New York, Inc., 1995.

[151] C. Burges, "A tutorial on support vector machines for pattern recognition," *Data mining and knowledge discovery*, vol. 2, no. 2, pp. 121–167, 1998.

[152] B. Scholkopf, K.-K. S., C. J. C. Burges, F. Girosi, P. Niyogi, T. Poggio, and V. Vapnik, "Comparing support vector machines with gaussian kernels to radial basis function classifiers," vol. 45, no. 11, pp. 2758–2765, 1997.

[153] M. Tipping, "Sparse Bayesian learning and the Relevance Vector Machine," *Journal of Machine Learning Research*, vol. 1, pp. 211–244, 2001.

[154] N. Downie and R. Heath, *Basic Statistical Methods*, ch. 2. Harper & Brothers, 1959.

[155] C. Chang and C. Lin, "LIBSVM: A library for support vector machines," *ACM Transactions on Intelligent Systems and Technology*, vol. 2, pp. 27:1–27:27, 2011.

[156] NICE, "Chest pain of recent onset: Assessment and diagnosis of recent cehst pain or discomfort of suspected cardiac origin," tech. rep., National Institute for Clinicial Excellence, March 2010.

[157] MedTronic, "Specificition for lifepak 15," tech. rep., Physio-Control, 2011.

[158] M. Wukitsch, M. Petterson, D. Tobler, and J. Pologe, "Pulse oximetry: Analysis of theory, technology and practice," *Journal of Clinical Monitoring*, vol. 4, no. 4, pp. 290–301, 1988.

[159] R. Marsan, Jr, K. Shaver, K. Sease, F. Shofer, F. Sites, and J. Hollander, "Evaluation of a clinical decision rule for young adult patients with chest pain.," *Acad Emerg Med*, vol. 12, pp. 26–31, Jan 2005.

[160] D. A. Morrow, E. M. Antman, A. Charlesworth, R. Cairns, S. A. Murphy, J. A. de Lemos, R. P. Giugliano, C. H. McCabe, and E. Braunwald, "TIMI risk score for ST-elevation myocardial infarction: A convenient, bedside, clinical score for risk assessment at presentation: An intravenous nPA for treatment of infarcting myocardium early II trial substudy.," *Circulation*, vol. 102, pp. 2031–2037, Oct 2000.

[161] M. Wolf, "Sinus arrhythmia in acute myocardial infarction," *Med J Aust*, pp. 2–52, 1978.

[162] R. Kleiger, J. Miller, J. J. Bigger, and A. Moss, "Decreased heart rate variability and its association with increased mortality after acute myocardial infarction," *American Journal of Cardiology*, vol. 59, no. 4, pp. 256–262, 1987.

[163] F. Lombardi, G. Sandrone, S. Pernpruner, R. Sala, M. Garimoldi, S. Cerutti, G. Baselli, M. Pagani, and A. Malliani, "Heart rate variability as an index of sympathovagal interaction after acute myocardial infarction.," *American Journal of Cardiology*, vol. 60, pp. 1239–1245, Dec 1987.

[164] M. T. LaRovere, J. T. Bigger, F. I. Marcus, A. Mortara, and P. J. Schwartz, "Baroreflex sensitivity and heart-rate variability in prediction of total cardiac mortality after myocardial infarction. atrami (autonomic tone and reflexes after myocardial infarction) investigators.," *Lancet*, vol. 351, pp. 478–484, Feb 1998.

[165] H. V. Huikuri, T. H. Mkikallio, C. K. Peng, A. L. Goldberger, U. Hintze, and M. Mller, "Fractal correlation properties of r-r interval dynamics and mortality in patients with depressed left ventricular function after an acute myocardial infarction.," *Circulation*, vol. 101, no. 1, pp. 47–53, 2000.

[166] M. Malik, A. J. Camm, M. J. Janse, D. G. Julian, G. A. Frangin, and P. J. Schwartz, "Depressed heart rate variability identifies postinfarction patients who might benefit from prophylactic treatment with amiodarone: a substudy of EMIAT (The European Myocardial Infarct Amiodarone Trial)," *J Am Coll Cardiol*, vol. 35, pp. 1263–1275, Apr 2000.

[167] P. K. Stein, R. M. Carney, K. E. Freedland, J. A. Skala, A. S. Jaffe, R. E. Kleiger, and J. N. Rottman, "Severe depression is associated with markedly reduced heart rate variability in patients with stable coronary heart disease.," *J Psychosom Res*, vol. 48, no. 4-5, pp. 493–500, 2000.

[168] O. Manfrini, C. Pizzi, D. Trer, F. Fontana, and R. Bugiardini, "Parasympathetic failure and risk of subsequent coronary events in unstable angina and non-ST-segment elevation myocardial infarction," *Eur Heart J*, vol. 24, pp. 1560–1566, Sep 2003.

[169] C. Carpeggiani, A. L'Abbate, P. Landi, C. Michelassi, M. Raciti, A. Macerata, and M. Emdin, "Early assessment of heart rate variability is predictive of in-hospital death and major complications after acute myocardial infarction," *Int J Cardiol*, vol. 96, pp. 361–368, Sep 2004.

[170] P. Stein, "Potential role of different components of heart rate variability for risk-stratification in critical care.," *Crit Care Med*, vol. 33, pp. 2128–2130, Sep 2005.

[171] F. Lombardi, A. Malliani, M. Pagani, and S. Cerutti, "Heart rate variability and its sympatho-vagal modulation.," *Cardiovasc Res*, vol. 32, pp. 208–216, Aug 1996.

[172] M. T. Spinnler, F. Lombardi, C. Moretti, G. Sandrone, V. Podio, T. Spandonari, D. Torzillo, A. Brusca, and A. Malliani, "Evidence of functional alterations in sympathetic activity after myocardial infarction.," *Eur Heart J*, vol. 14, pp. 1334–1343, Oct 1993.

[173] J. T. Bigger, J. L. Fleiss, L. M. Rolnitzky, R. C. Steinman, and W. J. Schneider, "Time course of recovery of heart period variability after myocardial infarction.," *J Am Coll Cardiol*, vol. 18, pp. 1643–1649, Dec 1991.

[174] Y. Goseki, T. Matsubara, N. Takahashi, T. Takeuchi, and C. Ibukiyama, "Heart rate variability before the occurrence of silent myocardial ischemia during ambulatory monitoring.," *Am J Cardiol*, vol. 73, pp. 845–849, May 1994.

[175] W. J. Kop, R. J. Verdino, J. S. Gottdiener, S. T. O'Leary, C. N. Bairey Merz, and D. S. Krantz, "Changes in heart rate and heart rate variability before ambulatory ischemic events(1)," *J Am Coll Cardiol*, vol. 38, pp. 742–749, Sep 2001.

[176] R. Kleiger, J. Miller, J. Bigger, and A. Moss, "Decreased heart rate variability and its association with increased mortality after acute myocardial infarction," *American Journal of Cardiology*, vol. 59, pp. 256–263, 1987.

[177] C. M. van Ravenswaaij-Arts, L. A. Kolle, J. C. Hopman, G. B. Stoelinga, and H. P. van Geijn, "Heart rate variability.," *Ann Intern Med*, vol. 118, pp. 436–447, Mar 1993.

[178] P. Stein and R. Kleiger, "Insights from the study of heart rate variability," *Annu Rev Med*, vol. 50, pp. 249–261, 1999.

[179] M. F. Hilton, R. A. Bates, K. R. Godfrey, M. J. Chappell, and R. M. Cayton, "Evaluation of frequency and time-frequency spectral analysis of heart rate variability as a diagnostic marker of the sleep apnoea syndrome," *Med Biol Eng Comput*, vol. 37, pp. 760–769, Nov 1999.

[180] Y. Goren, L. R. Davrath, I. Pinhas, E. Toledo, and S. Akselrod, "Individual time-dependent spectral boundaries for improved accuracy in time-frequency analysis of heart rate variability," *IEEE Journal of Biomedical Engineering*, vol. 53, no. 1, pp. 35–42, 2006.

[181] R. Bailon, P. Laguna, L. Mainardi, and L. Sornmo, "Analysis of heart rate variability using time-varying frequency bands based on respiratory frequency," in *Proc. 29th Annual Int. Conf. of the IEEE Engineering in Medicine and Biology Society EMBS 2007*, pp. 6674–6677, 2007.

[182] R. Bailon, G. Laouini, C. Grao, M. Orini, P. Laguna, and O. Meste, "The integral pulse frequency modulation model with time-varying threshold: application to heart rate variability analysis during exercise stress testing," *IEEE Trans Biomed Eng*, vol. 58, pp. 642–652, Mar 2011.

[183] D. Liao, R. W. Barnes, L. E. Chambless, R. Simpson, Jr, P. Sorlie, and G. Heiss, "Age, race, and sex differences in autonomic cardiac function measured by spectral analysis of heart rate variability–the ARIC study. Atherosclerosis Risk in Communities.," *Am J Cardiol*, vol. 76, pp. 906–912, Nov 1995.

[184] K. Jensen-Urstad, N. Storck, F. Bouvier, M. Ericson, L. E. Lindblad, and M. Jensen-Urstad, "Heart rate variability in healthy subjects is related to age and gender.," *Acta Physiol Scand*, vol. 160, pp. 235–241, Jul 1997.

[185] I. Antelmi, R. S. de Paula, A. R. Shinzato, C. Peres, A. Mansur, and C. Grupi, "Influence of age, gender, body mass index, and functional capacity on heart rate variability in a cohort of subjects without heart disease.," *Am J Cardiol*, vol. 93, pp. 381–385, Feb 2004.

[186] O. Rimoldi, R. Furlan, M. R. Pagani, S. Piazza, M. Guazzi, M. Pagani, and A. Malliani, "Analysis of neural mechanisms accompanying different intensities of dynamic exercise.," *Chest*, vol. 101, pp. 226S–230S, May 1992.

[187] S. W. Webb, A. A. Adgey, and J. F. Pantridge, "Autonomic disturbance at onset of acute myocardial infarction.," *Br Med J*, vol. 3, pp. 89–92, Jul 1972.

[188] H. Gao, A. McDonnell, D. Harrison, T. Moore, S. Adam, K. Daly, L. Esmonde, D. Goldhill, G. Parry, A. Rashidian, C. Subbe, and S. Harvey, "Systematic review and evaluation of physiological track and trigger warning systems for identifying at-risk patients on the ward," *Intensive Care Med*, vol. 33, pp. 667–79, 2007.

[189] R. Morgan, F. Williams, and W. M.M., "An early warning score for the early detection of patients with impending illness," *Clin Intens Care*, vol. 8, p. 100, 1997.

[190] C. Stenhouse, S. Coates, M. Tivey, P. Allsop, and T. Parker, "Prospective evaluation of a modified early warning score to aid earlier detection of patients developing critical illness on a general surgical ward.," *Br. J. Anaesth.*, vol. 84, p. 663, 2000.

[191] R. Schoenberg, D. Sands, and C. Safran, "Making ICU alarms meaningful: a comparison of traditional vs. trend-based algorithms.," *Proc AMIA Symp*, pp. 379–83, 1999.

[192] A. Otero, F. Palacios, S. Barro, and P. Felix, "A tool for the analysis and synthesis of alarms in patient monitoring," in *Seventh International Conference on Information Fusion*, pp. 951–958, 2001.

[193] C. Tsien and J. Fackler, "Poor prognosis for existing monitors in the intensive care unit," *Crit Care Med*, vol. 25, no. 614–619, 1997.

[194] T. Sukuvaara, E. Koski, A. Makivirta, and A. Kari, "A knowledge-based alarm system for monitoring cardiac operated patients–technical construction and evaluation," *Int J Clin Monit Comput*, vol. 10, pp. 117–26, 1993.

[195] S. Charbonnier and S. Gentil, "A trend-based alarm system to improve patient monitoring in intensive care units," *Control Engineering Practice*, vol. 15, no. 9, pp. 1039–1050, 2007.

[196] J. Quinn and C. Williams, "Known unknowns: Novelty detection in condition monitoring," in *Proc 3rd Iberian Conference on Pattern Recognition and Image Analysis* (J. Marti, J. Benedi, A. Mendonca, and J. Serrat, eds.), LNCS 4477, pp. 1–6, Springer-Verlag, 2007.

[197] L. Tarassenko, A. Hann, A. Patterson, E. Braithwaite, K. Davidson, V. Barber, and D. Young, "Biosign:multi-parameter monitoring for early warning of patient deterioration," *Proc. 3rd IEE International Seminar on Medical Applications of Signal Processing*, pp. 71–76, 2005.

[198] L. Clifton, D. Clifton, P. Watkinson, , and L. Tarassenko, "Identification of patient deterioration in vital-sign data using one-class Support Vector Machines," *IEEE Conference on Artificial Intelligence in Medical Applications*, pp. 125 – 131, 2011.

[199] A. Hann, *Multi-parameter Monitoring for Early Warning of patient Deterioration*. PhD thesis, University of Oxford, 2008.

[200] S. Fleming, M. Thompson, and L. Tarassenko, "Measuring respiratory rate using a pulse oximeter in children attending primary care.," in *SWSAPC Annual Research Meeting*, Mar. 2011.

[201] G. Moody and R. Mark, "Qrs morphology representation and noise estimation using the karhunen-loeve transform," in *Computers in Cardiology 1989, Proceedings.*, pp. 269–272.

[202] I. Silva, G. Moody, and L. Celi, "Improving the quality of ECGs collected using mobile phones: The PhysioNet/Computing in Cardiology Challenge 2011," *Computing in Cardiology*, vol. 38, pp. 273–276, 2012.

[203] M. R. Zong W, Moody GB, "Reduction of false arterial blood pressure alarms using signal quality assessment and relationships between the electrocardiogram and arterial blood pressure," *Med Biol Eng Comput*, vol. 42, p. 698706, 2004.

[204] G. Clifford, *Advanced Methods and Tools for ECG Data Analysis*, ch. Linear filtering methods, pp. 270–290. Artech House, 2006.

[205] V. Murthy, T. Grove, G. Harvey, and L. Haywood, "Clinical usefulness of ecg frequency spectrum analysis," in *Computer Application in Medical Care*, pp. 610–612, 1978.

[206] M. Saeed, M. Villarroel, A. T. Reisner, G. Clifford, L.-W. Lehman, G. Moody, T. Heldt, T. H. Kyaw, B. Moody, and R. G. Mark, "Multiparameter Intelligent Monitoring in Intensive Care ii (MIMIC-II): A public-access intensive care unit database," *Critical Care Medicine*, vol. 39, pp. 952–960, May 2011.

[207] G. Moody, W. Muldrow, and R. Mark, "A noise stress test for arrhythmia detectors," in *Proc. of Computers in Cardiology*, pp. 381–384, 1984.